Analytical and Numerical Techniques for the Optimal Design of Mineral Separation Circuits

Christopher Aaron Noble

Dissertation submitted to the Faculty of the
Virginia Polytechnic Institute and State University
in partial fulfillment of the requirements for the degree of

Doctor of Philosophy
in
Mining Engineering

Gerald H. Luttrell, Chair
Roe-Hoan Yoon
Gregory T. Adel
Emily A. Sarver
Serhat Keles

May 7, 2013
Blacksburg, Virginia

Keywords: Separation Circuit Analysis, Data Analysis, Circuit Simulation

Analytical and Numerical Techniques for the Optimal Design of Mineral Separation Circuits

Christopher Aaron Noble

(ABSTRACT)

The design of mineral processing circuits is a complex, open-ended process. While several tools and methodologies are available, extensive data collection accompanied with trial-and-error simulation are often the predominant technical measures utilized throughout the process. Unfortunately, this approach often produces sub-optimal solutions, while squandering time and financial resources. This work proposes several new and refined methodologies intended to assist during all stages of circuit design. First, an algorithm has been developed to automatically determine circuit analytical solutions from a user-defined circuit configuration. This analytical solution may then be used to rank circuits by traditional derivative-based linear circuit analysis or one of several newly proposed objective functions, including a yield indicator (the yield score) or a value-based indicator (the moment of inertia). Second, this work presents a four-reactor flotation model which considers both process kinetics and machine carrying capacity. The simulator is suitable for scaling laboratory data to predict full-scale performance. By first using circuit analysis to reduce the number of design alternatives, experimental and simulation efforts may be focused to those configurations which have the best likelihood of enhanced performance while meeting secondary process objectives. Finally, this work verifies the circuit analysis methodology through a virtual experimental analysis of 17 circuit configurations. A hypothetical electrostatic separator was implemented into a dynamic physics-based discrete element modeling environment. The virtual experiment was used to quantify the selectivity of each circuit configuration, and the final results validate the initial circuit analysis projections.

Parts of this work received financial support form FLSmidth Minerals. Unless otherwise indicated, all examples presented in this document are fictitious and only intended for demonstration. Any resemblance to real operations is purely coincidental.

Acknowledgments

The preparation of this dissertation has been an immensely rewarding undertaking. I would like to first thank the Lord for the many blessings I have experienced.

I want to acknowledge my research advisor, Dr. Jerry Luttrell. I know I could not have started this work without his teachings, and I know I could not have finished this work without his persistence. Though I have occasionally heard "you can't beat physics" in my sleep, I slept knowing that someone besides me wanted to see this work to completion. Jerry has been a constant friend and mentor throughout my time at Virginia Tech.

I cannot understate the role of my other committee members and mentors in motivating me to conduct this research. I owe original my interest in flotation to Dr. Roe-Hoan Yoon. His unquenchable thirst for understanding is both a silent and, at times, vocal motivator for continued success. Dr. Greg Adel, has provided solidarity and direction, while Dr. Emily Sarver has consistently offered pragmatic suggestions and advice on many professional levels. Finally, I thank Dr. Serhat Keles for the original genesis of much of this work. I am not sure if the graphical interface would have ever been attempted had he not invested countless hours in the beginning.

I also express gratitude to FLSmidth for the continued funding throughout parts of this project. I especially thank Asa Weber for his role facilitating and testing my ideas. His suggestions have taught me a lot about flotation as well as practicality and leadership.

I want to thank my current, former, and future students. They all motivate me every day to dig deeper, work harder, and discover more. I have learned a lot of patience serving them, and I hope I have repaid a fraction of the enlightenment and enjoyment that they have brought me.

I could not have completed this work without the constant love and support from my friends and family. I thank them for bearing with me throughout this process. Finally, I thank my *yeojachingu* Alice Lee . She is a constant source of love, hope, and joy.

Contents

List of Figures

List of Tables

Chapter 1

Introduction

1.1 Preface

Mineral processing is largely the science of particulate separation as it applies to the beneficiation of mining products. Run-of-mine material consists of one or more valuable components, designated as ore minerals, mixed with a significant portion of waste components, designated gangue minerals. The relatively low quality of the run-of-mine material often necessitates downstream processing to enhance the marketable value of the raw material. While the general quality of the final product may be defined by several indicators (average particle size, moisture content, bulk mechanical properties), the compositional purity (i.e., grade) of the final product often drives the economic unit value. Consequently, the most important objective of mineral processing is to physically separate the mineral constituents, so that the valuable portions may be retained for marketing or further processing, while the gangue may be properly disposed.

Mineral beneficiation is a costly portion of the raw material production chain, given the large overall throughputs required to recover material from low-grade deposits. As a result, the separation processes must increase the value of the final product to a level which justifies the cost of beneficiation. Since single unit operations are often incapable of producing sufficient separation, multiple cleaning stages are typically arranged in a circuit to produce synergistic efficiencies. The simple serial arrangement and interconnections of the circuit have the capacity to drastically alter the single-stage separation efficiency. Well-designed circuits can overcome various unit inadequacies, while poor configurations can actually degrade performance below that of a single unit.

In theory, a perfect separation can ultimately be achieved by a well-designed circuit of imperfect units, regardless of the magnitude of deficiency in the single unit. In practice, these ideal circuits are never fully pursued, since the cost of the required resources would greatly overcome the value of the pure separation products. Nevertheless, the optimal design of separation circuits is critical to maximizing beneficiation value, while minimizing required capital resources and processing costs.

This work is largely concerned with the identification of optimal circuit designs. While no single circuit is universally suitable in all instances, analytical and numerical tools can be used to guide the decisions of circuit designers as the site-specific, ore-specific, and time-specific conditions dictate. The resulting techniques are empowered by fundamental insight and streamline the otherwise haphazard and costly circuit design process.

1.2 History

Over the last 100 years, mineral processing has advanced from a crude, labor-intensive processes to a highly sophisticated scientific endeavor. While much of the progress has been spearheaded by the invention and development of froth flotation, other processing methods have also benefited from the more scientific outlook on mineral separation (Wills & Atkinson, 1991). One of the first exhaustive analyses of the design and operation of mineral processing plants was presented by Taggart (1927). This classic text marked the beginnings of the burgeoning scientific discipline.

Throughout the remainder of the century, the science of mineral processing grew to encompass numerous sub-disciplines, including surface chemistry, analytical chemistry, physical chemistry, mathematical modeling, data analysis, scientific computing, simulation, engineering economics, process control, fluid mechanics, machine design, and extractive metallurgy. Both the ever-increasing consumer demand for minerals as well as the heightened productivity of various separation processes are evident when considering the rapidly increasing global mineral production. Figure 1.1 shows global production statistics for 47 major mineral commodities (Kelly et al., 2010). While the production of some commodities has stagnated in recent years (e.g. lead, mercury, and tin), others have continually experienced long-term exponential growth since the beginning of the century (e.g. aluminum, copper, and rare earths).

Froth flotation is the most common and versatile separation methodology used in the mineral processing industry today. Since its development in the early 1900's (Sulman, Picard,

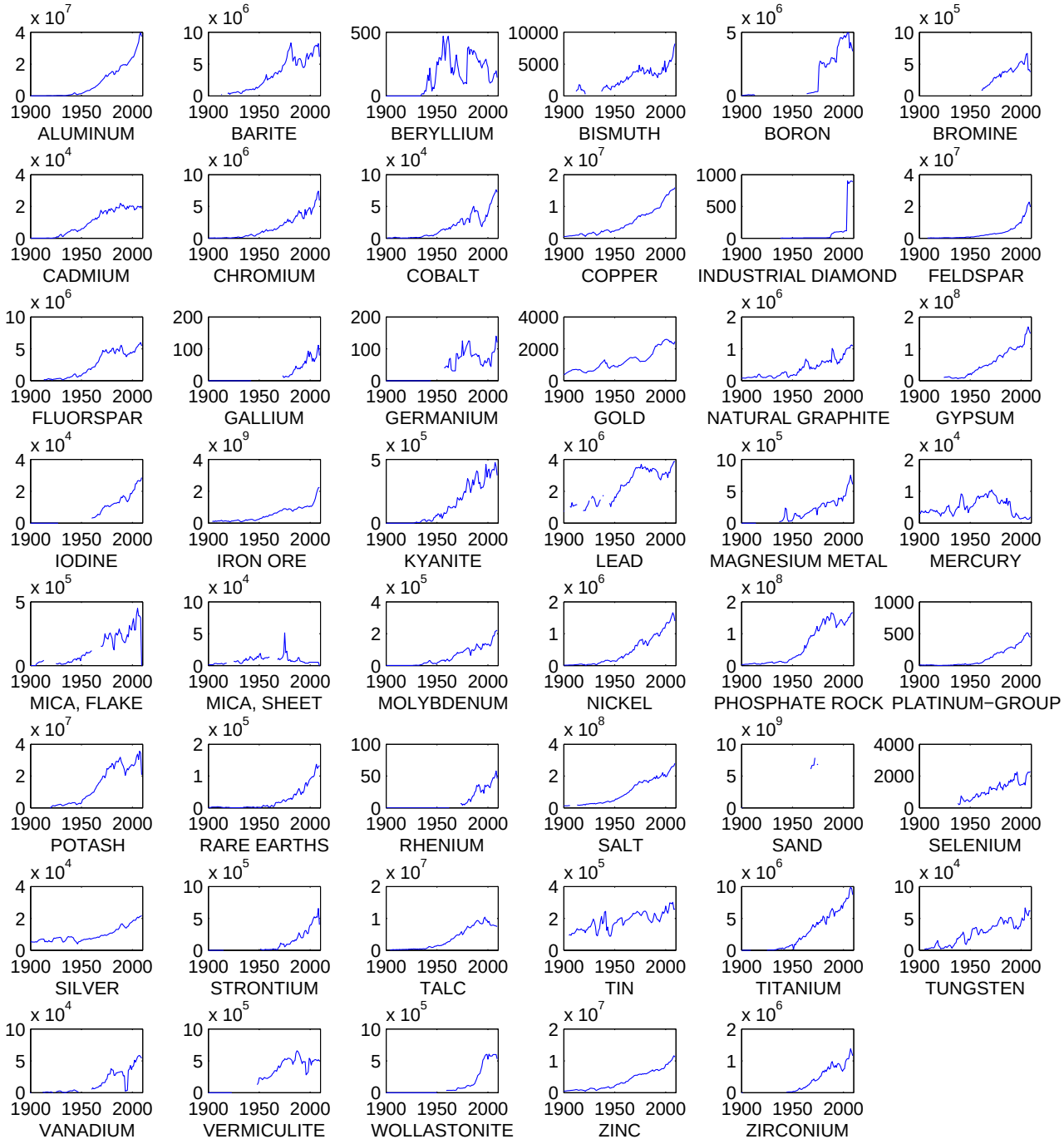

Figure 1.1: World production (shown in metric tonnes) for various major minerals from 1900 to 2009. Data after (Kelly et al., 2010).

& Ballot, 1905), most of the advancement in the mineral processing science have been driven by the dominance of the flotation process. Up until 1905, most base-metals and porphyry copper deposits were processed via simple gravity separation. Around this time, the poor separation performance and the ever-increasing ore complexity led to substantial milling deficiencies and lost revenue (Lynch, Watt, Finch, & Harbort, 2007). A large-capacity, highly selective industrial process was needed to ensure the economic stability of the world-wide base metal industry. Shortly after its inception, the froth flotation process fulfilled this role and quickly grew to one of the most crucial metallurgical processes . With the development of selective reagents in the 1930's, processing plants were beginning to use froth flotation as the sole separation process (Wills & Atkinson, 1991). While observing those industrial advancements, many academic researchers and engineers became curious on how to optimize flotation performance through fundamental understanding and rigorous laboratory experimentation. This initial growth period witnessed the prominence of authors such as Sutherland (1948), Gaudin (1957), and Harris (1976) whose work still withstands scrutiny today.

Given its prominence in the economic production of base metals, froth flotation has been described by several several authors as one of the most significant technological innovations of the 20th century (Klassen & Mokrousov, 1963; Napier-Munn, 1997; Fuerstenau, 1999; Lynch et al., 2007). Even outside of the minerals industry, flotation has alternatively been used as a separation process in waste water treatment (Wang, Fahey, & Wu, 2005), algae harvesting (Phoochinda, White, & Briscoe, 2004; Lynch et al., 2007), and paper recycling (Bloom & Heindel, 1997; Kemper, 1999; Gomez, Watson, & Finch, 1995). The ever-increasing importance of froth flotation as an industry-leading separation technique is evident in the exponential growth of the size of flotation units (Figure 1.2). Since the commercialization of the process in the early 1900's, the size of "large" flotation cells as reported in the literature has consistently followed an exponential curve, doubling in size every nine years.

Other separation methods have witnesses comparatively modest gains in prominence throughout the last century. These methods are often relegated to the few mineral industries where their simplicity and utility overcome their lack of robustness. For example, modern coal preparation plants largely employ gravity separation, given its effectiveness in separating simple coal and rock systems, especially in the larger size fractions. At least one author has claimed that gravity separation is realizing a small revival in base metal plants, where conditions favor their simple process control strategies (Wills & Napier-Munn, 2006, p. 225). Other separations, such as electromagnetic or magnetic are selected when the physical properties of the mineral systems allow their usage. Nevertheless, the gains in process knowledge originally driven by flotation have effectively benefited these industries, especially

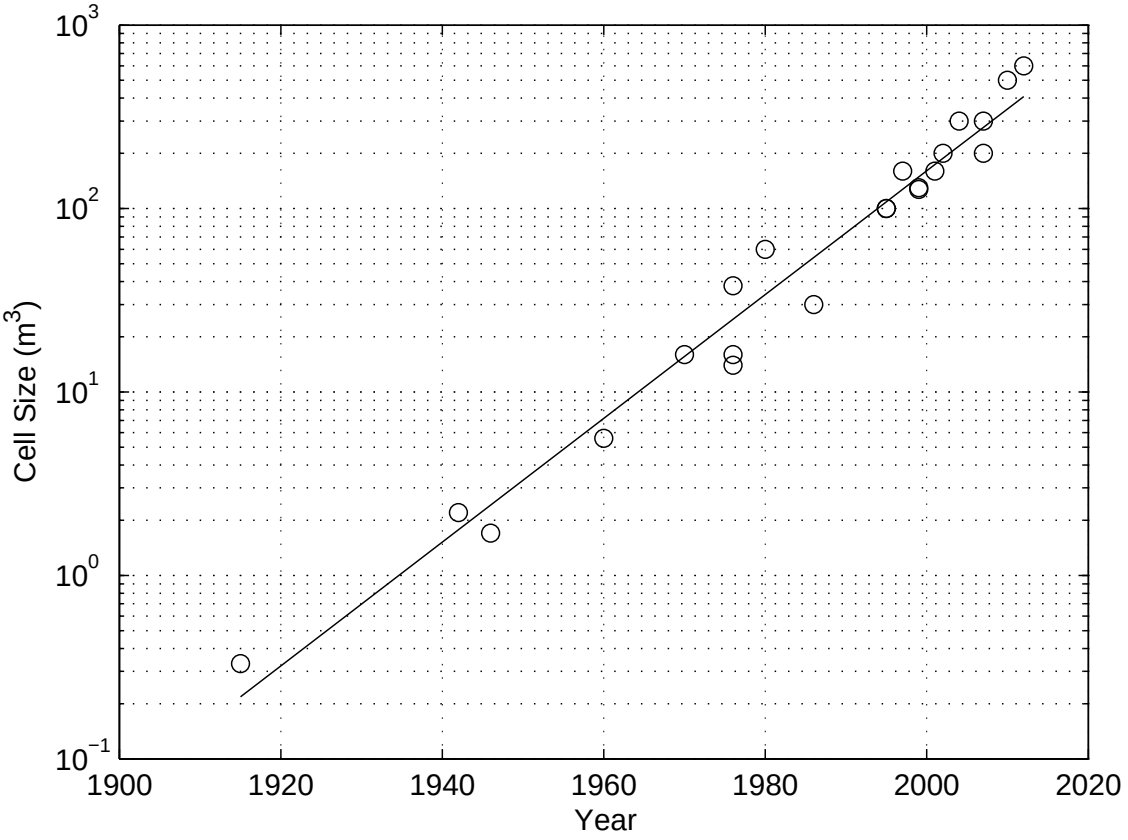

Figure 1.2: Size of large flotation cell sizes reported in literature since 1917. Data after (Taggart et al., 1945; Hanna et al., 1976; Weber et al., 1999; Meenan, 1999; Lynch et al., 2007; Gorain, 2007; Weber & Tracyzk, 2007; Oravainen & Allenius, 2007). Plot design after (Noble, 2012).

in the areas of process control, modeling and simulation, and circuit design.

1.3 Unit Operations

Mineral processing consists of two fundamental unit operations: comminution and separation. Comminution processes reduce the size of run-of-mine material prior to downstream separation processes. This size reduction step is usually required to liberate locked mineral particles; although, comminution may also perform a number of auxiliary functions, including enhancing mineral handleability, creating fresh surfaces, increasing surface area, and managing particle size.

From a purist perspective, the comminution process begins during the mining phase (i.e., drilling and blasting) and continues throughout the beneficiation phases. Size reduction in the comminution stage-proper is often achieved by both crushing and grinding, which may include dry and wet methods; however, unintentional size reduction and attrition may result from other downstream materials handling operations, such as pumping, tank mixing, and ore storage. Lynch and Rowland (2005) have provided a narrative on the historical influences of contemporary grinding methods. Other authors have provided technical reviews and critical analyses of comminution theory, modeling, and equipment design (Bond, 1952; Lynch & Bush, 1977; Veasey & Wills, 1991).

After the comminution stage, the liberated material is concentrated via one or more physical separation processes until the mineral component meets the required product quality specifications. Separation processes are often broadly classified by the chemical phase of the constituent products. Under this taxonomy, the following designations are given:

- *Solid-Solid Separation*: Processes which separate minerals of two different compositions, namely mineral and gangue components. These operations can be conducted wet or dry, depending on the specific application. Common examples include froth flotation, gravity separators, and magnetic separators.
- *Solid-Liquid Separation*: Drying processes which concentrate the solid phase of the mineral slurry or reduce the moisture of the product. These unit operations are required when the final product moisture is of concern, such as in coal preparation. Common examples of solid-liquid separation include thickeners, centrifuges, and thermal dryers.
- *Size-Size Separation*: Processes which classify minerals based on particle size. These unit operations are typically used to ensure that appropriate size reduction has been

achieved in the comminution stage. Additionally, size-size separation may be utilized when seeking to exploit the size dependency of many solid separation processes. Two common examples include screens and cyclones.

Separations involving two liquid phases or gaseous phases are not typically considered in the mineral processing discipline. These processes are more common to chemical engineering, particularly the studies of solvent extraction, adsorption, and distillation. A pragmatic review of various separation methods, including gas-gas separation, gas-solid separation, gas-liquid separation, and liquid-liquid separation has been presented by Schweitzer et al. (1979). Despite the differences in unit operations, many of the performance indicators and circuit design strategies for these techniques are founded in similar fundamental theory.

The focal point of most mineral separation plants is the solid-solid separation stage. These unit operations are solely responsible for producing a final product free of containments and of sufficient marketable concentration. As a result, the economic gains and losses of the entire plant are highly sensitive to the efficiency of these processes. The selection of the appropriate solid-solid separator is driven by contrasts in the physical or chemical properties of the mineral and gangue constituents. The following designations subdivide these processes by the property on which the separation is based (modified after, Wills & Napier-Munn, 2006, pp. 8 - 11):

- *Gravity-Based Separation*: Processes which separate minerals on basis of particle density. Feed particles are typically fluidized by air, water, or a heavy medium. The application of a centrifugal force is used to enhance the rate of separation. Common examples include cyclones, spirals, and dense-media vessels.
- *Surface-Based Separation*: Process which exploit contrasts in surface properties, such as hydrophobicity. Froth flotation is the most prominent example.
- *Conductivity/Magnetic Separation*: Processes which exploit the degree of a particle's conductivity or magnetic susceptibility. Common examples include high-intensity and low-intensity magnetic separators, high-tension separators, and matrix magnets.
- *Optical and Other Novel Separation*: Processes which can exploit any other property disparate between the valuable mineral and gangue material. One such example is a diamond ore sorter which uses X-ray diffraction to distinguish liberated diamonds from the host rock.

The efficiency of most separation processes is strongly influenced by the particle size of the feed material. Every unit operation performs optimally within a critical size range, and many processes cannot feasibly distinguish particles of extreme sizes. In most cases, these performance limitations are driven by the physical subprocesses that define the individual unit operations. For example, many gravity separators exploit the differences in the settling velocity of particles suspended in water. This settling velocity is a function of both density and particle size. As particles settle, those in a similar size range may be distinguished by differences in density; however, as the size range expands, the separation is influenced by both density and size. As a result, many gravity separations cannot distinguish a small, dense particle from a large, light particle. By expanding this example to include other separation methods, an effective particle size range may be determined for various separators by recognizing the mechanism by which particles are distinguished. Figure 1.3 shows various unit operations and their range of applicable particle sizes.

In addition to particle size and other physical limitations, all particulate separation processes are inherently probabilistic and subject to unavoidable imperfection. To overcome these inefficiencies, mineral processing plants typically include staged separation arrangements, where the products of a single unit may be further processed by other units or reintroduced at other points in the plant. The resulting structure which includes all of the specific unit operations and the flow patterns of the units' products is defined as the *separation circuit*. Over time, the mineral processing industry has trended toward a few basic circuit configurations which are adapted to account for site-specific considerations.

The fundamental element of a separation circuit is a *unit*. In a binary system, a separation unit (Figure 1.4a) is capable of accepting a single feed stream while producing two product streams, namely a concentrate and a tailings. A junction unit (Figure 1.4b) is capable of accepting two feed streams while producing a single product stream. Practically, a separation circuit may be a single flotation cell or any other unit operation, while a junction may be a sump or mixing tank (Meloy, 1983). A *bank* of units (Figure 1.4c) consists of two or more individual units which are serially staged such that the tailings product passes from one unit to the next. The concentrate product of each unit in the bank is typically combined to produce a single bank concentrate. Banks of flotation cells are common, as the recovery from a single unit is not substantial to justify standalone cells. Flotation banks range from 5 to 12 units, depending on the unit volume and the process requirements (Malghan, 1986). Industrial trends have recently favored larger cells with fewer cells in a bank, though the metallurgical and economic performance of such trending is debated (Harris, 1976; Abu-Ali & Sabour, 2003). Banks of individual units may then be configured to produce the overall *circuit*.

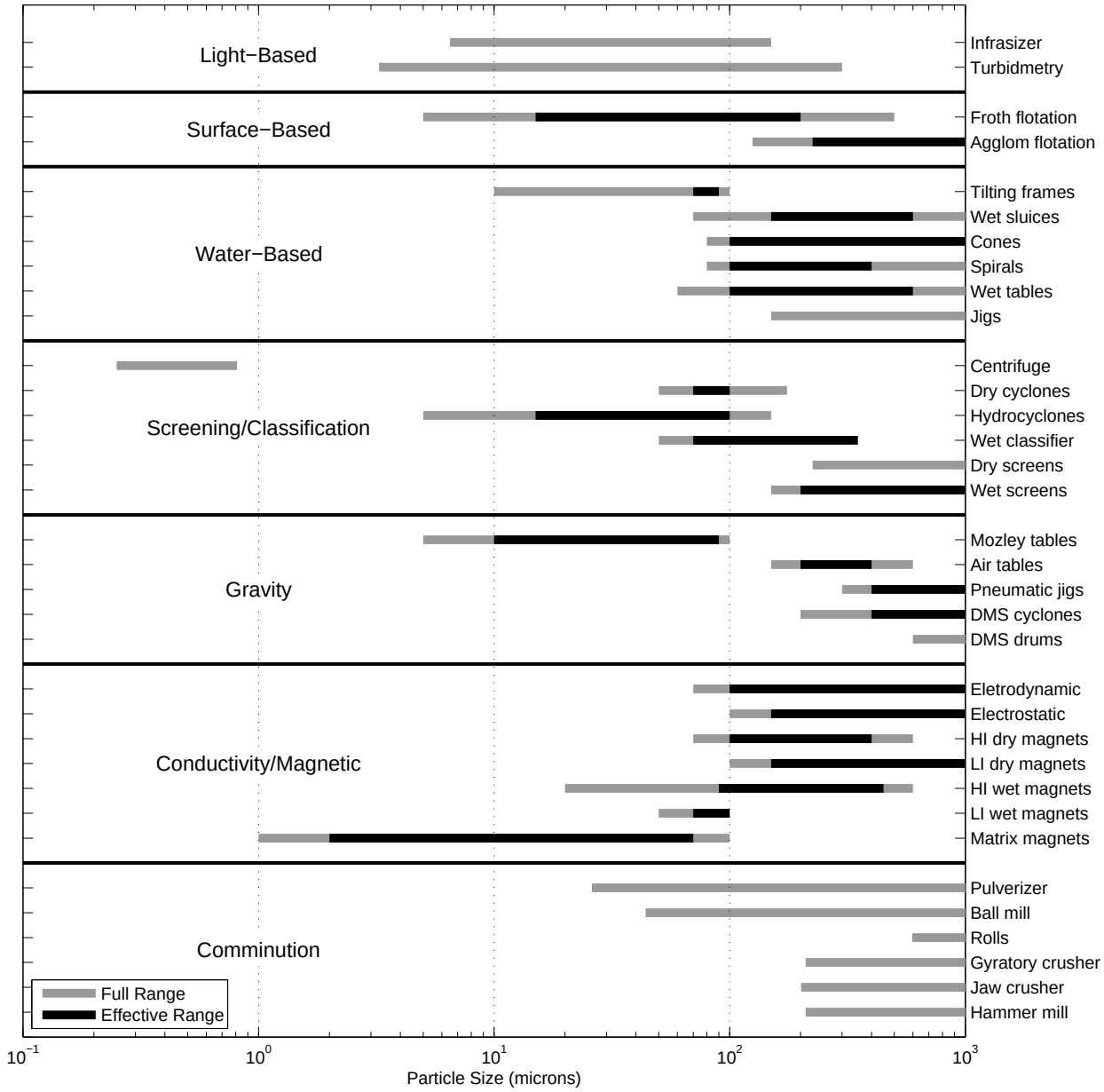

Figure 1.3: Effective particle size range for various separation processes. Data after (Glover, 1991; Wills & Napier-Munn, 2006).

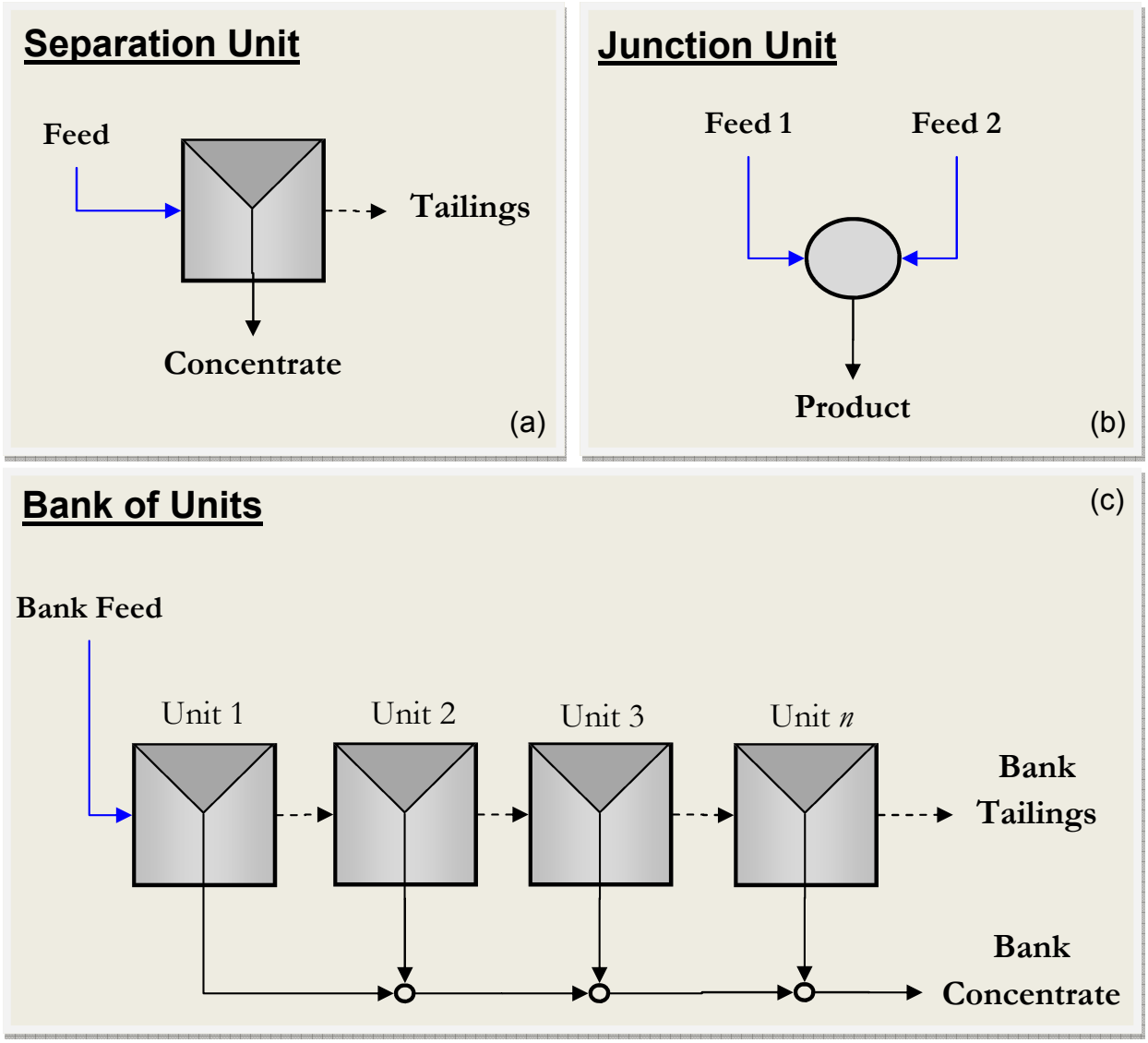

Figure 1.4: Definition of various fundamental separation circuit components.

Separation circuits are classified as open or recycle, depending on the presence of circulating loads (open circuits do not incorporate recirculating loads). The relative location of the bank within the circuit provides a means of designation (Williams & Meloy, 1989). *Rougher* banks are the initial separation which receives the plant feed. The rougher concentrate product is advanced to the *cleaner* bank which further upgrades the product until the final quality specifications are met. Finally, the rougher tailings product is sent to the *scavenger* to ensure that no valuable material has bypassed the rougher stage (Malghan, 1986). These definitions are illustrated in Figure 1.5.

In this work, *circuit design* encompasses all of the design decisions associated with the steady-state operation of separation circuits, whether the circuit under consideration is a greenfield design or a modification to an existing plant. Within this definition, the circuit designer must address several questions:

1. The selection of the appropriate separation process(es). While this selection is fairly definitive for a given mineral system, some flexible may be warranted in novel separation systems or where the economics support non-traditional processes, such as the choice to include or omit flotation as part of a fine coal cleaning circuit. Furthermore, specific equipment types should be considered in this decision, such as column versus conventional flotation cells.

2. The selection of the number and size of each unit in a bank. Especially in the case of rate separators (See Section 2.2.3), the separation performance of each unit is dependent on the mean residence time of particles in the vessel. Consequently, units must be sized to ensure sufficient residence time.

3. The optimization of the operational parameters unique to each unit. The steady-state performance of all separation units can be influenced by specific operational parameters. While dynamic control systems can alter these values to adapt to changing feed conditions, an ideal steady-state value should be determined by the circuit designer. This optimization may include reagent dosages for flotation plants or dense-media concentrations values in dense-media circuits.

4. The configuration of the flows between individual units and banks. This decision includes the required number of scavenger and cleaner banks, open or recycle circuit designation, and the point of reentry for recirculating loads.

While these design considerations have been presented sequentially, the actual circuit design process must consider all of these factors simultaneously while incorporated knowl-

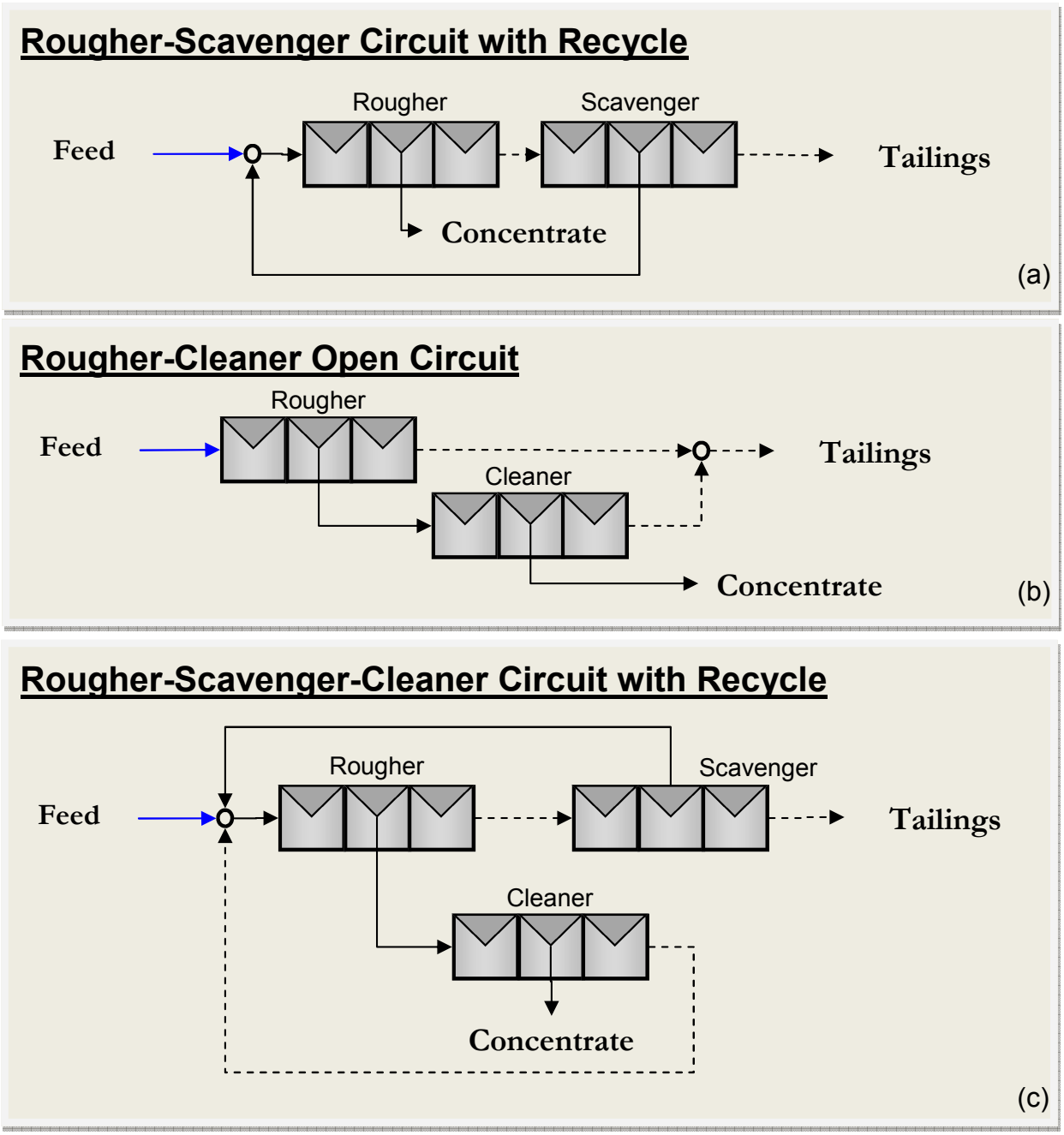

Figure 1.5: Examples of various generic circuit configurations.

edge gleaned from laboratory and pilot-scale experiments, process models, dynamics and control systems, common sense limitations, empirical insight, and operator preferences and biases. Given the complexity and interdependence of this knowledge base, circuit design unfortunately remains cumbersome and unsystematic. Numerous methods and engineering tools have been developed to assist the circuit designer; however, no comprehensive design methodologies have gained substantial usage in an industrial setting (Lucay, Mellado, Cisternas, & Galvez, 2012).

1.4 Objectives

The singular goal of this research is to develop and validate a methodology for separation circuit design based on new, existing, or refined analytical and numerical techniques. This methodology should streamline the circuit design process, by assimilating diverse process knowledge and fundamental scientific observations. The resultant tool-set should foster optimal design strategies throughout the entire circuit design process, from the initial concept generation to the final performance guarantee.

In summary, the itemized objectives of this study are to:

- Conduct a critical review of the recent developments in separation circuit design.
- Develop and asses a software platform for froth flotation circuit simulation. This simulator may be later used in the corroboration of novel circuit design methodologies.
- Develop an analytical methodology of circuit evaluation which rely on fundamental separation principles.
- Implement that methodology into a design software package which can streamline preliminary analysis and alternative selection for proposed circuit configurations.
- Experimentally validate the circuit design methodology with a known or novel separation process.

1.5 Organization

The body of this dissertation is organized into nine chapters, with the primary works presented individually as standalone papers describing a separate phase or objective of the

work. These primary phases constitute the seven informative chapters, while an introductory and a concluding chapter complete the dissertation. References are listed individually for each chapter.

Chapter 1 includes a description of the historical context of separation circuit design, general definitions, and an overview of the work completed as a part of this study.

Chapter 2 provides a comprehensive review of the state-of-the-art in engineering data analysis as it applies to mineral processing, process modeling, circuit simulation, and circuit optimization. This chapter shows the historic trends and recent developments in circuit design strategies. This review is largely reflective and descriptive; however, some meta-analysis is used to critically evaluate prior claims and methods.

Chapter 3 describes the development of a robust, graphically based simulator for froth flotation circuits, FLoatSim. A four-reactor flotation model, which is based on standard first-order rate equations, is described along with details of the simulation approach and software interface. Finally, this chapter presents a case study which utilizes the software in a coal flotation scale-up problem.

Chapter 4 presents a critical evaluation of rate-based simulation from the perspective of discretization detail. This chapters shows the derivation of "rate compositing formulas" unique for each reactor type. These formulas are used to calculate a single "apparent rate" value which produces the same recovery as a series of distributed rates at a given residence time. The utilization of these formulas is demonstrated by the error propagation which results from truncating the rate distribution. Sample calculations and examples are presented in this chapter.

Chapter 5 introduces the use of analytical circuit solutions in the design of optimal separation circuits. This chapter describes Meloy's (1983) algebraic method of analytical circuit solution determination, while noting the drawbacks and inefficiencies of the method. In light of the deficiencies, a new method for analytical circuit solution determination is introduced. The final algorithm is described and applied to evaluate several circuit configurations found in the literature.

Chapter 6 extends the utility of analytical circuit solutions, by describing the resultant optimization software: the Circuit Analysis Reduction Tool (CART^{TM}). The program uses analytical circuit solutions and the circuit partition sharpness to evaluate circuit configurations. The software also contains a custom algorithm which determines the optimal location in the circuit for an additional unit based on the greatest increase in the sharpness parameter. These tools and other applications of the software are presented.

Chapter 7 describes a new technical-economic performance indicator for partition separators: the moment of inertia. This chapter describes the theoretical background of the performance indicator and compares its utility of to that of more common measures, such as the partition sharpness and error area.

Chapter 8 validates the proposed circuit analysis and optimization methodologies through the use of a novel virtual separator.

Chapter 9 summarizes the key findings of this work, describes holistic conclusions, and introduces opportunities for further research and development.

1.6 Bibliography

Abu-Ali, M., & Sabour, S. A. (2003). Optimizing the design of flotation circuits: an economic approach. *Minerals Engineering*, *16*(1), 55–58.

Bloom, F., & Heindel, T. (1997). A theoretical model of flotation deinking efficiency. *Journal of Colloid and Interface Science*, *190*(1), 182–197.

Bond, F. (1952). The third theory of comminution. *Transactions*, *193*(2), 484–494.

Fuerstenau, M. (1999). Froth flotation: The first ninety years. In B. Parekh & J. Miller (Eds.), *Advances in flotation technology.* SME.

Gaudin, A. (1957). *Flotation.* McGraw-Hill.

Glover, T. (1991). *Pocket ref.* Sequoia.

Gomez, C., Watson, J., & Finch, J. (1995). Recycled-paper deinking using column flotation. In *The 3rd research forum on recycling* (pp. 41–44).

Gorain, B. (2007). Mechanical froth flotation cells, section i: Design, operating principles, and optimization of mechanical flotation cells. In M. Fuerstenau, J. G., & R. Yoon (Eds.), *Froth flotation a century of innovation* (pp. 637–656). SME.

Hanna, H., Somasundaran, P., & Fuerstenau, M. (1976). Flotationam gaudin memorial volume. *Am. Miner. Inst., New York*.

Harris, C. (1976). Flotation machines. In M. Fuerstenau & A. Gaudin (Eds.), *Flotation–a. m. gaudin memorial.* AIME.

Kelly, T., Matos, G., Buckingham, D., DiFrancesco, C., Porter, K., Berry, C., et al. (2010). *Historical statistics for mineral and material commodities in the united states*. US Geological Survey Reston, VA.

Kemper, M. (1999). State-of-the-art and new technologies in flotation deinking. *International Journal of Mineral Processing*, *56*(1), 317–333.

Klassen, V., & Mokrousov, V. (1963). *An introduction to the theory of flotation*. Butterworths.

Lucay, F., Mellado, M. E., Cisternas, L. A., & Galvez, E. D. (2012). Sensitivity analysis of separation circuits. *International Journal of Mineral Processing*, *110–111*, 30–45.

Lynch, A., & Bush, P. (1977). *Mineral crushing and grinding circuits: their simulation, optimisation, design and control* (Vol. 340). Elsevier.

Lynch, A., & Rowland, C. (2005). *The history of grinding*. SME.

Lynch, A., Watt, J., Finch, J., & Harbort, G. (2007). History of flotation technology. In M. Fuerstenau, J. G., & R. Yoon (Eds.), *Froth flotation a century of innovation* (pp. 65–92). SME.

Malghan, S. (1986). *Typical flotation circuit configurations*.

Meenan, G. (1999). Modern coal flotation practices. In B. Parekh & J. Miller (Eds.), *Advances in flotation technology* (pp. 309–319). SME.

Meloy, T. (1983). Analysis and optimization of mineral processing and coal-cleaning circuits circuit analysis. *International Journal of Mineral Processing*, *10*(1), 61–80.

Napier-Munn, T. (1997). Invention and innovation in mineral processing. *Minerals Engineering*, *10*(8), 757–773.

Noble, A. (2012). *Laboratory-scale analysis of energy-efficient froth flotation rotor design*. Unpublished master's thesis, Virginia Polytechnic Institute and State University.

Oravainen, H., & Allenius, H. (2007). Mechanical froth flotation cells, section ii: Development of outokumpu flotation machines. In M. Fuerstenau, J. G., & R. Yoon (Eds.), *Froth flotation a century of innovation* (pp. 656–666). SME.

Phoochinda, W., White, D., & Briscoe, B. (2004). An algal removal using a combination of flocculation and flotation processes. *Environmental technology*, *25*(12), 1385–1395.

Schweitzer, P., et al. (1979). *Handbook of separation techniques for chemical engineers.* McGraw-Hill New York.

Sulman, H., Picard, H., & Ballot, J. (1905). *British patent 7,803.* (Duplicated as U.S. Patent 835,120)

Sutherland. (1948). Physical chemistry of flotation. xi. kinetics of the flotation process. *The Journal of Physical Chemistry*, *52*(2), 394–425.

Taggart, A. (1927). *Handbook of ore dressing.* Wiley.

Taggart, A., Behre, H., Breerwood, C., & Callow, J. (1945). *Handbook of mineral dressing, ores and industrial minerals.* Wiley.

Veasey, T., & Wills, B. (1991). Review of methods of improving mineral liberation. *Minerals Engineering*, *4*(7), 747–752.

Wang, L., Fahey, E., & Wu, Z. (2005). Dissolved air flotation. *Physicochemical Treatment Processes*, 431–500.

Weber, A., & Tracyzk, F. (2007). Mechanical froth flotation cells, section iv: Dorr-oliver eimco flotation equipment. In M. Fuerstenau, J. G., & R. Yoon (Eds.), *Froth flotation a century of innovation* (pp. 672–680). SME.

Weber, A., Walker, C., Redden, L., Lelinski, D., & Ware, S. (1999). Scale-up and design of large-scale flotation equipment. In B. Parekh & J. Miller (Eds.), *Advances in flotation technology* (pp. 353–369). SME.

Williams, M., & Meloy, T. (1989). On the definition and separation of fundamental process functions. *International Journal of Mineral Processing*, *26*(12), 65–72.

Wills, B., & Atkinson, K. (1991). The development of minerals engineering in the 20th century. *Minerals Engineering*, *4*(7-11), 643–652.

Wills, B., & Napier-Munn, T. (2006). *Wills' mineral processing technology: an introduction to the practical aspects of ore treatment and mineral recovery.* Butterworth-Heinemann.

Chapter 2

Literature Review

(ABSTRACT)

Today, the process of designing circuits is largely driven by computer simulation. Simulations require extensive data defining the feed and unit operations, as well as process models which can relate these parameters to the separation performance. The circuit designer is then tasked with the selection of the separation units and their interconnections in a way that pursues a technical or economic objective. The task of optimizing these circuits has grown with the use of simulation. Several modern circuit optimization routines incorporate sophisticated nonlinear integer programming and genetic algorithms. Unfortunately, most industrial circuit designs do not use these methods, instead relying on trial-and-error simulation. This approach incorporates empirically-based heuristics and ultimately leads to non-ideal configurations requiring perpetual modification and redesign. This paper reviews the engineering tools, modeling paradigms, and optimization routines which encompass the circuit design problem.

2.1 Data Analysis

Data utilization and simulation are the most prominent engineering tools available to circuit designer. Both greenfield designs and plant modifications typically begin by gathering laboratory or plant data in order to develop benchmarks for current performance as well as prediction for the anticipated results. This data may also be used to build models or estimate the processing requirements for a given ore. While the modeling and simulation stages are of paramount importance in this approach (see Section 2.2), the role of data

Table 2.1: Summary of Common Metallurgical Performance Indicators

Name	**Symbol**	**Explanation**
Mass Flow	F, C, T	Amount of total mass in a given stream
Grade	f, c, t	Quality of given stream; mass of designated material component (%)
Yield	$Y = C/F$	Total amount of material which was produced as concentrate (%)
Recovery	$R = Cc/Ff$	Amount of desired material which was produced as concentrate (%)
Rejection	$J = Tt/Ff$	Amount of desired material which was produced as tailings (%)
Separation Efficiency	$SE = R_{valuable} - R_{waste}$	Amount of material that experienced ideal separation (%)

Note: F, C, and T refer to the feed, concentrate, and tailings streams, respectively.

acquisition, parameter estimation, and performance measurement cannot be understated. Not only are many process models limited by the veracity of the data used to build them, but routine plant evaluation relies on sound sampling and analytical principles (Wills & Napier-Munn, 2006). Errors at this stage may mask true performance levels and propagate misinformation throughout the entire circuit design process. As a result, standard procedures for material sampling, laboratory testing, and performance evaluation have been developed and are presented in this section.

2.1.1 Performance Indicators

Several common and widely accepted metallurgical performance indicators are used to evaluate the separation capacity of individual unit operations and entire circuits. While these calculations are well known, the definitions are included here for both completeness and precision. Certain performance indicators are more common to specific mineral industries, and colloquial terms may be used in place of (or in distortion of) the precise terms listed here. Table 2.1 details several common metallurgical performance indicators.

Some interdependence exists between the performance indicators listed in Table 2.1. For example, real processes experience a trade-off between grade and recovery. Evaluation

of mineral separation systems is usually conducted by comparing the grade-recovery curves for different process designs. Many researches have attempted to produce a single indicator which combines grade and recovery. The most accepted single index is the separation efficiency (SE) which theoretically indicates the percentage of feed which passes through an ideal separation (Schulz, 1970).

While separation efficiency and other standards indicate the metallurgical performance, they do no reveal any information on the economic performance. Conversely, the most common economic measure in the metal industry is the Net Smelter Return (NSR). This value is found by subtracting the smelter charges, penalties, and transport costs from the payment for the delivered metal. This value fluctuates with concentrate grade, though an optimum value is usually obtainable within the technical limitations of the system (Sosa-Blanco, Hodouin, Bazin, Lara-Valenzuela, & Salazar, 2000; Wills & Napier-Munn, 2006)

Given the complexity of most mineral separation plants, the generic terms given in Table 2.1 usually provide a sufficient starting point for the evaluation of metallurgical performance. Alternatively, coal preparation researchers have developed a number of plant-wide separation efficiency indicators, largely driven by the standard modes of laboratory evaluation in coal washing. Throughout the coal preparation plant, gravity techniques are predominantly used to separate the binary coal-ash mixtures. A *washability* (or float-sink) test is a standard laboratory procedure used to identify the relative density fractions of the feed coal (Osborne, 1988a; Leonard, 1991). This test effectively identifies the ideal separation potential at various density cut-points. By comparing the actual separation performance of the plant to the ideal separation determined from washability, several practical performance indicators may be determined. For example, the organic efficiency is defined as the percentage ratio between the plant yield and the theoretical yield determined at the actual ash content (with the theoretical values determined from washability testing). Similarly, the ash error is the percentage ratio between the ash content of the actual clean coal product and the theoretical ash content at the same yield. The International Standards Organization suggests that any statement describing the performance of a coal preparation plant should include these two indicators along with percentage of misplaced material in various size fractions and the total percentage of correctly placed material (Osborne, 1988b; Leonard, 1991).

Since washability analysis only applies to gravity separators and since flotation has become prominent in many modern preparation plants, researches have attempted to derive testing methods which identify the ideal flotation partition. The *release analysis* is one such method which utilizes successive batch flotation tests where the concentrate is re-floated multiple times. This procedure attempts to minimize entrained particles while forming an

ideal grade-recovery curve (Dell, 1964) Modifications to the original testing procedure have been introduced in order to minimize operator bias and increase testing ease (Honaker, 1996; Pratten, Bensley, & Nicol, 1989). While the release analysis has gained substantial backing in the flotation industry (especially in coal preparation), some criticism has undermined the theoretical backing of the technique (Meloy, Whaley, & Williams, 1998). Here, authors argue that the grade-recovery boundary is not unique to a given mineral system but is dependent on various operational characteristics of the release analysis (i.e. the type of cell, the operator's experience, and the levels of the analysis). The authors support these claims through an analytical evaluation of the of the possible outcomes of different test methods.

2.1.2 Material Sampling and Data Reconciliation

Most metallurgical decisions rely on the ability to gather mineral samples which are later subjected to further analysis. The downstream uses of these samples rarely consider the means in which they were retrieved, and non-representative samples often lead to errant decisions and wasted resources. The challenges of performing unbiased sampling of heterogeneous mineral systems has been well studied (Gy, 1979, 1992). While the mathematical approach of Gy is quite involved, the author provides practical, yet theoretically-supported, standards for material sampling. Most of the work is based on the probabilistic quantification of sampling errors and ways to minimize these errors during sampling processes. One general rule is that sampling should be probabilistic rather than deterministic: all particles in a given lot should have an equal probability of being sampled. In flowing streams, this rule is usually satisfied incrementally: either a portion of the stream is sampled for a long time or all of the stream is sampled for a short time. In general, the latter approach produces more reliable samples since mineral processing streams are often subjected to particle classification (e.g. heavy solids settle to the bottom of a horizontal pipe).

Data collected from experimental studies can be somewhat unreliable, even when proper sampling procedures are followed. Given the stochastic nature of mineral feed streams and separation processes, individual samples are subject to marginal discrepancies. When redundant data is collected, the assays must be reconciled prior to further analysis. One common example of "redundant data" collection is fulfilled by sampling the feed and products for a given unit. Since the feed assay can be back-calculated from the products, the feed assay, in this case, is said to be redundant. While ignoring, omitting, or avoiding redundant data is common, such actions represent poor uses of the collected information. Instead a standard data reconciliation method must be instituted to ensure that the final data set adheres to the conservation of mass principle. By definition, a steady-state process does experience

Table 2.2: List of Error Distribution Functions used in Data Reconciliation. After (Özyurt & Pike, 2004)

Name	**Equation**	**Sensitivity to Gross Errors**
Gaussian	$\sum e^2$	High
Fair	$c^2[\|e\|/c - \log(1 + \|e\|)/c)]$	Moderate
Lorentzian	$1/(1 + e^2/2)$	Very low
Tjoa-Biegler	$-\log((1 - \eta) * \exp(-e^2/2) + \eta/b * \exp(-e^2/(2 * b))) + \log(\sqrt{2 * \pi} * \sigma)$	Low

Legend: e = (measured - adjusted)/σ σ = tolerance
η = probability of gross error c = tuning parameter, between 10 - 20
b = ratio of large variance of gross error with respect to normal error

accumulation, and thus, the component mass of the products must equal the component mass of the feed. In the mineral processing discipline, the adjustment of data to meet this principle is deemed *mass balancing* (Luttrell, 1996).

One common way to mass balance data is to minimize the difference between the experimental data and the adjusted data while constraining the adjusted data to the mass-balanced condition (Reklaitis & Schneider, 1983; Luttrell, 1996; Wills & Napier-Munn, 2006). This linear optimization problem may be solved by one of several optimization routines (See Section 2.1.4). The objective function, representing the error between the adjusted and measured points can be determined by one of several means, depending on the desired influence of gross error. Four common error distribution functions are shown in Table 2.2 (Tjoa & Biegler, 1991; Özyurt & Pike, 2004). With the exception of the Lorentzian function, all others are minimized during the optimization process. Given the form of the Lorentzian, the value is maximized during optimization. Table 2.2 also shows the relative effect of gross error on the reconciliation. This designation indicates the influence of a single erroneous data points on the entire function. A highly sensitive method, such as the Gaussian, will allow gross error to influence the adjustments throughout the circuit. Alternatively, low sensitivity methods, such as the Lorentzian and Tjoa-Biegler, will localize the adjustments to the value which is expected to be in gross error.

2.1.3 Curve Fitting and Interpolation

Regression, curve fitting, and interpolation are common engineering tools crucial to the appropriate evaluation of mineral processing data. Within the mineral processing discipline, regression analysis has a marked influence on equipment comparison, evaluation of performance indicators, empirical modeling, and simulation.

Curve fitting is as an application of linear optimization. Curve fitting problems arise when a set of experimental data is to be approximated by a model of known functional form. In the linear case, analytical equations are readily available which can optimize the function parameters (i.e., the slope and intercept for linear functions) via least squares regression (Faires & Burden, 2003, p. 343). If the proposed model can be linearized, modified regression equations can be derived to calculate the linearized parameters. Unfortunately, many process models cannot be easily linearized, and more involved curve fitting must be conducted.

The generic curve fitting process begins by proposing a functional form with one or more unknown parameters. More parameters entail a better fit to the experimental data, while fewer parameters typically provide more physical meaning and understanding. Initial values for the parameters are selected, the proposed model is calculated over the range of the experimental data, and finally, the modeled values are compared to the experimental values. An error function is defined which quantifies this difference between the modeled parameters and the experimental parameters. For many curve fitting problems, some version of the squared error may be used. The mean squared error (MSE) represents the average error of each data point and is calculated by:

$$MSE = \sum_{i=1}^{n} (x_i - y_i)^2 / n$$

where x is the value of the experimental points, y is value of the modeled points, and n is the number of data points. Other error quantification methods may normalize the squared value by the absolute magnitude of the value or allow user-defined weightings.

The optimization routine progresses by minimizing the error function by changing the value of the model parameters. Various optimization strategies are presented in Section 2.1.4. Once the error function is minimized, the calculated model parameters represent the best fit to the experimental data (Faires & Burden, 2003). This process may also be termed *parameter optimization* to better reflect the mechanics of the calculations.

Depending on the knowledge of the appropriate functional forms and the veracity of the experimental data, a simple curve fit may not be appropriate. For example, if the

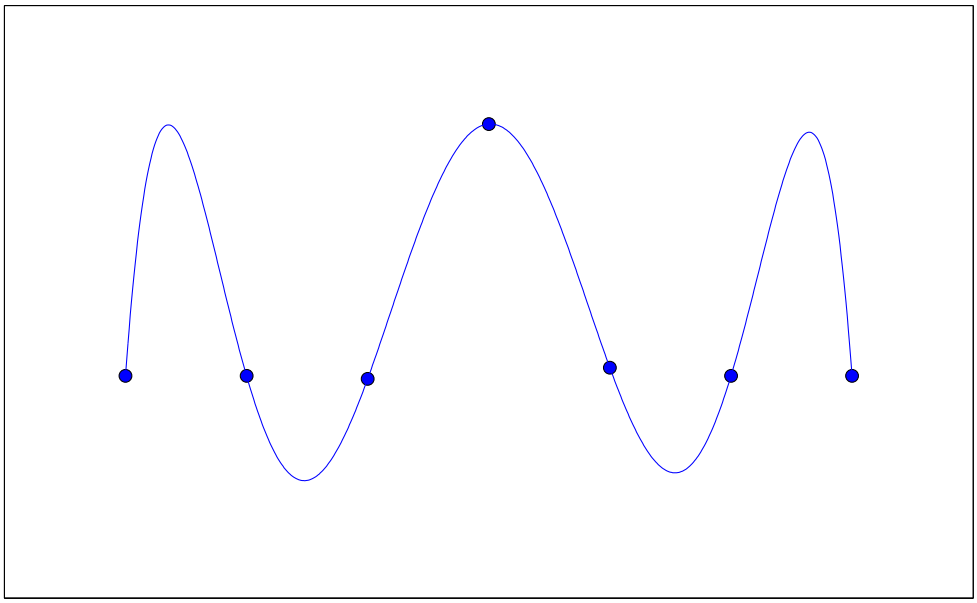

Figure 2.1: Example of undesired oscillation as a result of a high-order polynomial fit.

experimental data was gathered from a high precision land survey, a curve fit that does not pass through every point is not valid for interpolation. As an alternative curve fitting strategy, polynomial interpolation is often capable of producing much better approximations when compared to other simple functions. By definition, a polynomial of degree n can precisely represent a data set containing $n + 1$ members (i.e. a linear function can precisely fit two points, a quadratic function can precisely fit three points, etc.). While standard algebraic functions are available to calculate the parameters of polynomial fits, higher order polynomials are know to exhibit an unrealistic and undesired oscillation, as shown in Figure 2.1 (Faires & Burden, 2003). Furthermore, since higher-order polynomials require numerous fitting parameters, the actual parameters entail less physical meaning.

Alternatively, another method of exact interpolation is by splines. Physically, splines are graphical relics of hand plotting techniques which utilized French curves. Mathematically, a spline fit uses piece-wise polynomial approximation to precisely estimate a set of experimental data. A spline fit provides a unique polynomial for each consecutive pair of points. A first-order or linear spline is constructed by simply connecting the data point-to-point with straight lines. The disadvantage with linear splines is that the resulting piecewise function may have sharp corners and a thus a discontinuous derivative. Instead, the most common

spline is the cubic spline which connects pairs of points with cubic polynomials. This approach provides a continuous first and second derivative along the data range, producing a smooth, non-sharp curve.

To determine the cubic spline, four parameters must be solved for each pair of points (a cubic polynomial interpolation requires four parameters). The challenge in constructing splines is that while the interior polynomials have sufficient data to be fully constrained, information on the slope at the boundary conditions is lost. Consequently, the boundary slopes must be estimated. Many methods are available (Faires & Burden, 2003), though three are common: (1) the end cubics approach linearity, (2) the end cubics approach parabolas, and (3) the final slopes are a linear extrapolation from the neighboring points. A pragmatic guide to spline construction has been presented by Gerald and Wheatley (1994, p. 200). Figure 2.2 shows an arbitrary data set that has been estimated using various regression, curve fitting, and spline approximation techniques.

2.1.4 Optimization

Numerical optimization is a branch of engineering mathematics and computational research which is concerned with identifying extrema values of functions. Classical optimization problems are formulated by three mathematically defined parts: (1) the design vector, (2) the objective function, and (3) the constraint vector. The design vector contains all of the parameters which can be controlled by the designer. Often, a starting guess is required to initialize the design vector. The objective function defines the value which is to be minimized or maximized. This function is defined in terms of the elements of the design vector. Finally, optimization problems may be constrained or unconstrained, depending if physical or other limitations must be applied to various elements of the design vector. If the problem is constrained, these constraints are formulated in vector form as a function of the elements of the design vector.

A solution which meets the entire constraint set is said to be a *feasible* solution (Foulds, 1981). Optimization functions must be stated in the form of a single objective function. If more than one extrema outcome is desired (e.g. maximize profits while minimizing investor risk), a weighting factor may be used to combine both goals into a single objective function. Alternatively, the most important criteria may set by the objective function, while simply imposing constraints on the secondary objectives (Bhatti, 2000).

Most contemporary optimization techniques may be classified as either enumerative, random, or calculus-based (Foulds, 1981; Goldberg & Holland, 1988). Enumerative, or

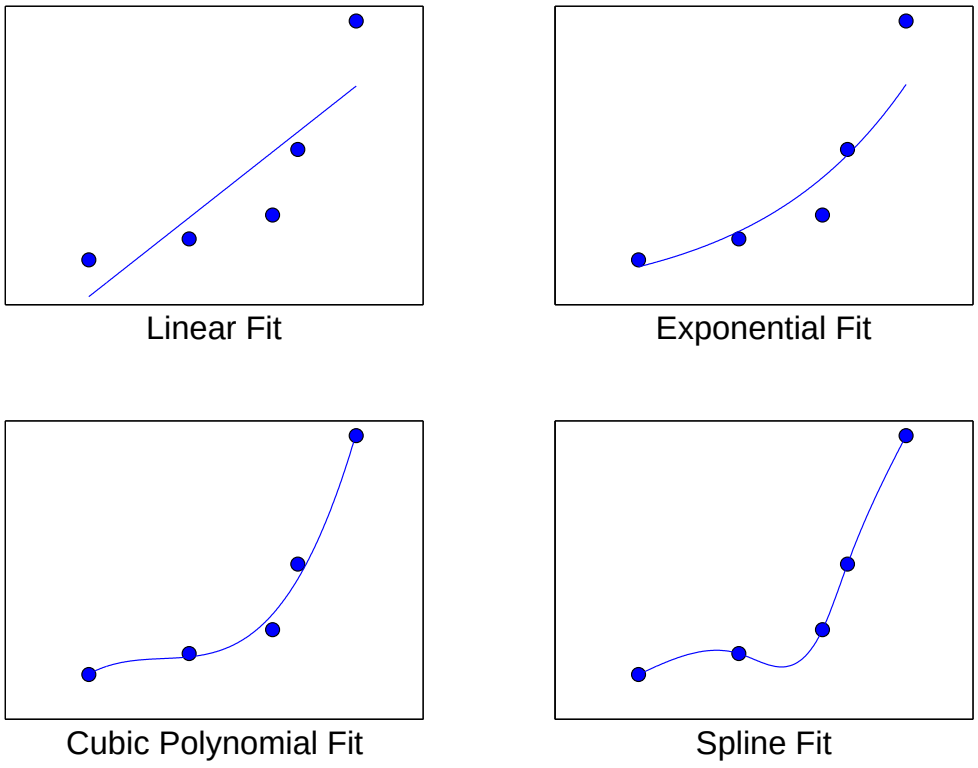

Figure 2.2: Various regression and approximation techniques applied to the same arbitrary data set.

direct-search, techniques are the most straightforward. The solution space of the design vector is partitioned as a grid, and every possible combination of parameters is tested and compared to determine the optimum configuration. Purely random techniques (i.e. random walks) institute a similar methodology, but the solution space is randomly sampled in an attempt to hasten the calculation time. Nevertheless, both direct-search and random optimization techniques are grossly inefficient and require substantial computation resources when considering even modest problems (Goldberg & Holland, 1988).

Calculus-based methods, such as linear programming and the simplex method rely on the gradient of the objective function to establish the search direction and step size. In practice, these search methods are akin to hill-climbing: the crest is determined by traversing in the direction of the steepest slope until one begins to descend. These and other calculus-based methods generally rely on known or estimated derivative and second derivative information in order to establish the slope gradients. As a result, the derivatives must generally be continuous and defined over the anticipated design vector range. With the additional auxiliary information, calculus-based methods are substantially more efficient than enumerative and random techniques; however, the added complexity results in a loss of robustness. Many calculus-based methods tend to isolate local, rather than global extrema, especially if the technique is ill-suited for the problem type (Bhatti, 2000). Furthermore, when the objective function is nonlinear, quadratic programming or other classical optimization methods (such as Newton's method) must be applied. Further subclasses of calculus-based optimization techniques are available for integer or binary-constrained design vector values (Foulds, 1981).

Since many conventional optimization techniques are limited by computation inefficiency, lack of robustness, and solution divergence, research has attempted to redefine the optimization paradigm by abandoning the calculus-based influences on which most traditional optimization theory is based. Holland (1975) created *genetic algorithms* to optimize functions in a manner similar to the evolutionary processes found in nature. Genetic algorithms utilize stochastic processes to "evolve" a design vector until an optimal solution is reached. Unlike calculus-based methods, genetic algorithms do no require any auxiliary information, and thus, even the existence of a first derivative is not necessary to efficiently obtain a solution. Genetic algorithms operate analogously to natural selection and biological evolution (Goldberg & Holland, 1988; Holland, 1992).

Genetic algorithms denote a substantial increase in solution robustness, especially in nonlinear and otherwise complex search spaces. In this regard, genetic algorithms differ from other searches in that they: initiate from a population rather than a single point, rely

simply on the value of the objective function rather than auxiliary information, and they utilize stochastic rather than deterministic operations (Goldberg & Holland, 1988).

2.2 Circuit Modeling and Simulation

2.2.1 Modeling of Process Unit Operations

Over the last 40 years, modeling and simulation of unit operations has advanced as one of the primary research areas in the discipline of mineral processing. In general, *modeling* refers to the process of describing a physical phenomenon in terms of mathematical equations, while *simulation* refers to the solving of those equations to predict potential outcomes. In the case of mineral processing, a process model is used to predict the concentrate and tailings product from a given unit operation when provided descriptions of the feed and operational parameters.

Most process models are classified in terms of the model fidelity, earning the distinction of either an empirical, phenomenological, or theoretical model. For much of the last century, empirical models have found the most widespread usage and availability (Wills & Napier-Munn, 2006). From a mathematical perspective, an empirical model does not actually consider the physical subprocesses of the separation system but is simply a curve-fit which seeks to consolidate experimental data. Despite their simplicity, empirical models are especially useful, since they are relatively easy to construct and apply (Napier-Munn & Lynch, 1992; Wills & Napier-Munn, 2006). Furthermore, the functional form of the resulting curve fit may indicate the ultimate form of a more theoretical model. The only requirements for empirical models are ample experimental data and curve-fitting or regression software. Unfortunately, empirical models are prone to catastrophic failure if simulation seeks to extrapolate beyond the range of experimental data used to build the model. A common example of this failure is given by the extrapolation of power versus mill load data in a ball mill grinding system (Figure 2.3).

Extrapolation fallacies, such as the one presented in Figure 2.3, illustrate the lack of predictive capacity inherent to data-driven models. On the other end of the fidelity spectrum, purely theoretical models (or transport phenomena models) require no initial experimental data and are entirely predictive when based on sound fundamental knowledge (Napier-Munn & Lynch, 1992). Unfortunately, the unit operations in the mineral processing industry are vastly complex and incorporate numerous physical and chemical subprocesses. Additionally,

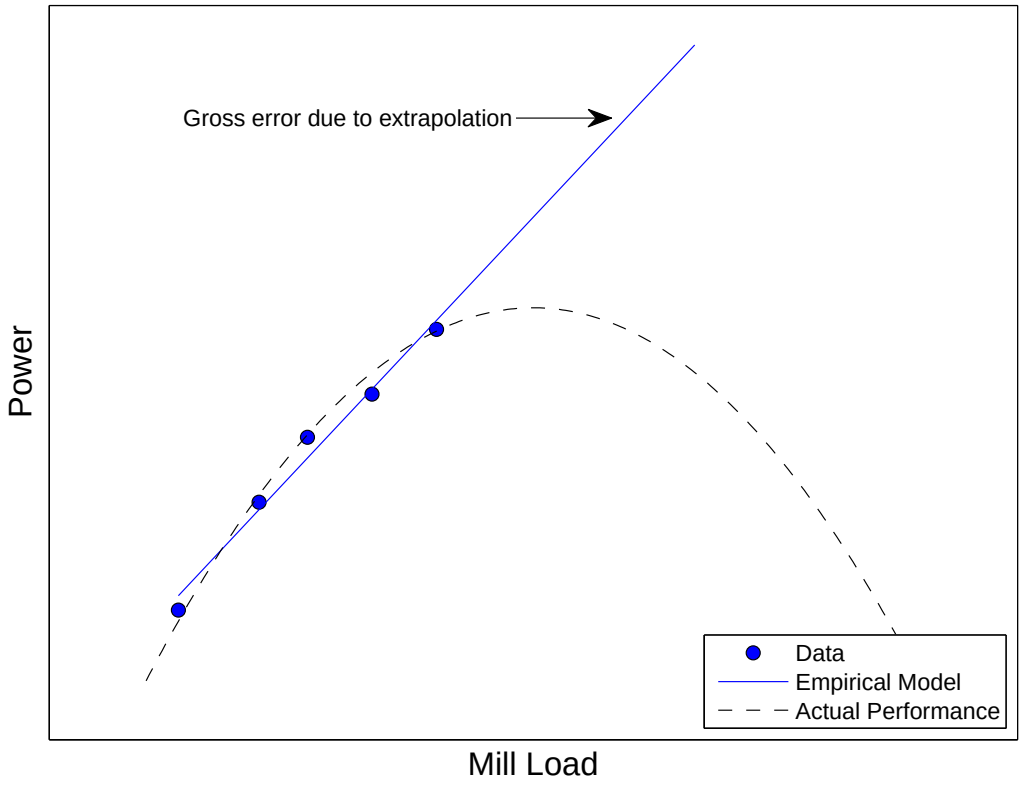

Figure 2.3: Example of catastrophic failure in empirical model predictions. Graph hypothetically compares power and mill load in a ball mill system for experimental data, the empirical model, and the actual performance.

comprehensive theoretical models must know or be able to predict the entire liberation state of each particle in the system, since most separation principles are largely dependent on liberation. Consequently, the development of comprehensive theoretical models has been deterred for most mineral processing systems; however, recent attempts have been made to model the flotation system from first principles (See Section 2.2.3).

In order to balance the benefits and detriments to either modeling paradigm, recent effort has been placed in phenomenological modeling. Generally, the phenomenological approach considers the various physical subprocesses to an extent in identifying the functional forms; however, experimentation, rather than fundamental science, is used to finalize the model parameters. Since these models are in part based on scientific principles, they are much less sensitive to catastrophic failure than empirical models. As a result, these models have found widespread integration in process scale-up and circuit simulation (King, 2001; Wills & Napier-Munn, 2006). The most common phenomenological approach, the population balance approach, essentially tracks the transport of individual particles throughout a separation system (Himmelblau & Bischoff, 1968). This modeling approach can be conveniently applied to dynamic or steady-state systems and provide fundamental insight when the model is well developed and vetted.

The most fundamental form of the population balance model states that the accumulation of particles is equal to the input minus the output plus net generation. For population balance models, this general articulation accounts for both the transport in physical space, as particles move throughout a system, as well as property space, as the characteristic property of individual particles changes within a process unit. Mathematically, the general microscopic population balance model is given by:

$$\frac{d\psi}{dt} + \frac{d}{dx}(v_x\psi) + \frac{d}{dy}(v_y\psi) + \frac{d}{dz}(v_z\psi) + \sum_{j=1}^{J} \frac{d}{d\varsigma_j}(v_j\psi) + \dot{D} - \dot{A} = 0$$

where ψ is the number concentration of particles, x, y, and z are directions in physical space; ς is the direction in property space; $\dot{D}$ is the rate of particle disappearance; and $\dot{A}$ is the rate of particle appearance. From this nomenclature, the first term ($d\psi/dt$) represents accumulation; the second, third, and fourth terms ($d/dx(v_x\psi)$, $d/dy(v_y\psi)$, and $d/dz(v_z\psi)$) represent the physical transport terms; the fifth term ($d/d\varsigma(v\psi)$) represents continuous changes in physical space; and the final two terms ($\dot{D}$ and $\dot{A}$) represent discrete changes in property or physical space. King (2001) has provided an extensive review of population balance models for various mineral processing unit operations, including size classification, comminution, dewatering, gravity separation, magnetic separation, and flotation.

Several commercial simulation packages are available which utilize various process models and data fitting routines. The most widely used software today include JKSimMet (Cameron & Morrison, 1991; Richardson, 2002), Modsim (King, 2001), and Limn (Nageswararao, Wiseman, & Napier-Munn, 2004; Hand & Wiseman, 2010). Each of these simulation packages is currently undergoing continuous research and development.

2.2.2 Modeling Partition Separators

One basic method of empirically modeling a separation system is by a partition curve. Partition curves were first developed by Tromp (1937) to evaluate the efficiency of various coal cleaning methods. A basic reduced partition curve is shown in Figure 2.4.

The reduced partition curve shows the probability of reporting to the concentrate product as a function of a dimensionless property. The property depicted on the horizontal axis is typically the property on which the separation is based (e.g. gravity, size, magnetic susceptibility) or the particle composition. The characteristic "S" shape of the curve indicates that the separation probability is normally distributed about a single value of the separation property. The true value of this central property is known as the "cut-point" since particles of this property have equal probability of reporting to either product. To normalize the horizontal axis in the reduced curve, all values of the property are divided by the cut-point, so that the 50% probability refers to the cut-point value of one. The ideal partition curve (also shown in Figure 2.4), has a probability of zero up to the cut-point and a value of one for all values greater than the cut-point. The area between the real curve and the ideal curve is sometimes distinguished as the "error area" (Wills & Napier-Munn, 2006).

Another significant characteristic of the partition curve is the slope of the curve at the 50% probability. This value is generally termed the "separation sharpness", though several precise mathematical interpretations or fitting parameters are found in the literature (E_p, I, λ, α) (Osborne, 1988a; Leonard, 1991; King, 2001; Wills & Napier-Munn, 2006). Of particular interest in dense-media separation is the probable error of separation or the Ecart probable (E_p) and the imperfection (I). These are given by:

$$E_p = \frac{d_{75} - d_{25}}{2}$$

$$I = \frac{E_p}{d_{50} - 1}$$

where d_{25}, d_{50}, d_{75} represent the property value at 25%, 50% , and 75% recovery, respectively.

The two remaining characteristics of the partition curve are the high and low bypass

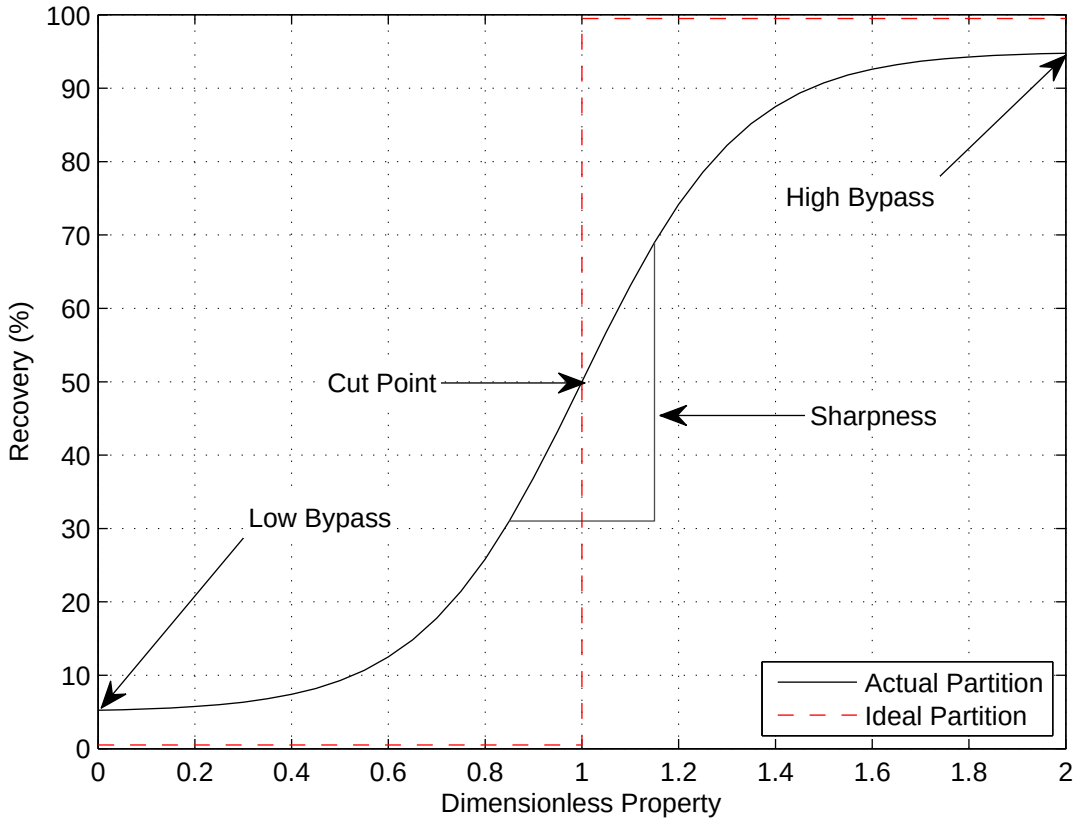

Figure 2.4: Recovery plotted against dimensionless property for a generic partition model.

values. These values are generally represented as the probabilities where the curve closes at the high and low extremes of the property values.

Though partition curves were originally developed to evaluate equipment performance, they may also be used for empirical simulation. The mathematical parameters of the partition curve are often independent of the feed composition and unique to specific separation units. Experimental testing can be used to identify the curve parameters at standard operational conditions, and further testing can derive empirical relationships to relate the partition function parameters to specific operational and equipment variables. Researchers have identified four qualities preferred in all proposed partition functions: (1) the existence of natural asymptotes, (2) the ability to express asymmetry about the cut-point, (3) mathematical continuousness, and (4) parameters which can be easily estimated by accessible methods (Stratford & Napier-Munn, 1986; Wills & Napier-Munn, 2006).

2.2.3 Kinetic Modeling of Flotation

Considerable effort has been placed in developing predictive models for flotation performance. The cause of this interest is likely a result of its dominance in the mineral processing industry as a separation process as well as the incredible complexity, plurality, and interdependence of the relevant subprocesses. To date, comprehensive and purely theoretical flotation models remain immature, though several recent authors have provided a foundation for this work (Sherrell, 2004; Do, 2010; Kelley, Noble, Luttrell, & Yoon, 2012). Nevertheless, empirical and partially phenomenological models have been well vetted and used extensively for many industrial simulation purposes. From a microscopic perspective, the complex mechanics of froth flotation may be described by several transport mechanisms. The most recent studies include the rate of pulp to froth transport by bubble attachment, the rate of material drop-back from the froth, the rate of water drainage from the froth, and the rate of entrainment. Most modeling approaches attempt to quantify the specific rates and interaction of these mechanisms.

Many researchers have empirically witnessed the kinetic behavior of bulk flotation recovery as a function of time. This evidence has prompted many to model flotation as a first-order rate process analogous to a chemical reaction (Sutherland, 1948; Tomlinson & Fleming, 1965; Fichera & Chudacek, 1992). Other order rate models have been postulated, but few have gained as much widespread applicability as the first-order model. The first-order rate model defines a constant proportionality between the depletion of mineral particles

(dN/dt) and the number of particle in the system (N):

$$dN/dt = kN \tag{2.1}$$

where k is a proportionality or *rate* constant.

From the first-order assumption, Equation 2.1 may be solved at various boundary condition to determine the recovery (R) as a function of flotation time (τ) for both a plug-flow reactor (Equation 2.2) and a perfectly-mixed reactor (Equation 2.3), depending on the residence time distribution (Levenspiel, 1999). These equations have been used to model the flotation process in scaling from a laboratory to an industrial flotation unit:

$$R_{Plug} = 1 - e^{-k\tau} \tag{2.2}$$

$$R_{Mixed} = \frac{k\tau}{1 + k\tau}. \tag{2.3}$$

Several modifications to these models have been proposed to incorporate a theoretical maximum recovery and a flotation delay time (Dowling, Klimpel, & Aplan, 1985; Gorain, Franzidis, Manlapig, Ward, & Johnson, 2000; Sripriya, Rao, & Choudhury, 2003). Additionally, some researchers have suggested that industrial cells (especially column cells) substantially deviate from the perfectly-mixed assumption (Dobby & Finch, 1988; Luttrell & Yoon, 1991). Coinciding with the aforementioned chemical reaction analogy, these authors have suggested the axially-dispersed reactor model (ADR) which defines recovery as a function of the degree of axial mixing, via the Peclet number (Pe) (Levenspiel, 1999):

$$R_{ADR} = 1 - \frac{4A \exp\{Pe/2\}}{(1+A)^2 \exp\{(A/2)Pe\} - (1-A)^2 \exp\{(-A/2)Pe\}}$$

$$A = \sqrt{1 + 4k\tau/Pe}.$$

For extreme values of the Peclet number, the behavior of the ADR model approaches that of the perfectly-mixed and plug-flow models (Equations 2.2 and 2.3). For high Peclet numbers (> 99), plug-flow behavior is experienced, while low Peclet number (< 0.001) produce perfectly-mixed results. Figure 2.5 compares these three rate recovery models. The ADR model is shown for two different Peclet numbers.

While the general rate-based approach to flotation modeling has substantial empirical justification, researchers and practitioners have realized that not all particles of a given mineral in a flotation system exhibit the same kinetics. This observation has led to the

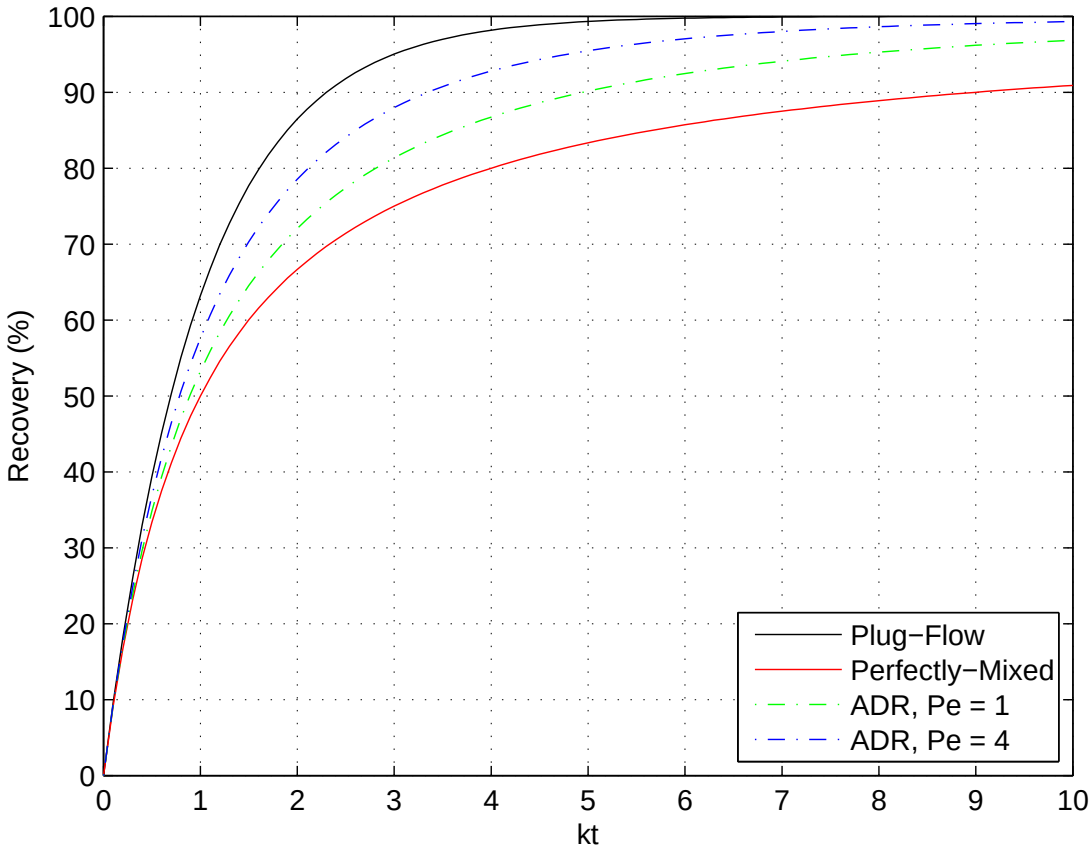

Figure 2.5: Recovery plotted against dimensionless kt value for perfectly-mixed, plug-flow, and axially-dispersed reactor models.

development of distributed parameter rate models (Fichera & Chudacek, 1992). Various researchers have identified properties to justify the distribution, with one of the more prevalent parameters being particle size. Gaudin, Schuhmann Jr, and Schlechten (1942) first experimentally measured the dependence of flotation rate on particle size, noting the substantial degradation in flotation rate for large particles. This observation was later given a more thorough theoretical consideration which investigated the streamline hydrodynamics for given bubble and particle sizes (Sutherland, 1948).

A more general approach to model parameterization was conducted by Imaizumi and Inoue (1965). This modeling approach considers distributed floatability classes which lump together the combined effects of particle size, shape, and other surface properties. Most contemporary flotation models include some form distributed flotation classes, often in the form of a double distributed model which includes size and floatability (Fichera & Chudacek, 1992).

Further attempts to add fundamental insight to the empirical first-order observation have led many to propose analytical expressions for the flotation rate constant. These expressions generally suggest a strong dependence of gas dispersion on the flotation rate. One such model suggests that the rate constant is proportional to the bubble surface area flux (S_b) and a generic probability or collection efficiency term (P) (Jameson, Nam, & Young, 1977; Yoon & Mao, 1996; Gorain, Franzidis, & Manlapig, 1997; Gorain, Napier-Munn, Franzidis, & Manlapig, 1998):

$$k = 0.25 P S_b.$$

Here, S_b is a derived term which defines the degree of aeration present in the cell (Finch & Dobby, 1990; Gorain et al., 1997; Gorain, Napier-Munn, et al., 1998). S_b mathematically balances the superficial gas velocity (J_g) and the mean bubble size (d_b):

$$S_b = \frac{6 J_g}{d_b}.$$

This model has been very successful at normalizing flotation performance when the gas dispersion variables are known. The linear $k - S_b$ relationship has been experimentally verified for various minerals and at various scales (Gorain, Napier-Munn, et al., 1998; Hernandez-Aguilar, Rao, & Finch, 2005; Noble, 2012). The overall acceptance of this model has led to several comprehensive studies in characterizing and quantifying gas dispersion in flotation cells (Finch, Xiao, Hardie, & Gomez, 2000; Tavera, Escudero, & Finch, 2001; Kracht, Vallebuona, & Casali, 2005; Schwarz & Alexander, 2006; Miskovic, 2011).

Other models have proposed a purely theoretical expression for k, based on surface chemistry and hydrodynamic variables (Luttrell & Yoon, 1992, 1991; Mao & Yoon, 1997;

Sherrell, 2004; Do, 2010). These models were originally applicable for predicting rate constants under quiescent conditions, such as in column cells. More recently, the fundamental models have addressed the turbulent hydrodynamic conditions found in conventional cells. Additionally, these approaches have added fundamental or semi-empirical models to describe material drop-back and fluid drainage from the froth. All of these fundamental models are based on a compartment paradigm which independently defines the flotation rate constant as a combination of probabilities of collision (P_c), attachment(P_a), and detachment (P_d):

$$k = PS_b = (P_c P_a (1 - P_d))S_b.$$

In these models, the probability terms have been analytically defined using fundamental hydrodynamic variables (such as turbulent kinetic energy) and surface energies calculated from the Van Der Waals, electrostatic, and hydrophobic force components. The extended DLVO theory is invoked to define the composite interaction of these forces (Yoon & Wang, 2007; Kelley et al., 2012). Ultimately these fundamental models predict flotation performance as a function of intensive mineral properties and machine characteristics which are either well known or do not change with scale (Kelley et al., 2012).

In addition to the aggregate recovery models, other recent studies have focused on the inclusion of other transport mechanisms, such as froth recovery and entrainment. Such models consider flotation to be a two stage process, while modeling the pulp and the froth as independent reactors. Most of the pure pulp recovery models invoke analytical forms similar to the rate models presented above with some empirical correction to negate the ever-present froth effects (Gorain, Harris, Franzidis, & Manlapig, 1998; Vera et al., 2002).

Similar to pulp recovery, froth drop-back has been identified as a rate process which can be modeled as a plug-flow reactor considering the interaction of a rate constant and residence time (Equation 2.2) (Gorain, Harris, et al., 1998). When the independent froth (R_f) and pulp (R_p) recoveries are known, the overall recovery may be calculated by (Finch & Dobby, 1990):

$$R = \frac{R_f R_p}{1 - (1 - R_f)R_p}.$$

Since the identification of the two compartment flotation modeling approach and the kinetics of froth drop-back, researchers have attempted to gain further fundamental, especially with regard to froth residence time (Vera et al., 2002). Most simply, froth residence time can be determined by dividing the froth height by the superficial gas rate for the cell ($\tau_f = h/J_g$) (Mathe, Harris, O'Connor, & Franzidis, 1998). Since this calculation does not accommodate for different cell geometries and froth travel distances, many have proposed

revisions to the initial calculation, while retaining the kinetic plug-flow model. Gorain, Harris, et al. (1998) suggest the inclusion of the distance from the center of the flotation cell to the launder, while Lynch, Johnson, Manlapig, and Thorne (1981) base the calculation on the volumetric slurry flow through the froth.

2.3 Circuit Analysis and Optimization

2.3.1 Design Principles

Since staged separation is often necessary to meet final product requirements, circuit designers must designate the flow configuration between various process units. This set of decisions, constituting *circuit design*, may involve the selection of different unit operations, different equipment models or sizes, different operational parameters, and different unit interconnections. To assist circuit designers, researchers have attempted to establish standard design methodologies which involve various analytical techniques and tools. These tools are typically guided by some optimization strategy and a generic process model applicable for the given separation.

Circuit design analysis and optimization methods can be described on a continuum scale depicting the level of direct mathematical involvement and intensity (Figure 2.6). On the lower portion of the scale are purely heuristic methods. These circuit analysis techniques utilize rules and guidelines which may or may not be based on sophisticated mathematical integration. Conversely, purely numerical optimization routines define the higher portion of the scale. These methods have incorporated various optimization algorithms, including linear programming, non-linear programing, gradient-based optimization, and genetic optimization. Both extremes of this scale introduce numerous advantages and disadvantages. Recent trends are seemingly favoring high-tech numerical algorithms to accommodate the nonlinear, discontinuous design parameters associated with separation circuits; however, contemporary industrial practice still favors more heuristic solutions. Consequently, several active research projects are developing strategies at all points along the continuum. This section will review the state-of-the art in these optimization strategies while noting the merits and drawbacks to the various methods.

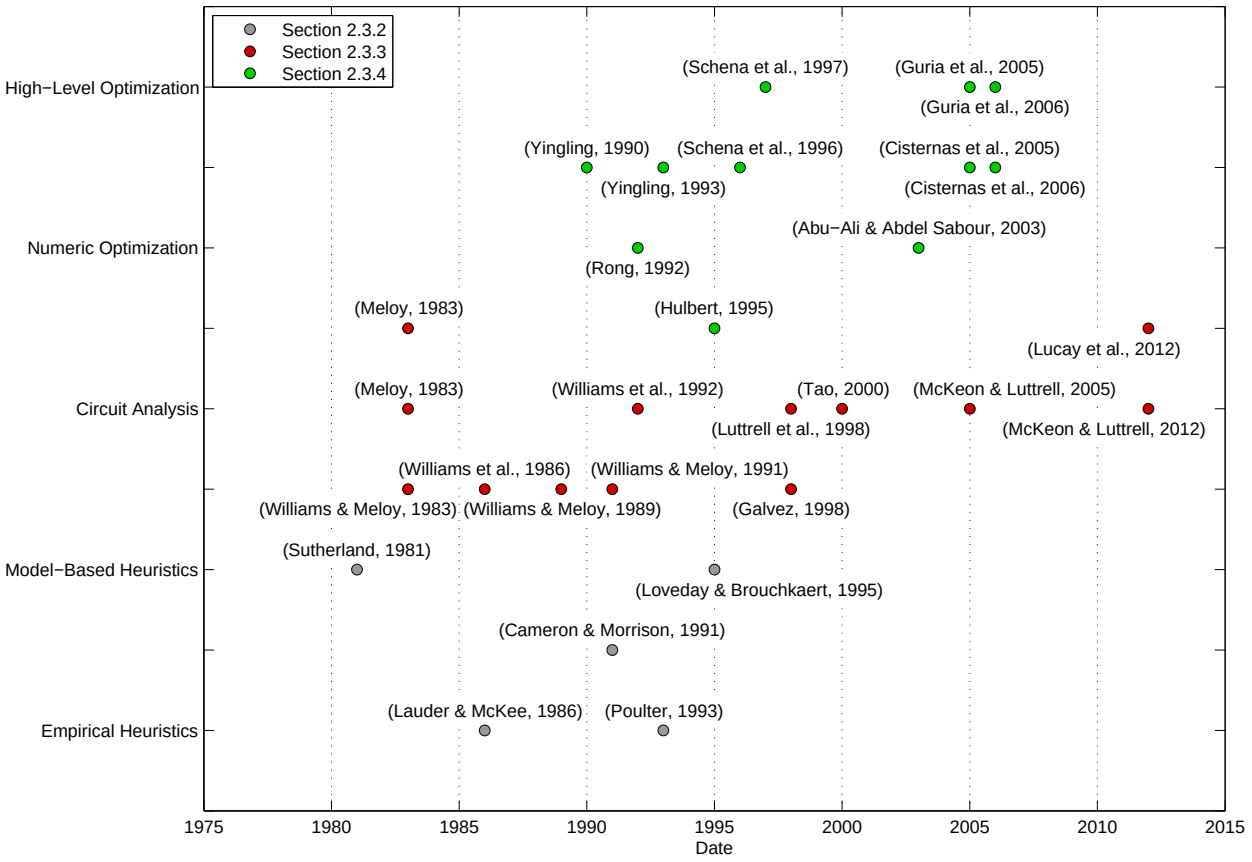

Figure 2.6: Survey of literature describing various methods of separation circuit design and optimization. Vertical axis is a qualitative scale indicating the perceived degree of mathematical influence in circuit optimization. Lower points represent purely observational design methods, while higher points represent purely mathematical optimization techniques. Color coding denotes the section of this chapter in which the technique is reviewed. This figure does not exhaustively describe the literature included in this review.

2.3.2 Classic Heuristic Methods

In general, the term *heuristic* refers to a learned behavior derived from a set of loosely-defined rules. With reference to separation circuit design, a heuristic approach refers to the use of established operator practices, accepted "rules-of-thumb", or quantitative design regulations when generating preliminary alternatives (Wills & Napier-Munn, 2006). In this review, the pure heuristic approaches presented in the literature have been classified into two groups: (1) those that simply impose design principles from empirical observation and (2) those which derive the heuristics from process models. While the heuristic methods appear less scientifically-sound than high level analytical and numerical approaches, their lack of sophistication is convalesced in their ability to accommodate operator experience and common-sense design constraints. Additionally, when well-formulated and valid, heuristics are the most easy to implement, since no analytical or computational resources are required. Unfortunately, many reported heuristics are dependent on the process model validity, or they are only applicable in the specified site conditions. Furthermore, model-based heuristics may provide conflicting solutions, if all of the rules cannot be satisfied simultaneously.

Much of preliminary circuit design is driven by trial-and-error and accepted industry practices (Lauder & McKee, 1986; Wills & Napier-Munn, 2006; Lucay, Mellado, Cisternas, & Galvez, 2012). This approach has driven the industry for much of the known past and continues to be the method of choice for many circuit designers. Malghan (1986) notes that regional bias may also influence the general paradigm or approach to circuit design. At the time of his publication, poly-metallic sulfides and porphyry copper deposits were primarily processed by bulk flotation in the Americas, sequential copper-lead-zinc flotation in Australia, and low-throughput, complex circuits in Scandinavia. Furthermore, Malghan claims that open-circuits (those lacking recycle streams) were becoming increasingly common. The author also suggests simple design principles loosely based on a kinetic model of flotation. For example, high-grade material is claimed to float quicker than lower-grade middling material. In the instances where the rougher concentrate from the first cell meets product specifications, the floated material may be immediately directed to the final concentrate. The author also describes other common flotation practices including:

- The sizing of units based on the residence time required for desired recovery;
- The regrind of middling material produced as scavenger concentrate;
- The inclusion of sufficient units in a bank to prevent short-circuiting;
- The addition of conditioning or agitation tanks to accommodate circuit flexibility;

- The selection of the type of flotation cells, perhaps considering columns for cleaner flotation;
- Common flowsheets for copper flotation, copper-lead-zinc flotation, molybdenite flotation, nickel flotation, feldspar flotation, and phosphate flotation.

These principles are simply presented as the state of the industry at the time of publication. The author makes no claim that the rules and design principles are applicable in all circumstances or that they represent optimal solutions (Malghan, 1986). Despite the age of this study, many of these principles are still in use today.

At the same time, Lauder and McKee (1986) presented a more data-driven, empirical critique of circuit design, focusing on the parameter of circulating loads in flotation plants. Earlier theory had suggested that improved separation performance is achieved by increasing the circulating load if the plant had the available capacity (Loveday & Marchant, 1972). In the present study, two circuits were tested in parallel to definitively validate this claim. Both circuits were operated identically, with the only variation being the rougher volume. By altering the rougher volume between the two circuits, the amount of rougher concentrate was controlled, and subsequently, varying circulating loads were produced in downstream operations. The parallel arrangement of the circuits ensured similar chemistry and mineralogy; therefore, the measured performance differences were solely attributed to the variations in circuit design. The authors conclude that increased circulating load (and thus circuit configuration, in general) is capable of increasing both grade and recovery simultaneously. While other operational changes move the performance along the same grade-recovery curve, the circuit arrangement is capable of moving the values to a new curve. Despite the plurality of available literature on modeling and circuit design at the time (e.g., D. Sutherland, 1981; Meloy, 1983b, 1983a; M. Williams & Meloy, 1983; M. Williams, Fuerstenau, & Meloy, 1986; Chan & Prince, 1986), the authors argue that the lack of fundamental insight on circulating loads and the lack of a widely accepted flotation model contribute to the overwhelmingly empirical circuit design process. Furthermore, the introduction of either of these tools would be beneficial in balancing the metallurgical gain of increased circulating loads with the loss of processing resources. Their oversight of the available scientific literature does not suggest deliberate neglect, but rather, the lapse is likely an indicator of the lack of technology transfer between industry and academia prevalent at the time.

As a transitional point between the empirical and model-based heuristic methodologies, Cameron and Morrison (1991) describe approaches to both steady-state and dynamic optimization using the technologies developed at the Julius Kruttschnitt Mineral Research Centre (JKMRC). First, the term *optimum* is given contextual meaning. The authors confide

that *optimum* may have different meanings on the given operation and corporate culture. Typically, plant personnel suffer from compartmentalized optimization which may focus on limited factors without considering downstream effects. In summary, the authors state that unless an optimum is related to specific parameters (i.e. "optimize quarterly profits"), the term is essentially meaningless. As a result, they show how JKSimMet and other model-based simulation software have been used to increase performance at various operations. No attempt is made to generalize the optimization strategies, rather the authors simply state how their software can be adapted and applied at various sites.

Conversely, one decade prior to Cameron and Morrison, D. Sutherland (1981) provided a general strategy to optimize resource allocation in rougher-scavenger-cleaner flotation plants using simulations derived from simple kinetic flotation models. In this analysis, Sutherland assumed that the flotation process can be effectively described by a first-order rate constant which does not change between various stages of flotation, and each individual cell was modeled as a perfectly-mixed reactor (Equation 2.3, given in Section 2.2.3). Finally, to simplify the calculations, Sutherland assumed a constant solids hold up throughout the circuit. Since a generic circuit configuration was selected (rougher-scavenger-cleaner with recycle), the simulations were conducted to assess how residence time should be split between the three units to yield the best separation performance.

In the study, Sutherland hypothetically established four flotation/grade classes: fast floating mineral, slow floating mineral, fast flotation gangue and slow floating gangue. Reasonable values were selected for the flotation rates and grades of these classes. Next, simulations were performed for various residence times in the rougher, scavenger, and cleaner. To constrain the system of equations to a single independent variable, fixed values were selected for the total plant size and the desired plant recovery. Hence, the size of one unit was selected independently, and the other two were calculated from the equations describing the full plant recovery and the total plant size. By varying the size of the cleaner bank, the final product grade was determined as a function of the number of cleaner cells for a fixed plant recovery and plant size. This result was plotted as product grade versus the ratio of residence times in the cleaner and the rougher. The simulations indicate that the highest grade (and thus best separation efficiency) is achieved when the residence times in the rougher and cleaner are nearly equal. However, in the examples shown by Sutherland, the final product grade was highly insensitive to changes in resource allocation for most normal operational cases. The data showed significant benefits were only witnessed when the plant was being pushed for high recovery or when a gross imbalance existed between the stages. As a result, Sutherland stresses that selectivity in the individual stages is much more crucial to plant performance than simple resource allocation. Thus, optimization efforts should focus on the

study of chemical and operational parameters.

A similar model-based optimization strategy was proposed by Loveday and Brouckaert (1995). Here, the authors based the optimization on maximizing the partition separation sharpness (see Section 2.2.2). For case of flotation, Loveday and Brouckaert define the separation sharpness as the slope of the recovery versus rate plot where the recovery equals 50%. A higher slope at this point indicates an increased ability to distinguish middling material. The authors show that in the case of single stage flotation, the separation sharpness is very poor. Therefore, multiple stages and increased recirculating loads are necessary to produce acceptable separation performance in a flotation plant. The authors postulate that the optimum recycle is achieved when the maximum slope of the recovery-rate plot is at the $R = 50\%$ point. As shown in the paper, the maximum slope starts at $R = 0\%$ for no recycle and increases exponentially as the amount of recirculation increases. The authors then show the calculation steps needed to determine the appropriate recycle to achieve this goal and the cell volumes required. The initial calculation was shown for a single-rougher cleaner circuit, but the calculation is then repeated for several counter-current circuit configurations. The conclusions of their paper highlight the need for extensive batch and pilot testing to characterize the flotation kinetics and rate distribution of the ore.

2.3.3 Linear Circuit Analysis and Analytical Heuristics

The concept of linear circuit analysis (LCA) was first derived by Meloy (1983a) in order to provide a method of optimizing multi-unit separation circuit configurations. This original paper eventually developed into a series of publications examining various aspects and applications of the methodology. The impact of these papers in the literature spanned nearly two decades with much of the original developments occurring in the early 1980's. In the groundbreaking work, a series of circuit design principles were generated from fundamental observations on the algebra concerning binary separation units. First, a separation unit's yield of a particular particle type is defined by a transfer function (or probability, P). The mass of material in the concentrate stream is simply the product of the yield and the feed mass (PF), while the transfer function to the tailings stream constitutes the remaining material ($1 - P$). By extending this algebra over many units, the recovery for the entire circuit may be analytically defined in terms of each unit's recovery. Figure 2.7 shows examples of this algebra applied to common circuit configurations. The power of all LCA applications is then derived from the analytical solution.

The LCA methodology is constrained by linearity assumptions. Meloy (1983a) presents

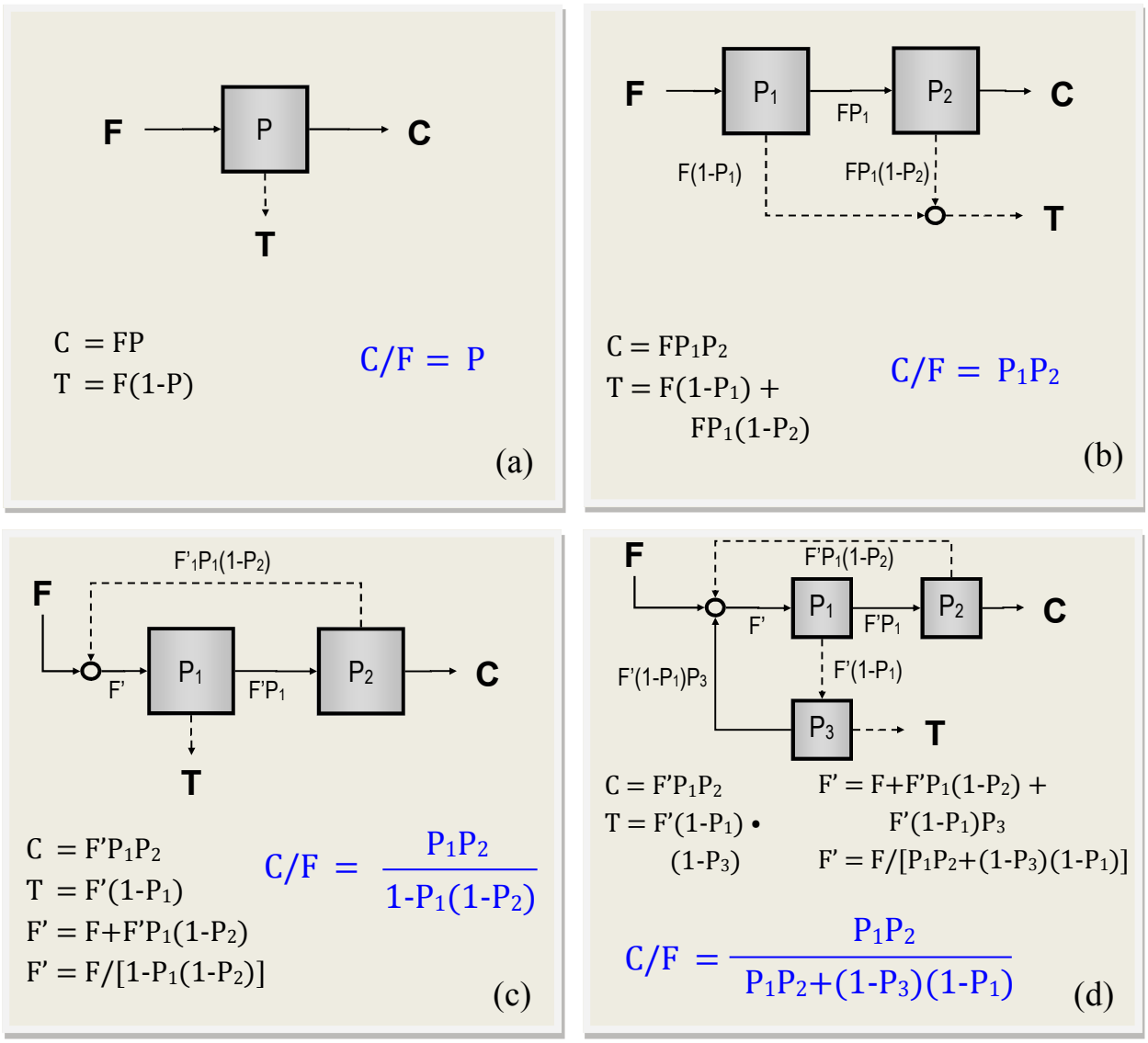

Figure 2.7: Examples of linear circuit analysis applied to several simple configurations.

a formal definition of these restrictions, but in summary, linearity states that a unit's partition curve is not influenced by feed composition or feed rate. While this assumption is not wholly valid for operating units, Meloy states that during the design phase, a larger or smaller unit may be selected to accommodate the required tonnages. Thus, this approach is valid for new circuit designs. Furthermore, the same author has suggested that literature contains support for linearly operated process units and that experimental investigations have confirmed linearity in some cases (Harris & Cuadros-Paz, 1978; M. Williams & Meloy, 1983; M. Williams et al., 1986).

In the original LCA paper, the analytical solution is used to determine the relative separation sharpness of a circuit to a single unit (Meloy, 1983a). The slope of the partition curve is used as a general indicator of separation capability, and Meloy shows that this slope can be determined for the full circuit by calculating the derivative of the circuit's analytical recovery at a value where the circuit recovery equals 50%. From this method, the incorporation of circulating loads are shown to increase separation sharpness; however, staged units may affect the cut-point of partition-based separators, even if all units are operating similarly. Finally, Meloy presents a means of analyzing unit bypass, such as the entrainment phenomenon witnessed in flotation (King, 2001; Wills & Napier-Munn, 2006).

Meloy (1983b) later expanded upon the analysis procedure to define a methodology for circuit optimization. In this paper, four functions fundamental to separation processes are described mathematically: feed, selectivity, composition, and criteria. The former three functions are defined by three variable types, particle property, operational, and compositional, though not all functions are defined by all variables. Finally, the criteria function defines the value to be optimized, typically grade or recovery. The optimization then proceeds by (1) defining the criteria function in terms of the three other functions; (2) differentiating with respect to the operational variables; (3) setting the resulting derivative equal to zero; and (4) solving for the operational derivatives. If more than one process variable exists, the procedures may be expanded by taking partial derivatives of the criteria function with respect to each operational variable. This array of equations is then set equal to zero and solved simultaneously. Meloy states that the required data are easily determined by assays or other experimental studies. Furthermore, the process may be applied to various mineral processing unit operations, including flotation, gravity separation, magnetic and electrostatic circuits. As a final contribution, Meloy notes that the optimum grade and the optimum recovery never occur at the same operational point.

The principles of LCA were also used to analyze dynamic flotation cell models (M. Williams & Meloy, 1983), multi-feed multistage separators (M. Williams et al., 1986), and the effect

of density variations in heavy media circuits (Meloy, Clark, & Glista, 1986). First, the analytical circuit solutions derived from LCA were coupled with a dynamic, rate-based lumped parameter flotation model to analyze the dynamic response of flotation circuits to sinusoidal feed variations (M. Williams & Meloy, 1983). The authors compared the dynamic behavior of counter-current and co-current circuits, concluding that co-current circuits are better in all applications. This result was based on the deficiencies of counter-current circuits , including larger required volumes and longer dynamic response times. Finally, co-current flotation banks were shown to be non-oscillatory, while counter-current circuits exhibit osculation frequencies that increase with flotation rate and retention time.

Another paper in the LCA series addresses the optimization of a rougher-scavenger-cleaner dense-media coal cleaning circuit (Meloy et al., 1986). Here, the authors seek to address whether the media density in multistage coal cleaning circuits can be optimized to improve overall performance. The authors note that rougher-scavenger-cleaner circuits are not common in coal preparation, especially in gravity separation circuits. This design principle is likely supported by the relatively high separation efficiencies naturally found in dense-media vessels (Osborne, 1988a, p. 259; Wills & Napier-Munn, 2006, p. 260). Nevertheless, the authors conduct the optimization exercise utilizing a standard partition function for the selection function of the dense-media separator. This partition function is dependent on the separation sharpness and the dense-media cut-point. The LCA methodology is used to determine the product function for the entire rougher-scavenger-cleaner circuit, and an incremental approach (by taking the second derivative of the analytical expression) is used to determine the affect of the gravity set point in each unit on the final recovery, grade, concentrate, and circulating load. This analysis is repeated and the results are plotted as a function of the units' original sharpness value. The results show that the best benefit occurs at relatively low sharpness values. Furthermore, additional benefits can be experienced by increasing the scavenger gravity and decreasing the cleaner gravity. This result is expected, since such modifications will increase the circulating load to the rougher and increased circulating loads are known to enhance separation performance.

Collectively, the mathematical approach of LCA is used to derive a common set of principles which guide separation circuit design. These principles have been summarized, most recently by McKeon and Luttrell (2005, 2012):

- Only circuit configurations involving recycle to prior units are capable of increasing the separation sharpness;
- Perfect separation is obtainable as the number of units down the scavenger and cleaner branch approach infinity;

- Products generated after the first separator should not cross between the scavenger and cleaner branches of the circuit without first being recycled through the initial separator;
- Units positioned off of the main scavenger and cleaner legs do not increase separation sharpness.

These authors go on to show the application of circuit analysis in evaluating and reconfiguring a heavy mineral sands spiral separation circuit. By adapting and implementing these principles the authors were able to simplify the plant configuration by reducing the number of spirals from 686 to 542. Furthermore, the new circuit was able to produce a higher grade material at an increased recovery. Previously, concentrate material was reprocessed seven times in order to produce the specified grade at a 93.0% recovery. After the modification, the circuit was able to obtain a 94.7% recovery at the desired grade in only a single pass (McKeon & Luttrell, 2012). In other instances similar performance gains have been obtained by implementing circuit analysis principles to coal spiral separators (Luttrell, Kohmuench, Stanley, & Trump, 1998) and flotation columns (Tao, Luttrell, & Yoon, 2000).

Despite this evidence for circuit analysis and the value of well configured recycle streams, some authors have ignored these considerations in their circuit designs. In particular, Poulter (1993) has described the overhaul of the zinc circuit at the Rosebery concentrator. Among other advancements involving process mineralogy and feed characterization, the author described a "circuit simplification" process which occurred during 1992. The prior flotation circuit, shown schematically in Figure 2.8a involved three cleaner stages and counter current flow, recycling each tailings product to the feed of the prior unit. Poulter indicates several deficiencies inherent to this circuit, including: complicated process control, high circulating loads, inhibited performance of fast floating material, and little perceived benefit from the latter cleaner states.

After 1993, the operators installed modifications to the circuit, including split conditioning for the feed and regrind product, froth booster plates, and a revised flowsheet (shown schematically in Figure 2.8b). Worth noting, when evaluated by the LCA methodology, the modified circuit represents a much weaker configuration. According to Meloy (1983a), the modified circuit should witnessed inhibited separation capability. Nevertheless after describing these modifications, the author states that the new circuit design has increased operational ease and metallurgical performance. The data presented by Poulter (Figure 2.9) shows increased grade in the latter months of the study; however, further meta-analysis shows that the new circuit experienced no significant increase in actual separation efficiency (Figure 2.10). While the author has noted the achievement of several auxiliary goals (i.e increased

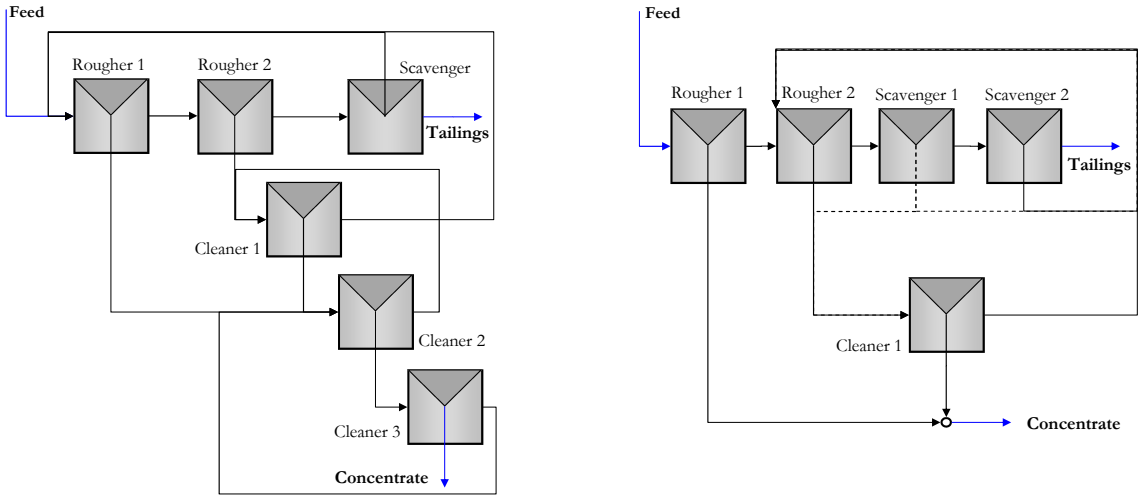

(a) Original Rosebery Circuit

(b) Modified Rosebery Circuit

Figure 2.8: Schematic circuit configurations for Rosebery flotation plant, circa 1992-1993. Flowsheet after (Poulter, 1993).

process control, reduced uncertainty, reduced flowsheet complexity), increased metallurgical performance, should not be included. The gains in equipment retrofitting were seemingly canceled by the reduction in circuit strength. Despite the errant conclusion, Poulter does raise the concern that auxiliary process goals (e.g. flowsheet complexity) sometimes trump simple septation capacity. Currently, LCA does not include a methodology for addressing these alternative goals.

To supplement their core work in LCA, M. Williams and Meloy later suggested two alternative approaches to circuit configuration design. Both methods were derived from theories similar to LCA; however, the authors sought to reduce the cumbersome mathematics associated circuit analysis. The first of these methods presents precise definitions for the common colloquial circuit functions: roughers, scavengers, and cleaners (M. Williams & Meloy, 1989). According to M. Williams and Meloy, a rougher is unit whose feed is the circuit feed, a cleaner is a unit fed by a concentrate stream, and a scavenger is fed by a tailings stream. In most processing plants, a single unit will fulfill several of these functions. For example, the rougher in a standard rougher-scavenger-cleaner recycle circuit (Figure 1.5c) is actually a rougher, scavenger, and cleaner, since it is processing feed, concentrate, and tailings from various units. M. Williams and Meloy argue that a better approach is to

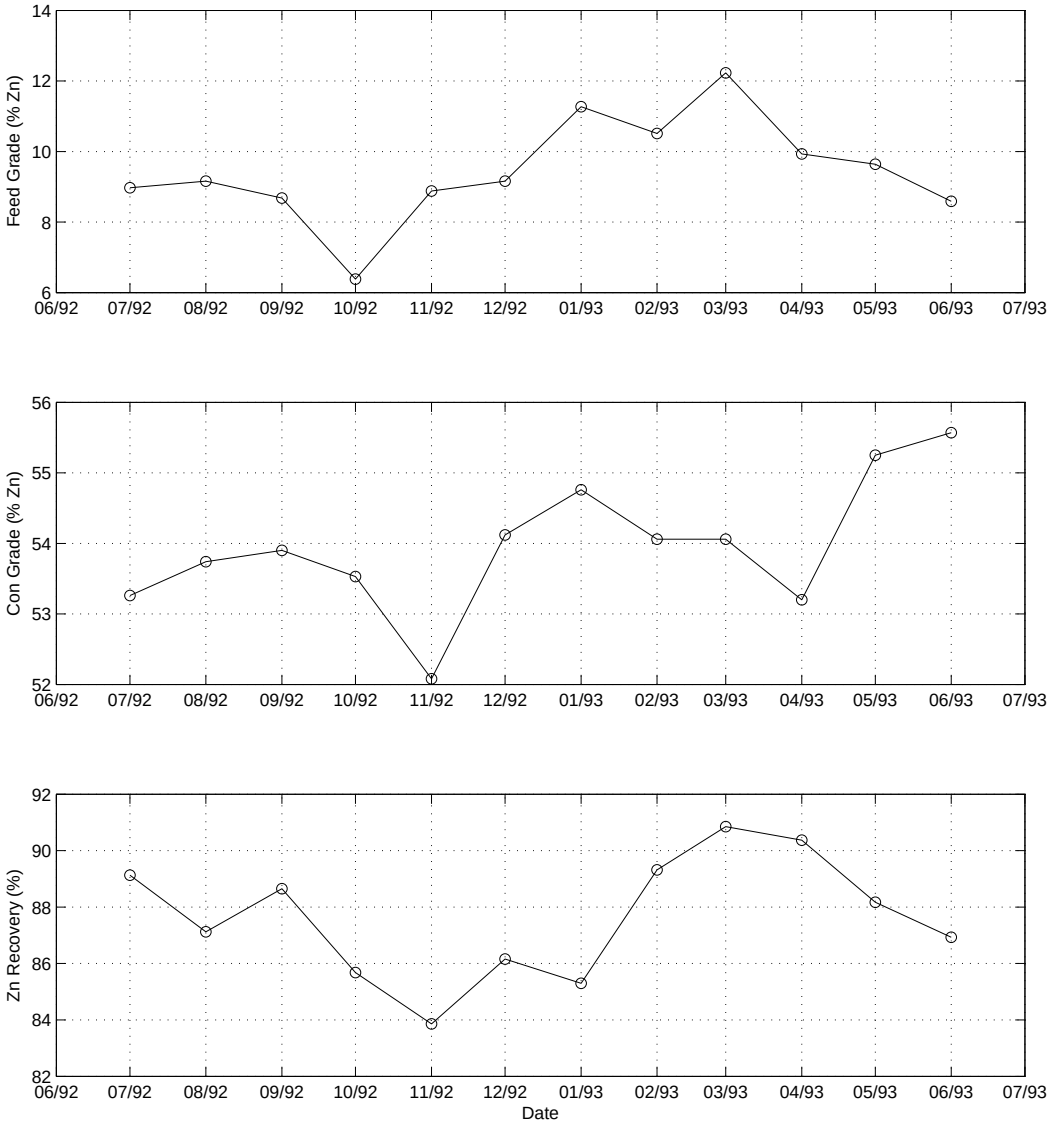

Figure 2.9: Raw metallurgical data at the Rosebery concentrator during period of circuit modification. Data after (Poulter, 1993).

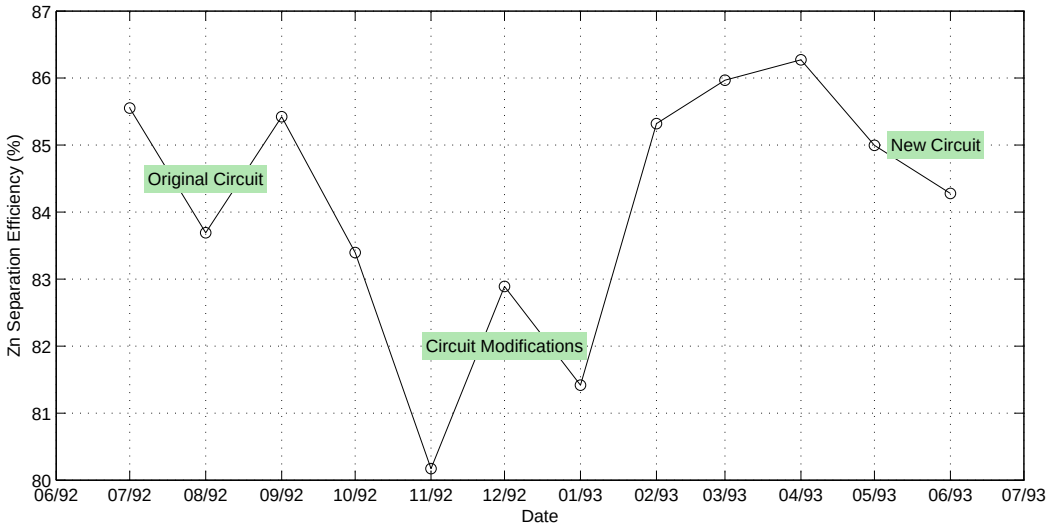

Figure 2.10: Calculated separation efficiency at the Rosebery concentrator during a period of circuit modification.

design circuits so that the individual unit operations are only fulfilling a single function. This strategy promotes specialized operation for individual cells, since each is pursuing a different process goal. Furthermore, by developing circuits which exploit specialized functions, the feed loading to each unit is substantially reduced. In the paper, the authors use LCA to show four equivalent circuits, each representing a higher degree of specialization. The authors then use the analytical solution to show the degree to which specialization can reduce feed loading, and in many cases, increase metallurgical performance (M. Williams & Meloy, 1989).

The second alternative circuit design approach defined mathematical solutions to three circuit design criteria: (1) the required number of stages, (2) the stage where the feed enters the circuit, (3) the configuration of the product streams (M. Williams & Meloy, 1991). This approach begins by assuming a generic cleaner-type circuit of indeterminate size, with each concentrate advancing serially to the next unit. Tailing streams are recycled to a prior point in the circuit, such that the the grade of the recycle stream is greater than or equal to the grade at the point of reentry, a principle originally suggest by Taggart, Behre, Breerwood, and Callow (1945). By establishing this generic superstructure, the three design criteria may be solved algebraically if four desired/operational parameters are specified: (1) the desired global product recovery, (2) the desired global ratio of product to waste, (3) the product to waste ratio achievable for each unit, and (4) the feed component ratio. These algebraic functions are intended to guide an initial circuit design, since they will inherently produce

non-integer values. By rounding and manipulating different combinations of values, the design criteria which achieve the desired results may be determined. These configurations constitute the "feasible designs" from which a more thorough optimization or design process may originate (M. Williams & Meloy, 1991).

A later reaction paper by Galvez (1998) proposed slight alterations to the "feasibility method" employed by M. Williams and Meloy. This paper begins by describing potential pitfalls to the original feasibility method, such as: the assumption of identical transfer function for each unit, the conversion of recycle streams to waste streams when the recycle parameter was ambiguous, and the lack of a standard methodology when non-integer values were calculated. Rather than first generically defining the number of stages for the entire plant, Galvez assumes that each circuit will have one rougher stage, and an indeterminate number of scavenger and cleaner stages. The number of units in each stage is calculated independently using equations which relate the waste specification to the number of scavenger stages and the concentrate specification to the number of cleaner stages. Next, the reentry point of the concentrate waste streams is determined by implementing the same recycle principle proposed by Taggart et al. (1945) and employed by M. Williams and Meloy (1991): namely, the waste stream must be recycled back such that it enters a stream with a lower or equal grade. An analogous approach is taken for the reentry of the scavenger concentrate products. After the calculation of these four parameters Galvez proposed three rules to guide selection when non-integer values are calculated: (1) the number of recycle stages must be greater than or equal to one, (2) all recycle streams must be recycled into the circuit (i.e. no open circuits), and (3) values for the number of cleaner and scavenger units should be rounded up, unless they are extremely close to the floor value. The final rule provides added conservatism since the initial calculations do not consider the influence of recycle streams. Even after these rules are applied, several feasible solutions may persist. In these cases, Galvez suggests either an economic analysis or a decision based on the separation factor, the beneficiation ratio, or the valuable component recovery.

Noting the utility of LCA and the analytical solution, M. C. Williams, Fuerstenau, and Meloy (1992) derived a methodology to rapidly produce analytical solutions to separation circuits. In this paper, the authors note the drawbacks to traditional circuit analysis, namely the cumbersome required mathematics, as well as the deficiencies of numerical optimization approaches, such as the inability to introduce common sense principles from the designer. This approach, tailored from the principles of graph theory, provides a technique of relating the recovery of individual units to the full circuit recovery. In their nomenclature, separation units are designates as modules which are connected by branches by identifying loops in the circuit configuration, the overall circuit recovery may be calculated by a standard approach.

The authors present an example from the literature which contains five units and required the simultaneous solution of 12 equations (Davis, 1964) . M. C. Williams et al. suggest that, when mastered, the graph theory approach should take ten minutes for a similarly-sized problem.

A recent adaptation of LCA is sensitivity analysis (*SA*) (Lucay et al., 2012). The authors present SA as an ideal trade-off between empirical and heuristic insight and numerical optimization strategies. Since global optimization through experiments is nearly impossible, SA is used to determine the nodes in the circuit which produce the greatest impact. Subsequently, empirical insight and experiments can be used to optimize or improve performance at those nodes. In SA, each unit is examined individually and the final results are compared to determine the most influential unit. As in LCA, the first required step is to determine an analytical expression for the circuit yield in terms of each unit operation's independent recovery function. In defining this expression, terms referring to units not under scrutiny are lumped into a single, constant parameter. By mathematically manipulating this global recovery function, an expression can be determined which indicates if a species is being diluted or concentrated, depending on the value of the lumped parameter. Next, the partial derivative of the global recovery function is determined with respect to the recovery of the unit under scrutiny. The magnitude of this partial derivative is then determined and plotted for various expected values of the individual recovery functions. Local minima and maxima in the plots are noted. This process is then repeated by taking the partial derivative with respect to each unit, the behavior of the plots are identified, and the overall magnitude of each partial derivative is compared to determine the unit with greatest influence on the circuit. Unfortunately, the behavior of the sensitivity graph changes, depending on the performance of other units in the circuit. However, if the general behavior of an operating circuit is known, SA may be used to determine the unit which merits the most attention. Once the operation of this unit is altered, the circuit will produce a new high sensitivity unit and the process may be repeated. Lucay et al. conclude the paper by demonstrating the method on a hypothetical flotation circuit using a standard perfectly-mixed reactor model.

2.3.4 Numerical Circuit Optimization Methods

Several authors over the last 25 years have used calculus-based optimization and, to a limited extent, genetic algorithms in the circuit design problem. A comprehensive review on the application of numerical optimization to circuit design has been recently presented by Mendez, Galvez, and Cisternas (2009). These authors present circuit design as a synthetic design process which can (and potentially should) be approached as a traditional engineering

optimization problem. However, as common to many synthesis problems, the initial solution approach is usually trial-and-error. The industrial result has been non-optimal circuits which later require substantial plant modification. These retrofits are still based on non-optimal solutions which in turn introduce new deficiencies. Alternatively, limitations to the optimization strategies generally arise from insufficient resources, unrealistic process models, and sporadic laboratory data. Mendez et al. note that historic strategies used circuit simulation to drive the trial-and-error process. Many times these solutions pursued enhanced metallurgical performance, at the expense of disregarding process economics. To overcome these limitations, modern circuit design research has used numerical optimization to pursue technical and economic objectives.

Mendez et al. found four approaches to circuit design in the literature. In general, the circuit designers were tasked with identifying the operational characteristics of each unit and the interconnection between the units which optimized some technical-economic objective function. In the first two groups (labeled A and B in the review), an overall circuit superstructure was first established. In the literature, the *superstructure* refers to all possible combinations of circuit configurations. Typically, this superstructure is represented mathematically by directing the products of each separation unit to a flow distribution node. This node can ambiguously split the flow to any other point in the circuit. The optimization routine is then tasked with calculating the proper split portions for these nodes. In an example, the concentrate of a scavenger may be directed to a flow distribution node. This node splits the concentrate to either return the rougher feed or proceed to the final concentrate. The optimization routine then determines the appropriate split based on the objective function. This node splitting paradigm is repeated throughout the entire circuit so that all possible (or plausible) circuit configurations are contained in the superstructure. Groups A and B of Mendez et al. utilize the superstructure approach with the designation being Group A allows any value for the split portion, while Group B only allows integer values. As described in the original research, the incorporation of only integer values marks a substantial increase in the algorithm complexity.

Since the superstructure approach often leads to extremely non-conventional circuit designs, other researchers have attempted more heuristic optimization approaches. Some of these examples explain additive circuits which continually build up a better configuration without necessarily optimizing the result. This class of techniques are labeled Group C by Mendez et al.. Finally, Group D includes those researches which have utilized genetic algorithms to produce optimal circuit solutions. Mendez et al. state that these papers show the power of genetic algorithms but do not necessarily identify a global optimum.

Beyond the simple classification scheme Mendez et al. (2009) provides an exhaustive analysis of the flotation models and additional design selections incorporated into the optimization algorithms. Options such as regrind mills, existence of column cells, and existence of feed splitting are compared for each group of techniques. Furthermore, the various objective functions are listed and compared. Some examples include maximizing recovery, maximizing grade, maximize quantity of valuable species in concentrate, maximize net smelter return, maximize profit. These objectives have evolved over time, with recent trends incorporating capital and operating costs, Nonetheless, many models today are limited by deterministic projections of uncertain market factors (i.e. mineral selling price). The authors also conclude that the lack of a comprehensive flotation model limits the state of global circuit optimization since the results are largely driven by the models. Finally, a stronger effort needs to be made in incorporating sustainability within the problem of circuit design.

Many of the papers described by Mendez et al. (2009) are included in the "higher-level" design approaches shown in Figure 2.6. The remainder of this section will analyze these papers individually, commenting on factors either omitted or generalized.

One of the early systemic uses of mathematical optimization to set operating parameters for a fixed circuit layout is presented by (Rong, 1992). Earlier work by the same author had investigated a direct-search technique (Rong & Lyman, 1985), though the 1992 paper described the use of this technique within the framework of a coal preparation flowsheet simulator. The simulator is intended to predominantly serve the Chinese preparation market, and therefore includes models for roll crushers, rotary breakers, jigs, dense-media cyclones, as well as prepackaged flowsheets (not user-defined). The optimization engine utilizes the Rosenbrock direct-search technique and can identify the optimal screen apertures, cut densities, flotation time, and circuit layout to optimize a the objective function. This technical-based value relates the simulated final ash with a specified final ash value. The author does indicate the number of iterations required to achieve the optimum but does indicate that the solution converges "rapidly even for the complex optimization tested" (Rong, 1992).

Yingling (1990, 1993a, 1993b) highlighted the need for robust mathematical optimization in the circuit design problem, despite the nonlinear objective functions and discrete selection variables which complicate the underlying mathematics. Yingling's first paper introduces a novel approach to the mathematical representation of the circuit configuration based on the theory of steady-state evolution in Markov chains. This formalistic approach to probabilistic separation was formed as an extension of Linear Circuit Analysis (see Section 2.3.3). Yingling notes the desire for an analytical circuit solution (especially in optimization

problems), but discredits the case-by-case algebraic approach taken by Meloy (1983a). Instead, Yingling proposes a flowgraph reduction strategy based on elementary reduction rules (Yingling, 1988). With the Markov assumption, the separation state of a given unit is not dependent on the prior states of the process. Combining this approach with potential theory of Markov chains, Yingling is able to produce a more efficient, but mathematically equivalent, solution for the steady-state behavior of the circuit. This approach incorporates the circuit superstructure with flow distribution nodes. The state of this superstructure along with the operational parameters is defined as the circuit control policy which is varied to optimize an economically-driven reward function. The optimization algorithm proposed by the author is based on stochastic dynamic programming with extended techniques to account for the multiple particle classes present in flotation systems. This optimization relies on discrete layout alternatives, defined by the circuit designer; however, Yingling (1990) is regarded as one of the first authors to provide a formalistic approach to the circuit superstructure concept and an economic objective function.

Yingling's later two-part series (1993a, 1993b) reviewed prior work in circuit optimization and extended the original work in Markov chains. Yingling's review categorized prior work into two classifications: (1) those that use direct search techniques to optimize the operational parameters and the circuit layout simultaneously and (2) those that use a two-stage optimization to first establish the configuration before solving the parameters. Yingling notes that many of authors in the first group produce solutions that contain too many flow streams, as the optimization algorithms blindly attempt to expand the circuit optimization problem. The second group of authors rarely consider the impact of stream flows in the circuit configuration step and generally ignore economic considerations. Yingling concludes that neither approach is ultimately sufficient for the circuit design problem. In response, the final paper (1993b) extends the procedures developed in the original (Yingling, 1990). Most notably, a new optimization routine was developed which allows for both discreet and continuous stream splitting nodes. This algorithm is stated to be more efficient and actually more robust than many direct search methods which cannot determine the appropriate number of cells within a flotation bank. A similar ambiguous, though economically-based, objective function is used. Examples of the solution robustness are presented.

Further economic factors were later integrated into the circuit optimization objective function (Schena, Villeneuve, & Nol, 1996; Schena, Zanin, & Chiarandini, 1997). The initial paper largely builds upon Yingling's inclusion of financial reward functions. Schena et al. criticize Yingling's adherence to the linearity assumption originally proposed by Meloy (1983a). Schena et al. discusses the available flotation models and the lack of linearity in these models. The authors further propose the use of a direct-search technique to optimize the profit after

considering capital cost, operating cost, smelting cost, refining cost, and overall revenue. Constraints may be placed on the minimum acceptable grade as well as other factors, and the design vector includes the number of cells in the rougher and scavenger bank, as well as the number of cleaning stages. Cell selection in the case of expanding an existing plant is handled by weighting existing cells at no capital cost, while unavailable cells are weighted at exorbitantly high capital costs. Other constraints are liberally applied to reduce the feasible solution space and enhance the optimization efficiency. The first paper (Schena et al., 1996) largely introduces these principles in general terms, while the second paper (Schena et al., 1997) provides more pragmatic analysis. In the second paper, both flotation and grinding models are included to create optimal circuit configuration from scratch without an initial recommendation from the circuit designer. The algorithm handles nonlinearities by solving linearized subproblems, and thus, has the capacity to design a full circuit from merely user inputted feed and operational data. The authors note that the approach is unfortunately limited by the fidelity of the process models.

Abu-Ali and Sabour (2003) further formalized the inclusion of economics in optimizing portions of a flotation circuit by considering the simple case of adding cells to a flotation bank. They conclude that the optimal bank size is determined when the incremental cost of adding the cell is zero. The flotation recovery is determined by a simple perfectly-mixed, in-series model which accounts for an infinite-time recovery. Equations are derived which define the capital and operating costs for a bank of cells as a function of cell size and cell number. The assumptions of the analysis consider that the feed rate, feed grade, and required grade are known. Furthermore, the mean residence time of the bank remains constant as the bank size is increased (i.e. smaller cells are used as more units are added to the bank). The flotation model and operational cost estimation equations are combined to calculate the present value of the annual revenue as a function of the various operational, contractual, and assumed parameters. This equation is added to the capital cost estimation to produce a final expression for the net present value. Finally, the authors evaluate the derivative of the new present value, and solve for the number of cells which causes the derivative to equal zero. This value is denoted as the optimal solution. For the hypothetical low grade copper example, the optimal bank size to achieve a target 80% recovery was evaluated to be 16 cells, each having a volume of 24 cubic meters.

A novel optimization strategy, based on the McCabe-Thiele technique for multi-column distillation, was presented by Hulbert (1995). The author introduces a new structure for the modeling of counter-current flotation based on so-called "enrichment functions." This approach is comparable with the rate principles of flotation modeling, though it does not directly consider rate constants and residence times which lead to nonlinear, numerical op-

timization. Rather, the recovery relationships are based on concentration, as similar to chemical equilibrium processes. For the case of flotation, the concentration of mineral in the concentrate is shown to be a function of the concentration in the feed and the rate of removal or mass pull (which can then be related back to operational parameters such as air flow for reagent dosage) The result is that an analytical optimum can be determined for counter-current flotation system, by evaluating the partial derivate of the enrichment function. McCabe-Thiele "staircase" diagrams can be determined for operating plants to assist in interpreting the optimization. From the exercise, the authors define optimal performance by the following heuristic: at the optimum, small changes in the mass pull of each internal concentrate stream must not alter the concentration of any other stream nor alter the concentration of the local pulp (Hulbert, 1995).

Finally, two fully comprehensive approaches to circuit optimization have been presented. The first uses mixed integer linear programming (MILP) to determine the circuit configuration, bank vs. column selection, regrind selection, and operational parameters (Cisternas, Gálvez, & Mendez, 2005; Cisternas, Mndez, Glvez, & Jorquera, 2006). The second uses the elitist, binary-coded, non-dominated sorting genetic algorithm with the modified jumping gene (NSGA-II-mJG) to simultaneously solve the configuration and the operational parameters of a flotation system (Guria, Verma, Gupta, & Mehrotra, 2005; Guria, Varma, Mehrotra, & Gupta, n.d.).

The first approach (Cisternas et al., 2005, 2006) uses a hierarchal superstructure to determine the circuit configuration. The highest level (the separation task superstructure) is composed of three subsystems: the feed processing superstructure, the tail processing superstructure, and the concentrate processing superstructure. The separation tasks superstructure controls the relative splits between the three components. For example, a flow distribution node in the separation tasks superstructure controls the amount of the feed processing superstructure's tailings which proceed to final tailings versus the amount that enters the the tailings processing superstructure. The individual subcomponents then have similarly designed components consisting of individual bank cells, as well as an equipment selection superstructure which decides upon potential regrind mills or column cells when appropriate. A simple perfectly-mixed in series model is used to determine the bank cell recovery, while an axially-dispersed reactor model is used for column cells. The objective function is financially based, calculating the Net Smelter Return as a function of refining charges, grade penalties, operating hours, feed rate, capital and operating cost for the equipment, and revenue generated for the concentrate product. An application example is shown to demonstrating that unlike prior superstructure-based optimization, this MILP model typically does not produce large-scale stream splitting or high numbers of individual streams.

A sensitivity analysis shows that the metal price is a significant factor in the optimization, however, the valuable mineral mass distribution (i.e., grade) may be more significant. The results imply that a specific circuit design may only be valid for a given mineral price and feed condition.

The second comprehensive approach (Guria et al., 2005, n.d.) allows multiple objective optimization via specific genetic optimization algorithms (NSGA-II-mJG). The authors show that four earlier examples in the literature used gradient-based or direct search techniques which eventually converged to a local optimum. Conversely, the genetic algorithm described in the paper produced superior circuit configurations while pursuing the same objective function. The optimization routine accounts for standard assumptions in flotation modeling, including perfectly-mixed reactors and rate constant distributions for particle species. The objective function is defined by the profit of producing material at a certain grade, with a penalty for values below the contract value. No equipment costs are considered. Constraints are set on the total plant size, the loss of valuable mineral to the final tailings, the existence of split streams, as well as other case-specific parameters. Specific details of the four example problems are presented. The authors report the solution time for each problem which ranged from 4.5 to 9 hours on standard desktop computers using 100,000 generations in the genetic algorithm (Guria et al., 2005).

In the follow up paper (Guria et al., n.d.), the authors describe methodologies for optimizing multi-objective functions using the same NSGA-II-mJG algorithm. The number simultaneous objectives ranged from two to four, including maximizing recovery at a fixed grade, minimizing number of streams, and minimizing the total cell volume. These examples further demonstrate the robustness of the optimization technique in identifying potential circuit designs which may be selected from the designer's experience.

2.4 Summary and Conclusions

This paper has reviewed the methodologies for separation circuit design in the mineral processing industry. Over the last century, mineral beneficiation has grown from a rudimentary, laborious art to an efficient, highly mechanized industrial process. In this period of growth, the froth flotation process has advanced as the most utilized and robust separation process in the industry. Full understanding of the flotation process requires deep consideration of the chemical and physical transport phenomena driving the various subprocesses. The desire to understand and optimize the flotation process has led to a more fundamental, rather than empirical, approach to process engineering. The consequences of this transition

have also led to various benefits in the optimization of all unit operations.

One engineering problem common to mineral processing is the design of the separation circuit. Since all separation units are inherently imperfect, individual units are staged in an attempt to produce synergistic efficiencies so that the final circuit product can meet contract specifications. In order to design a process circuit, four questions must be addressed: (1) the selection of the appropriate separation process(es); (2) the selection of the number and size of individual units; (3) the selection of the various operational parameters for each unit; and (4) the configuration of the flows between units. While many circuit designers approach these questions sequentially, a more comprehensive methodology must realize the interdependence of the various selections and answer these questions simultaneously.

Circuit designers have access to a number of process engineering tools which can aid in the design process. Today, most circuit design is driven by computer simulation which requires extensive information on the expected feed conditions, the operational details of the equipment, the desired circuit layout, and the process models which relate all of these parameters to the quantity and quality of the final product. In this design approach, laboratory data is typically collected and analyzed first.

Several approaches to process modeling have been used with success in the past. The most common in the mineral processing industry is simple empirical modeling. In this approach, the process model is simply an arbitrary curve which best interprets the existing data. The model does not inherently reflect the physics of the process; however, empirical models are easy to develop and can be related to a number of operational parameters given sufficient experimental data. One common fallacy is using empirical models to extrapolate beyond the experimental range. Since the model has no knowledge of the physics, gross error is common once the process transitions to a different operational condition. Phenomenological models overcome many of these drawbacks while balancing utility and development time. This modeling approach uses the physical subprocesses to define the functional forms, while still using experimental data to determine the final model parameters. Phenomenological models are more difficult to develop than empirical fits, but they are less prone to gross error when extrapolation is required. The higher-order fundamental models extend this concept using theory to completely define the model form and parameters. Unfortunately, fundamental models are largely immature, given the complexity of most mineral separation processes.

The literature defines several methodologies for optimizing the circuit configuration and parameters. Before the original insurgence of modeling and simulation, most circuit configurations were designed from historic and legacy perspectives. This empirical evidence led to

simple heuristics which imposed design rules, based on prior results. Modeling and simulation led to more sophisticated and scientifically-based heuristics; but the final solutions are strongly dependent on the applicability of the underlying assumptions and the robustness of the process model. During this time, circuit analysis ascended as an alternative methodology which considered the fundamental capacity of the circuit itself, omitting the need for a vetted process model. The ultimate adaptation to circuit analysis is realized in numeric circuit optimization. Once again, process models must be known, but this approach allows the sensitivity of the model to be analyzed with respect to the final solution. With the widespread availability of high-performance desktop computers, numeric optimization has become more accessible, and various, highly sophisticated optimization methods have been developed exclusively for the circuit design problem.

From this review, four key opportunities for further research are:

1. The data analysis and simulation of separation circuits utilizes engineering tools which are common to many other disciplines, most notably in the area of numeric methods. Very little work has analyzed the effect of sensitivity or error propagation that these methods inherently impose. Few authors have investigated the influence of uncertainty on simulation. The breakdown between systemic uncertainty (i.e. from data fits, error propagation) and natural uncertainty (feed variations) has not been discussed.

2. No consensus exists on the objective function utilized in the circuit optimization problem. While the objective has evolved over time from a purely technical value to a financially-based optimum, researched have still not agreed on the best value to optimize. Questions remain on whether on how operating costs, capital costs, the cost of more complex circuits, and sustainability costs should be incorporated into an optimization routine.

3. While many authors have expressed the utility of an analytical circuit solution, no author has provided a simple, computer-based algorithm capable of producing one for a user-defined circuit. Therefore, the utility of the analytical solution is severely limited by the inability to quickly produce solutions for alternate circuit designs.

4. Despite the availability of circuit optimization and analysis methods, none have gained sufficient utilization in industrial circuit designs or modifications. This result is likely due to the perceived complexity or the lack of applicability which accompanies the current methods.

2.5 Bibliography

Abu-Ali, M., & Sabour, S. A. (2003). Optimizing the design of flotation circuits: an economic approach. *Minerals Engineering*, *16*(1), 55–58.

Bhatti, M. (2000). *Practical optimization methods: with mathematica applications*. Telos Pr.

Cameron, P., & Morrison, R. (1991). Optimisation in the concentrator - the practical realities. In *Mining industry optimisation conference, sydney, june l991.*

Chan, W., & Prince, R. (1986). Application of the chain rule of differentiation to sequential modular flowsheet optimization. *Computers and Chemical Engineering*, *10*(3), 223–240.

Cisternas, L. A., Gálvez, E. D., & Mendez. (2005). *Optimal design of flotation circuits including selection of bank cells, column cells, and regrinding mills.* Rio de Janeiro, Brazil.

Cisternas, L. A., Mndez, D. A., Glvez, E. D., & Jorquera, R. E. (2006). A milp model for design of flotation circuits with bank/column and regrind/no regrind selection. *International Journal of Mineral Processing*, *79*(4), 253–263.

Davis, W. (1964). The development of a mathematical model of the lead flotation circuit at the zinc corporation ltd. *Proc. Australas., Inst. of Mining and Met*, *212*, 61–89.

Dell, C. (1964). An improved release analysis procedure for determining coal washability. *Journal of the Institute of Fuel*, *37*, 149–150.

Do, H. (2010). *Development of a turbulent flotation model from first principles*. Unpublished doctoral dissertation.

Dobby, G., & Finch, J. (1988). Flotation column scale-up and modeling. *Can. Inst. Min. Metall. Bull.*, *79*(889), 89–96.

Dowling, E., Klimpel, R., & Aplan, F. (1985). Model discrimination in the flotation of a porphyry copper ore. *Minerals and Metallurgical Processing*, *2*(2), 87–101.

Faires, J., & Burden, R. (2003). *Numerical methods*. Thomson Learning.

Fichera, M., & Chudacek, M. (1992). Batch cell flotation models–a review. *Minerals Engineering*, *5*(1), 41–55.

Finch, J., & Dobby, G. (1990). *Column flotation* (Vol. 9). Pergamon Press Oxford.

Finch, J., Xiao, J., Hardie, C., & Gomez, C. (2000). Gas dispersion properties: bubble surface area flux and gas holdup. *Minerals Engineering*, *13*(4), 365–372.

Foulds, L. (1981). *Optimization techniques: an introduction*. Springer-Verlag.

Galvez, E. (1998). A shortcut procedure for the design of mineral separation circuits. *Minerals Engineering*, *11*(2), 113–123.

Gaudin, A., Schuhmann Jr, R., & Schlechten, A. (1942). Flotation kinetics. ii. the effect of size on the behavior of galena particles. *The Journal of Physical Chemistry*, *46*(8), 902–910.

Gerald, & Wheatley. (1994). *Applied numerical analysis*. Addison Wesley.

Goldberg, D., & Holland, J. (1988). Genetic algorithms and machine learning. *Machine Learning*, *3*(2), 95–99.

Gorain, B., Franzidis, J., & Manlapig, E. (1997). Studies on impeller type, impeller speed and air flow rate in an industrial scale flotation cell. part 4: Effect of bubble surface area flux on flotation performance. *Minerals Engineering*, *10*(4), 367–379.

Gorain, B., Franzidis, J., Manlapig, E., Ward, K., & Johnson, N. (2000). Modeling of the mount isa rougher-scavenger copper flotation circuit using size-by-liberation data. *Minerals and Metallurgical Processing(USA)*, *17*(3), 173–180.

Gorain, B., Harris, M., Franzidis, J., & Manlapig, E. (1998). The effect of froth residence time on the kinetics of flotation. *Minerals Engineering*, *11*(7), 627–638.

Gorain, B., Napier-Munn, T., Franzidis, J., & Manlapig, E. (1998). Studies on impeller type, impeller speed and air flow rate in an industrial scale flotation cell. part 5: Validation of k-sb relationship and effect of froth depth. *Minerals Engineering*, *11*(7), 615–626.

Guria, C., Varma, M., Mehrotra, S. P., & Gupta, S. K. (n.d.). Simultaneous optimization of the performance of flotation circuits and their simplification using the jumping gene adaptations of genetic algorithm-ii: More complex problems. *International Journal of Mineral Processing*, *79*(3), 149–166.

Guria, C., Verma, M., Gupta, S. K., & Mehrotra, S. P. (2005). Simultaneous optimization of the performance of flotation circuits and their simplification using the jumping gene adaptations of genetic algorithm. *International Journal of Mineral Processing*, *77*(3), 165–185.

Gy, P. (1979). *Sampling of particulate materials: theory and practice.* Elsevier.

Gy, P. (1992). *Sampling of heterogeneous and dynamic material systems: theories of heterogeneity, sampling, and homogenizing.* Elsevier.

Hand, P., & Wiseman, D. (2010). Addressing the envelope. *Journal of the South African Institute of Mining & Metallurgy*, *110*(7), 365.

Harris, C., & Cuadros-Paz, A. (1978). Species interaction in flotation: A laboratory-scale semi-batch study. *International Journal of Mineral Processing*, *5*(3), 267–283.

Hernandez-Aguilar, J., Rao, S., & Finch, J. (2005). Testing the k-sb relationship at the microscale. *Minerals Engineering*, *18*(6), 591–598.

Himmelblau, D., & Bischoff, K. (1968). *Process analysis and simulation: Deterministic systems.* Wiley.

Holland, J. (1975). *Adaptation in natural and artificial systems: An introductory analysis with applications to biology, control, and artificial intelligence.* University of Michigan Press.

Holland, J. (1992). Genetic algorithms. *Scientific American*, *267*(1), 66–72.

Honaker, R. (1996). A modified release analysis procedure using advanced froth flotation mechanisms. *Illinois Clean Coal Institute Annual Report*, 71.

Hulbert, D. (1995). Optimization of counter-current flotation circuits. *The Chemical Engineering Journal and the Biochemical Engineering Journal*, *59*(1), 7–13.

Imaizumi, T., & Inoue, T. (1965). Kinetic consideration of froth flotation. *6th Int. Mineral Processing congr., Cannes, 1963*, 581–593.

Jameson, G., Nam, S., & Young, M. (1977). Physical factors affecting recovery rates in flotation. *Minerals Science and Engineering*, *9*(3), 103–18.

Kelley, K., Noble, A., Luttrell, G., & Yoon, R. (2012). Development of a model-based flotation simulator. In C. Young & G. Luttrell (Eds.), *Separation technologies for minerals, coal, and earth resources* (pp. 699–708). SME.

King, R. (2001). *Modeling and simulation of mineral processing systems.* Elsevier.

Kracht, W., Vallebuona, G., & Casali, A. (2005). Rate constant modelling for batch flotation, as a function of gas dispersion properties. *Minerals Engineering*, *18*(11), 1067–1076.

Lauder, D., & McKee, D. (1986). The impact of circulating loads on flotation circuit performance. In *l3th congress the council of mining and metallurgical institutions, singapore, 6 volumes* (p. 7).

Leonard, J. (1991). *Coal preparation, 5th ed.* SME.

Levenspiel, O. (1999). *Chemical reaction engineering.* Wiley.

Loveday, B., & Brouckaert, C. (1995). An analysis of flotation circuit design principles. *The Chemical Engineering Journal and the Biochemical Engineering Journal*, *59*(1), 15–21.

Loveday, B., & Marchant, G. (1972). Simulation of multicomponent flotation plants. *Journal of the South African Institute of Mining and Metallurgy*, *72*, 288–294.

Lucay, F., Mellado, M. E., Cisternas, L. A., & Galvez, E. D. (2012). Sensitivity analysis of separation circuits. *International Journal of Mineral Processing*, *110–111*, 30–45.

Luttrell, G. (1996). Analyzing common mass balance problems using spreadsheet tools. In *Sme preprint number 96-186* (p. 7). SME.

Luttrell, G., Kohmuench, J., Stanley, F., & Trump, G. (1998). Improving spiral performance using circuit analysis. *Minerals & Metallurgical Processing*, *15*(4), 16–21.

Luttrell, G., & Yoon, R. (1991). A flotation column simulator based on hydrodynamic principles. *International Journal of Mineral Processing*, *33*(1-4), 355–368.

Luttrell, G., & Yoon, R. (1992). A hydrodynamic model for bubble–particle attachment. *Journal of Colloid and Interface Science*, *154*(1), 129–137.

Lynch, A., Johnson, N., Manlapig, E., & Thorne, C. (1981). *Mineral and coal flotation circuits.* Elsevier.

Malghan, S. (1986). *Typical flotation circuit configurations.*

Mao, L., & Yoon, R. (1997). Predicting flotation rates using a rate equation derived from first principles. *International Journal of Mineral Processing*, *51*(1), 171–181.

Mathe, Z., Harris, M., O'Connor, C., & Franzidis, J. (1998). Review of froth modelling in steady state flotation systems. *Minerals Engineering*, *11*(5), 397–421.

McKeon, T., & Luttrell, G. (2005). Application of linear circuit analysis in gravity separator circuit design. In *Heavy minerals.*

McKeon, T., & Luttrell, G. (2012). Optimization of multistage circuits for gravity concentration of heavy mineral sands. *Minerals & Metallurgical Processing*, *29*(1), 1-5.

Meloy, T. (1983a). Analysis and optimization of mineral processing and coal-cleaning circuits circuit analysis. *International Journal of Mineral Processing*, *10*(1), 61–80.

Meloy, T. (1983b). Optimizing for grade or profit in mineral processing circuits circuit analysis. *International Journal of Mineral Processing*, *11*(2), 89–99.

Meloy, T., Clark, N., & Glista, J. J. (1986). Effect of density variations in heavy-media rougher-cleaner-scavenger cells circuit analysis. *International Journal of Mineral Processing*, *16*(34), 169–178.

Meloy, T., Whaley, D., & Williams, M. (1998). Flotation tree analysis reexamined. *International Journal of Mineral Processing*, *55*(1), 21–39.

Mendez, D. A., Galvez, E. D., & Cisternas, L. A. (2009). State of the art in the conceptual design of flotation circuits. *International Journal of Mineral Processing*, *90*(14), 1–15.

Miskovic, S. (2011). *An investigation of the gas dispersion properties of mechanical flotation cells: An in-situ approach.* Unpublished doctoral dissertation, Virginia Polytechnic Institute and State University.

Nageswararao, K., Wiseman, D., & Napier-Munn, T. (2004). Two empirical hydrocyclone models revisited. *Minerals Engineering*, *17*(5), 671–687.

Napier-Munn, T., & Lynch, A. (1992). The modelling and computer simulation of mineral treatment processes current status and future trends. *Minerals Engineering*, *5*(2), 143–167.

Noble, A. (2012). *Laboratory-scale analysis of energy-efficient froth flotation rotor design.* Unpublished master's thesis, Virginia Polytechnic Institute and State University.

Osborne, D. (1988a). *Coal preparation technology, volume 1.* Norwell, MA (USA); Kluwer Academic Publishers.

Osborne, D. (1988b). *Coal preparation technology, volume 2.* Norwell, MA (USA); Kluwer Academic Publishers.

Özyurt, D., & Pike, R. (2004). Theory and practice of simultaneous data reconciliation and gross error detection for chemical processes. *Computers & Chemical Engineering*, *28*(3), 381–402.

Poulter, S. (1993). Zinc flotation at rosebery - complex but not difficult. In *World zinc '93* (p. 6).

Pratten, S., Bensley, C., & Nicol, S. (1989). An evaluation of the flotation response of coals. *International Journal of Mineral Processing*, *27*(3), 243–262.

Reklaitis, G., & Schneider, D. (1983). *Introduction to material and energy balances*. Wiley.

Richardson, R. (2002). Jksimmet: A simulator for analysis, optimisation and design of comminution circuits. *Mineral Processing Plant Design, Practice, and Control Proceedings*, *1*, 442.

Rong, R. (1992). Optimization of complex coal preparation flowsheets. *International Journal of Mineral Processing*, *34*(12), 53–69.

Rong, R., & Lyman, G. (1985). Computational techniques for coal washery optimization-parallel gravity and flotation separation. *Coal Preparation*, *2*(1), 51–67.

Schena, G., Villeneuve, J., & Nol, Y. (1996). A method for a financially efficient design of cell-based flotation circuits. *International Journal of Mineral Processing*, *46*(12), 1–20.

Schena, G., Zanin, M., & Chiarandini, A. (1997). procedures for the automatic design of flotation networks. *International Journal of Mineral Processing*, *52*(23), 137–160.

Schulz, N. (1970). Separation efficiency. *Transactions*, *247*, 81.

Schwarz, S., & Alexander, D. (2006). Gas dispersion measurements in industrial flotation cells. *Minerals Engineering*, *19*(6-8), 554–560.

Sherrell, I. (2004). *Development of a flotation rate equation from first principles under turbulent flow conditions*. Unpublished doctoral dissertation.

Sosa-Blanco, C., Hodouin, D., Bazin, C., Lara-Valenzuela, C., & Salazar, J. (2000). Economic optimisation of a flotation plant through grinding circuit tuning. *Minerals Engineering*, *13*(1011), 999–1018.

Sripriya, R., Rao, P., & Choudhury, B. (2003). Optimisation of operating variables of fine coal flotation using a combination of modified flotation parameters and statistical techniques. *International Journal of Mineral Processing*, *68*(1), 109–127.

Stratford, K., & Napier-Munn, T. (1986). Functions for the mathematical representation of the partition curve for dense medium cyclones. In *Submitted to apcom symposium.*

Sutherland. (1948). Physical chemistry of flotation. xi. kinetics of the flotation process. *The Journal of Physical Chemistry*, *52*(2), 394–425.

Sutherland, D. (1981). A study on the optimization of the arrangement of flotation circuits. *International Journal of Mineral Processing*, *7*(4), 319–346.

Taggart, A., Behre, H., Breerwood, C., & Callow, J. (1945). *Handbook of mineral dressing, ores and industrial minerals.* Wiley.

Tao, D., Luttrell, G., & Yoon, R.-H. (2000). An experimental investigation on column flotation circuit configuration. *International Journal of Mineral Processing*, *60*(1), 37–56.

Tavera, F., Escudero, R., & Finch, J. (2001). Gas holdup in flotation columns: laboratory measurements. *International Journal of Mineral Processing*, *61*(1), 23–40.

Tjoa, I., & Biegler, L. (1991). Simultaneous strategies for data reconciliation and gross error detection of nonlinear systems. *Computers & Chemical Engineering*, *15*(10), 679–690.

Tomlinson, H., & Fleming, M. (1965). Flotation rate studies. In *International mineral processing congress* (Vol. 6, pp. 563–579).

Tromp, K. (1937). New methods of computing the washability of coals. *Colliery Guardian*, *154*, 955–959.

Vera, M., Mathe, Z., Franzidis, J., Harris, M., Manlapig, E., & O'Connor, C. (2002). The modelling of froth zone recovery in batch and continuously operated laboratory flotation cells. *International Journal of Mineral Processing*, *64*(2), 135–151.

Williams, M., Fuerstenau, D., & Meloy, T. (1986). Circuit analysisgeneral product equations for multifeed, multistage circuits containing variable selectivity functions. *International Journal of Mineral Processing*, *17*(12), 99–111.

Williams, M., & Meloy, T. (1983). Dynamic model of flotation cell banks circuit analysis. *International Journal of Mineral Processing*, *10*(2), 141–160.

Williams, M., & Meloy, T. (1989). On the definition and separation of fundamental process functions. *International Journal of Mineral Processing*, *26*(12), 65–72.

Williams, M., & Meloy, T. (1991). Feasible designs for separation networks: a selection technique. *International Journal of Mineral Processing*, *32*(34), 161–174.

Williams, M. C., Fuerstenau, D., & Meloy, T. (1992). A graph-theoretic approach to process plant design. *International Journal of Mineral Processing*, *36*(12), 1–8.

Wills, B., & Napier-Munn, T. (2006). *Wills' mineral processing technology: an introduction to the practical aspects of ore treatment and mineral recovery*. Butterworth-Heinemann.

Yingling. (1988). *Optimum synthesis of probabilistically-governed separation system with applications to mineral processing circuits*. Unpublished doctoral dissertation, University of Pittsburgh.

Yingling. (1990). Circuit analysis: optimizing mineral processing flowsheet layouts and steady state control specifications. *International Journal of Mineral Processing*, *29*(34), 149–174.

Yingling. (1993a). Parameter and configuration optimization of flotation circuits, part i. a review of prior work. *International Journal of Mineral Processing*, *38*(12), 21–40.

Yingling. (1993b). Parameter and configuration optimization of flotation circuits, part ii. a new approach. *International Journal of Mineral Processing*, *38*(12), 41–66.

Yoon, R., & Mao, L. (1996). Application of extended dlvo theory, iv:: Derivation of flotation rate equation from first principles. *Journal of Colloid and Interface Science*, *181*(2), 613–626.

Yoon, R., & Wang, L. (2007). Hydrophobic forces in foam films. *Colloid Stability*, 161–186.

Chapter 3

Development of a Flotation Circuit Simulator Based on Reactor Kinetics

(ABSTRACT)

A robust and user-friendly flotation simulation software package (*FLoatSim*) was developed to provide a numerical approach to flotation circuit design. This simulation software incorporates a unique four-reactor modeling paradigm which considers rate-based pulp recovery, non-selective froth recovery, partition-based entrainment recovery, and physical carrying capacity limitations. Each of the four sub-models are defined by well-published and industry-accepted principles. The final software package includes two data analysis and parameter estimation modules which extract information from batch or continuous flow testing. The resulting data is imported into the primary simulation program, which provides flowsheet construction tools, unique calculation algorithms, and stream legend data visualization. This chapter describes the modeling approach, simulation strategy, and software user interface development. A final case study is presented and analyzed to demonstrate the software's applicability to a coal flotation scale-up problem.

3.1 Introduction

Currently, process modeling and circuit simulation are the most common engineering tools used during the circuit design process. When well formulated and appropriately used, models and simulations can predict ultimate circuit performance as a function of various operational inputs. This capability supports a trial-and-error design approach, where the

circuit designer can propose a potential circuit solution (often from prior experience) and then use the simulator to evaluate the final performance. If this performance is inadequate, other potential solutions may then be proposed and simulated. While labor intensive, this approach provides tangible performance criteria (i.e. circuit recovery, grade) by which the circuit designer can base a final decision.

While often used analogously, the terms *modeling* and *simulation* distinctively refer to two independent but related tasks. Modeling denotes the act of describing physical processes via mathematical equations, while simulation signifies the act of solving the model equations to predict future performance. The aptitude of a given process model is most readily described by the model's *fidelity*. In general, fidelity refers to the ability of a model to successfully portray real physical systems. In mineral processing, the model fidelity is often described as empirical, phenomenological, or theoretical, with higher fidelity reflecting increased knowledge of the relevant physical subprocesses (See Chapter 2.2).

Alternatively, the aptitude of a simulation is driven by resolution. For mineral processing simulations, resolution is analogously described as the level of data *discretization*. Process models often relate separation performance to the physical properties of the system's particles. Since the actual properties of every particle include an infinite range of continuous values, simulations often lump similar particles into a finite number of particle classes. The model equations are then solved for each class of particle rather than for each particle independently. This truncation introduces systemic error which is inversely proportional to the resolution or number of particle classes. A greater number of particle classes will generally produce a more realistic simulation, in the same way that a photograph with a higher number of pixels will produce a clearer image. *Discretization* is the decision of how these particle classes may be formed while balancing the computational efficiency, data availability, and systemic error.

This chapter describes the development of a robust froth flotation circuit simulation software package (*FLoatSim*). The software includes a kinetics-based flotation model, suitable for scaling laboratory and plant data to full-scale user-defined circuits. This model uses a novel four-reactor framework, while incorporating widely-published and industry-accepted subprocess models. The software provides tools to optimize and scale these these models for case-specific flotation systems through laboratory testing. This chapter describes the model theory, simulation theory, and software interface unique to the FLoatSim simulator. The approach is in the section is largely deductive. The holistic framework and global models are described first, while the proceeding discussions focus on the constituent components and sub-models.

3.2 Modeling Theory

3.2.1 Overall Recovery

The FLoatSim software uses a unique four-reactor flotation model framework was generated which combines industry-accepted rate models, partition models, and physical restrictions. The overriding assumption in this paradigm is that four predominant factors contribute to flotation recovery: pulp recovery, froth recovery, entrainment, and carrying capacity. In the FLoatSim model, these factors (with the exception of carrying capacity) have been modeled independently. Small changes in the value of one factor do not directly influence the value of the other two. Nevertheless, indirect influences may persist due to the nature of the carrying capacity model (i.e. increased pulp recovery may cause the overall recovery to exceed the carrying capacity limitation, which would, in-turn, cause a reduction of froth recovery).

The interdependence of these four reactors is shown schematically in Figure 3.1. Material recovered from the pulp reports to the froth and is then eligible for recovery to final concentrate. Material not recovered in the froth is returned to the pulp feed and may be recovered or rejected from the pulp. The pulp tailings reports to the entrainment reactor. Material recovered via entrainment bypasses the froth stage and is eligible for direct recovery to the final concentrate. Material rejected in the entrainment reactor reports to the final tailings. All material recovered from the froth and entrainment reactors is finally subjected to the carrying capacity restriction. This reactor imposes a maximum achievable concentrate flow rate. Material recovered in excess of this restriction is returned to the flotation cell feed. From a modeling perspective, the froth and pulp reactors are represented by rate models, the entrainment reactor is represented by a partition model, and the carrying capacity is a conditional restriction.

Using this serial arrangement of unit reactors, the analytical expression for recovery to final concentrate (R_{Final}) is derived as a function of pulp recovery (R_p), froth recovery (R_f), and entrainment recovery (E):

$$R_{Final} = \frac{R_f R_p (1 - E)}{1 - (1 - R_f) R_p} + E. \tag{3.1}$$

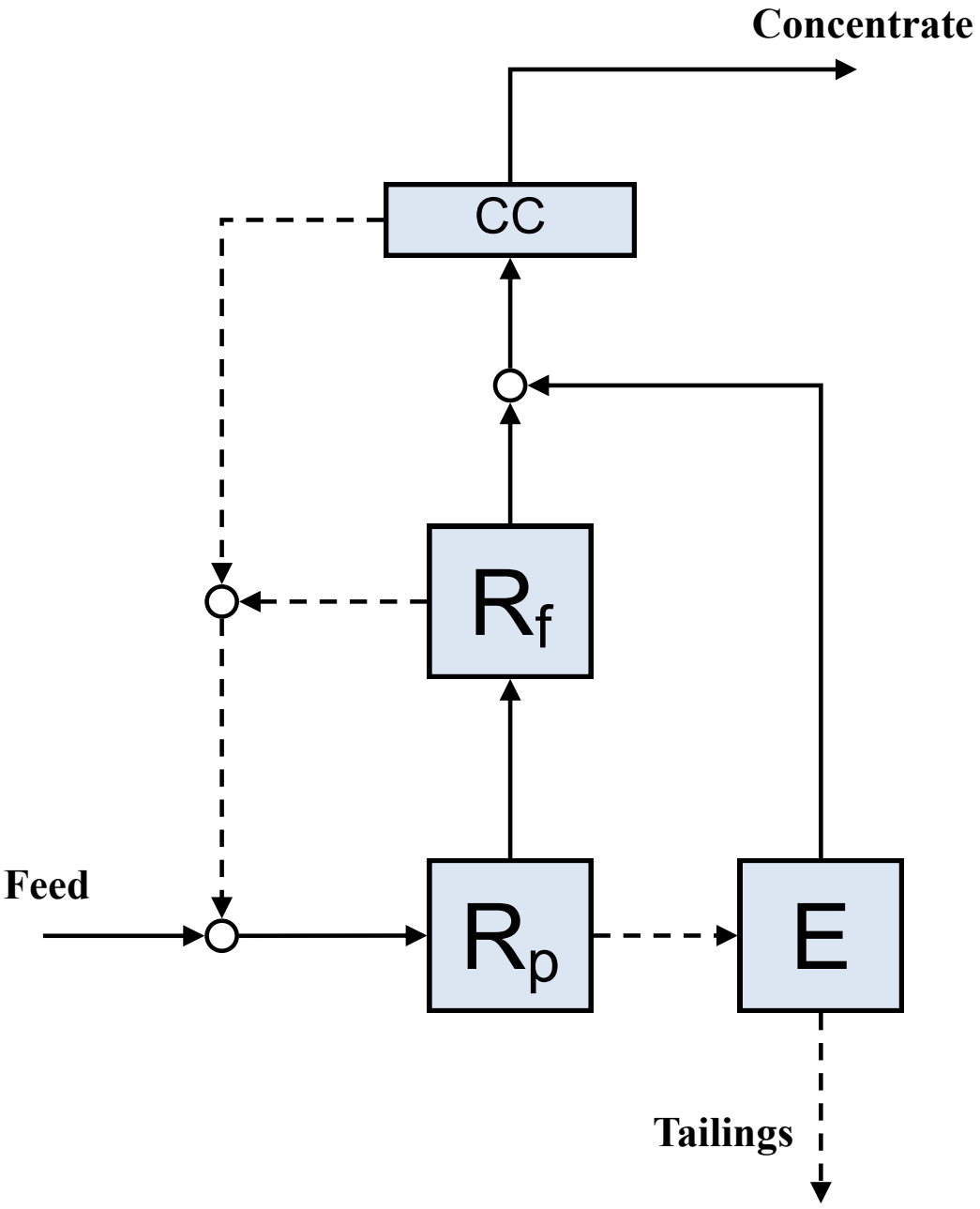

Figure 3.1: Four Reactor Flotation Model Schematic.

3.2.2 Carrying Capacity

In real flotation cells, physical limitations, such as the carrying capacity, may prevent the flotation cell from achieving the recovery value calculated in Equation 3.1. Carrying capacity (CC) is the maximum concentrate mass flow rate (i.e. tonnes per hour) and is theoretically a function of the cell's gas flow rate (Q_g), the particle size (D_p), the bubble size (D_b), and a bubble-particle packing efficiency (β). When the expression is simplified, the theoretical maximum carrying capacity is also function of the bubble surface area flux (S_b) and the particle density (ρ):

$$CC_{Theoretical} = \frac{4Q_g D_p \beta}{D_b} = (2/3) S_b D_p \rho \beta. \tag{3.2}$$

Pragmatically, other factors, such as the froth removal rate, total froth surface area, and the cell's weir lip length also factor into the maximum carrying capacity. In the FLoatSim software, the carrying capacity is calculated from a user-specified unit carrying capacity value (tonnes per hour of concentrate per square meter of froth area). This number is highly application specific, given the effect of particle size and density on carrying capacity (Equation 3.2). Empirical relationships or prior process knowledge define this value for a given simulation.

Once the unit carrying capacity and the cell dimensions are defined, the total carrying capacity (CC, given in tonnes per hour of concentrate) is calculated. This number is then compared to the total mass flow of concentrate ($R_{Final} * Feed$) for all flotation classes (i):

$$\sum_{i=1}^{N} R_{Final,i} * Feed_i \leq CC \tag{3.3}$$

If the normal cell recovery exceeds the carrying capacity limitation, the recovery must be reduced until the restriction is met. This reduction is assumed to take place in the froth. Namely, the froth recovery (described in Section 3.2.4) is incrementally reduced until the carrying capacity restriction is met. The FLoatSim software uses a non-trivial matrix application of Newton's method to solve the froth recovery value which forces the total recovery (summed from each particle class) to be equal to the carrying capacity restriction. Since froth recovery is inherently non-selective, the reduction due to froth recovery is also non-selective.

3.2.3 Pulp Recovery

Pulp recovery (often distinguished as *true recovery*) represents the fraction of material which is transported from the pulp to the froth via bubble-particle attachment. As described in Chapter 2.2.3, the recovery of particles in a flotation cell is generally accepted to be a rate-based process and is modeled analogously to a chemical reaction. Traditional flotation models use the plug-flow model to describe the batch cell and the perfectly-mixed model to describe the industrial cell. However, recent trends have shown drastic increases in the size of industrial flotation cells (Noble, 2012). Larger flotation cells tend to deviate (sometimes catastrophically) from perfectly-mixed behavior, especially as the cell's power intensity (kW/m^3) is reduced. Consequently, the perfectly-mixed assumption used in traditional flotation models may not be appropriate for contemporary large commercial flotation cells.

To account for deviations from the perfectly-mixed assumptions, Levenspiel's (1999) axially dispersed reactor model for intermediate flows is utilized in the FLoatSim model. This model uses the Peclet number (Pe) as an indicator of tank mixing. Residence time studies are required to derive the Peclet number, and typical values for large conventional cells range from 1 to 4 (smaller Peclet numbers indicate that a tank is more well-mixed). Once the Peclet number is known for a given cell, the pulp recovery (R_p) for a given mineral class may be calculated from the cell residence time (τ) and the mineral's kinetic coefficient (k):

$$R_p = 1 - \frac{4A\exp\{Pe/2\}}{(1+A)^2\exp\{(A/2)Pe\} - (1-A)^2\exp\{(-A/2)Pe\}} \tag{3.4}$$

$$A = \sqrt{1 + 4k_p\tau/Pe}.$$

The FLoatSim flotation model utilizes laboratory data to predict full-scale performance. To account for changes in the bubble surface area flux (S_b) between the two scales, the kinetic coefficient determined from laboratory testing (k_{lab}) is scaled by a user-defined S_b ratio prior to being used in Equation 3.4:

$$k_p = k_{lab}\left(\frac{S_{b-FullScale}}{S_{b-LabScale}}\right). \tag{3.5}$$

Flotation residence time is determined by the calculated feed rate (Q_{Feed}). This approach typically produces a conservative solution as opposed to using the flow rate of the

tailings. The overall cell volume (V_{Total}) is de-rated to account for the user-defined air holdup (ε):

$$\tau_p = \frac{V_{Total}(1-\varepsilon)}{Q_{Feed}}. \tag{3.6}$$

3.2.4 Froth Recovery

Froth recovery (often inversely described as froth drop-back) is the portion of material previously recovered from the pulp phase which ultimately survives the froth phase and is recovered to the final concentrate. Many researchers have described froth recovery (R_f) with a plug-flow reactor model (e.g., Gorain, Harris, Franzidis, & Manlapig, 1998; Mathe, Harris, O'Connor, & Franzidis, 1998; Yianatos, Bergh, & Cortes, 1998; Vera, Franzidis, & Manlapig, 1999; Vera et al., 2002; Yianatos, Moys, Contreras, & Villanueva, 2008):

$$R_f = \exp(-k_{DB}\tau_f) \tag{3.7}$$

where k_{DB} is the rate of froth drop-back, and τ_f is the froth residence time. While most researchers agree on the functional form, much debate has surrounded the calculation of k_{DB} and τ_f.

Repeated experimental evidence has shown that k_{DB} is the same for all mineral classes in a flotation system (Yianatos et al., 2008). Consequently, froth recovery is described as a non-selective process. Simply, all minerals classes, regardless of hydrophobicity or pulp recovery rate are expelled from the froth at the same rate.

Most contemporary flotation models use one of two methods to define froth residence time. The first method describes froth residence time to be proportional to the superficial gas rate and the froth height ($\tau_f = H/J_g$) (Gorain et al., 1998); whereas, the second method uses the ratio between the froth volume and volumetric flow of concentrate ($\tau_f = V_f/Q_c$) (Vera et al., 2002). While the latter option produces a better fit to experimental data, it requires knowledge of the concentrate flow rate. For simulation purposes, this value is difficult to predict without first knowing the froth recovery and the water recovery. While these values are known in cell diagnostic studies, accurate simulation would require former knowledge of the anticipated solution, thus eliminating the need for simulation altogether. Alternatively, the former calculation ($\tau_f = H/J_g$) includes values which are known prior to simulation.

To allow different calculations of the froth recovery, the current FLoatSim model includes froth recovery as a direct input to the simulation. Nevertheless, to coincide with the appropriate functional form, the inputted value is scaled according to the inputting S_b ratio,

which reflects the dependence of froth residence time on gas flow rate. Using the plug-flow model, the S_b adjusted froth recovery rate ($R_{f,Adj}$) is calculated:

$$R_{f,Adj} = \exp\left\{(-k_{DB}\tau_f)\left(\frac{1}{SBR}\right)\right\}. \tag{3.8}$$

Since the original froth recovery is an input to the simulation, k_{DB} and τ_f are not known explicitly. Rather, the combined parameter ($k_{DB}\tau_f$) may be calculated from the inputted froth recovery ($R_{f,Input}$) by mathematically manipulating Equation 3.7:

$$(k_{DB}\tau_f) = \ln[R_{f,Input}]. \tag{3.9}$$

By substituting, the combined value of ($k_{DB}\tau_f$) calculated in Equation 3.8 into Equation 3.9, the simplified calculation for $R_{f,Adj}$ is produced. FLoatSim uses this equation to calculate the ultimate froth recovery from the inputted values $R_{f,Input}$ and SBR:

$$R_{f,Adj} = \exp\left\{\ln\left[R_{f,Input}\right]\left(\frac{1}{SBR}\right)\right\}. \tag{3.10}$$

3.2.5 Entrainment and Water Recovery

Entrainment is a non-selective recovery mechanism whereby particles which are not attached to air bubbles are carried into the concentrate by the flow of water. Given their reduced inertial resistance, low density and fine particles have a much higher susceptibility to entrainment. Recovery via entrainment (E) is known to be proportional to the recovery of water (R_{Water}) and a degree of entrainment factor (DoE) (Vianna, 2011):

$$E = R_{Water}DoE. \tag{3.11}$$

In the FLoatSim simulator, the DoE factor is determined by size class from the laboratory kinetics testing or a user-defined value may be specified. Given the aforementioned theory, this factor is expected to decrease as particle size increases.

The water recovery is determined using a two-reactor model similar to the four-reactor particle recovery model (Figure 3.1) with the omission of the entrainment reactor (i.e. water cannot be "entrained" to the concentrate) and the carrying capacity restriction. Water recovery from the two-reactor model may be calculated from the water pulp recovery (R_p) and the water froth recovery (R_f):

$$R_{Water} = \frac{R_f R_p}{1-(1-R_f)R_p}. \tag{3.12}$$

Equation 3.1 reduces to Equation 3.12 when $E = 0$. The water pulp recovery and water froth recovery are calculated by the same methodology used for particle recovery (Equation 3.4 and Equation 3.9). The kinetic coefficient for water recovery may be determined from a laboratory batch flotation test which tracks the mass recovery of water along with the particle recovery.

3.3 Simulation Theory

3.3.1 Model Discretization

In order to solve the model equations as a circuit simulation, three aspects of the simulation methodology must be established: the degree of model discretization, the model parameters, and the calculation strategy. As mentioned above, discretization directly refers to simulation resolution. The models presented in the prior section only apply to individual particles with identical physical properties and kinetic coefficients. To solve these equations, the particles must be grouped into a finite number of classes, with each class representing a group of particles which behave similarly. The number and type of flotation classes must balance the data limitations and the desired simulation accuracy. A larger number of classes will produce a more realistic simulation; however, more extensive data must be acquired and analyzed.

By default, the FLoatSim simulator incorporates three dimensions of discretization. Each dimension correlates to a parameter which is known to influence flotation performance and has values that can be easily identified in laboratory analysis. Each dimension has a standard resolution limit within the FLoatSim software:

1. *Particle Size.* Size-by-size analysis of batch flotation data shows that particles of different size classes generally float at different rates. This observation is especially true for particles less than 10 microns and greater than 200 microns. Additionally, small particles less than 10 microns will witness a significantly increased degree of entrainment. FLoatSim allows up to 10 particle classes.

2. *Mineral Type.* In multicomponent flotation systems, particles of different mineral types are known float at different rates. For example, in a three component system consisting of chalcopyrite, molybdenite, and gangue, a different set of kinetic coefficients should be determined for each of the three components. FLoatSim allows up to 4 valuable mineral classes with an ever-present "other" gangue class.

3. *Floatability Class.* Particles of the same mineral type and size class still exhibit slight variations in flotation rate due to numerous known and unknown factors (collector adsorption, particle shape, degree of oxidation, etc.). To retain simplicity, all of these factors are generally lumped into a single discretization class known as floatability. FLoatSim allows up to three floatability classes which are given the generic designations fast-floating, slow-floating, and non-floating.

Each discretized element (e.g. 35 micron fast floating chalcopyrite) is characterized by its mass percent of the total feed and a pulp kinetic coefficient. These values are determined through the data fitting of the laboratory testing. Other means (e.g. QEMSEM) may be applied but are not included in the default FLoatSim package. The grade of the discretized element is determined by the mineral type, and the degree of entrainment is identical for all classes of a similar particle size. The froth recovery is identical for all particles, thus invoking the non-selective assumption for froth drop-back.

3.3.2 Model Fitting and Parameter Estimation

After the data discretization strategy has been identified, the kinetic coefficients and mass proportions must be determined for the flotation system under inspection. These parameters are best estimated from batch kinetics tests conducted with feed material and chemical dosages which most closely resemble the expected plant conditions. The batch kinetics test with mass balanced size-by-size recovery, grade, and water recovery data as a function of time may be used to establish all of the parameters needed for a plant simulation. The software package includes a laboratory data fitting module (*LabDataFitting*) which estimates the kinetic and mass proportion parameters by weighted sum-of-the-squared-error minimization between the experimental data and a plug-flow reactor model applicable for batch systems. Recovery between the various classes is summed and used with the experimental grade data to determine the mass proportions of the various mineral and floatability classes.

Continuous flow data (full-scale, pilot-scale and locked-cycle testing) may be used additionally or alternatively to batch kinetics data. The FLoatSim *PlantDataFitting* module estimates the kinetic parameters from mass balanced plant data and equipment operating conditions (cell volume, cell Peclet number, etc.). Similar to the lab data fit, this module minimizes the weighted sum-of-the-squared errors between the experimental data and the full-scale, four-reactor flotation cell model described in the prior section (Equation 3.1).

While full-scale and pilot-scale data minimize scaling uncertainty, they are often derived from tests conducted at a single residence time or plant operating point. This lack of time-dependent data decreases the amount of available information used to fit the models. As a result, the validity of the model decreases rapidly as the simulations deviate from the tested residence time (See Section 4. Furthermore, additional mineralogical data or assumptions on the floatability class distribution must be invoked in order to properly determine the mass proportions of the discretized elements. In the absence of this information, the data fit may only be used to determine the kinetic coefficients for a single composite rate class. Simulations conducted solely with these data sets must be carefully considered, given the various sources of model uncertainty.

Material in a batch flotation cell often floats much quicker than similar material in an industrial cell. While various scaling factors (energy dissipation, froth volume, and gas rate) contribute to this difference, the simple difference in reactor type cannot be understated. As shown in Figure 2.5, the plug-flow reactor shows considerably elevated recovery values within the typical operating region of 2 to 6 $k\tau$ units. To further illustrate this point, Figure 3.2 shows recovery for batch and continuous flotation tests conducted under similar conditions (Noble, 2012). In these test, all operational parameters (material type, energy intensity, cell dimensions, froth height, and chemical dosage) were held constant, while only varying the reactor type and superficial gas rate. The data from the batch test was used to fit a plug-flow model, and the derived kinetic parameters were then used to predict the continuous performance via a perfectly-mixed model (the energy intensity of the small cell was sufficient to justify this assumption as opposed to an intermediate flow model). The results show good agreement, and more importantly that in some cases, a five-fold increase in residence time may be required to produce batch-derived recovery in a continuous cell (see residence time required to achieve 70% recovery: 1.8 minutes in batch cell, 9.9 minutes in continuous cell).

3.3.3 Calculation Strategy

After the specific models have been built from experimental data, simulations may finally be conducted to determine how user-specified operational and equipment conditions (i.e. feed rate, water addition, gas rate, circuit arrangement, equipment specifications) influence the plant's final recovery and grade. The models presented in the preceding sections are only applicable to a single cell. During simulation, these model calculations are extended so that the predictions are applicable for a circuit of interconnected and interdependent unit cells.

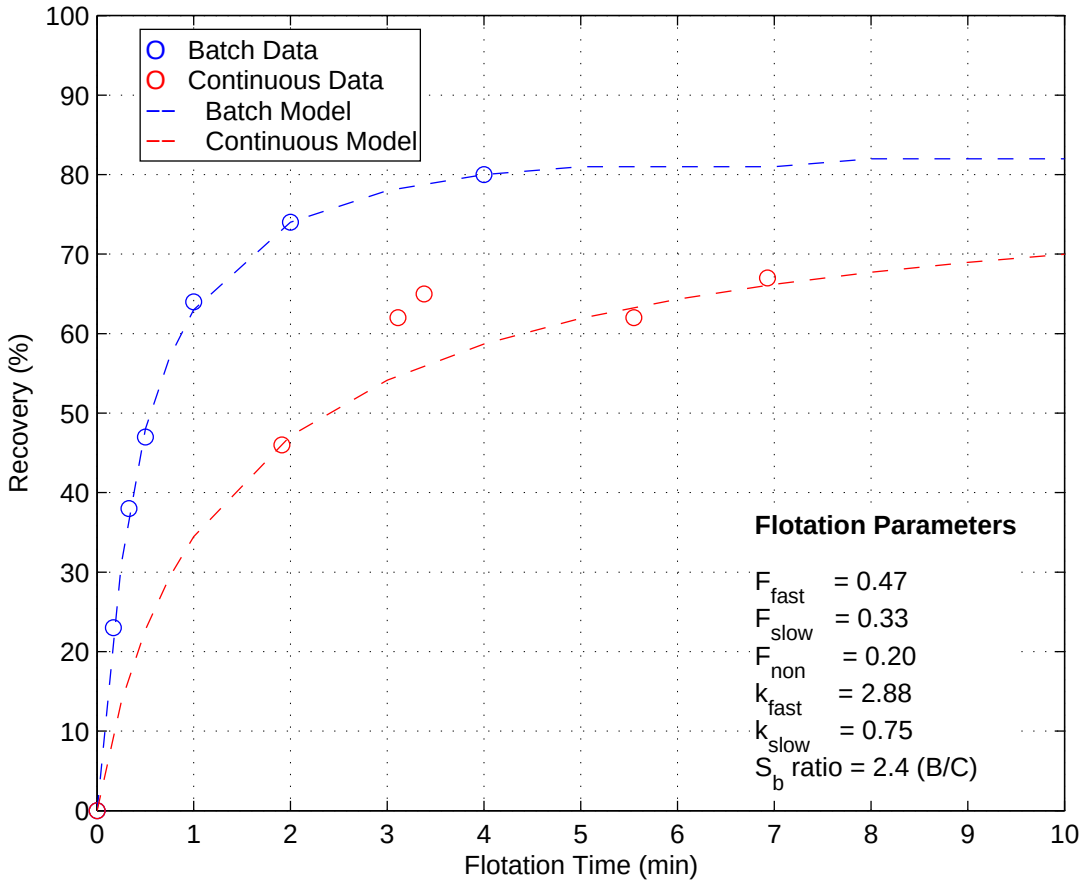

Figure 3.2: Comparison of data collected from batch and continuous flotation testing. Parameter optimization was used to fit experimental batch test data to a plug-flow model. Derived kinetic coefficients were then implemented into a perfectly-mixed equation to form continuous model. Parameters of the model fit are shown. Data after (Noble, 2012).

The calculation approach used in FLoatSim is sequential modular with iteration. The simulation begins with the specified feed conditions and passes that information to the first unit. The operational parameters and established models unique to that unit are used to determine the recovery to concentrate and the rejection to tailings for each discretized element. Those data are sent to the downstream units, and the calculations are repeated. If recycle streams are present, the simulation iterates until a stable steady-state is reached. After the first iteration, the recycle streams are determined and the flowsheet is reevaluated with considerations from the updated values. This procedure is then repeated until a desired threshold is established. An simple example of the sequential modular iteration algorithm is shown in Figure 3.3.

The error associated with an iterative circuit solution is governed by the number of iterations and the circuit complexity. For a given circuit, the simulation error is reduced exponential by increasing the number of iterations. Furthermore, as the complexity of the circuit increases, the number of iterations required to achieved a desired accuracy increases. An example of this principle is shown in Figure 3.4. The circuits under consideration in this example are simple counter-current cleaner configurations of a designated size (two to five units). The concentrate from each unit passes serially to the next, while the tailings pass to the prior unit. Final circuit concentrate is produced from the concentrate of the final cell, while the final circuit tailings are produced from the tailings of the first cell.

3.4 Software Development and User Interface

3.4.1 Overall Simulation Work Flow

The FLoatSim software suite includes a graphic interface which permits user-defined circuit configurations, the flotation models and simulation routines, as well as two supplementary data fitting modules for laboratory and pilot-scale data analysis. All of the software has been implemented as a subset to the Microsoft Excel platform. FLoatSim uses many of Excel's native functions and capabilities, while the models and graphical user interface have been embedded using the Visual Basic for Applications (VBA) programming language. The ubiquity of Excel's interface minimizes user startup time and provides a number of familiar analytical tools (i.e. plotting, data comparison, etc.), while minimizing development time and new programming requirements. Furthermore, the VBA language easily allows the implementation of new or user-defined models. VBA's inherent simplicity extends this feature to users with little or no programming experience.

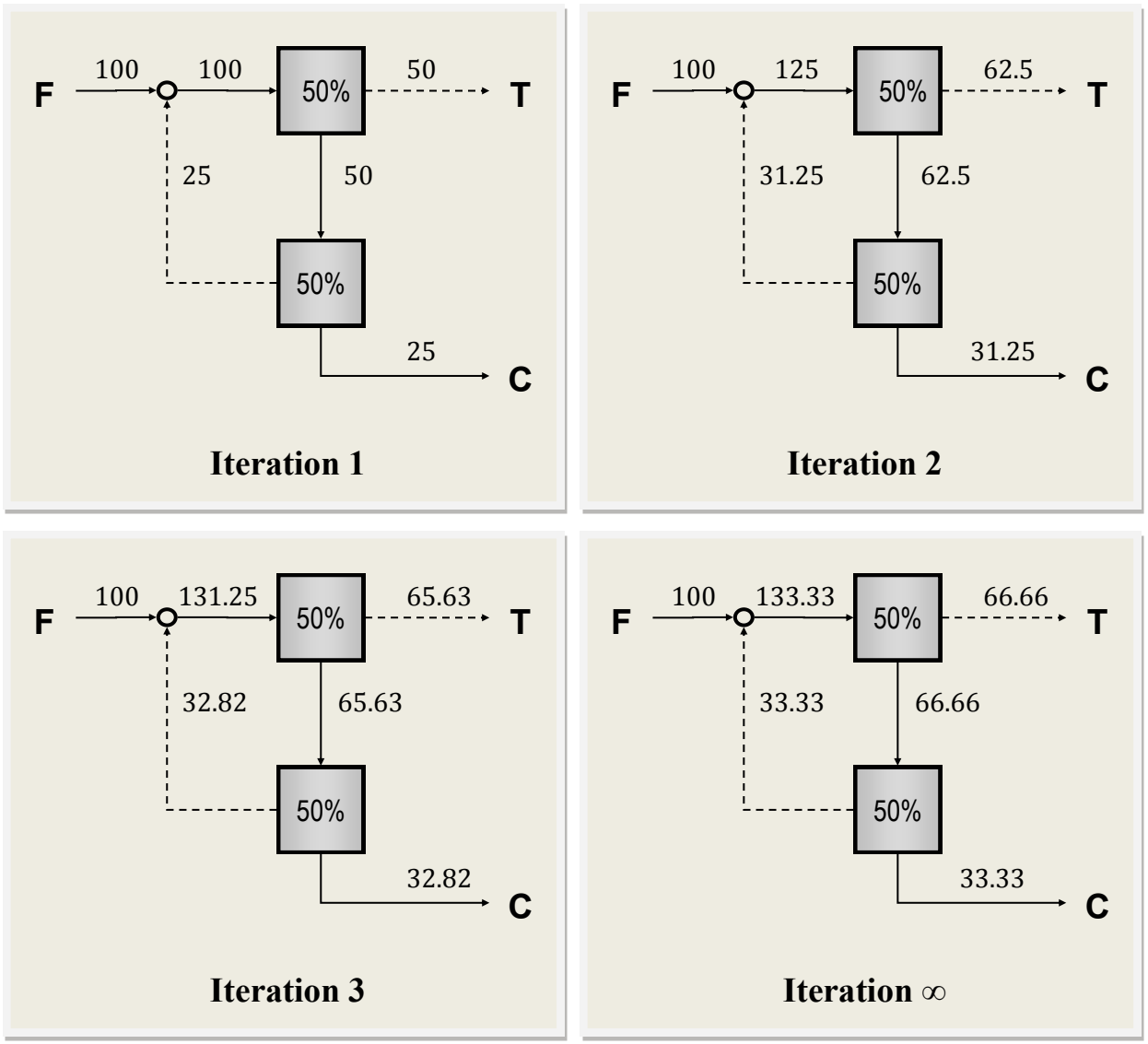

Figure 3.3: Example of sequential modular iteration calculation for a two-unit cleaner circuit.

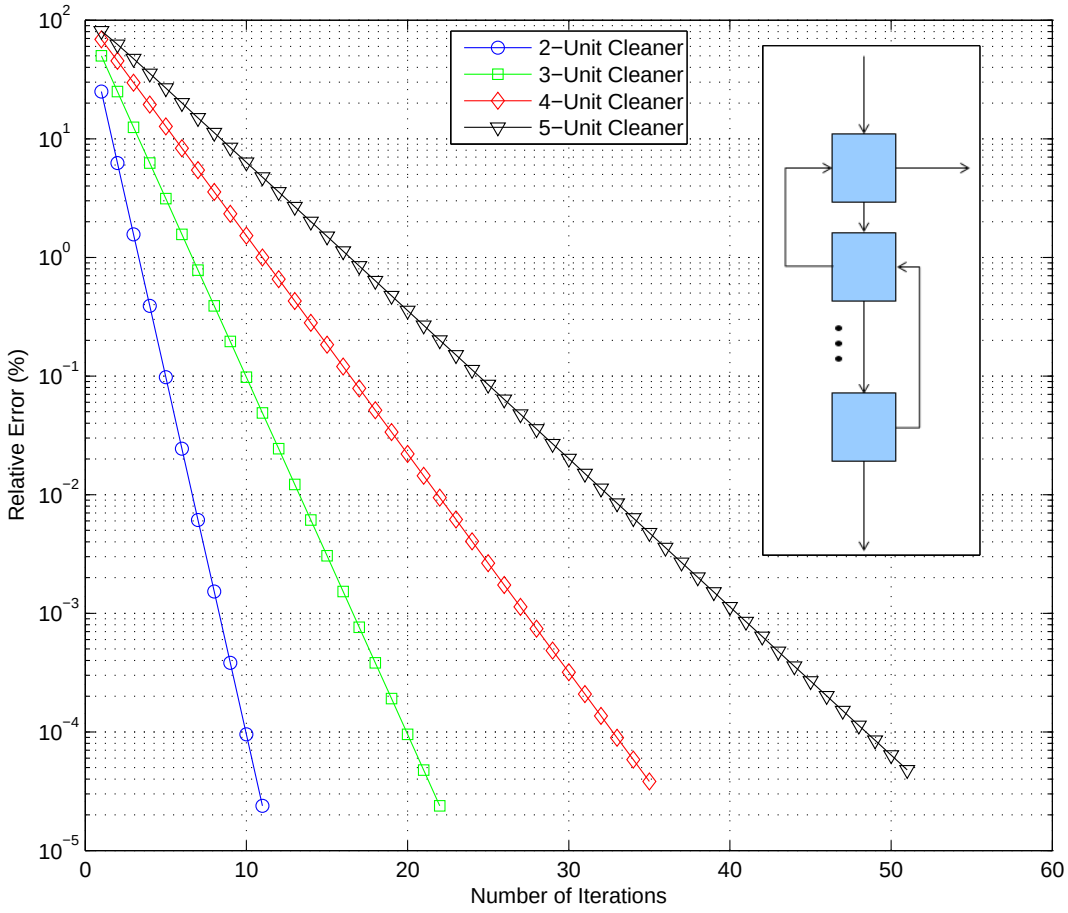

Figure 3.4: Iterative calculation error plotted against number of iterations for circuits of varying complexity. Relative error is defined as the percent difference between the solution at the given iteration level and the ultimate analytical solution. Different data series correspond to cleaner circuits of different sizes.

Figure 3.5 shows the overall work-flow diagram describing the generic simulation approach utilized by the FLoatSim software. The start terminator segregates into three process paths: one which analyzes and synthesizes the experimental data, one which defines the operational parameters, and one which specifies the equipment. These three paths reunite to define the flotation models immediately prior to the simulation. The simulation steps which are enclosed in the dashed rectangles are part of FLoatSim's standard analytical tools, either by the data fitting modules (blue) or the simulation package (red). The data analysis process path (the right side) is significantly more complex than the other two, given the various data types and analysis steps required. This complexity gives rise to the data analysis modules which use FLoatSim's model library to predict flotation rates from laboratory, pilot, full-scale, or locked-cycle data. The FLoatSim suite also includes standard import and export data features (depicted as green arrows in Figure 3.5). The data import function retrieves kinetic and mass parameters from the laboratory fitting module, while the data export function produces a summary of user-specified simulation outputs.

3.4.2 Data Fitting Software

The FLoatSim software suite includes two data fitting modules which provide a standard methodology for data acquisition and analysis: *RateFittingLab* and *RateFittingPlant*. These modules interface with the modeling and simulation routines to allow quick data import and export. Since the procedures for laboratory kinetics testing are fairly standardized, the data analysis for the RateFittingLab module benefit from a straightforward interface. Figure 3.6 shows the workspace for this module.

To ensure the most valid and scalable kinetic coefficients, the batch flotation test should be carefully planned and conducted. The chemical conditions and feed material used in the test must closely mimic the expectations of the full-scale plant. If a paddle is used to pull froth from the cell, the froth pull rate should remain constant throughout the test, even as the froth volume lessens in the latter stages. A steady pull rate may be verified by analyzing the water recovery versus time plot. Since water is a single component, the results should show that the same rate adequately predicts recovery throughout the entire test. The identification of multiple water rates is usually an indication that the pull rate was not constant throughout the test. Finally, if a paddle is used, only froth should be pulled by the paddle. If the paddle pulls pulp along with the froth, the test data will overestimate entrainment. As water is removed from the cell, fresh water must be added to maintain a constant level. The amount of water added should be monitored and recorded to properly determine the final water recovery.

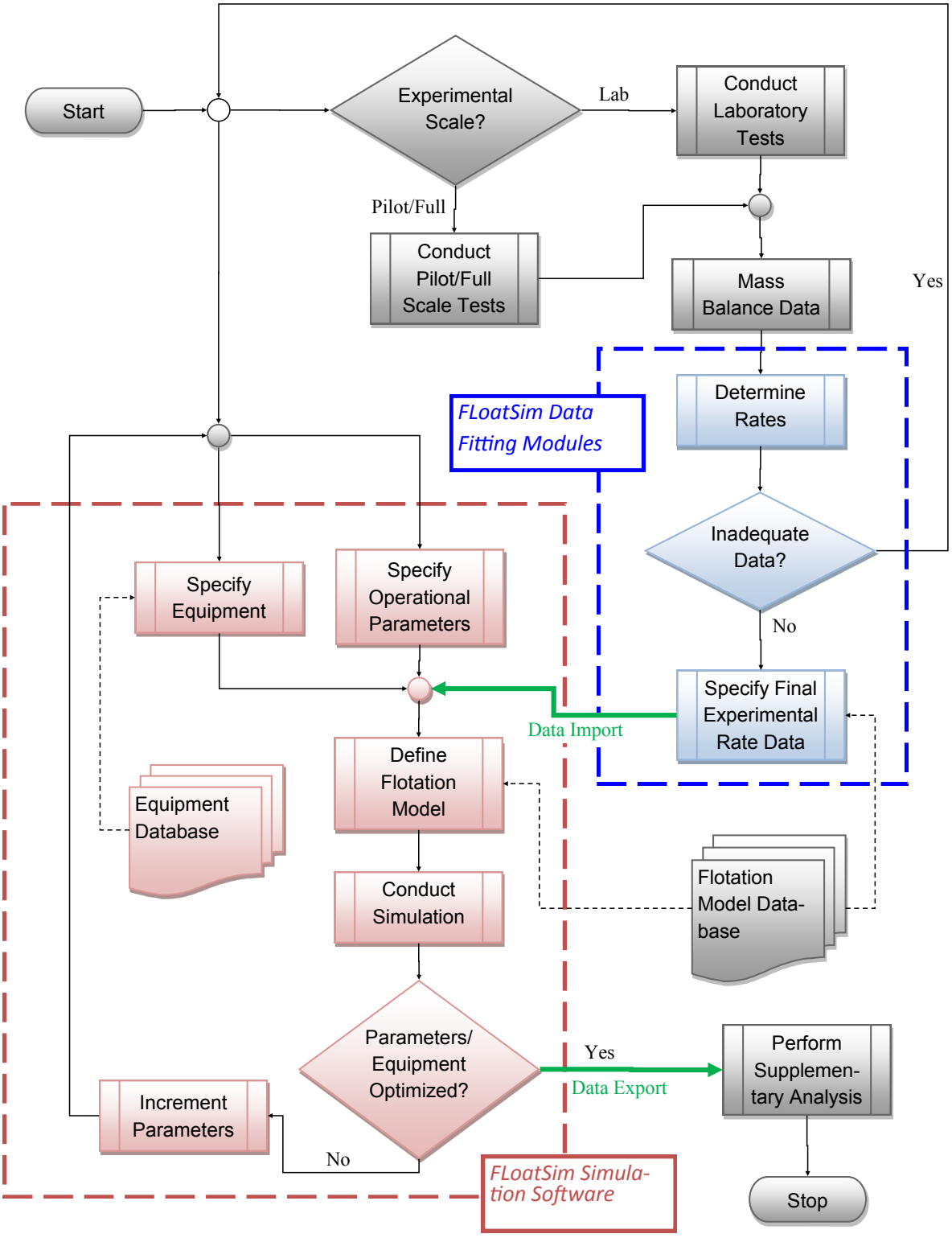

Figure 3.5: FLoatSim software suite work-flow diagram.

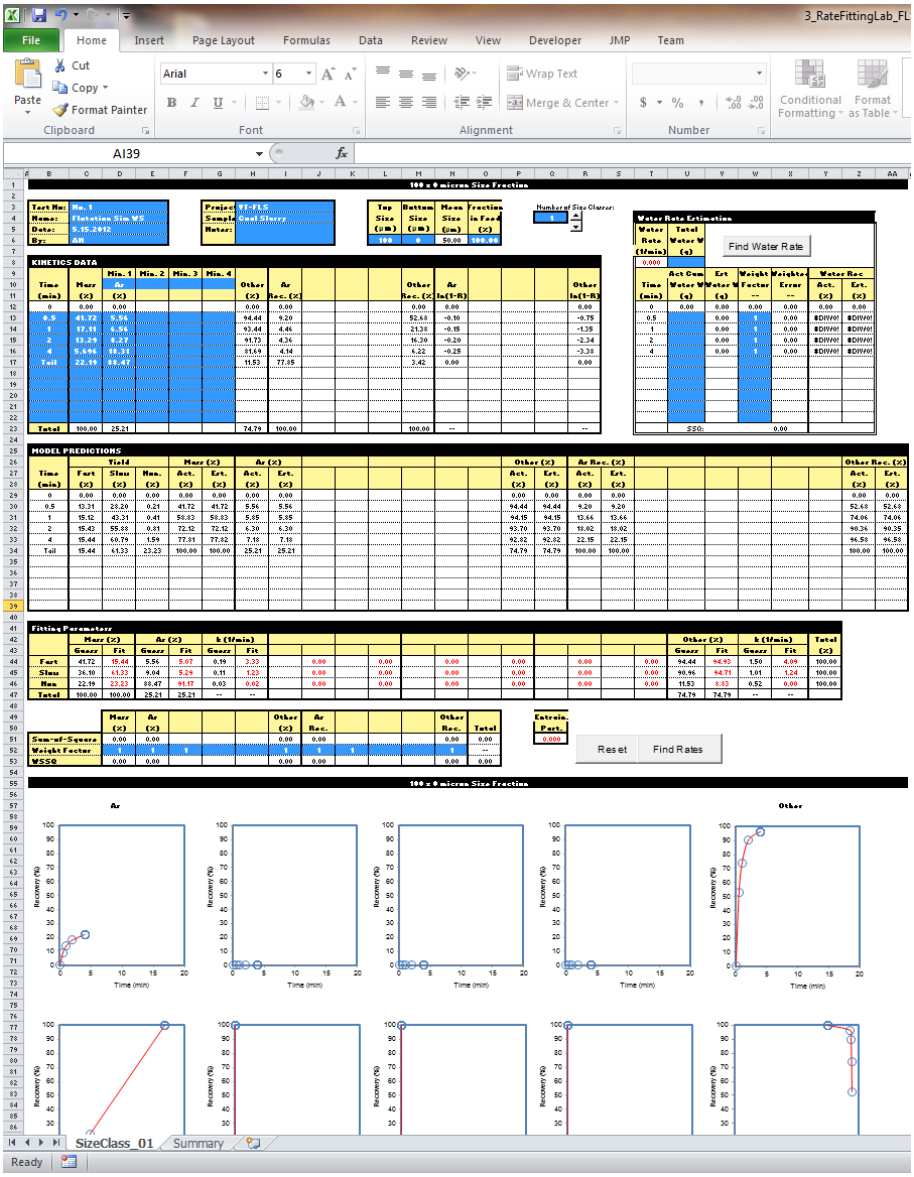

Figure 3.6: FLoatSim RateFittingLab workspace.

The best data sets will track the water recovery and take advantage of size-by-size analysis. Since particle size is known to influence bubble-particle collision rates and entrainment susceptibility, more particle size classes will inherently produce more accurate simulations. The FLoatSim software has been designed to accommodate up to ten size classes. While simulations can be conducted with just one size class, at least three (fine, medium, and large) should properly account for entrainment effects in most flotation systems. The water recovery data can be used to predict entrainment in the lab test as well as the final water recovery for the plant.

Assays from experimental data usually indicate elemental assays (e.g. %Cu); however, flotation behavior is largely driven by mineral components. Particulate chalcopyrite, rather than elemental copper is recovered in a flotation cell. Mineralogical information, unique to the flotation system under inspection, must be known in order to convert elemental assays to mineral assays. FLoatSim has been designed to accept non-stoichiometric mineral formulas (e.g. Fe2.5S3.7) as a means to account for multi-mineral, similar element systems. For example, a flotation system may be known to contain three copper bearing minerals: chalcocite (Cu_2S), chalcopyrite ($CuFeS_2$), and cuprite (Cu_2O). The most accurate simulations would track the flotation rate for each of these minerals separately. Unfortunately, such a simulation would require mineralogical data for each time interval of the batch test in order to distinguish the elemental copper assay into each of the constituent minerals. Conversely, if the mineralogical distribution of the feed is known, the user may make a simplifying assumption and lump all of these copper-bearing minerals into a single hypothetical copper mineral that has non-stoichiometric element coefficients and floats at a single rate. Obviously, this approach introduces a simplifying assumption with may reduce the simulation's validity, but few reliable and efficient alternative approaches exist, beyond time-dependent mineralogical analysis.

The RateFittingPlant module is used to interpret and analyze data collected from continuous flow tests, including pilot plants, full-scale plants, and locked cycle tests. The data from these tests are usually collected at a single residence time, unlike batch kinetics data which is collected at a range of flotation times. Consequently, the derived rate data is only valid for a narrow operating range around the tested residence time. Furthermore, the single data point derived from continuous flow tests is not sufficient to meaningfully fit floatability class distributions. Without introducing an assumed distribution, the RateFittingPlant module can only fit rates for a single class (e.g. fast floating with no slow or non-floating components).

Since the experimental procedure and circuit arrangements vary considerably between

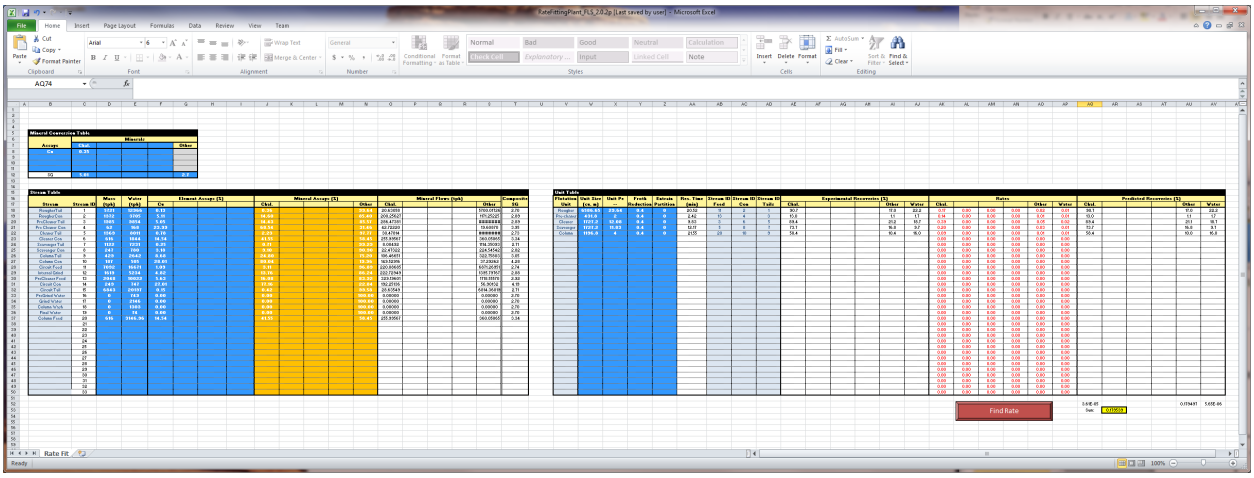

Figure 3.7: FLoatSim RateFittingPlant workspace.

different continuous flow tests, the interface for this module is more open-ended and requires more consideration from the user compared to the batch fitting routines. The workspace for the RateFittingPlant module is shown in Figure 3.7.

Both modules use Excel's Solver routine to perform the final parameter estimation optimization problem. This routine determines the kinetic coefficients by minimizing the weighted sum of the squared error ($WSSQ$) between the experimental data and the predicted performance. Since Solver uses a gradient-based simplex search routine, the "optimized" solution is susceptible to localized minima. To avoid this problem, FLoatSim ensures that the best starting guesses (as predicted by the experimental data) are utilized.

3.4.3 Simulation Software

After the kinetic coefficients have been determined from laboratory analysis, the FLoatSim simulation package may be used to predict the performance of various circuit configurations and equipment specifications. The work flow for conducting a simulation is driven by the custom ribbon tab icons. These icons and their respective descriptions are shown in Figure 3.8 and Table 3.1.

The FLoatSim software contains a custom user interface which allows streamlined flowsheet generation, data entry, and solution visualization. Figure 3.9 shows the standard steps in the FLoatSim simulation process. First, the user enters a custom flowsheet. Excel's standard drawing tools are used to draw flotation cells, splitters, junctions, slurry streams, water streams, and feed streams. These items may then be connected to form a user-specified

Table 3.1: Summary of FLoatSim Toolbar Buttons

Toolbar Button	Action
Flotation Cell	Places a flotation cell in the flowsheet drawing tab.
Junction	Places a junction in the flowsheet drawing tab.
Splitter	Places a splitter unit in the flowsheet drawing tab.
Feed	Places a feed stream in the flowsheet drawing tab.
Water	Places a water stream in the flowsheet drawing tab.
Stream	Places a general stream in the flowsheet drawing tab.
Create Simulation	Generates the circuit connection matrix and model tabs for the current flowsheet configuration.
Get Feed Data	Imports feed data from the lab data fitting module.
Get Rate Data	Imports kinetic data for current flotation model tab.
Calculate	Calculates flowsheet (resets iteration).
Carrying Capacity	Applies carrying capacity restriction.
Add Stream Info	Adds stream info boxes for all streams.
Delete Stream Info	Deletes all stream info boxes.
Reroute Connections	Reroutes stream box connections.
Back to Flowsheet	Navigates back to the flowsheet tab.
Clear Flowsheet	Deletes current simulation.
Export Data	Exports user-defined simulation data.
Help	Opens help menu.

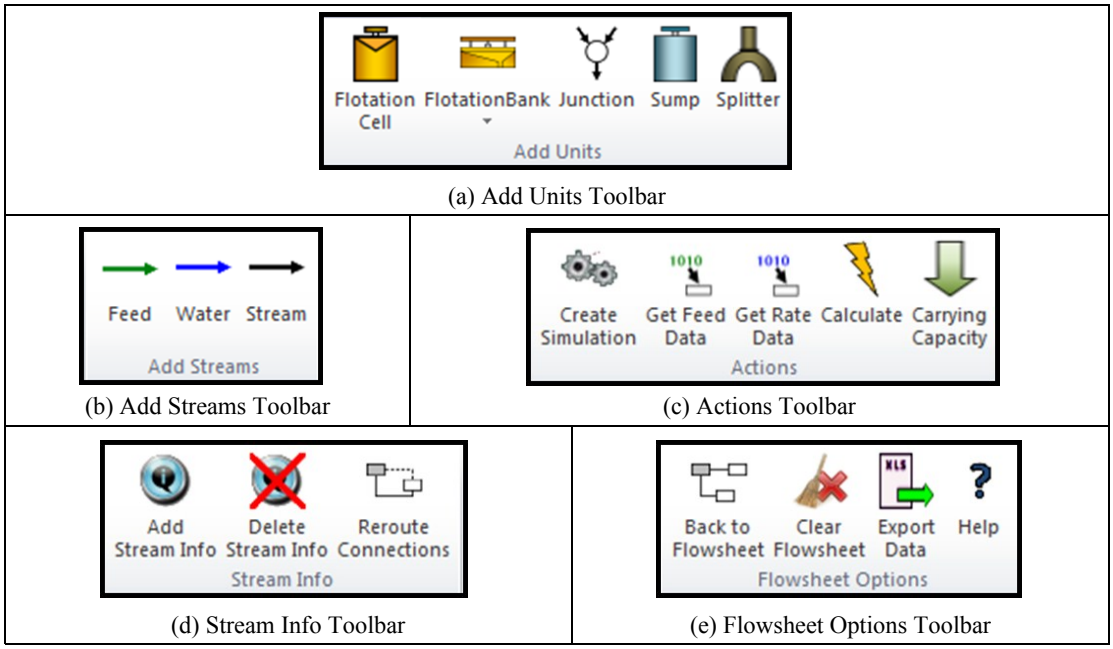

Figure 3.8: FLoatSim Custom Ribbon Toolbars.

circuit configuration.

After the flowsheet is drawn, the initial conditions and simulation parameters are entered. The FLoatSim simulator requires three main types of data to build the models and conduct the simulation: equipment characteristics, kinetic coefficients, and operational characteristics. The equipment characteristics (flotation cell size, froth surface area, and weir lip length) are extracted from a user-defined equipment database. Other values, such as unit Peclet number, air holdup and bank dimensions (number of parallel rows and cells in series) are user-specified. Each flotation cell element drawn on the flowsheet may be used to represent a different cell type. The kinetic coefficients are manually entered or imported from the data fitting modules. Finally, the operational parameters (feed rate and feed percent solids) are entered manually onto the appropriate spreadsheet tab.

Once all the data and simulation parameters are input, the simulation may be calculated. FLoatSim uses Excel's standard iterative calculation engine to resolve recirculating loads. However, the FLoatSim calculation algorithm contains a hard zero-value reset to ensure that the iteration does not produce a divergent or erroneous solution. The default iteration convergence criteria is an absolute change of 0.001 of any spreadsheet value or 100

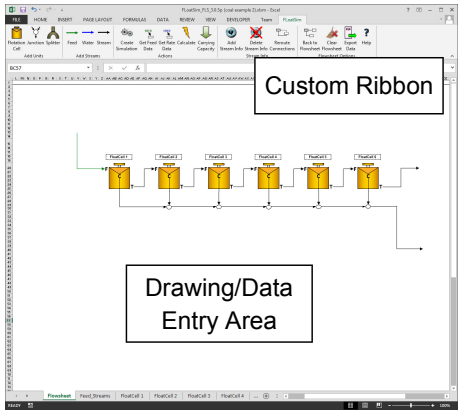

(1) Draw Flowsheet

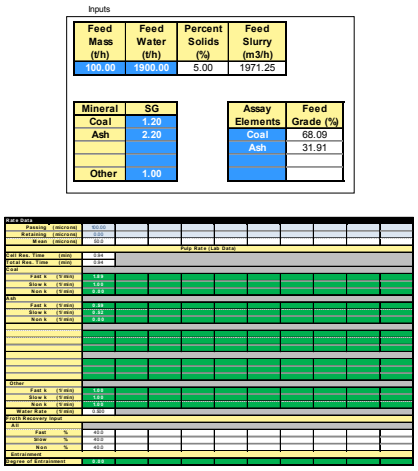

(2) Enter Feed/Rate Data

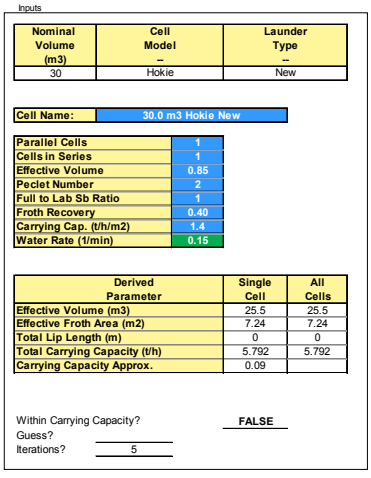

(3) Enter Equipment Parameters

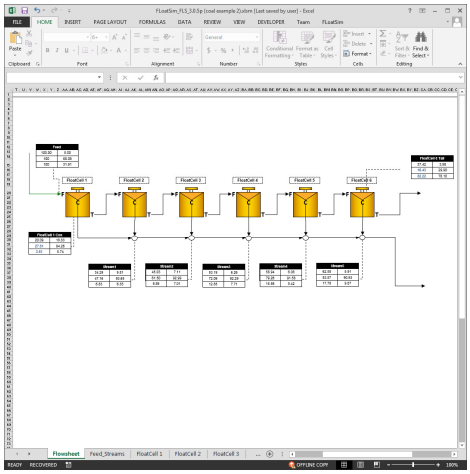

(4) Calculate/Review Results

Figure 3.9: Standard Steps for FLoatSim Simulation Usage.

Table 3.2: Coal Case Study: Laboratory Data

Product	**Weight**	**Assay (%)**	
(min)	**(%)**	**Ash (dry)**	**Combustible**
0.25	17.00	5.91	94.09
0.50	16.60	6.52	93.48
1.00	10.20	10.81	89.19
2.00	11.10	12.45	87.55
3.00	7.80	17.59	82.41
5.00	5.00	22.54	77.46
Tail	32.30	76.89	23.11
Con Total	67.70	10.44	89.56
Calc. Head	100.00	31.91	68.09

iteration. Additional iterations may be requested by the user. Once the calculation is complete, the user may analyze the results by custom stream legends or via FLoatSim's data export feature.

3.5 Case Study: Coal Flotation

3.5.1 Raw Data

To demonstrate the capability of the FLoatSim suite, a coal flotation scale-up simulation study was conducted. Batch kinetics data was acquired for the circuit feed. The mass balanced data report delivered by the metallurgical lab is included in Table 3.2. This laboratory data is presented for the composite feed (no size-by-size analysis) and includes assay information for ash and combustible matter.

3.5.2 Rate Fitting

This system was discretized using the two component assays: ash and coal. These components represent the prominent distinctions of floatable and non-floatable particulate matter in the feed material. Since no size data was recorded, the simulation utilized a single

KINETICS DATA																
Time (min)	Mass (%)	Min. 1 Coal (%)	Min. 2 Ash (%)	Min. 3	Min. 4	Other (%)	Coal Rec. (%)	Ash Rec. (%)			Other Rec. (%)	Coal ln(1-R)	Ash ln(1-R)			Other ln(1-R)
0	0.00	0.00	0.00			0.00	0.00	0.00			0.00	0.00	0.00			0.00
0.25	17.0	94.09	5.91			0.00	23.49	3.15			#DIV/0!	-0.27	-0.03			#DIV/0!
0.5	16.6	93.48	6.52			0.00	22.79	3.39			#DIV/0!	-0.62	-0.07			#DIV/0!
1	10.2	89.19	10.81			0.00	13.36	3.46			#DIV/0!	-0.91	-0.11			#DIV/0!
2	11.1	87.55	12.45			0.00	14.27	4.33			#DIV/0!	-1.34	-0.15			#DIV/0!
3	7.8	82.41	17.59			0.00	9.44	4.30			#DIV/0!	-1.79	-0.21			#DIV/0!
5	5.0	77.46	22.54			0.00	5.69	3.53			#DIV/0!	-2.21	-0.25			#DIV/0!
Tail	32.3	23.11	76.89			0.00	10.96	77.84			#DIV/0!	0.00	0.00			#DIV/0!
Total	100.00	68.09	31.91			0.00	100.00	100.00			#DIV/0!	--	--			--

Figure 3.10: RateFittingLab data entry field for coal case study.

size class. Finally, the rate fitting module automatically assumed three floatability classes. As a result, this simulation was discretized into six total classes: fast, slow and non-floating for coal and ash.

The mass balanced laboratory data as presented in Table 3.2 is well formulated for entry into the RateFittingLab module. The mass recoveries are expressed as a percent of the total mass, and the relevant assays are identified. The data entry section of the RateFittingLab module is shown in Figure 3.10. Since this data set did not include water recovery or percent solids information, the water rate estimation table was not used.

After entering the assay information into the data entry fields, the weight factors were set. Since no information was available to justify an increased or decreased weight among the various assays, all factors were held constant at a value of 1. After the data and weight factors were entered into the spreadsheet, the parameter estimation algorithm was used to find the model parameters. The recovery and assay graphs (Figure 3.11) show good agreement between the experimental data and the fitted parameters, and the final summarized data set (Table 3.3) includes reasonable values. No further adjustments were made, and the final analyzed data set was deemed suitable for further simulation.

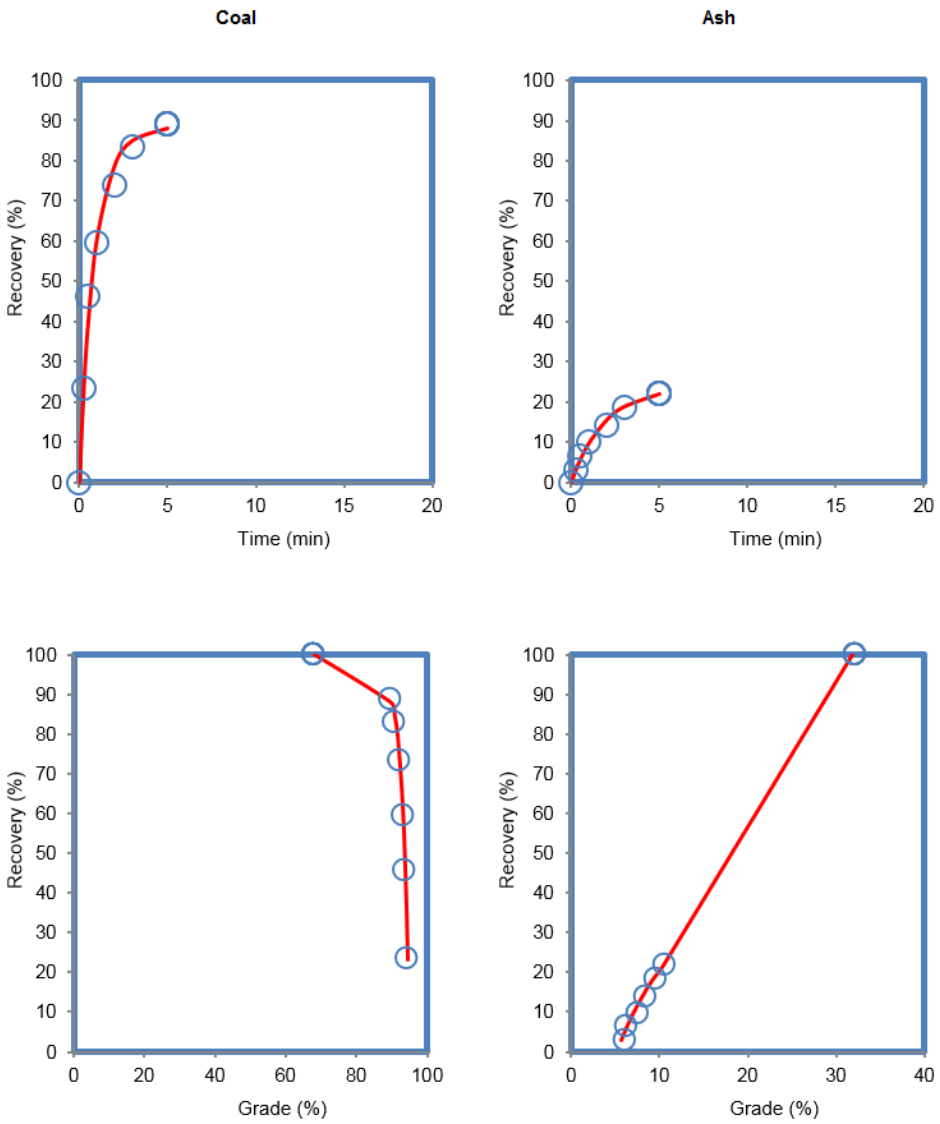

Figure 3.11: RateFittingLab experimental/predicted graphs for coal case study. Blue circles indicate experimental data while red lines indicate the model fits. Kinetic and grade-recovery plots are shown for coal and ash.

Table 3.3: Coal Case Study: Kinetic Parameter Summary

	Total Mass	**Coal**	**Ash**
Distributions (%)			
Fast	17.12	93.97	6.03
Slow	50.68	87.20	12.80
Non	32.20	24.25	75.75
Rates (1/min)			
Fast	–	1.89	0.59
Slow	–	1.00	0.52
Non	–	0.00	0.00

3.5.3 Simulation

After collecting the laboratory data, performing the mass balance adjustments, and determining the rate constants, the flotation models were constructed and the desired circuit configuration was simulated. For this case study, the simulator was used to determine the expected ash and yield from six 30 m^3 cells in series, as well as the cumulative ash and yield from each cell down the bank. The feed rate was set to 100 metric tonnes per hour at 5% solids.

The 30 m^3 cells have a standard froth area of 7.24 m^2. Historical data shows that the Peclet number for this unit is 2, and the unit carrying capacity for a fine coal application is 1.4 tph/m^2. No scaling is expected between the batch and full-scale S_b values, and the air hold up is expected to be 15% (i.e. 85% effective volume). A froth recovery of 40% is assumed.

Since no water recovery data was recorded in the batch test, a simplifying assumption was made to estimate the water recovery in the simulation. In the laboratory analysis, the batch test data reported a tailings water recovery between 4.5 and 4.0%. This value is a reasonable estimation for cell-to-cell performance, and a feed percent solids in this range will not be deleterious to downstream flotation. Consequently, the water recovery rate of each cell was adjusted until the tailings percent solids was between 4 and 4.5%. Second, since no information was available to justify a decision, a value of zero was assumed for the entrainment partition. While this assumption deviates from reality, the non-zero rate constants for the ash components already account for some gangue recovery, since entrainment was not

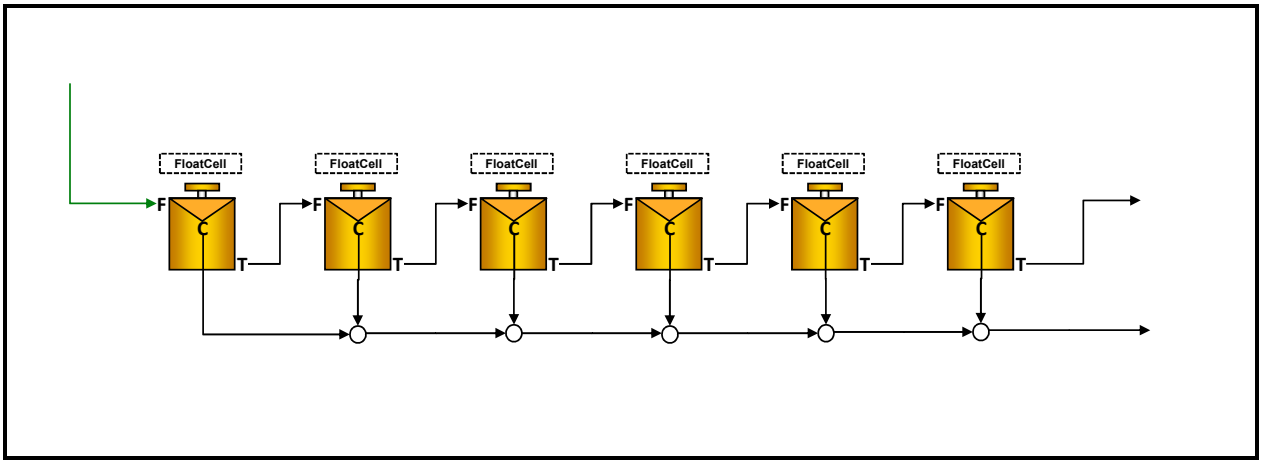

Figure 3.12: Coal case study simulation flowsheet.

used to fit the data.

After the assumptions and input data were resolved, the FLoatSim software was used to conduct the simulation. The flowsheet drawing tools were used to construct six cells in series, using a node after each cell to show the cumulative froth product. The final flowsheet is shown in Figure 3.12.

After the flowsheet was constructed, feed data was entered into the appropriate cells of the Feed Streams tab (Figure 3.13). The feed mass (100 tph) was entered, and Excel's "goal seek" command was used to determine the feed water required to attain 5% solids. The rest of the sheet was completed using data from other laboratory analyses.

Next, the model tabs were generated by FLoatSim's create simulation algorithm. An individual tab was created for each of the six flotation cells and five junctions shown on the flowsheet. Using the assumptions and input data described above, each model tab was completed sequentially. The equipment database on each tab was adjusted to include the desired cell geometry, and the get rate data button was used to import the kinetic parameters from the RateFittingLab module. The data entry field for the flotation cell tabs is shown in Figure 3.14.

After all of the basic data was entered, the calculate button was pressed to initialize the cell-by-cell modular calculations. At this point, neither the water recovery nor the carrying capacity limitations were included in the calculations. When the laboratory data is sufficient, the water recovery rate for each cell can be determined by fitting an experimental kinetic coefficient. With the water recovery for each cell known, the carrying capacity button could be used to implement the carrying capacity limitation for all cells simultaneous. Unfortu-

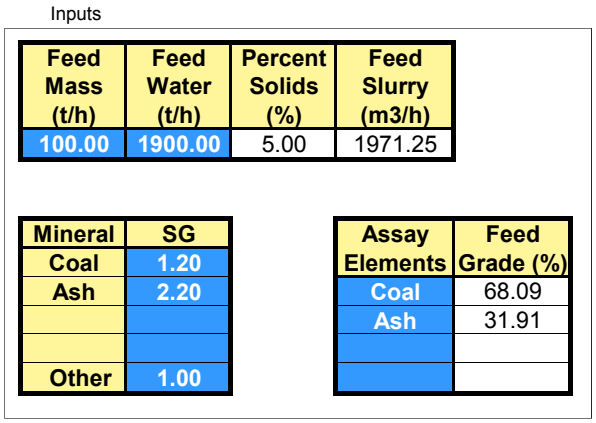

Inputs

Feed Mass (t/h)	Feed Water (t/h)	Percent Solids (%)	Feed Slurry (m3/h)
100.00	1900.00	5.00	1971.25

Mineral	SG
Coal	1.20
Ash	2.20
Other	1.00

Assay Elements	Feed Grade (%)
Coal	68.09
Ash	31.91

Figure 3.13: Data entry fields for coal case study feed information.

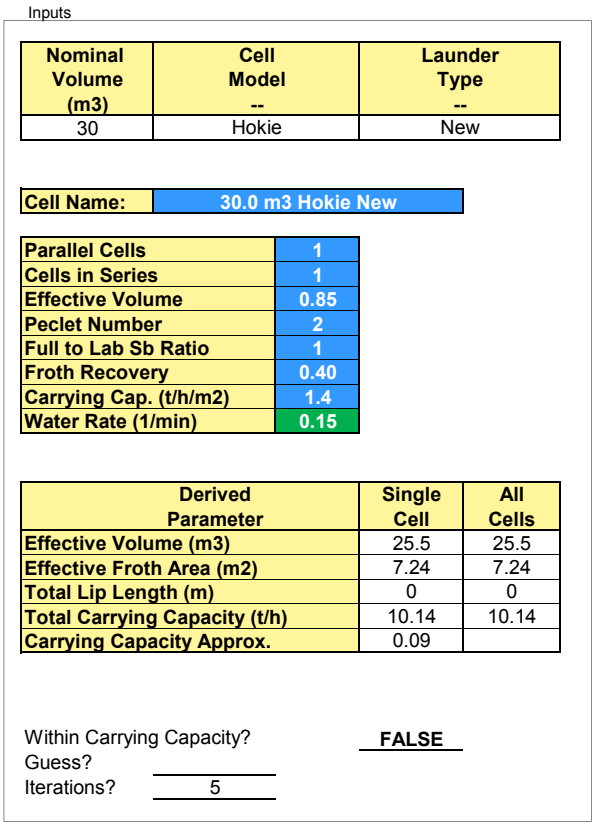

Inputs

Nominal Volume (m3)	Cell Model --	Launder Type --
30	Hokie	New

Cell Name:	30.0 m3 Hokie New

Parallel Cells	1
Cells in Series	1
Effective Volume	0.85
Peclet Number	2
Full to Lab Sb Ratio	1
Froth Recovery	0.40
Carrying Cap. (t/h/m2)	1.4
Water Rate (1/min)	0.15

Derived Parameter	Single Cell	All Cells
Effective Volume (m3)	25.5	25.5
Effective Froth Area (m2)	7.24	7.24
Total Lip Length (m)	0	0
Total Carrying Capacity (t/h)	10.14	10.14
Carrying Capacity Approx.	0.09	

Within Carrying Capacity? FALSE
Guess?
Iterations? 5

Figure 3.14: Input parameters for FloatCell tab in coal case study.

Table 3.4: Coal Case Study: Froth Recovery and Water Rate Values

Cell	**Water Rate Input (1/min)**	**Froth Recovery Input (%)**
Float Cell 1	0.10	0.16
Float Cell 2	0.10	0.20
Float Cell 3	0.50	0.26
Float Cell 4	0.55	0.33
Float Cell 5	0.45	0.40
Float Cell 6	0.25	0.40

nately, the work flow for this simulation was altered to account for the unique assumption used to determine the water recovery. As mentioned above, the water recovery was adjusted until the tailings percent solids was between 4.0 and 4.5%. The tailings percent solids is dependent upon the mass recovery which is dependent upon the status of the carrying capacity. Furthermore, the solid and water recovery of downstream cells is dependent upon the performance of prior cells. As a result of these dependencies, the order of the adjustments was logically considered.

First, the carrying capacity limitation for the first cell was imposed. The water recovery from the first cell will not influence this value; however, the desired tailings percent solids is influenced by this value. As a result, the overall solids recovery must be reconciled before the water recovery. The carrying capacity for Cell 1 was implemented by overwriting the standard froth recovery (0.4) with the value required to meet carrying capacity (in this case, 0.16). Next, the water recovery was adjusted until the desired value was reached. This procedure was then repeated cell-by-cell, down the bank. Table 3.4 summarizes the final froth reduction values and water rate values for each cell which satisfy the original assumptions.

After all values were input, the the final simulation was calculated. To analyze the results, stream info boxes were added to the flowsheet, showing the distribution and grades of various components for each stream (Figure 3.15). Finally, the export data button was used to conduct further analysis on the values produced from the simulation. This post-processing shows the percent yield and percent ash as a function of residence time down the bank (Table 3.5).

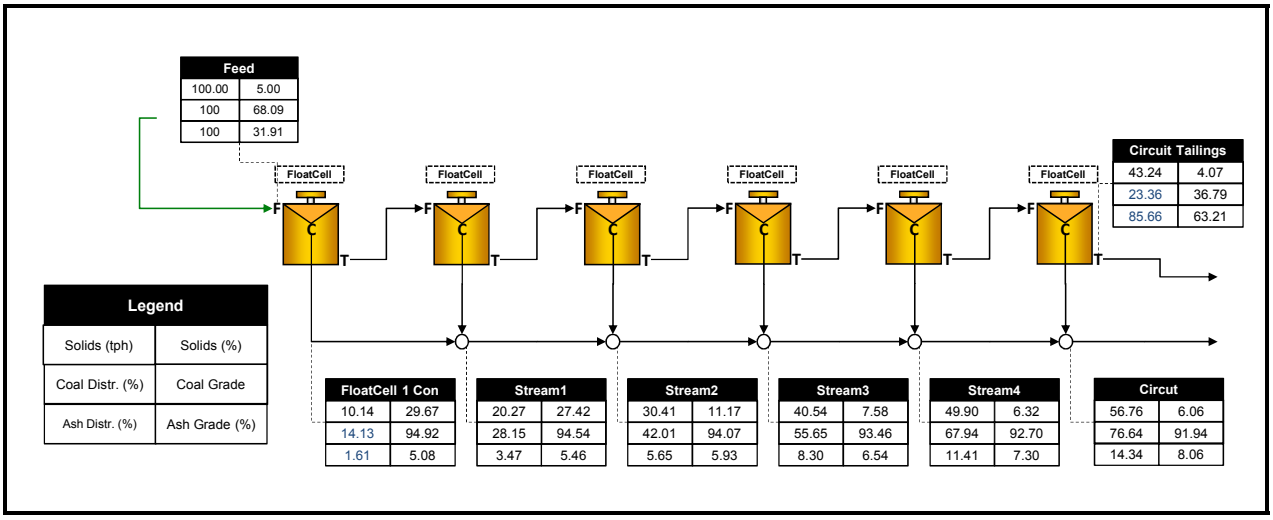

Figure 3.15: Final simulated flowsheet for coal case study.

Table 3.5: Coal Case Study: Final Cumulative Results

Cell	**Cumulative Res. Time (min)**	**Cumulative Yield (%)**	**Cumulative Ash (%)**
Float Cell 1	0.78	10.14	5.08
Float Cell 2	1.57	20.27	5.46
Float Cell 3	2.37	30.41	5.93
Float Cell 4	3.27	40.54	6.54
Float Cell 5	4.33	49.90	7.30
Float Cell 6	5.61	56.76	8.06

3.5.4 Discussion

The results of the case study simulation demonstrate the simulator's capability and highlight some of the fundamental differences between batch and continuous reactor kinetics. As described in Section 3.3.2, batch data from the laboratory is fitted by a plug-flow reactor model, while the plant data is projected using an axially-dispersed reactor model. While this mere difference in reactor type promotes some deviation between the experimental and simulated data, the implementation of a carrying capacity restriction in the simulation further propagates distinction.

Cumulative yield and cumulative ash for the experimental and simulated data is presented as a function of flotation time in Figure 3.16. Along with the experimental data and the standard simulation (which includes carrying capacity restrictions), a third data series is plotted showing the simulation results assuming the carrying capacity restriction was ignored (labeled the "Kinetic Only" data series, since recovery in this simulation is driven entirely by kinetics). This data is included to isolate the difference between the plug-flow and axially-dispersed reactor models as well as the true influence of the cell carrying capacity. These three curves together indicate that a simple cells-in-series plant will never outperform the batch cell in terms of yield at a given residence time. This phenomenon is largely driven by the difference in reactor models. In theory, as more cells are added in series, the axially-dispersed reactor can approach the plug-flow behavior; however, moderate deviation is expected when only six cells are utilized. The magnitude of this difference is quantified by comparing the batch data and the kinetic only curves in Figure 3.16.

Alternately, the difference between the kinetic only data series and the carrying capacity limited data series is driven by the imposed restriction in concentrate flow rate. The cell geometry and metallurgical conditions in this case study, dictate that the concentrate weir has a maximum flow capacity of 10.14 tph, regardless of the kinetic prediction. This physical restraint can substantially reduce the expected yield at a given residence time. For example at a four minutes of residence time, kinetic simulation dictates that the yield should be 65%; however, the available froth surface area in the plant is not capable of physically producing this amount of concentrate. According to the carrying capacity limited simulation, the anticipated yield will instead be 45% at that residence time. For the case study simulation, the first four cells in the bank were all restricted by carrying capacity, while the last two were the only cells restricted by kinetics.

The cumulative ash plot in Figure 3.16 shows that the reduction in yield of the simulated plant is compensated by in increase in product quality. At a given residence time, the

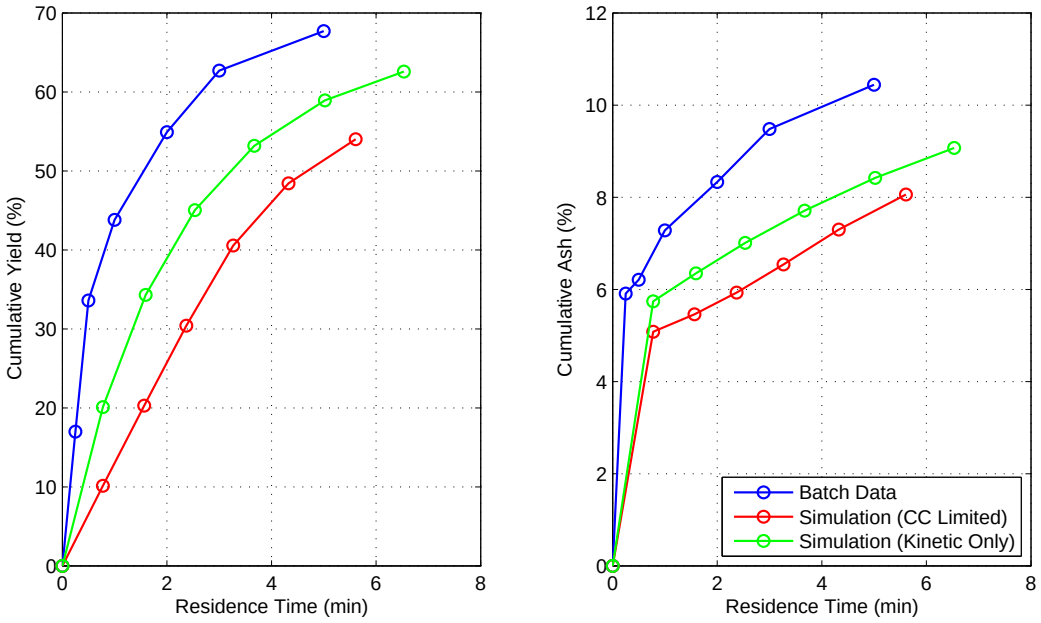

Figure 3.16: Cumulative yield and cumulative ash plotted as a function of residence time for experimental and simulated values. The batch data series shows the experimental data gathered from bench-scale laboratory testing. The carrying capacity (CC) limited data series corresponds to the case study simulation which included realistic carrying capacity restrictions, while the kinetic only data series corresponds to a purely kinetic simulation which ignores carrying capacity limitations.

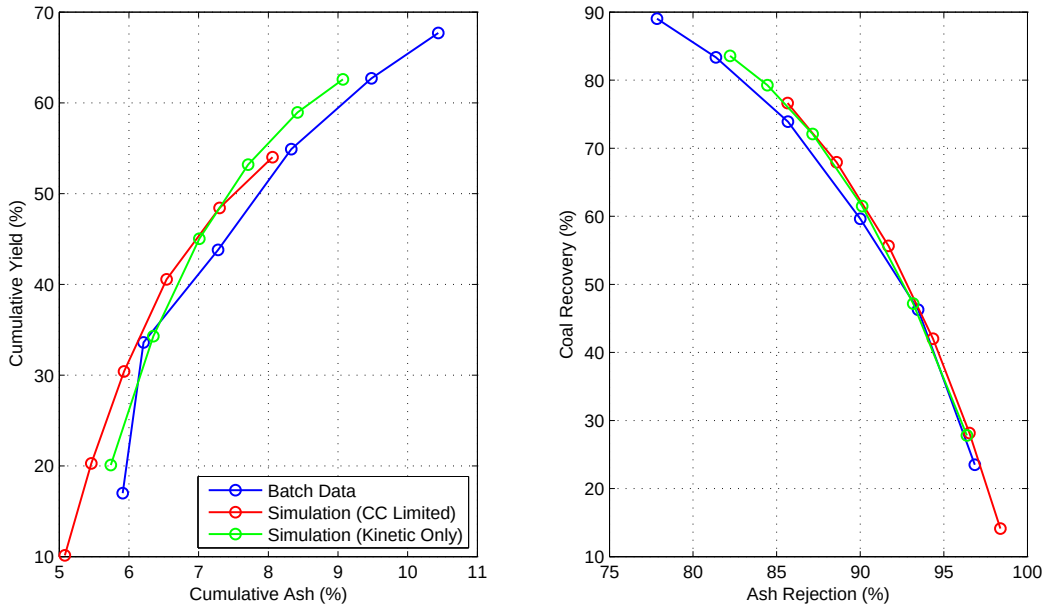

Figure 3.17: Separation efficiency plots for experimental and simulated values. The batch data series shows the experimental data gathered from bench-scale laboratory testing. The carrying capacity (CC) limited data series corresponds to the case study simulation which included realistic carrying capacity restrictions, while the kinetic only data series corresponds to a purely kinetic simulation which ignores carrying capacity limitations.

simulation shows substantially reduced product ash when compared to the same residence time in the batch case. In both plots, the carrying capacity limited simulation shows a strong deviation from the standard kinetic curve. Rather than the typical rate-based recovery curves, the carrying capacity limited curve shows more linear behavior for the cells influenced by carrying capacity.

Given the balance of reduced yield but increase product quality, the experimental data and the simulated data are roughly equivalent in terms of separation efficiency. Figure 3.17 shows cumulative yield plotted against cumulative ash as well as carbon recovery plotted against ash rejection. Both of these plots are commonly used in coal preparation as indicators of separation efficiency. In the yield-ash curve, points approaching the northwest corner(high yield, low ash) represent the greatest separation efficiencies, while the high ash rejection, high carbon recovery points (northeast corner) are desired in the latter graph. Since the same feed characteristic were used in both cases, either curve is capable of producing a fair comparison.

Typically, a plug-flow reactor should be more selective than an axially-dispersed reactor.

However, the case study simulation shows that both cases are quite similar, and either is capable of producing a greater efficiency at different points on the curve. Moving left to right along the cumulative yield - cumulative ash curve (or right to left along the carbon recovery - ash rejection curve), the carrying capacity simulated curve shows the best efficiency at the low product ash (or high ash rejection) points. These points correspond to the low residence time values in the data sets. Alternatively, along the midpoints, the batch data shows the greatest efficiency, while the carrying capacity limited curve regains the optimal position at the high product ash (or low ash rejection).

This deviation from the reactor-theory expectations is explained by the inclusion of a froth drop-back model. If the simulator only included a pulp recovery model, the batch data curve would always outperform the simulator curve. However, the froth drop-back generates a refluxing action. Material that is rejected from the froth returns to the pulp and has an opportunity to re-float. While the froth drop-back model is non-selective, the inclusion of froth reflux increases the selectivity of the entire process, by re-exposing rejected particles to the selective pulp reactor. The degree of the selectivity increase is directly related to the magnitude of the froth drop-back. For this simulation, the froth drop-back in the carrying capacity limited cases was extremely high, sometimes as great as 84% (Table 3.4). The resulting balance between the selectivity enhancing froth drop-back and the selectivity decreasing axially-dispersed reactor model causes the simulation curves to "intertwine" with the batch data curves.

The selectivity-enhancing phenomenon associated by froth drop-back is further demonstrated by comparison of the kinetic only and carrying capacity limited simulation data. While the magnitude of difference is extremely low, the carrying capacity limited simulation always exhibits a higher separation efficiency than the kinetic only curve. This difference is most evident in the low residence time points (low cumulative ash, high ash rejection), and it diminishes as the residence time increases. The greatest difference in froth drop-back between the two simulations is at the low residence times, where the carrying capacity limitation is most pronounced. The increased froth drop-back at these points causes a higher degree of reflux and thus a greater separation efficiency. At the higher residence time points (where the carrying capacity limited simulation is actually driven by kinetics), the separation efficiency of the two simulations is identical.

From a practical standpoint, the separation efficiencies in all three cases are roughly equivalent. The predominant difference between the carrying capacity limited simulation, the kinetic only simulation, and the batch data is the residence time required to achieve a desired yield. The extremely high refluxing in the first carrying capacity constrained cell may

lead to enhanced separation performance, but this difference is quickly reduced as further products are added down the bank. This simulation indicates that operational enhancements which can mitigate carrying capacity restrictions will allow substantial reductions in required cell volume.

3.6 Summary and Conclusions

This section has described the the FLoatSim software suite. The flotation modeling theory is derived from a unique four-reactor model which independently considers pulp recovery, froth recovery, entrainment recovery, and carrying capacity. The pulp recovery model is based on intermediate flow conditions in an axially-dispersed reactor. As a result, pulp recovery is a function of the particles' kinetic coefficients, the cell's residence time, and the cell's degree of mixing (or Peclet number). The froth recovery model is user-specified but derives from a plug-flow model influenced by the gas residence time in the froth and a rate of froth drop-back. The entrainment model shows that entrainment recovery is proportional to the water recovery and a size-dependent degree of entrainment fitting parameter. Finally, the carrying capacity imposes a strict limit on the maximum concentrate flow rate which may be produced per unit of cell surface area. In cases that exceed the carrying capacity restriction, the cell's froth recovery is incrementally reduced until the physical constraints are met.

Data from laboratory, pilot-scale, or full-scale testing is used to determine the unique fitting parameters to the general discretized models. FLoatSim's data fitting modules adjust the model parameters (kinetic coefficients and mass proportions) to minimize the weighted-sum-of-the-squared errors between the experimental data and the model predictions for the experimental condition under investigation. This data analysis approach uses a three-level discretization which can include up to ten size classes, five mineral classes, and three floatability classes.

FLoatSim's sequential modular calculation approach extends the single cell models to a user-specified plant configuration. Equipment characteristics (cell size, froth dimensions, and unit Peclet number) as well as operational conditions (feed rates, water addition rates, and gas rates) are used with the model parameters to ultimately predict the plant performance characteristics, including grade, recovery, and residence time. These parameters may then be adjusted, and subsequent simulation can indicate optimal performance strategies.

The overall work-flow has been demonstrated for a coal flotation case study. This

exercise shows how the simulation package may be used to analyze batch data and predict performance, in this case, for a simple rougher bank. Post-processing of the simulated data demonstrates how the difference in the reactor model as well as the carrying capacity limitations explain the significant deviations between the laboratory test results and the projected full-scale performance.

Acknowledgments

The author would like to thank Dr. Serhat Keles for his initiative in designing the user interface and providing ideas and suggestions for general software usability. Financial support for the FLoatSim Software package was provided by FLSmidth Minerals.

3.7 Bibliography

Gorain, B., Harris, M., Franzidis, J., & Manlapig, E. (1998). The effect of froth residence time on the kinetics of flotation. *Minerals Engineering*, *11*(7), 627–638.

Levenspiel, O. (1999). *Chemical reaction engineering*. Wiley.

Mathe, Z., Harris, M., O'Connor, C., & Franzidis, J. (1998). Review of froth modelling in steady state flotation systems. *Minerals Engineering*, *11*(5), 397–421.

Noble, A. (2012). *Laboratory-scale analysis of energy-efficient froth flotation rotor design*. Unpublished master's thesis, Virginia Polytechnic Institute and State University.

Vera, M., Franzidis, J., & Manlapig, E. (1999). Simultaneous determination of collection zone rate constant and froth zone recovery in a mechanical flotation environment. *Minerals Engineering*, *12*(10), 1163–1176.

Vera, M., Mathe, Z., Franzidis, J., Harris, M., Manlapig, E., & O'Connor, C. (2002). The modelling of froth zone recovery in batch and continuously operated laboratory flotation cells. *International Journal of Mineral Processing*, *64*(2), 135–151.

Vianna, S. (2011). *The effect of particle size, collector coverage and liberation on the floatability of galena particles in an ore*. Unpublished doctoral dissertation, The University of Queensland.

Yianatos, J., Bergh, L., & Cortes, G. (1998). Froth zone modelling of an industrial flotation column. *Minerals Engineering*, *11*(5), 423–435.

Yianatos, J., Moys, M., Contreras, F., & Villanueva, A. (2008). Froth recovery of industrial flotation cells. *Minerals Engineering*, *21*(12), 817–825.

Chapter 4

Derivation of Rate Constant Compositing Formulas

(ABSTRACT)

Several mineral processing unit operations are described by first-order kinetic reactor models. Nearly all contemporary froth flotation models incorporate one or more kinetic models to describe various sub-processes, including pulp recovery and froth recovery. Furthermore, contemporary approaches utilize a "lumped parameter" model which describes the bulk flotation behavior as the sum of various components (fast, slow, and non-floating). In order to express a distribution of rate constants as a single apparent rate, the values must be composited. Unlike other physical properties, rate constants cannot be easily combined by simple mass or volume weighted averages. This chapter describes the derivation and application of more sophisticated reactor-dependent rate constant compositing formulas. These formulas are shown to be time dependent, as the time in which the rates are composited influences the apparent bulk rate. Sample calculations are shown for the various formulas and two applications of this theory are presented, explaining the role of compositing in the observable rate limits and simulation discretization error.

4.1 Introduction

Kinetic models are often used in mineral processing to describe unit operations which have a strong time dependency. The most common example of this modeling approach is given by flotation (Sutherland, 1948; Tomlinson & Fleming, 1965; Lynch, Johnson, Manlapig,

& Thorne, 1981; Fichera & Chudacek, 1992), though other metallurgical processes, such as grinding (Lynch & Bush, 1977), pelletization (Fuerstenau, Kapur, & Mitra, 1982), and leaching (Beolchini, Papini, Toro, Trifoni, & Vegliò, 2001; Mellado, Cisternas, & Gálvez, 2009) have also be modeled as kinetic reactors.

Despite the range of potential applications and physical environments, performance in a kinetic reactor is defined in terms of the reactor type, the mean particle residence time (τ), and a kinetic coefficient (k). For a plug-flow reactor, the kinetic recovery is given by:

$$R_{plug} = 1 - e^{-k\tau}. \tag{4.1}$$

The perfectly-mixed model is given by:

$$R_{mixed} = \frac{k\tau}{1 + k\tau}. \tag{4.2}$$

Finally, the axially-dispersed model is given by:

$$\begin{aligned} R_{ADR} &= 1 - \frac{4A \exp\{Pe/2\}}{(1+A)^2 \exp\{(A/2)Pe\} - (1-A)^2 \exp\{(-A/2)Pe\}} \\ A &= \sqrt{1 + 4k\tau/Pe}. \end{aligned} \tag{4.3}$$

where the degree of axially mixing is given by the Peclet number (Pe) (Levenspiel, 1999).

In each of these models, τ represents the mean residence time of reactive (or in the case of flotation, *floatable*) particles which exhibit a reaction (or *flotation*) rate of k. Often, these two factors are combined to form the dimensionless $k\tau$ factor. In the case of flotation, the kinetic coefficient is modeled to be an intrinsic physical property of the material which has a defined value for a given experimental condition and particle properties. For example, experiments show that particles of similar composition but different sizes float at different rates (Gaudin, Schuhmann Jr, & Schlechten, 1942). These disparities cause many researchers to use a distributed parameter rate model, with the the distribution classes referencing the various driving forces of rate constant disparity. For example, most flotation models at least include mineral and size classes, reflecting the knowledge that particles of different mineral types and of different size classes float at different rates (Fichera & Chudacek, 1992).

Despite this distributed parameter approach, researchers have shown that even particles of similar size and composition still exhibit a distribution of rate constants (Polat & Chander, 2000). Consequently, additional factors beyond size and mineral composition drive changes in the rate constant. Some of these factors may include physical or hydrodynamic

properties such as particle shape, particle zeta potential, particle contact angle, degree of surface oxidation, bubble-particle collision turbulence, the kinetic energy of detachment, or the film thinning rate (Sutherland, 1948; Sherrell, 2004; Do, 2010; Kelley, Noble, Luttrell, & Yoon, 2012). To account for these various ill-defined and poorly-understood characteristics, a general approach to model parameterization is often used (Imaizumi & Inoue, 1965). In this approach, the models lump together all of these combined effects to form a loosely-defined "floatability class." In most flotation systems, the full distribution of floatability classes is truncated to three colloquial distinctions: fast, slow, and non-floating. Most contemporary flotation models include some form of distributed flotation classes, often via double or triple distributed models which include size, composition, and floatability (Fichera & Chudacek, 1992, also see Chapter 3.3.1).

In general, when a continuous distribution of values is truncated to a finite number of distribution classes, some of the information is lost and error is introduced. As the distribution is truncated to fewer classes, the magnitude of the potential error increase. Historically, the standard use of two or three floatability classes limits the degree of potential error while providing meaningful values which can be estimated from the available data set. Mathematically, the extent of the original data set defines the number of potential classes which can be estimated. Occasionally, the lack of an extensive data set or the desire to make a single point comparison leads practitioners to estimate the full distribution of rate constants with a single rate constant that produces the same result. This approach is commonly required when recovery data has only been collected at a single residence time.

For most physical properties, the calculation required to truncate a distribution of values to a single value is trivial; however, the resultant value is often quite useful, despite the loss of information. The single truncated value provides a simple means to compare two varying distributions. Furthermore, the truncated value can be used to predict the average behavior that the distribution will exhibit. As a common example, the mass mean particle size may be used to truncate a full distribution of particle sizes to a single value. Similarly, an average density may be determined to represent the apparent density that a particle composed of many component densities will exhibit. In both of these cases, the calculation only entails a simple weighted average.

Unfortunately, the mathematical nature of rate constants do not lend themselves to a simple compositing expression. For example, consider a two component system which contains 500 kg of material with a rate constant 1.4 min^{-1} and 1,500 kg of material with a rate constant of 0.2 min^{-1}. The composited rate constant for this system should be a single value which produces the same recovery as the two component system when utilized in the

reactor model. A simple weighted average shows that the combined system should exhibit a rate constant of 0.5 min^{-1} ($[500 \times 1.4 + 1500 \times 0.2]/[500 + 1500] = 0.5$). However, the recovery calculations for a batch reactor (at a residence time of 2 minutes, for example) do not support this approach:

$$\begin{aligned} R_{Composited} &\stackrel{?}{=} R_{Distributed} \\ M_T(1 - e^{-k^*\tau}) &\stackrel{?}{=} M_1(1 - e^{-k_1\tau}) + M_2(1 - e^{-k_2\tau}) \\ (2000)(1 - e^{-(0.5)(2)}) &\stackrel{?}{=} (500)(1 - e^{-(1.4)(2)}) + (1500)(1 - e^{-(0.2)(2)}) \\ (2000)(0.632) &\stackrel{?}{=} (500)(0.939) + (1500)(0.330) \\ 1264 &\stackrel{?}{=} 470 + 495 \\ 1264 &\neq 965 \end{aligned}$$

Several observations surface from this example. First, simple weighted averages are not suitable for rate compositing estimation. Second, this example subtly shows that the true composited rate must consider both the residence time and the reactor type, since these values influence the equations used to determine recovery from a kinetic coefficient. Finally, the math involved in this example establishes the framework for the derivation.

The remainder of this paper will work through the derivation and implications of accurate rate compositing formulas. Expressions will be derived for the plug-flow, perfectly-mixed, and axially-dispersed reactor models. Sample calculations are shown to demonstrate the utilization and verification of the derived expression. Finally, composite optima and discretization error are presented as two practical applications of this rate compositing theory.

4.2 Derivation

In order to derive a general expression for a composite rate constant, several precise definitions must first be established. The composite rate constant (k^*) for a set of data is defined as the single rate constant which yields a recovery value (R^*) identical to the sum of all component rate constants (k_i), with each component having a known mass value (M_i). From the example presented in the previous section, unique expressions for the composite rate constant must be derived for each of the three reactor types. Also, the expressions must have a time dependence.

Mathematically, R^* is defined as the weighted average of the component recovery values:

$$R^* = \frac{R_1 M_1 + R_2 M_2 + \cdots + R_N M_N}{M_1 + M_2 + \cdots + M_N} = \frac{\sum_{i=1}^{N} R_i M_i}{\sum_{i=1}^{N} M_i} \tag{4.4}$$

where R_i is the recovery of particle class i, M_i is the mass fraction of particle class i, and N is the total number of particle classes.

In order to derive the composite rate constant from the constituent rate constants, the appropriate reactor-dependent recovery equation is substituted for R in Equation 4.4, and by mathematical manipulation, the composite rate constant is solved in terms of the class rate constants (k_i), the class mass fractions (M_i), and the test residence time (τ).

For a plug-flow reactor, Equation 4.1 is substituted into Equation 4.4 and solved for k^*_{plug}. The final relationship is given by:

$$k^*_{plug} = \left(- \ln \left[\frac{\sum_{i=1}^{N} M_i e^{-k_i \tau}}{\sum_{i=1}^{N} M_i} \right] \right) \tau^{-1}. \tag{4.5}$$

This equation indicates that the apparent rate constant is dependent on the residence time in which the compositing takes place. In the case of experimental data, this compositing time is simply the residence time in which the test data was acquired.

A similar mathematical approach is extended to account for the other reactor types. By substituting Equation 4.2 into Equation 4.4, the apparent rate constant for a perfectly mixed reactor (k^*_{mixed}) may be derived in a similar manner as Equation 4.5. This final relationship is given by:

$$k^*_{mixed} = \left(\frac{\left[\sum_{i=1}^{N} M_i \right] \left[\prod_{i=1}^{N} (1 + k_i \tau) \right]}{\sum_{i=1}^{N} \left[\frac{M_i \left[\prod_{j=1}^{N} (1 + k_j \tau) \right]}{(1 + k_i \tau)} \right]} - 1 \right) \tau^{-1}. \tag{4.6}$$

Given the complexity of the axially-dispersed reactor equation, an explicit analytical expression for k^* is not possible. Alternatively, Newton's method may be used to solve the system of equations numerically. The formulation of Newton's method requires the equation in question to be set equal to zero so that the roots may be determined. This derivative of this function with respect to the variable in question (in this case, k^*_{ADR}) must also be known. For the axially-dispersed reactor model, the Newton's method formulation is given

by:

$$f(x) = \sum_{i=1}^{N}(R_{ADR,i}M_i) - R^*_{ADR}\sum_{i=1}^{N} M_i \tag{4.7}$$

$$f'(x) = -\frac{\partial R^*_{ADR}}{\partial k}\sum_{i=1}^{N} M_i. \tag{4.8}$$

To determine a manageable expression for $f'(x)$, R_{ADR} is subdivided into different components representing the numerator(R_{num}) and two denominator (R_{denA} and R_{denB}) expressions:

$$R_{num} = 4A\exp\{Pe/2\} \tag{4.9}$$

$$R_{denA} = (1+A)^2\exp\{(A/2)Pe\} \tag{4.10}$$

$$R_{denB} = -(1-A)^2\exp\{(-A/2)Pe\} \tag{4.11}$$

$$R_{ADR} = 1 - \frac{R_{num}}{R_{denA} + R_{denB}}. \tag{4.12}$$

The partial derivative of each component is then defined individually:

$$\frac{\partial A}{\partial k} = \frac{2\tau}{PeA} \tag{4.13}$$

$$\frac{\partial R_{num}}{\partial k} = 4\exp\{Pe/2\}\left(\frac{\partial A}{\partial k}\right) \tag{4.14}$$

$$\frac{\partial R_{denA}}{\partial k} = \exp\left\{\left(\frac{A}{2}\right)Pe\right\}(1+A)\left[\left(\frac{Pe}{2}\right)(1+A)+2\right]\left(\frac{\partial A}{\partial k}\right) \tag{4.15}$$

$$\frac{\partial R_{denB}}{\partial k} = -\exp\left\{\left(\frac{-A}{2}\right)Pe\right\}(1-A)\left[\left(\frac{-Pe}{2}\right)(1-A)-2\right]\left(\frac{\partial A}{\partial k}\right). \tag{4.16}$$

Table 4.1: Kinetic Data Used for Rate Compositing Examples

Floatability Class	**Mass (%)**	**Grade (% $CuFeS_2$)**	**Rate (1/min)**
Fast	3	60	1.20
Slow	9	30	0.40
Non	88	1	0.01
TOTAL	100	5.38	–

Equations 4.9 - 4.16 are finally combined to define the full partial derivative of the axially dispersed reactor model with respect to k:

$$\frac{\partial R_{ADR}}{\partial k} = \frac{-(R_{denA} + R_{denB})\frac{\partial R_{num}}{\partial k} - R_{num}\left[\left(\frac{\partial R_{denA}}{\partial k}\right) + \frac{\partial R_{denB}}{\partial k}\right]}{(R_{denA} + R_{denB})^2} \tag{4.17}$$

This partial derivative is then substituted into Equation 4.8 to form the final formulation of Newton's method. Equations 4.7 and 4.8 may then be solved iteratively to determine k^*_{ADR} for a given set of data.

4.3 Sample Rate Compositing Calculations

To illustrate the usage of the compositing equations, a series of sample calculations is provided. These examples show how a simple three floatability class flotation system can be truncated to a single equivalent rate constant using the aforementioned expressions. The data used for these examples is a chalcopyrite flotation system with the kinetic data prescribed in Table 4.1.

To calculate the composite rate of chalcopyrite ($CuFeS_2$) at a residence time of 6 minutes, the relative "units" of chalcopyrite (M_i) in the three rate classes must first be determined. These values are calculated by simply multiplying the mass fractions in the floatability class by the chalcopyrite grade for that those classes. The resulting values are 180, 270, and 88 for the fast, slow, and non-floating classes, respectively. Once the units, rate constants, and test residence time are known, Equation 4.5 may be used to determine the

composited rate constant assuming a plug flow system:

$$k^*_{plug} = \left(-\ln \left[\frac{\sum_{i=1}^{N} M_i e^{-k_i \tau}}{\sum_{i=1}^{N} M_i} \right] \right) \tau^{-1}$$

$$= \left(-\ln \left[\frac{(180)e^{-(1.2)(6)} + (270)e^{-(0.40)(6)} + (88)e^{-(0.01)(6)}}{(180) + (270) + (88)} \right] \right) (6)^{-1}$$

$$= \left(-\ln \left[\frac{(0.134) + (24.5) + (82.9)}{538} \right] \right) (6)^{-1}$$

$$= (-\ln[0.1998])(6)^{-1} = 0.268.$$

This calculation indicates that in a plug-flow reactor, the chalcopyrite in the discretized system (Table 4.1) will appear to float at a rate constant of 0.268 if the recovery measurement is taken at 6 minutes. The following calculation verifies this result.

$$\begin{aligned}
R_{Composited} &\stackrel{?}{=} R_{Distributed} \\
M_T(1 - e^{-k^*\tau}) &\stackrel{?}{=} M_1(1 - e^{-k_1\tau}) + M_2(1 - e^{-k_2\tau}) + M_3(1 - e^{-k_3\tau}) \\
(538)(1 - e^{-(0.268)(6)}) &\stackrel{?}{=} (180)(1 - e^{-(1.2)(6)}) + (270)(1 - e^{-(0.4)(6)}) + (88)(1 - e^{-(0.01)(6)}) \\
(538)(0.80) &\stackrel{?}{=} (180)(0.999) + (270)(0.909) + (88)(0.058) \\
430 &\stackrel{?}{=} 180 + 245 + 5 \\
430 &= 430
\end{aligned}$$

Despite the apparent complexity of the perfectly-mixed compositing equation, the calculations can easily be performed in a programming environment using a series of nested for loops. As a manual example of the procedure, the kinetic data from the prior example (Table 4.1) is reproduced here to calculate the perfectly-mixed composite rate at a residence time of 6 minutes:

$$k^*_{mixed} = \left(\frac{\left[\sum_{i=1}^{N} M_i\right]\left[\prod_{i=1}^{N}(1+k_i\tau)\right]}{\sum_{i=1}^{N}\left[\frac{M_i\left[\prod_{j=1}^{N}(1+k_j\tau)\right]}{(1+k_i\tau)}\right]} - 1 \right) \tau^{-1}$$

$$\left[\sum_{i=1}^{N} M_i\right] = [(180) + (270) + (88)] = 538$$

$$\begin{aligned}\left[\prod_{i=1}^{N}(1+k_i\tau)\right] &= [(1+(1.2)(6)) * (1+(0.4)(6)) * (1+(0.01)(6))] \\ &= [(8.2) * (3.4) * (1.06)] = 29.55\end{aligned}$$

$$\begin{aligned}\sum_{i=1}^{N}\left[\frac{M_i\left[\prod_{j=1}^{N}(1+k_j\tau)\right]}{(1+k_i\tau)}\right] &= \left[(180)\frac{(1+(1.2)(6)) * (1+(0.4)(6)) * (1+(0.01)(6))}{(1+(1.2)(6))}\right] \\ &\quad + \left[(270)\frac{(1+(1.2)(6)) * (1+(0.4)(6)) * (1+(0.01)(6))}{(1+(0.4)(6))}\right] \\ &\quad + \left[(88)\frac{(1+(1.2)(6)) * (1+(0.4)(6)) * (1+(0.01)(6))}{(1+(0.01)(6))}\right]\end{aligned}$$

$$\begin{aligned}&= [(180) * (3.4) * (1.06)] + [(270) * (8.2) * (1.06)] + [(88) * (8.2) * (3.4)] \\ &= [649] + [2347] + [2453] = 5449\end{aligned}$$

$$k^*_{mixed} = \left(\frac{[538][29.55]}{[5449]} - 1\right)(6)^{-1}$$

$$= (1.920)(6)^{-1} = 0.320.$$

Under identical conditions, the plug-flow reactor exhibited a rate of 0.268, while the perfectly-mixed reactor exhibited a higher rate of 0.320. The following calculation verifies

this result.

$$
\begin{aligned}
R_{Composited} &\stackrel{?}{=} R_{Distributed} \\
M_T\left(\frac{k^*\tau}{1+k^*\tau}\right) &\stackrel{?}{=} M_1\left(\frac{k_1\tau}{1+k_1\tau}\right) + M_2\left(\frac{k_2\tau}{1+k_2\tau}\right) + M_3\left(\frac{k_3\tau}{1+k_3\tau}\right) \\
(538)\left(\frac{(0.320)(6)}{1+(0.320)(6)}\right) &\stackrel{?}{=} (180)\left(\frac{(1.2)(6)}{1+(1.2)(6)}\right) + (270)\left(\frac{(0.4)(6)}{1+(0.4)(6)}\right) + (88)\left(\frac{(0.01)(6)}{1+(0.01)(6)}\right) \\
(538)(0.657) &\stackrel{?}{=} (180)(0.878) + (270)(0.706) + (88)(0.057) \\
354 &\stackrel{?}{=} 158 + 191 + 5 \\
354 &= 354
\end{aligned}
$$

For the sake of brevity, an compositing example for the axially dispersed model is left to the reader. For the aforementioned kinetic data, the ADR composite rate constant is 0.310, given a composite time of 6 minutes and a Peclet number of 2.

4.4 Rate Compositing Optima

4.4.1 Application

Equations 4.5, 4.6, and 4.7 show that the apparent rate constant is strongly influenced by the residence time at which the compositing takes place (e.g. the residence time when the test data was collected). Along a continuum of residence times, the apparent rate constant transitions from a theoretical maximum observable rate constant to theoretical minimum observable rate constant. For the perfectly-mixed and plug-flow cases, these theoretical optima can be found by setting the first derivative of the analytical expressions (Equations 4.5 and 4.6) to zero and solving for the residence time. Predictably, this procedure reveals that the maximum composite rate constant is found at $\tau = 0$ and the minimum is found at $\tau = \infty$. The values of the optima can then be determined by finding the limit as the analytical expressions approach 0 and infinity. These results are given in Table 4.2.

The behavior of the transition between the two optima can be analyzed by plotting the composite rate constant as a function of the compositing time for three reactor models. An example of this transition plot, specific to the chalcopyrite data used in the aforementioned example, is shown in Figure 4.1. While the specific features of the graph (slope, asymptotes) are unique to the data set, the overall trends are consistent for all rate compositing problems. The slope of the plug-flow transition is always steeper than the perfectly mixed transition,

Table 4.2: Theoretical Observable Optima For Rate Constant Composites

	Minimum	**Maximum**
Time	$\tau = \infty$	$\tau = 0$
Plug-Flow	$\min(k_i)$	$\frac{\sum_{i=1}^{N} k_i M_i}{\sum_{i=1}^{N} M_i}$
Perfectly Mixed	$\left(\frac{[\sum_{i=1}^{N} M_i][\prod_{i=1}^{N} k_i]}{\sum_{i=1}^{n} \left[\frac{M_i \prod j=1^{N}(k_j)}{k_i} \right]} \right)$	
Axially Dispersed	Pe Dependent	

while the ADR curve is typically bounded by the two. All reactor models converge to the same maximum composite, while the minimum composite is reactor-dependent with the perfectly mixed composite always being lower than the plug-flow composite. As shown in in Table 4.2, the maximum composite is defined as the weighted average of the component rates, while the minimum for the plug-flow case is simply the minimum value for all rates.

4.4.2 Discussion

Though the compositing formulas are grounded in abstract theory, several practical implications of this curve can be derived. The sample data set used to build this curve includes reasonable values for most flotation systems. The rate composite transition curve (Figure 4.1) shows that the steepest transition for all reactor types occurs between residence times of 1 minute and 15 minutes. Unfortunately, most typical flotation cells operate within this range. As a result, small deviations in residence time at the test condition will lead to proportionally large changes in the apparent rate constant. To fully account for uncertainty, projections and simulations from this apparent rate constant must consider this steep transition.

With respect to the rate constant measurements, the only component rate constant that can be *directly* derived from the test data is the slow rate constant in the plug-flow reactor. This measurement requires recovery information at relatively long residence times. While Figure 4.1 shows the close approach to the asymptote occurring at 90 to 100 minutes of residence time, this value is strongly dependent on the specific component data. For the perfectly-mixed reactor, the apparent rate constant is always influenced by remnant fast floating material. Consequently, the apparent slow rate at very long residence times will always over-predict the true rate of the slow-floating component.

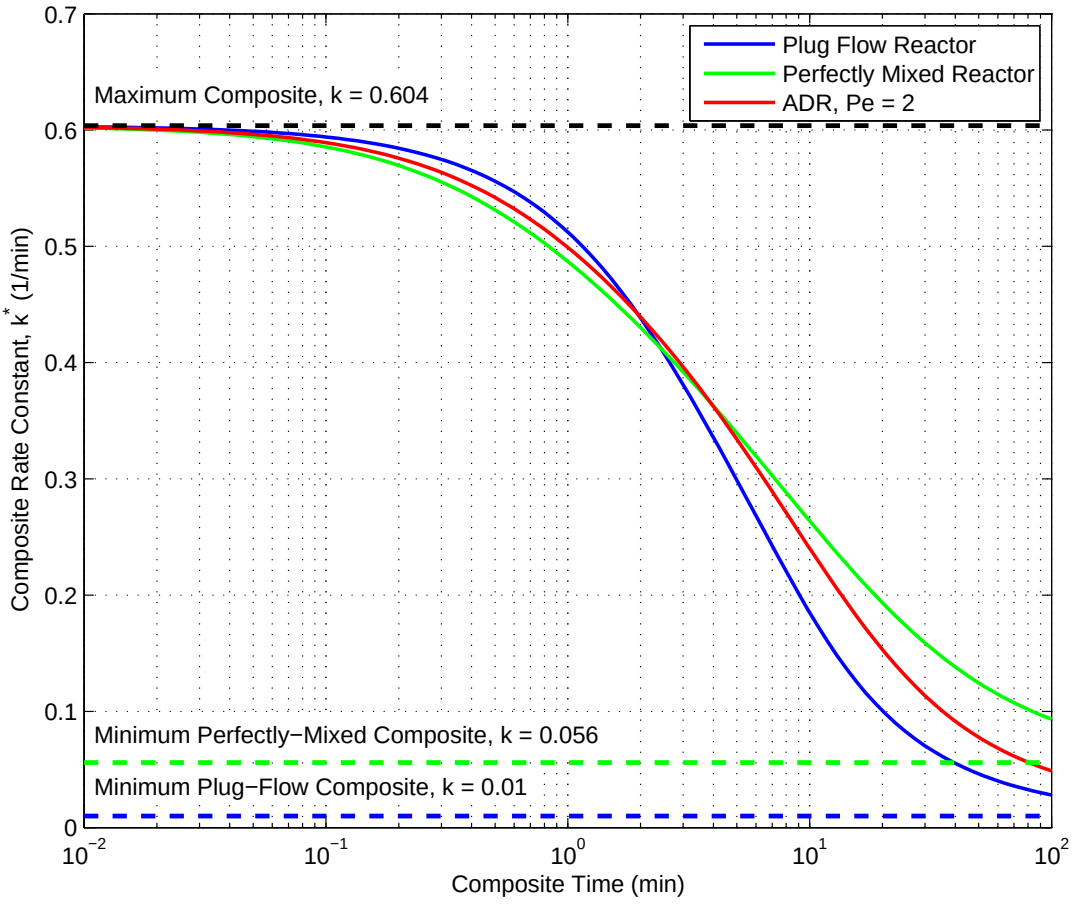

Figure 4.1: Composite rate constant plotted against the composite time for different reactor types (semi-log x-axis). Optima values are indicated on the chart for the plug-flow and perfectly-mixed reactor types. Plot is derived from kinetic data presented in Table 4.1.

Predictions for the fast floating-floating rate have a similar limitation. Even at infinitesimally small residence times, the apparent rate constant is influenced by the presence of slow-floating material. Without the information on the full distribution, the true fast floating rate cannot be directly calculated with data from any reactor type. For example, the data used to derive Figure 4.1 indicates that the true fast rate is 1.2; however, the greatest directly measurable rate constant is only 0.604. Furthermore, at practically measurable residence times (30 seconds to 1 minute), the apparent rate constant is already within the transition phase. To better illustrate the practical implications of rate compositing, the rate transition curve is reproduced in Figure 4.2 with a linear time axis and a practical range of measurable residence time values.

4.5 Discretization Error

4.5.1 Application

As a second application of the rate compositing theory, the apparent rate equations allow the determination of discretization error in simulations. When data is gathered from pilot or full-scale testing, the recovery data is often not time-dependent. As a result, only a single rate constant can be determined, rather than the real distribution of rate constants which were combined to form the apparent rate. By definition, the measured rate is the composite rate as determined from Equations 4.5, 4.6, and 4.7. Future projections or simulations which use this rate will deviate from the real behavior as the simulated residence time deviates from the residence time in which the data was collected. In order to demonstrate this application, the data from the prior example was extended to include rate data for a gangue particle class (Table 4.3).

Figure 4.3 illustrates this discretization error principle, assuming a perfectly-mixed reactor. In this example, the "Distributed Rate" curve represents the real behavior that is determined from the full distribution of rate constants; whereas, the "Composite Rate" curve represents the behavior derived from the single composite rate. From a practical standpoint, this single rate constant would be the experimental value derived from pilot-scale or full-scale testing. For this example, the rate data was composited at a residence time of six minutes which would reflect experimental data taken at a mean residence time of six minutes. As anticipated, the two curves overlap at this point, but as the residence time deviates from the composite time, the discretization error increases rapidly.

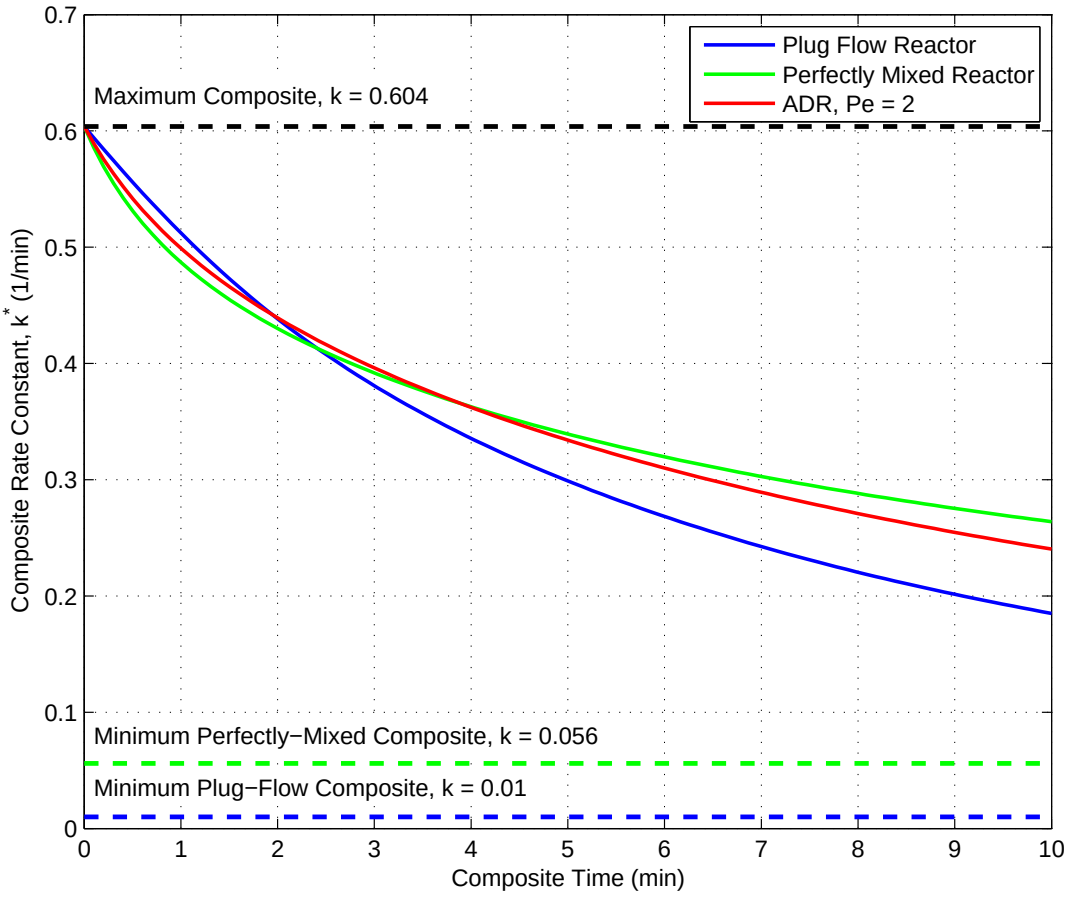

Figure 4.2: Composite rate constant plotted against the composite time for different reactor types (linear x-axis). Optima values are indicated on the chart for the plug-flow and perfectly-mixed reactor types. This plot has been cropped to show the values relevant for most flotation systems. Plot is derived from kinetic data presented in Table 4.1.

Table 4.3: Kinetic Data Used for Discretization Error Quantification Example

		Fast	**Slow**	**Non**
Mass	(%)	3	9	88
Grade (%)	$CuFeS_2$	60	30	1
	Gangue	40	70	99
Rate (1/min)	$CuFeS_2$	1.2	0.4	0.01
	Gangue	0.2	0.01	0

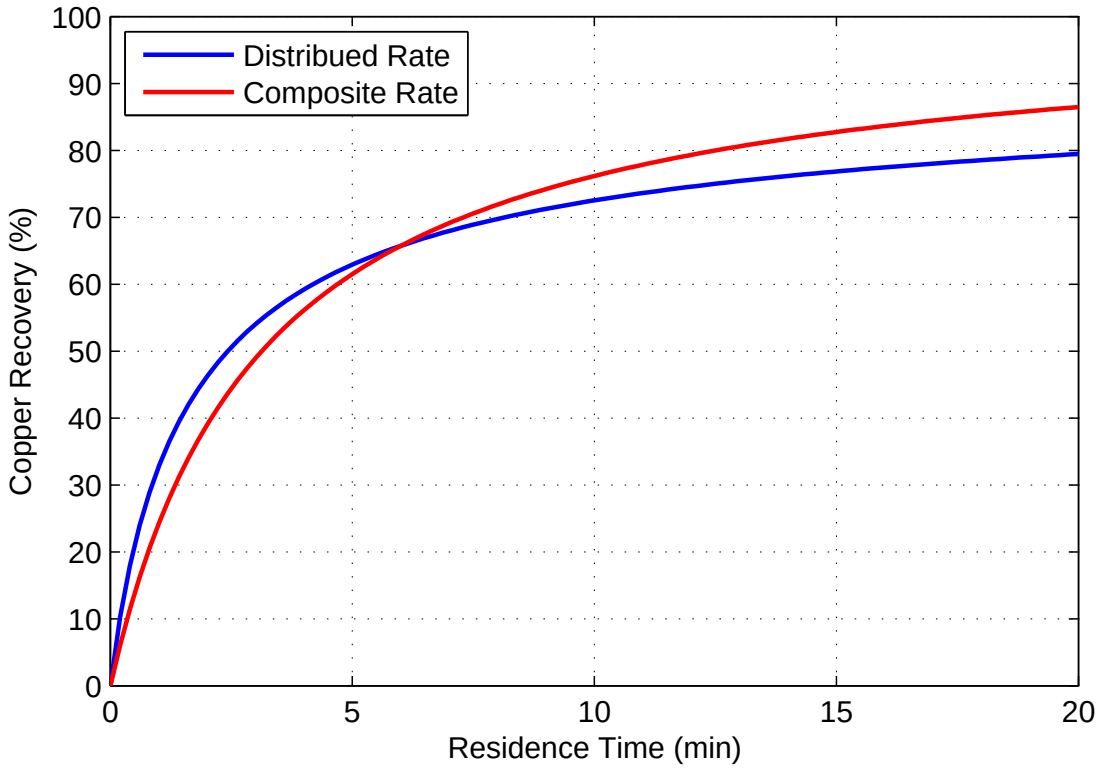

Figure 4.3: Recovery as a function of residence time for distributed and composited rate constant values. The distributed curve reflects information on the full distribution of kinetic coefficients, while the composite curve is derived from a single rate constant determined at a single flotation time ($\tau = 6$). A perfectly-mixed recovery model was used for this plot.

The single component, single reactor example shown in Figure 4.3 is extended to include the gangue component and other reactor types. This example demonstrates not only how rate constant compositing influences recovery of a second component but also how the procedure influences grade projections. Figure 4.4 shows the distributed and composited rate projections for copper recovery, gangue recovery, and copper grade for each of the three reactor types. The axially-dispersed reactor was calculated for a Peclet number of 2. As in the prior example, the "Distributed Rate" curve reflects the three rate data (fast, slow, and non-floating rate constants), while the "Composite Rate" curve reflects projections from a single rate constant which is the composite of the data at a residence time of six minutes. Figure 4.5 presents this same data as a percent error between the two curves, assuming the Distributed Rate curve represents the "true" values. Positive error reflects overestimates from the distributed curve while negative errors represent underestimates from the distributed curve.

4.5.2 Discussion

Though this data reflects one specific case, the behavior of the plots reveal several general trends. First, for residence times lower than the composite time, the composite curve always under-predicts the true recovery, regardless of the reactor type or the relative magnitude of the rate constant values. Conversely, for residence times greater than the composite time, the composite rate always over-predicts the recovery. This result coincides with logical expectations. The composite rate corresponds to a snapshot at a single point in time. The apparent rate a this snapshot reflects a specific mixture of fast and slow floating material. In the real system, the recovery beyond this residence time will begin to curtail because the fast floating material is being removed from the system at a faster rate than the slow floating. Alternatively, projections from the composite rate assume the same mixture of fast and slow material for all residence times, with the assumed mixture being equal to the mixture that was present at the composite time. For residence times beyond the composite time, the projection assumes a greater portion of fast floating material than the true distribution in the real system. As a result, the projection always over-predicts real recovery.

Second, the magnitude of the over or under-prediction is dependent upon the relative magnitude of the original rate data. In this example, the gangue recovery is much more susceptible to over-prediction than the copper recovery. Also, the original rate data for the gangue components are roughly one order of magnitude lower than the original rate data for the chalcopyrite. For example, Figure 4.5 shows that at a residence time of 20 minutes

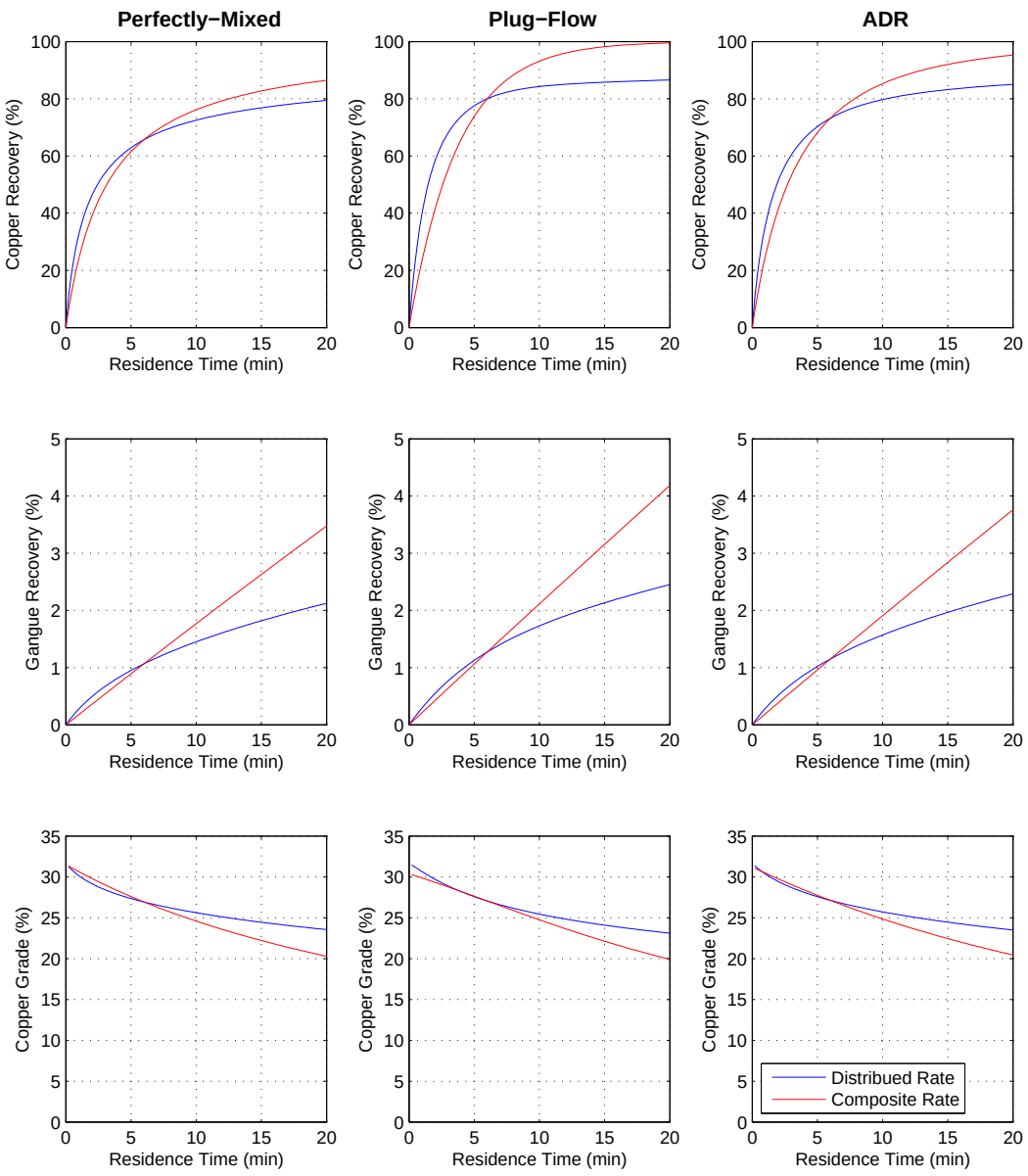

Figure 4.4: Simulation deviation plots. Top row shows copper recovery as a function of residence time, middle row shows gangue recovery as a function of residence time, and bottom row shows copper grade as a function of residence time. Columns reflect the different reactor types. The ADR reactor calculated for $Pe = 2$. The distributed curve reflects information on the full distribution of kinetic coefficients, while the composite curve is derived from a single rate constant determined at a single flotation time ($\tau = 6$).

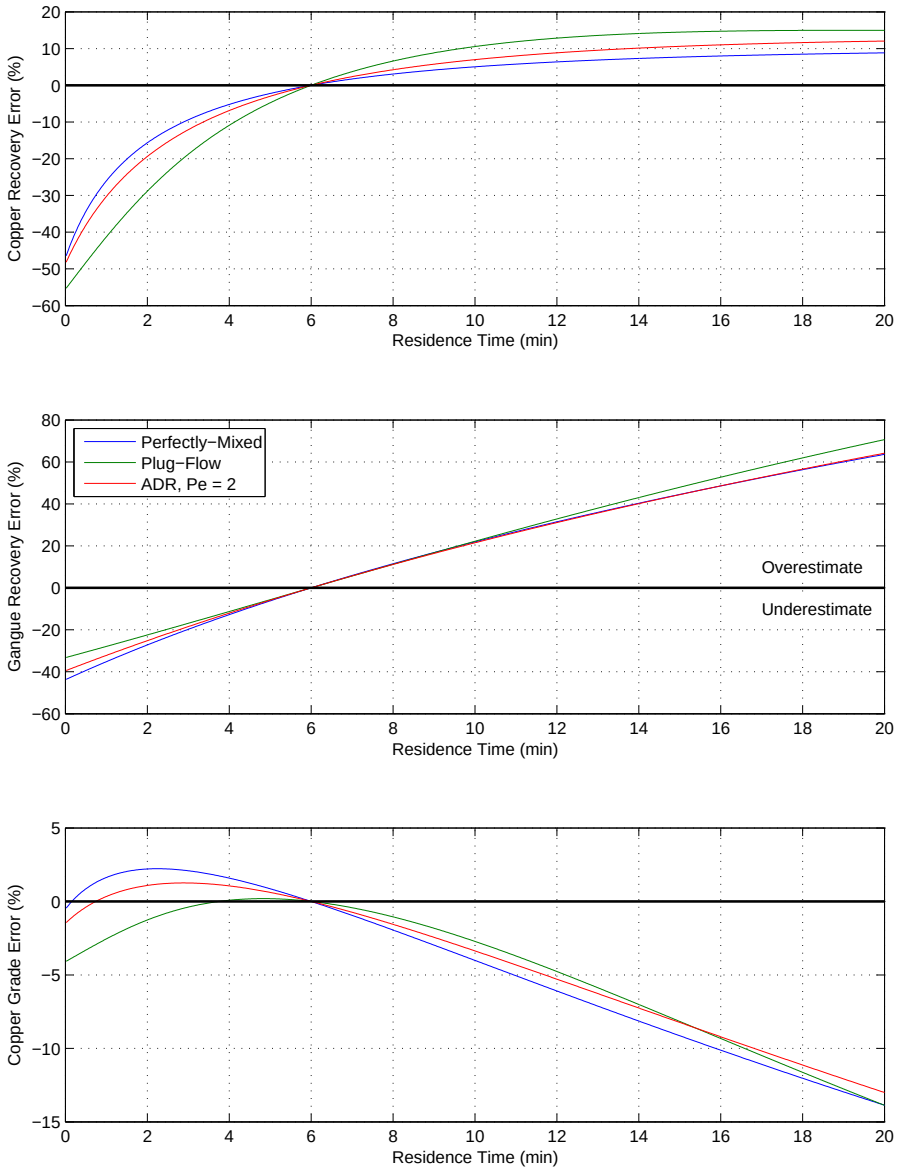

Figure 4.5: Simulation error plots. Top plot shows copper recovery error as a function of residence time, middle plot shows gangue recovery error as a function of residence time, and bottom row shows copper grade error as a function of residence time. *Error* is defined as the percent difference between the "true" distributed rate constant-derived values and the composite rate-derived values.

in a plug-flow reactor, the gangue recovery error is approximately 70%, while the copper recovery error is only 15%. Once again, this result coincides with logical expectation. The relatively high rate values for the chalcopyrite components indicate that the recovery is likely on the flat portion of the kinetic curve. In this region, small changes in the $k\tau$ value do not correspond to large changes in recovery. Alternatively, the low rate values for the gangue components likely indicate that the recovery is on steep portion of the kinetic curve, where small changes in $k\tau$ correspond to large changes in recovery. Since the copper recovery values are bounded by the upper recovery limit, over-predictions should show diminishing error as the residence time is increased.

The difference in error magnitude is further supported by the 0 rate constant for the non-floating gangue class. In the distributed system, the observable recovery will eventually reach a limit since some portion of the material is truly non-floatable. The distributed rate data for gangue recovery in Figure 4.4 shows this behavior for all three reactor types. However, in the composited data set, this non-floatable class is assumed to float at the single composite value. Thus the composite rate does not account for this truly non-floatable material, leading to further deviation in the overestimation.

One notable case where this principle is especially important is in plant modification. A common problem for flotation circuit designers is adding additional residence time to an existing rougher bank. If the data set used to design the rougher bank only reflects one residence time (e.g. the recovery and grade from the existing rougher bank), the projection will always overestimate the expected recovery and underestimate the expected grade. To alleviate this situation and minimize the discretization error associated with the projection, data from multiple residence times (e.g. batch flotation) should be collected to ascertain more elements of the floatability distribution.

4.6 Summary and Conclusions

This paper has presented the derivation of several rate constant compositing formulas. While particles of similar size and composition are known to exhibit a distribution of rate constants, the truncation of this distribution is often desired to form simple comparisons or is mandated when the available data is not sufficient to derive the full distribution. Unlike other physical properties, rate constants cannot be composited by simple weighted averages. Instead, time-dependent and reactor-specific equations must be used to determine the apparent rate constant that yields the same recovery as a the sum of all component rate constants.

For a plug-flow reactor, the composite rate constant (k^*) is given by:

$$k^*_{plug} = \left(-\ln \left[\frac{\sum_{i=1}^{N} M_i e^{-k_i \tau}}{\sum_{i=1}^{N} M_i} \right] \right) \tau^{-1}$$

while in a perfectly-mixed reactor, the composite rate constant is given by:

$$k^*_{mixed} = \left(\frac{\left[\sum_{i=1}^{N} M_i \right] \left[\prod_{i=1}^{N} (1 + k_i \tau) \right]}{\sum_{i=1}^{N} \left[\frac{M_i \left[\prod_{j=1}^{N} (1 + k_j \tau) \right]}{(1 + k_i \tau)} \right]} - 1 \right) \tau^{-1}.$$

The axially-dispersed reactor model is too complicated to yield an analytical expression for k^*. Rather, a numerical procedure using Newton's method has been described.

From this investigation, three key conclusions are derived:

1. All three rate compositing formulas are time dependent. The resulting functions produce semi-log transitions as the composite rate constant varies through a continuum of residence times.

2. The maximum observable rate constant at an infinitesimally small time is the simple mass weighted average of the component rate constants. The minimum observable rate constant at infinitely long residence times is reactor dependent, but only equal to minimum component rate in the plug-flow reactor.

3. The composite rate constant formulas may be used to quantify discretization error when a distribution of rate constants is truncated to a single value by single-residence time experimental testing. In all cases, projections beyond the test residence time show an over-prediction of recovery, while projections lower than the test residence time always show an under-prediction of recovery.

The utility of these equations may also be extended to other data fitting and rate comparison analyses. While these examples have only used two or three component systems, the formulation of the equations promote unlimited scalability.

4.7 Bibliography

Beolchini, F., Papini, M. P., Toro, L., Trifoni, M., & Vegliò, F. (2001). Acid leaching of manganiferous ores by sucrose: kinetic modelling and related statistical analysis. *Minerals Engineering*, *14*(2), 175–184.

Do, H. (2010). *Development of a turbulent flotation model from first principles*. Unpublished doctoral dissertation.

Fichera, M., & Chudacek, M. (1992). Batch cell flotation models–a review. *Minerals Engineering*, *5*(1), 41–55.

Fuerstenau, D., Kapur, P., & Mitra, A. (1982). Dry pelletization of kaolin. *Powder Technology*, *32*(1), 101–106.

Gaudin, A., Schuhmann Jr, R., & Schlechten, A. (1942). Flotation kinetics. ii. the effect of size on the behavior of galena particles. *The Journal of Physical Chemistry*, *46*(8), 902–910.

Imaizumi, T., & Inoue, T. (1965). Kinetic consideration of froth flotation. *6th Int. Mineral Processing congr., Cannes, 1963*, 581–593.

Kelley, K., Noble, A., Luttrell, G., & Yoon, R. (2012). Development of a model-based flotation simulator. In C. Young & G. Luttrell (Eds.), *Separation technologies for minerals, coal, and earth resources* (pp. 699–708). SME.

Levenspiel, O. (1999). *Chemical reaction engineering*. Wiley.

Lynch, A., & Bush, P. (1977). *Mineral crushing and grinding circuits: their simulation, optimisation, design and control* (Vol. 340). Elsevier.

Lynch, A., Johnson, N., Manlapig, E., & Thorne, C. (1981). *Mineral and coal flotation circuits*. Elsevier.

Mellado, M. E., Cisternas, L. A., & Gálvez, E. D. (2009). An analytical model approach to heap leaching. *Hydrometallurgy*, *95*(1), 33–38.

Polat, M., & Chander, S. (2000). First-order flotation kinetics models and methods for estimation of the true distribution of flotation rate constants. *International Journal of Mineral Processing*, *58*(1), 145–166.

Sherrell, I. (2004). *Development of a flotation rate equation from first principles under turbulent flow conditions*. Unpublished doctoral dissertation.

Sutherland. (1948). Physical chemistry of flotation. xi. kinetics of the flotation process. *The Journal of Physical Chemistry*, *52*(2), 394–425.

Tomlinson, H., & Fleming, M. (1965). Flotation rate studies. In *International mineral processing congress* (Vol. 6, pp. 563–579).

Chapter 5

An Algorithm for Analytical Solutions and Analysis of Mineral Processing Circuits

(ABSTRACT)

Traditional simulations of mineral processing circuits are solved by straightforward numerical techniques which require iteration to accommodate recirculating loads. Depending on the complexity of the simulated circuit, this solution technique can be inexact, computationally intensive, and potentially unstable. In this communication, an alternate calculation approach is presented, wherein an exact analytical solution is determined as a function of the individual units' separation probabilities. All the stream data, including recirculating loads, may be solved simultaneously, negating the need for iteration. Furthermore, with a symbolic solution available, linear circuit analysis may then be used to diagnose the relative separation potential of the circuit. By integrating these tools, the authors have developed a software package for evaluating circuit configurations. This paper presents the theory, development, and limitations of the software's methodology along with industrial examples which highlight the tool's applicability to industrial circuits.

5.1 Introduction

The ultimate goal of all mineral and coal processing operations is the separation of valuable components from the invaluable. Regardless of the sophistication or complexity, all

Table 5.1: Comparison of Circuit Evaluation Methods

Comparison Criteria	**Empirical Experience**	**Computer Simulation**	**Circuit Analysis**
Implementation Ease	●	○	○
Perceived Applicability	●	◐	○
Deterministic Insight	○	●	◐
Fundamental Insight	○	◐	●
Required Data	◐	○	●
Required Resources	●	○	◐
Advantages	Practice Driven	Numerical Results	Insightful
Disadvantages	No Insight	Time, Cost	Cumbersome

○= Poor, ◐= Marginal, ●= Good

single-stage separation processes are inherently imperfect. To ameliorate this imperfection, engineers and metallurgists have implemented staged-processes or *circuits* to pursue specific performance goals. The complexity and breadth of the process circuit can vary widely, depending on the value of the desired commodity.

The engineering design of process circuits has traditionally been driven by three distinct paradigms representing varying degrees of complexity: 1) empirical experience and operationally-conceived best practices, 2) computer simulation, 3) fundamental analytical techniques. Table 5.1 summarizes the trade-offs between these methods.

Empirical experience draws upon prior knowledge and operator bias. Circuits designed solely by these principles may work well in a given condition, but as feed characteristics change, the operator will have little insight on how performance may vary. Nevertheless, sound process knowledge is fundamental to the successful implementation of other tools.

Conversely, computer simulation typically integrates a more phenomenological approach (Wills & Napier-Munn, 2006; King, 2001). By invoking fundamental knowledge of the relevant sub-processes, simulation can provide a more deterministic quantification of the proposed circuit's performance. Unfortunately, computer simulation typically requires extensive data describing the feed material and the separation processes. Furthermore, the data processing, data analysis, simulation set-up, and simulation execution may require a substantial labor resources to provide a reasonably accurate solution. Depending on the number of

circuit configurations proposed during the design phase, computer simulation may not be a viable option to compare each alternative.

Finally, analytical circuit evaluation represents a more balanced trade-off between required resources (data and time) and value gained. Unfortunately, these methods are often unheeded due to the cumbersome mathematics required for multi-unit configurations and the perceived inapplicability depending on the assumptions invoked.

When designing a process circuit, the balance between the aforementioned tools is crucial. Each tool serves a specific purpose, and if utilized inappropriately, the tool may produce erroneous and inaccurate predictions. For example, simulations and circuit analysis are best implemented under the critical direction of experienced personnel. If simulations are "blindly" conducted or do not reflect empirically observed limitations, the reliability of the results may be substantially compromised. Therefore, the best approach to circuit design is to utilize each of the three tools in their own context, while acknowledging the merits and weaknesses of each.

This communication presents a refined approach to an analytical procedure originally described by Meloy (1983). The concept, generically coined *linear circuit analysis*, draws upon a simple mathematical approach to binary separators. By using these concepts to determine an algebraic solution to the circuit streams, mathematical indicators may be determined and used to compare circuit designs. This paper will provide a general review of circuit analysis and the underlying theory. Next, the details of the current refinements and the development of a circuit analysis software package will be described. Finally, the software's utility will be defined within the context of an industrial application.

5.2 Theory

5.2.1 Partition Curves

The primary purpose of circuit implementation is to overcome the inherent imperfection of single-stage separators. Consequently, any analytical circuit evaluation technique must account for the reduction of these imperfections in various circuit configurations; thus, the imperfections must somehow be mathematically defined. In the past, several researchers have used partition functions to generically model various separation processes (King, 2001). Partition functions rely on the predication that a simple separator receives feed which is characterized by individual particles having a given distribution of a specified property (e.g.,

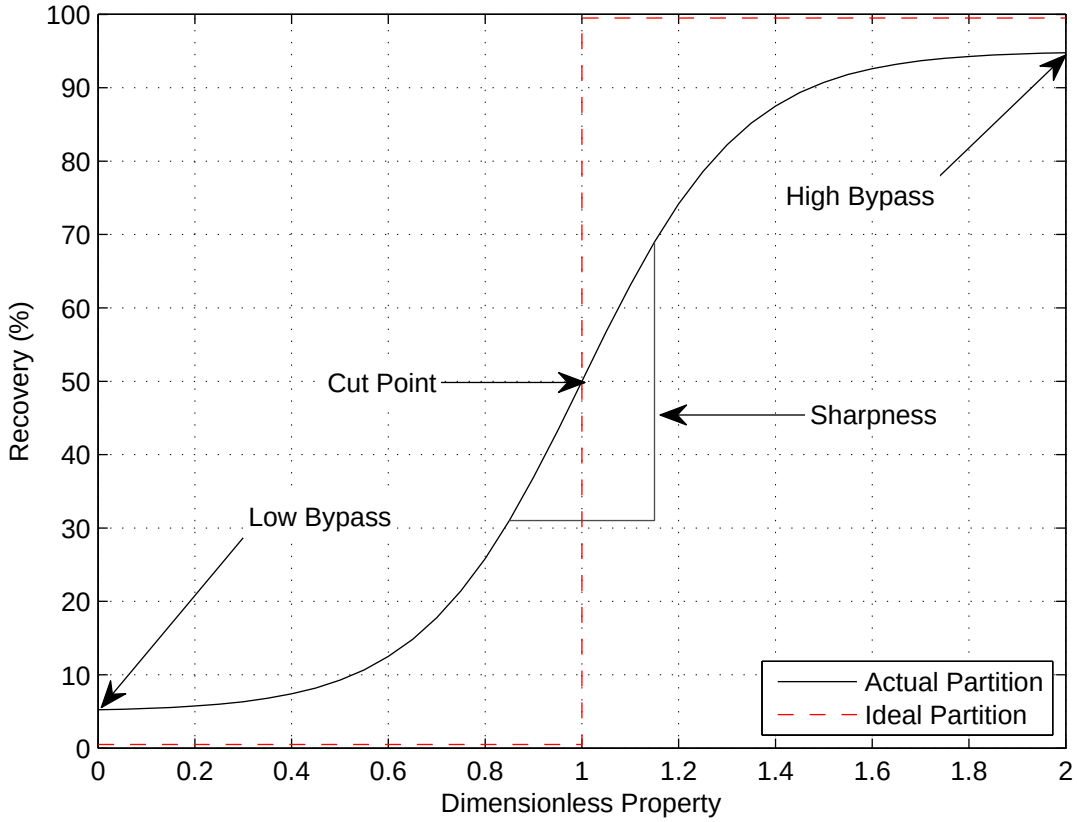

Figure 5.1: Typical partition function with the primary parameters labeled: cut-point, sharpness, high bypass, and low bypass.

10,000 tons of sand with a defined particle size distribution). The separator then distributes that feed to one of two products in a proportion dependent on the individual particle's magnitude of the property. This distribution of the feed to the two products may be interpreted as a probability (e.g. a 1,000 micron particle has a 100% chance of going to screen overflow; a 150 micron particle has a 20% chance of going to screen overflow).

The function defining these probabilities may be visualized as a smooth S-shaped curve, as shown in Figure 5.1. The horizontal axis may be manifested as any property, either tangible or abstract, which a separation process can be based on (e.g., size, density, magnetic susceptibility, conductivity, Stokes diameter, floatability, color, boiling temperature, shape, hardness, etc.). Furthermore, the vertical axis may represent the recovery to either product, depending on the system.

While several researchers have proposed mathematical fits to the partition function,

all essentially rely on four parameters: high bypass, low bypass, cut-point, and separation sharpness (King, 2001). High bypass is the percentage of high property material that reports to the desired product. Graphically, this is the location maximum asymptote of the partition function. Similarly, the low bypass is the amount of low property that reports to the incorrect product or they low asymptote of the partition function. The cut-point is the property value at which a particle has a 50% chance of reporting to either product. Finally, the separation sharpness is the slope of the curve at this 50% point. A higher slope indicates that the separator can better distinguish middling particles. Intuitively, each parameter of the partition function reveals some information on the separation capability of a single unit.

One mathematical form of the partition function is given by:

$$P = (\theta_H - \theta_L)\frac{1}{1 + \exp(\alpha(1 - Z))} + \theta_L \tag{5.1}$$

where P is the partition probability, θ_H is the high bypass, θ_L is the low bypass, α is the separation sharpness, and Z is the property normalized by the cut-point (X/X_{50}) (King, 2001). In a perfect separator, the partition curve is a step function, i.e., particles lower than the desired separation point will have a zero probability of reporting to the product, while particles with a higher property will have a 100% probability of reporting to product.

5.2.2 Circuit Analysis

Linear circuit analysis is an approach originally described by Meloy (1983). In the past, this tool has been used to evaluate heavy mineral circuits (McKeon & Luttrell, 2005), coal spiral circuits (Luttrell, Kohmuench, Stanley, & Trump, 1998), and magnetic separators (Luttrell, Forrest, & Mankosa, 2002). This procedure provides a systemic approach to the evaluation of processing circuits and the ability of these circuits to overcome partition imperfections. In order to evaluate the strength of a circuit, an analytical solution for the circuit recovery is first required. Fundamentally, recovery is simply defined as the proportion of mass that reports to the concentrate relative to the original feed mass (C/F). This proportion can be defined for the total mass of the stream (i.e., yield) or of a particular component (i.e., recovery). To determine this analytical expression, the recovery of each unit is defined by a probability value, P. This P value may be considered a deterministic, single value for a given property class or a functional value, such as a partition function. For a single unit, the solution is trivial (Figure 5.2). The concentrate mass (C) is the P value multiplied by the feed mass (F):

$$C = PF.$$

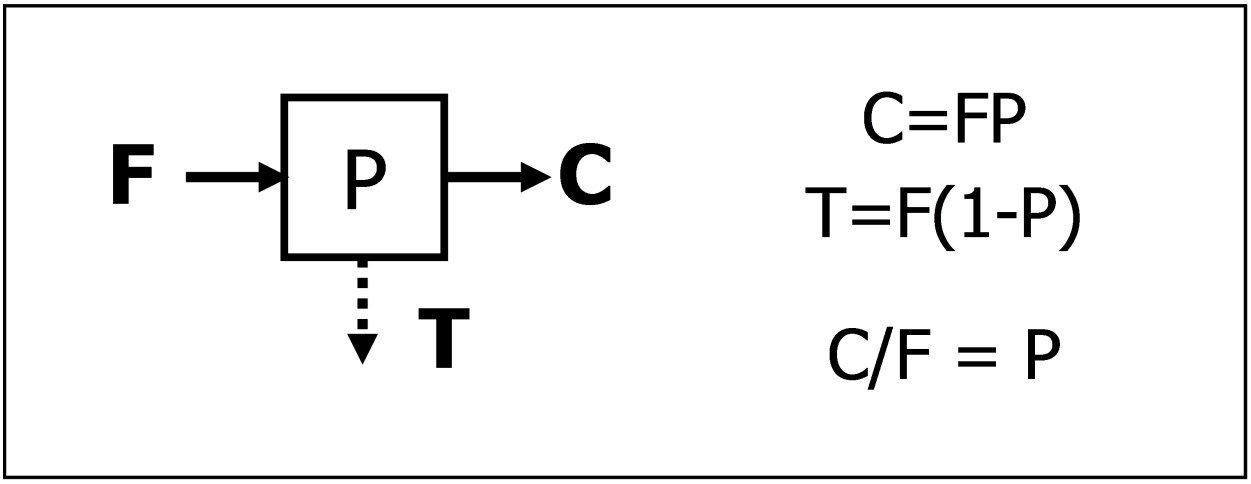

Figure 5.2: Circuit analysis solution for a single cell.

Following similar logic, the tailings mass (T) may be calculated by:

$$T = (1 - P)F.$$

Extending this procedure, the circuit concentrate and tailings streams can be calculated for any circuit configuration. As a simple example, consider a rougher-cleaner circuit, with no recycle (Figure 5.3). The first unit produces the same solutions presented in the trivial case. If the first unit's concentrate (FP_1) is then introduced as feed to the second unit, the final concentrate and final tails can be calculated by:

$$\begin{aligned} C &= FP_1P_2 \\ T &= F(1 - P_1) + FP_1(1 - P_2). \end{aligned}$$

If a recycle stream is introduced to the rougher-cleaner circuit, an additional equation must be written to account for the additional unknown. In this example, the first unit's feed is not explicitly known, so an arbitrary F' variable is assigned. However, by adding another equation to account for the initial node, F' can be solved in terms of F, and the appropriate substitutions can be made to solve for C/F. These procedures are shown in Figure 5.4.

Once an analytical solution to the recovery has been obtained, various parameters of the circuit strength may be evaluated. One of the most useful parameters presented by Meloy is relative separation sharpness. By re-examining the partition function (Figure 5.1), the α value is defined as the slope of the partition function at $P = 0.50$. Extending the concept, the partition function may be applicable for a single unit, or for an entire circuit. If the circuit's

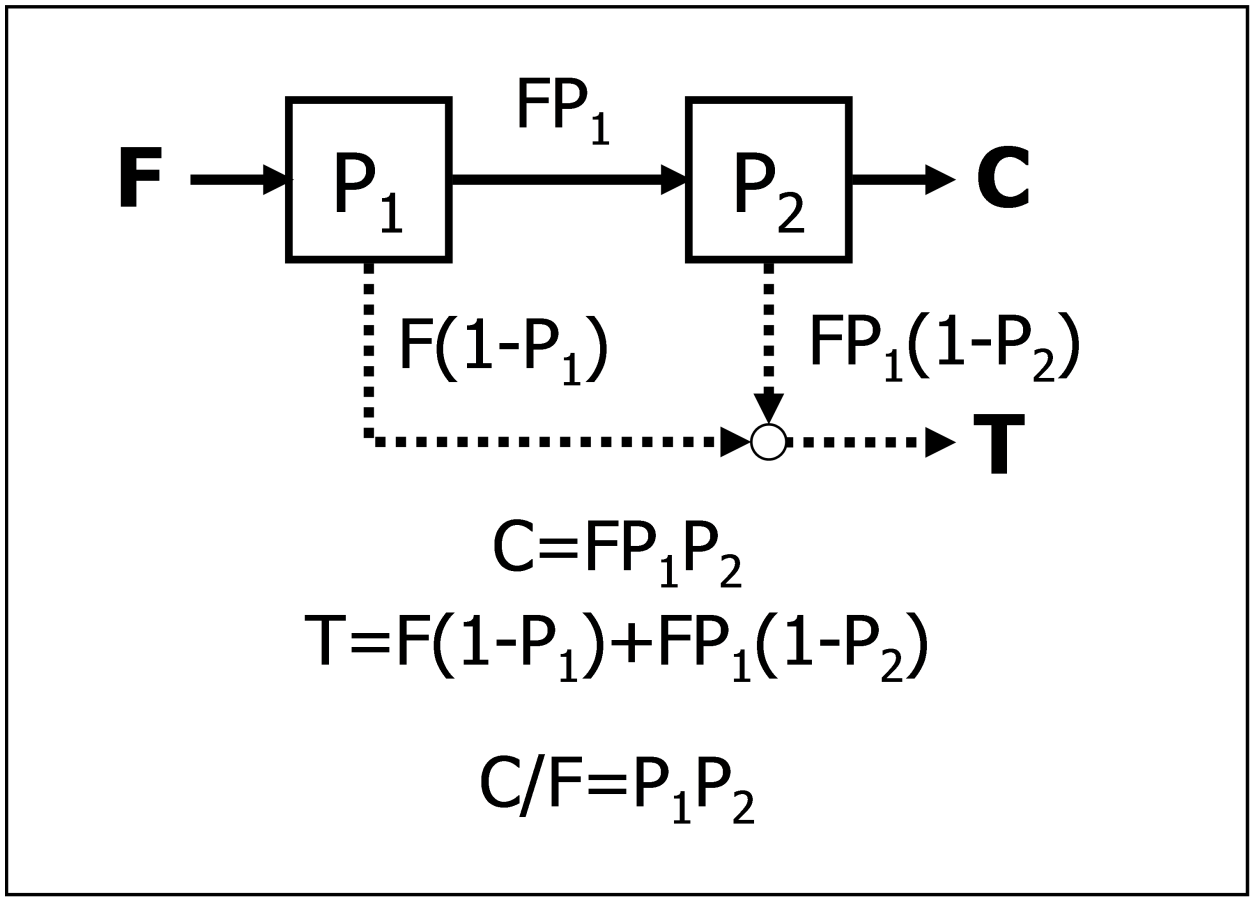

Figure 5.3: Circuit analysis solution for rougher-cleaner open circuit.

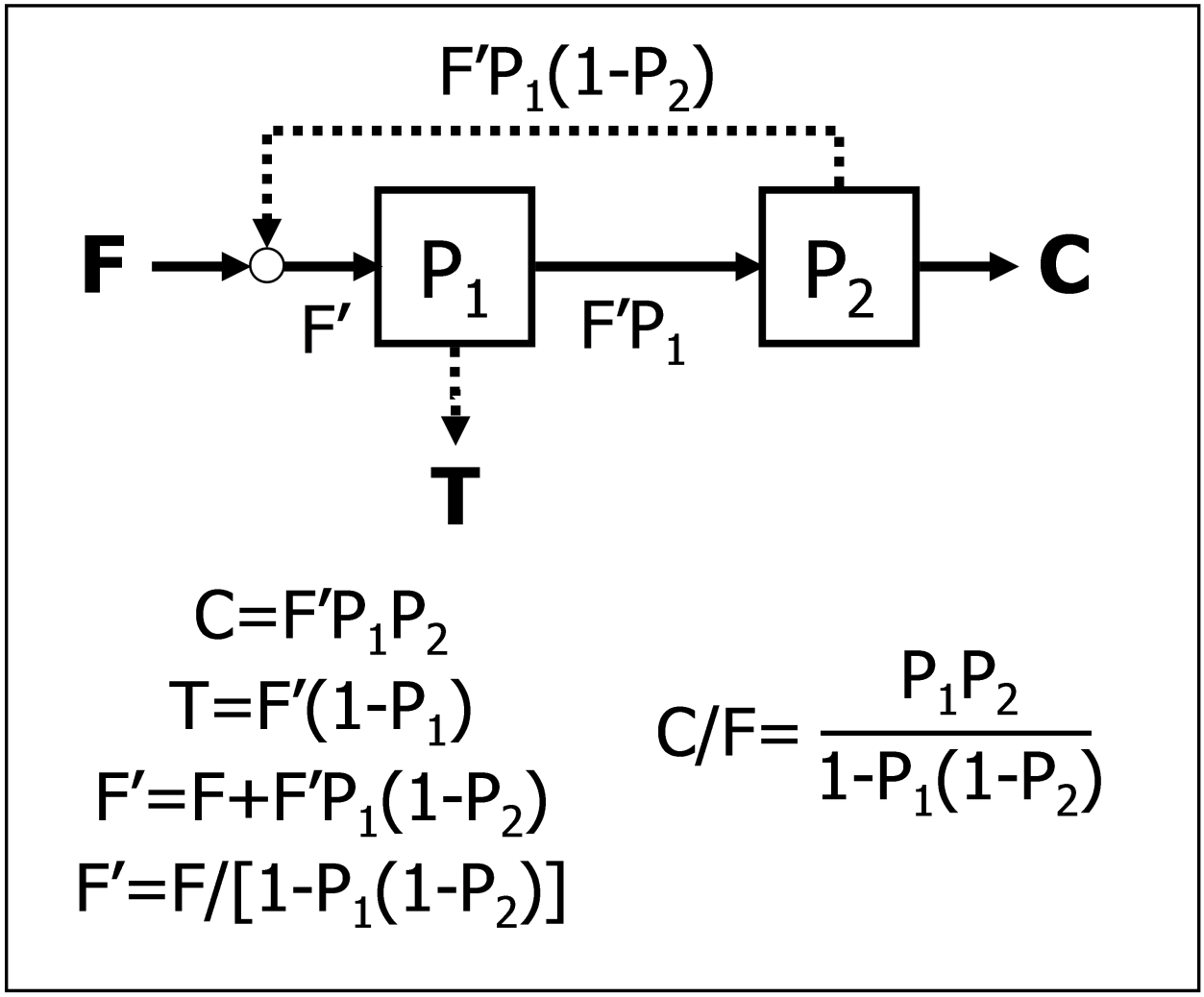

Figure 5.4: Circuit analysis solution for rougher-cleaner circuit with recycle.

recovery function (i.e. C/F) is analytically known, the derivative of this function may be calculated with respect to Z at $P = 0.50$ to determine the circuit's separation sharpness. In order to simplify the problem, all the units may be assumed to have the same probability. Mathematically, this expression is given by:

$$\frac{\partial(C/F))}{\partial Z} = \frac{\partial P}{\partial Z}.$$

For a single unit ($C/F = P$), the derivative of the recovery function is 1.00 along the entire curve. Consequently, when this calculation is repeated for more complex circuits, the value may be compared to 1.00 in order to determine the circuit's relative separation sharpness when compared to sharpness of a single unit. Physically, this value represents the circuit's ability to distinguish middling material. Circuits with enhanced separation sharpness will be characterized by a better grade-recovery curve.

When $P1 = P2$, the derivative analysis for the rougher-cleaner circuit without recycle (Figure 5.3) yields:

$$\begin{aligned}\frac{\partial(C/F))}{\partial Z} &= \frac{\partial(P^2)}{\partial Z} \\ &= 2P \\ &= 2(0.5) = 1\end{aligned}$$

In this case, the circuit's separation sharpness is no better than that of a single unit. Extending this analysis to the rougher-cleaner circuit with recycle (Figure 5.4) yields:

$$\begin{aligned}\frac{\partial(C/F))}{\partial Z} &= \frac{\partial(P^2/(1-P+P^2))}{\partial Z} \\ &= \frac{2P(1-P+P^2) - P^2(-1+2P)}{(1-P+P^2)^2} \\ &= \frac{-P^2+2P}{(1-P+P^2)^2} \\ &= \frac{-(0.5)^2+2(0.5)}{(1-(0.5)+(0.5)^2)^2} = 1.33\end{aligned}$$

Thus, by recycling the cleaner tailings back to the head of the circuit, the separation sharpness is enhanced 33%.

The circuit analysis method described above is restricted by the assumption of linearity. As defined by Meloy (1983), linearity implies three conditions (i) particle-particle interactions

do not affect the probability that a particle will report to a given stream, (ii) the fraction of particles of a given property in each stream remains unchanged as feed rate increases, and (iii) the partition curve is feed independent. Simply, these assumptions state that the partition function for a given unit is fixed, with respect to the feed rate and composition. While real processing circuits do not necessarily adhere to the linearity assumption, Meloy argues that for the design-case, all circuits are linear, since the size or number of the units has not yet been determined. Consequently, the equipment may be sized to accommodate any feed rate such that linear behavior is achieved.

5.3 Software Development

5.3.1 Matrix Reduction Analytical Solution Algorithm

The value of circuit analysis lies in its ability to provide fundamental evaluation without extensive data or computational resources. Unfortunately, when the circuit size extends beyond three or four units, the math becomes overly cumbersome, and the value of the final solution is diluted by the effort needed to achieve it. In order to overcome this deterrent, a graphically-based software program was developed to compute circuit analysis solutions. The resulting platform integrates a Microsoft Excel graphical user interface and a new matrix reduction solution algorithm to determine analytical stream solutions for circuits of any magnitude and any potential configuration.

To apply the matrix reduction algorithm, three circuit-descriptive arrays must first be constructed: the feed matrix ($\mathbf{F}$), the products matrix ($\mathbf{P}$), and the initial condition vector ($\vec{C}$). The two matrices have dimensions of $M \times N$ where M is the number of streams, and N is the number of units. The initial condition vector has dimensions of $M \times 1$. In constructing the feed vector, each element is given a value of 1 or 0. A value of $\mathbf{F_{m,n}} = 1$ indicates that stream m feeds unit n, while a value of 0 indicates that stream m does not feed unit n. The mathematical representation is given by:

$$\mathbf{F_{m,n}} = \begin{array}{c} \\ Stream_1 \\ Stream_2 \\ \vdots \\ Stream_M \end{array} \begin{array}{c} \begin{array}{cccc} Unit_1 & Unit_2 & \cdots & Unit_N \end{array} \\ \begin{pmatrix} F_{1,1} & F_{1,2} & \cdots & F_{1,N} \\ F_{2,1} & F_{2,2} & \cdots & F_{2,N} \\ \vdots & \vdots & \ddots & \vdots \\ F_{M,1} & F_{M,2} & \cdots & F_{M,N} \end{pmatrix} \end{array}.$$

The products matrix follows a similar construction. Here the matrix element value

represents the analytical or numeric transfer function which relates stream m to unit n. For separation units, a value of P_n or $(1 - P_n)$ is used to describe the concentrate or tailings products, respectively. For junction units, the appropriate matrix element is given a value of 1 to indicate that all of the product is produced in the single stream. Finally, products of a non-selective splitter unit may be described by the numeric fraction indicating the split. For example, 0.5 indicates one product of a 50-50 split. Formally, $\mathbf{P}$ is given by:

$$\mathbf{P_{m,n}} = \begin{array}{c} \\ Stream_1 \\ Stream_2 \\ \vdots \\ Stream_M \end{array} \begin{array}{c} \begin{array}{cccc} Unit_1 & Unit_2 & \cdots & Unit_N \end{array} \\ \begin{pmatrix} P_{1,1} & P_{1,2} & \cdots & P_{1,N} \\ P_{2,1} & P_{2,2} & \cdots & P_{2,N} \\ \vdots & \vdots & \ddots & \vdots \\ P_{M,1} & P_{M,2} & \cdots & P_{M,N} \end{pmatrix} \end{array}.$$

The initial condition vector simply indicates the value of the circuit feed. If the m^{th} stream is a circuit feed stream, a value of 1 is assigned; otherwise, each element is given a value of 0. The vector is formally defined:

$$\vec{C_{m,1}} = \begin{array}{c} Stream_1 \\ Stream_2 \\ \vdots \\ Stream_M \end{array} \begin{pmatrix} C_{1,1} \\ C_{2,1} \\ \vdots \\ C_{M,1} \end{pmatrix}.$$

Once all three circuit-descriptive arrays have been defined, the analytical circuit solution may be solved by formulating the following linear system:

$$(\mathbf{I} - \mathbf{P} \times \mathbf{F}')\vec{A} = \vec{C} \tag{5.2}$$

where $\mathbf{I}$ is the $M \times M$ identity matrix, and $\vec{A}$ is the circuit analytical solution $(M \times 1)$ for each stream.

To illustrate the utilization of this matrix reduction methodology, consider the rougher-cleaner recycle circuit given in Figure 5.4. First, the feed and products matrices are con-

structured:

$$\mathbf{F_{6,3}} = \begin{array}{c} \\ Cell_1Tail \\ Cell_1Con \\ Cell_2Tail \\ Cell_2Con \\ Feed \\ F' \end{array} \begin{array}{c} \begin{array}{ccc} Junction & Cell_1 & Cell_2 \end{array} \\ \begin{pmatrix} 0 & 0 & 0 \\ 0 & 0 & 1 \\ 1 & 0 & 0 \\ 0 & 0 & 0 \\ 1 & 0 & 0 \\ 0 & 1 & 0 \end{pmatrix} \end{array}$$

$$\mathbf{P_{6,3}} = \begin{array}{c} \\ Cell_1Tail \\ Cell_1Con \\ Cell_2Tail \\ Cell_2Con \\ Feed \\ F' \end{array} \begin{array}{c} \begin{array}{ccc} Junction & Cell_1 & Cell_2 \end{array} \\ \begin{pmatrix} 0 & 1-P_1 & 0 \\ 0 & P_1 & 0 \\ 0 & 0 & 1-P_2 \\ 0 & 0 & P_2 \\ 0 & 0 & 0 \\ 1 & 0 & 0 \end{pmatrix} \end{array}.$$

Next, the initial condition vector identifies the fifth stream as the circuit feed:

$$\vec{C_{6,1}} = \begin{array}{c} \\ Cell_1Tail \\ Cell_1Con \\ Cell_2Tail \\ Cell_2Con \\ Feed \\ F' \end{array} \begin{array}{c} \\ \begin{pmatrix} 0 \\ 0 \\ 0 \\ 0 \\ 1 \\ 0 \end{pmatrix} \end{array}.$$

The linear system may now be formulated according to Equation 5.2:

$$(\mathbf{I} - \mathbf{P} \times \mathbf{F}')\vec{A} = \vec{C}$$

$$\begin{pmatrix} 1 & 0 & 0 & 0 & 0 & P_1 - 1 \\ 0 & 1 & 0 & 0 & 0 & -P_1 \\ 0 & P_2 - 1 & 1 & 0 & 0 & 0 \\ 0 & -P_2 & 0 & 1 & 0 & 0 \\ 0 & 0 & 0 & 0 & 1 & 0 \\ 0 & 0 & -1 & 0 & -1 & 1 \end{pmatrix} \begin{pmatrix} A_1 \\ A_2 \\ A_3 \\ A_4 \\ A_5 \\ A_6 \end{pmatrix} = \begin{pmatrix} 0 \\ 0 \\ 0 \\ 0 \\ 1 \\ 0 \end{pmatrix}.$$

Solution of the linear system yields:

$$\vec{A_{6,1}} = \begin{matrix} Cell_1Tail \\ Cell_1Con \\ Cell_2Tail \\ Cell_2Con \\ Feed \\ F' \end{matrix} \begin{pmatrix} -(P_1 - 1)/(P_1P_2 - P_1 + 1) \\ P_1/(P_1P_2 - P_1 + 1) \\ -(P_1(P_2 - 1))/(P_1P_2 - P_1 + 1) \\ (P_1P_2)/(P_1P_2 - P_1 + 1) \\ 1 \\ 1/(P_1P_2 - P_1 + 1) \end{pmatrix}.$$

This matrix reduction methodology produces an analytical solution to every circuit stream in terms of individual unit transfer functions. The expression for the final circuit product (Stream 4: $Cell_2Con$) is mathematically equivalent to the expression formed algebraically in Figure 5.4. Finally, the procedure is infinitively scalable and can accommodate circuits with any number of streams and units.

5.3.2 Software Interface

The matrix reduction analytical solution algorithm is incorporated into a Excel-based software package which provides graphically-based circuit drawing tools. The software uses a custom ribbon tab on the Microsoft Excel program to access the drawing and other calculation tools. The available drawing components are limited to nodes, simple separators, and streams. By using Excel's drawing tools, the user can input the flowsheet, identify the feed and concentrate streams, and calculate the circuit analysis solution. Figure 5.5 shows a screenshot of the program's interface (a), and the custom ribbon tab highlighted (b).

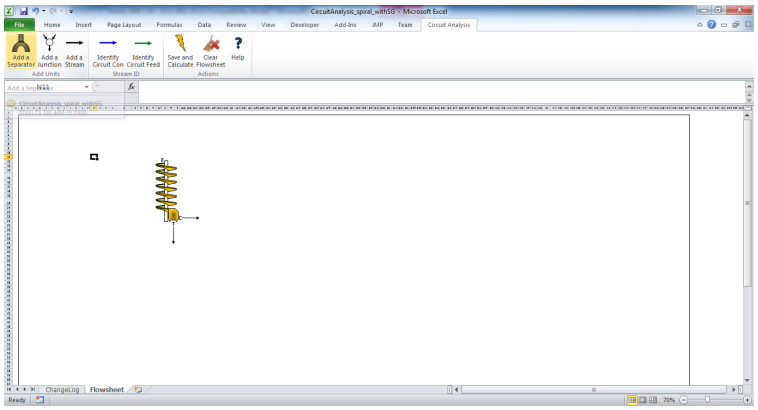

(a) Microsoft Excel platform

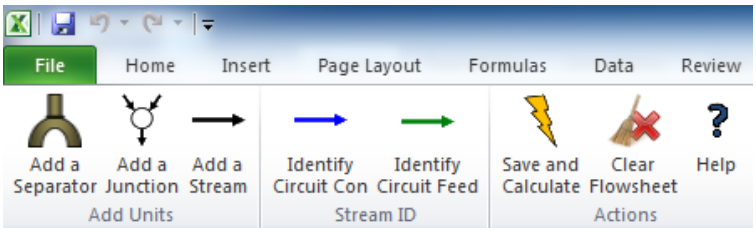

(b) Custom ribbon tab.

Figure 5.5: Circuit analysis software interface.

Once prompted, the software calculates several values indicative of a circuit's strength and presents these in a dialog window. The user is then free to alter the flowsheet, recalculate, or start over.

5.3.3 Analysis Features

The most significant output of the software is the analytical solution to the C/F value. The software next uses a numerical technique to compute the derivative of the C/F function at $P = 0.5$, assuming all P values are equal. The result is Meloy's relative separation sharpness value which is a good single indicator of circuit performance.

Further study beyond the separation sharpness has shown that the other parameters of the circuit's partition function (bypass values and relative cut-point) can also be determined once the analytical circuit solution is known. The low bypass (θ_L) defines a particular probability for the smallest property class. If given a circuit's recovery (C/F) function, the circuit's bypass may be calculated by substituting in each P value which corresponds to θ_L.

Mathematically, this calculation is defined as:

$$\theta_{L,Circuit} = C/F(P = \theta_{L,Unit})$$

For example, consider the rougher-cleaner, no recycle circuit ($C/F = P^2$). If both units have a low bypass of 10%, the circuit's low bypass may be calculated as $P^2 = (10\%)^2 = 1\%$. Likewise, the high bypass may be calculated in a similar fashion, substituting the appropriate value for P.

In order to predict the circuit's cut-point, a functional form must be given to the P value. For the circuit analysis software, Equation 5.1 is used. The choice of this function is based on calculation simplicity and is rather arbitrary. Most known partition functions predict similar behavior around the cut-point, so significant deviation is not expected regardless of the specific function chosen (King, 2001). By incorporating the partition functional form, the analytical circuit solution, and proprietary solution algorithms, the circuit analysis software is able to analytically predict the circuit's relative change in cut-point as a function of each unit's α value

5.4 Applications

5.4.1 Simple Examples

To demonstrate the power of the software, the results of several simple two- and three-unit circuits are presented. Figure 5.6 shows the two-unit circuit configurations, Figure 5.7 shows the three-unit circuit configurations, and Table 5.2 summarizes the analytical circuit solutions and the calculated parameters of the circuits' partition functions.

Since the relative cut-point is dependent on an inputted α value for each unit, an arbitrary value of 4 was chosen for this analysis, in order to show the relative change between the circuit configurations. A higher α value would result in a smaller change in the cut-point, while a lower α value will result in a greater change. Furthermore, the high and low bypass values were calculated by assuming a low bypass of 10% for each unit and a high bypass of 90% for each unit.

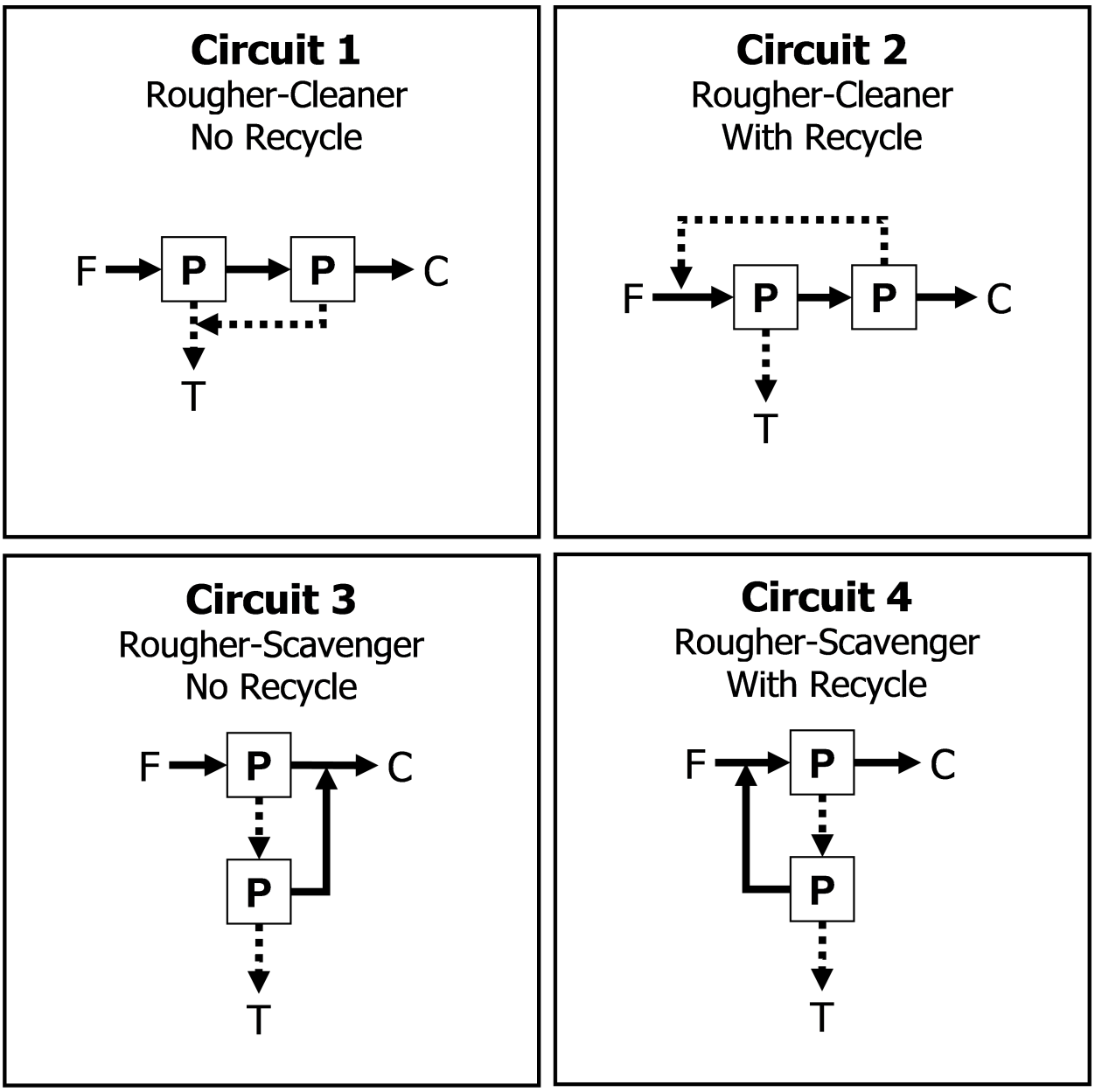

Figure 5.6: Simple two-unit circuits.

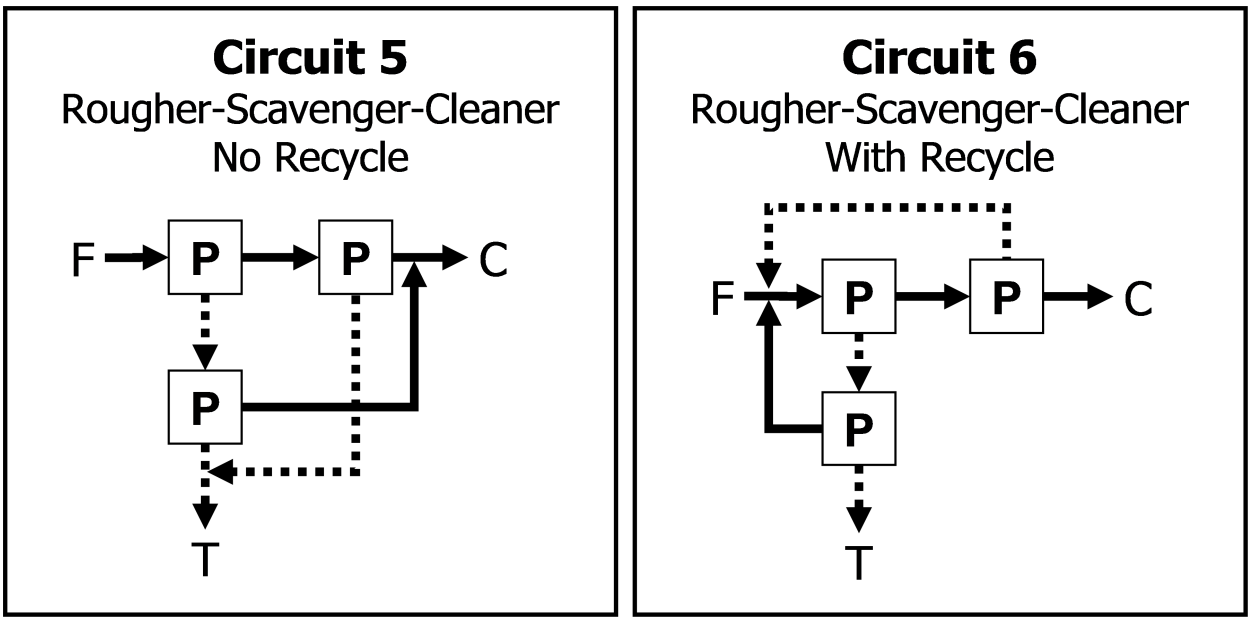

Figure 5.7: Simple three-unit circuits.

Table 5.2: Circuit analysis data for two and three-unit circuits.

Circuit Designation	**Analytical Solution**	**Relative Cut-Point**	θ_H **(90%)**	θ_L **(10%)**	**Relative** SE
1: R-C (n)	P^2	1.22	81%	1.00%	1.00
2: R-C (r)	$P^2/(1-P+P^2)$	1.12	89%	1.10%	1.33
3: R-S (n)	$2P-P^2$	0.78	99%	19.00%	1.00
4: R-S (r)	$P/(P^2-P+1)$	0.88	99%	11.00%	1.33
5: R-S-C (n)	P	1.00	90%	10.00%	1.00
6: R-S-C (r)	$P^2/(2P^2-2P+1)$	1.00	99%	1.20%	2.00

5.4.2 Discussion

The analysis of the simple circuits leads to several suggestive results. First, by examining the separation sharpness values for the two-unit circuits, the immediate conclusion is that enhanced sharpness can only result from recycle streams. This conclusion was presented in the original circuit analysis paper (Meloy, 1983).

The relative cut-point and bypass values follow an expected pattern. For the two-unit circuits, the greatest change in cut-point is realized by the non-recycling circuits. The cleaner circuits, which reprocess high property material, tend to increase the cut-point while scavenger circuits decrease the cut-point in equal portion. Since the three-unit circuits are both symmetric, the cut-point is not changed.

Additionally, a trade-off exists for the bypass values of the two-unit circuits. The rougher-cleaner, no recycle circuit substantially reduces the low bypass, at the expense of misplacing more high-property material, while the rougher-scavenger circuit reduces high bypass at the expense of misplaced low-property material.

Interestingly, Circuit 5 shows no improvement in any parameter from that of a single unit, despite the increased resources. This result implies that in more complex circuits, inappropriately implemented separation units may be completely inert.

5.4.3 Industrial Application

In a prior communication, McKeon and Luttrell (2005) used the fundamentals of circuit analysis to modify a heavy mineral sands wet plant. The original plant consisted of 686 spiral units with 14 stages of upgrading. The modified plant greatly reduced this requirement, as it consisted of 542 units with 11 stages of upgrading. Given the magnitude and complexity of these plants an analytical circuit solution and relative separation sharpness were not presented. Rather, the authors reported actual performance gains which are summarized in Table 5.3. While the modified circuit did not substantially enhance the ultimate recovery (94.7% vs. 93.0%), it did significantly reduce the number of passes needed to achieve this recovery (7 to 1).

To verify the suggestions and industrial applicability of the circuit analysis software, these two circuits were analyzed to determine the analytical circuit solution and the relative separation sharpness. For the analysis, all units were assumed to have the same P value. Furthermore, since these spirals produced three products (concentrate, middlings, and tail-

Table 5.3: Summarized data for heavy mineral sands plants as presented by (McKeon & Luttrell, 2005).

Parameter	**Original Circuit**	**Modified Circuit**
Ultimate Recovery	93.0%	94.7%
Number of Required Passes	7	1
Number of Stages	14	11
Number of Spirals	686	542

ings), each unit was modeled as two units in series. Figure 5.8 shows a screenshot from the software after calculating the analytical solution (C/F) and the relative separation sharpness (SE) for the original circuit. Figure 5.9 shows a similar screenshot for the modified circuit.

The software confirms the original authors' claims. The second circuit showed a greater separation sharpness (4.29 compared to 2.36) which was anticipated by the plant modifications and verified by the enhanced plant performance.

5.5 Summary and Conclusions

A software package has been developed which integrates Meloy's circuit analysis concept with solution algorithms that minimize the cumbersome algebra. The result is a tool which can provide efficient and quick insight on mineral processing circuits without the need for extensive data sets and computing resources. The implications of this tool are to provide insight and guidance. The circuit analysis software will never completely offset the need for simulation or empirical experience; however the solution algorithm may offset iterative calculation for process simulations. Predictions of grade, recovery, and other performance indicators will still require numeric simulation when a deterministic result is expected, and empirical experience is still needed to ensure that common-sense limitations are not exceeded. Nevertheless, this tool is intended to limit the required number of simulations. Rather than designing a circuit by performing multiple simulations on random and experience-driven circuit configurations, the principles can guide the design and limit the field of proposed designs. Such guidance can hasten the design process while providing truly engineered circuit solutions.

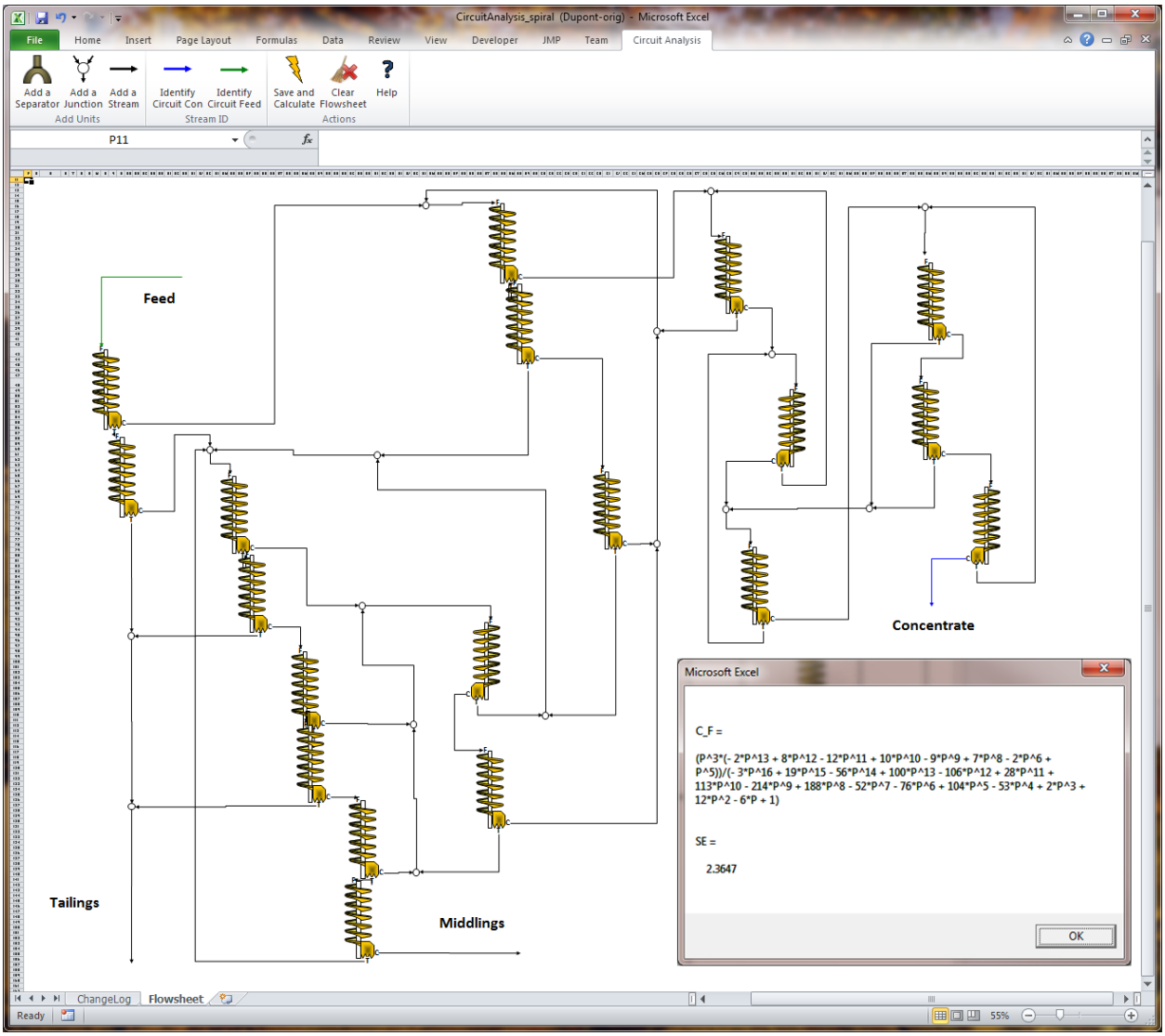

Figure 5.8: Circuit analysis software screenshot showing the analytical solution (C/F) and relative separation sharpness (SE) to the original circuit. Circuit flowsheet after (McKeon & Luttrell, 2005).

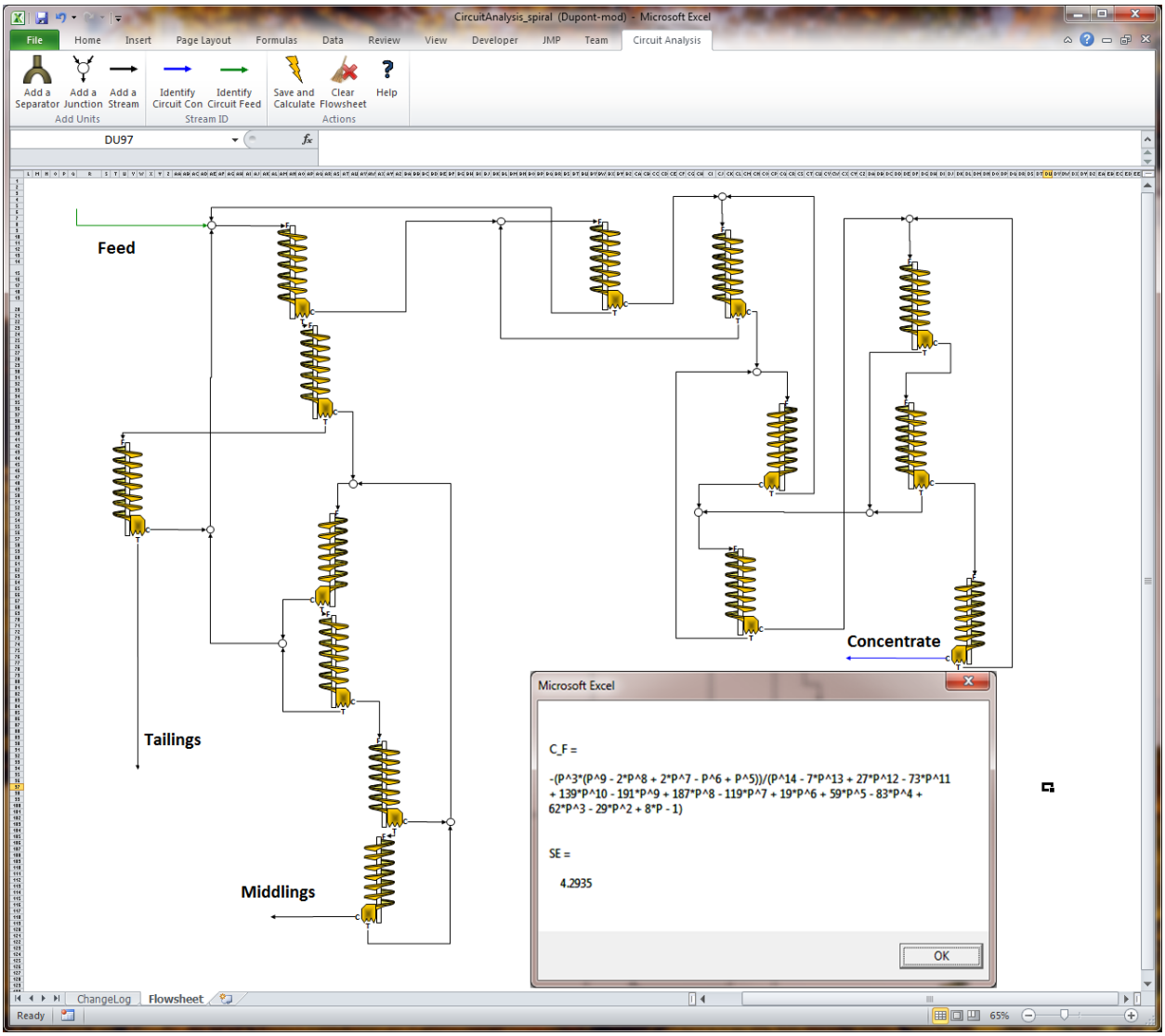

Figure 5.9: Circuit analysis software screenshot showing the analytical solution (C/F) and relative separation sharpness (SE) to the modified circuit. Circuit flowsheet after (McKeon & Luttrell, 2005).

Acknowledgments

The author would like to thank Dr. Serhat Keles for his initiative in designing the user interface and providing ideas and suggestions for general software usability.

5.6 Bibliography

King, R. (2001). *Modeling and simulation of mineral processing systems.* Elsevier.

Luttrell, G., Forrest, W., & Mankosa, M. (2002). Development of an ideal separation curve for dry beneficiation. In *Sme preprint number 02-178* (p. 8). SME.

Luttrell, G., Kohmuench, J., Stanley, F., & Trump, G. (1998). Improving spiral performance using circuit analysis. *Minerals & Metallurgical Processing*, *15*(4), 16–21.

McKeon, T., & Luttrell, G. (2005). Application of linear circuit analysis in gravity separator circuit design. In *Heavy minerals.*

Meloy, T. (1983). Analysis and optimization of mineral processing and coal-cleaning circuits circuit analysis. *International Journal of Mineral Processing*, *10*(1), 61–80.

Wills, B., & Napier-Munn, T. (2006). *Wills' mineral processing technology: an introduction to the practical aspects of ore treatment and mineral recovery.* Butterworth-Heinemann.

Chapter 6

CART^{TM}: A Fundamental Tool for Process Circuit Design

(ABSTRACT)

The design of separation circuits can be a complex, labor-intensive and costly process. While the engineer's experience along with extensive data sets and simulation are crucial tools for determining the final solution, a more fundamental approach is suitable to compare preliminary options and reduce the number of potential alternatives. In light of this need, the authors have developed the Circuit Analysis Reduction Tool (CART^{TM}). This software package relies on the fundamental principles of linear circuit analysis; however, the solution methodology has been streamlined to automatically incorporate stream splitting and unique separation performance for each unit. The resulting tool allows preliminary analysis of circuit designs without the need of detailed feed characterization. In addition to the basic analytical approach, this paper supports the veracity of the methodology with a simulated lead flotation example.

6.1 Introduction

6.1.1 Background

The fundamental goal of mineral processing is to increase the value of mining products to a degree that sufficiently justifies the upgrading costs. This upgrade is achieved by separating

the valuable and invaluable components of the run-of-mine material. In solid-solid mineral systems, these constituents are often labeled ore and gangue. Nevertheless, a more general interpretation can be applied to consider the separation of any component which ultimately increases profitability from any component which ultimately decreases profitability. For example, coal drying can be viewed as a beneficiation process which separates the dry coal material from the water to a point which sufficiently justifies the drying cost.

Given various physical limitations, the efficiency of separation in standalone units is severely limited. To overcome this deficiency, mineral processing plants often employ staged separation which can incorporate numerous separation devices of different sizes and operational characteristics. The unit operations and the interconnection between individual units are collectively described as the separation circuit.

The design of separation circuits is an open-ended, ill-defined engineering problem mostly experienced in two contexts: plant modifications and greenfield designs. The plant modification problem involves adding resources to an existing plant to pursue the enhancement of one or two process objectives (e.g. add a unit to increase overall recovery of fine material). Plant modification problems often entail a constrained solution, and comparisons between the initial and modified plant determine the real performance gains. The modifications may be limited to a specific section of the plant, as the costs, benefits, and risks of the modifications are balanced.

Alternatively, the greenfield problem usually entails more creativity and enhanced risk. The greenfield site does not have an existing plant to establish or compare site-specific process objectives, so historic indicators and experimental data must be used to establish benchmarks. Often, the circuit designer leverages prior experience to define a starting point, while laboratory and pilot-scale analyses are used to refine the specific operational parameters to produce in the final solution.

In both the greenfield designs and plant modifications, the final solution must answer four questions:

1. Which separation processes are to be utilized?
2. What is the total size and number of units needed?
3. What are the standard operational parameters for each unit?
4. How should the interconnection between the units be configured?

Circuit designers often approach the four circuit design problems independently while

incorporating knowledge from three paradigms: (1) empirical observation/traditional knowledge; (2) simulation and phenomenological predictions; (3) circuit analysis and optimization.

6.1.2 Separation Circuit Design Techniques

Today, many state-of-the-art solutions largely utilize process models. Over the last 40 years, the fidelity of these models has increased from low-level empirical curve fits, to phenomenological and other physics-based predictive models. Many mineral processing unit operations have mature phenomenological models which require experimental testing to tune the parameters. In general, the reliability of the simulation is principally dependent on the size and accuracy of the data set. As a result, substantial experimental work must be performed to ensure validity and repeatability. Several commercial software packages incorporate these contemporary models and data analysis software. The most widely used examples include Limn (Nageswararao, Wiseman, & Napier-Munn, 2004; Hand & Wiseman, 2010), JKSimMet (Cameron & Morrison, 1991; Richardson, 2002), and Modsim (King, 2001). At a higher level of fidelity, purely theoretical models are in development for some unit operations, but are still largely considered immature (Do, 2010; Kelley, Noble, Luttrell, & Yoon, 2012). Furthermore, computation fluid dynamics (CFD) and discrete element method (DEM) simulations are becoming increasingly popular as an alternative to experimental testing.

Despite the sophistication of current process modeling and simulation, the circuit designer's experience cannot be understated or denigrated as a design tool. The circuit designer can consider pragmatic factors not inherent to standard process models (e.g. brand loyalty, maintenance familiarity, process control complexity, etc.).

Lastly, circuit analysis and optimization is a broad category of design tools which incorporate fundamental analytics and numeric optimization. Some of these tools, such as Meloy's linear circuit analysis (Meloy, 1983), predate contemporary simulation since they rely on simple algebra, rather than computationally intensive mathematics. Other examples of analytical tools include procedures for determining the overall circuit size (M. Williams & Meloy, 1991; Galvez, 1998), the relative size between parts of the circuit (Sutherland, 1981), the amount of material recirculated (Loveday & Marchant, 1972; Lauder & McKee, 1986; Loveday & Brouckaert, 1995), the point of reentry for recirculating loads (M. Williams & Meloy, 1991; Galvez, 1998), and the unit which most greatly influences the overall circuit performance (Lucay, Mellado, Cisternas, & Galvez, 2012).

Most recently, researches have attempted to synthesize the analytical techniques, the

modeling and simulation tools, and to a limited extent, the empirical insight, in order to form robust circuit optimizers. An extensive review of circuit optimization strategies has been given by (Mendez, Galvez, & Cisternas, 2009). While older optimizers solved the problems of stream interconnection and unit parameters separately, more modern tools resolve both questions simultaneously. Often, the optimizers impose a generic circuit superstructure which contains all of the possible solutions originally established by the circuit designer. The final circuit is generated from this superstructure. Researchers have utilized numerous optimization algorithms, including: genetic search algorithms (Guria, Verma, Gupta, & Mehrotra, 2005; Guria, Varma, Mehrotra, & Gupta, n.d.) mixed-integer linear programming (Cisternas, Mndez, Glvez, & Jorquera, 2006), integer programming, as well as other various search strategies (e.g. Schena, Villeneuve, & Nol, 1996; Schena, Zanin, & Chiarandini, 1997). Unfortunately, many of these methods have been criticized for the complexity of the final circuit solutions, and the inclusion of impractical circuit elements, such as stream splitting nodes.

Despite the veracity and plurality of circuit design tools, many remain underutilized, ignored, or poorly understood with respect to industrial integration. Much of circuit design (especially Question 4) is driven by trial-and-error, either in simulation or laboratory testing. Realistic simulation requires extensive laboratory data which may be unavailable or untimely, especially during the preliminary design phases. Analytical tools, such as linear circuit analysis usually involve cumbersome mathematics which often outweighs the perceived benefits of the techniques. As a result, separation circuit design remains a labor-intensive and costly process.

This paper presents a software package which may be used to assist the circuit designer in both greenfield and plant modification problems, especially in the absence of detailed feed and separation data. The Circuit Analysis Reduction Tool (CART ^{TM}) provides rapid analytical solutions to user-defined circuit layouts. These analytical solutions may then be used in numeric simulation, sensitivity analysis, or other various circuit design tools. In particular, the integration of linear circuit analysis provides one basis for fundamental circuit comparison. This paper provides a detailed review of prior work which has utilized analytical circuit solutions, namely Meloy's linear circuit analysis (1983) and Lucay's Sensitivity Analysis (2012). Next, the CART^{TM}software is described and presented in context of these various analytical solution uses. An optimization approach to the circuit modification problem is presented, and finally, the utility of the software is validated by an application example. Opportunities for refinement and further study are described in the conclusions.

6.2 Utilization of Analytical Circuit Solutions

Of the analytical circuit design tools, Meloy's linear circuit analysis (LCA) and Lucay's sensitivity analysis (SA) are the most generally applicable for all separation systems, since they are based on modular separation fundamentals rather than unique model-dependent heuristics. Both methods of circuit analysis require the final circuit concentrate to be presented as an analytical function of the generic transfer functions for each unit.

6.2.1 Linear Circuit Analysis

Meloy first presented a method of determining the analytical circuit solution via simple algebra. Several authors have described and utilized Meloys algebraic technique (Luttrell, Kohmuench, Stanley, & Trump, 1998; Luttrell, Forrest, & Mankosa, 2002; McKeon & Luttrell, 2005, 2012). In summary, each unit is assumed to be a binary separator with a generic transfer function, P_n. As a result, each unit produces a concentrate product, $FP + n$, and a tailings product, $F(1 - P_n)$. The algebra is extended by determining the downstream unit feed values in terms of other transition functions. The final concentrate and overall circuit transition function (C/F) are solved in terms of the various P_n values. Figure 6.1 shows a simple example of this algebra.

Meloy's LCA uses this analytical solution to determine the relative separation efficiency between the circuit and a single unit. The slope of a single unit's partition curve at 50% recovery is a reasonable estimation of the unit's efficiency. For many separators, this value entails identifiable meaning as the imperfection or Ep value. By evaluating the derivative of the analytical function at the 50% recovery point, the overall separation sharpness of the circuit is identified. This value roughly corresponds to the relative increase in separation sharpness from an individual unit to the overall circuit (in this paper, the value is termed "Meloy's circuit strength parameter"). A more rigorous description of the mathematics is presented by Meloy (1983).

6.2.2 Sensitivity Analysis

Lucay's SA is a more recent utilization of analytical circuit solutions. In SA, each unit in the circuit is evaluated to determine its influence on the overall circuit. By identifying the most influential unit, experimental and optimization efforts can be directed to specific areas of the circuit which will return the greatest benefits. In the procedure, the analytical

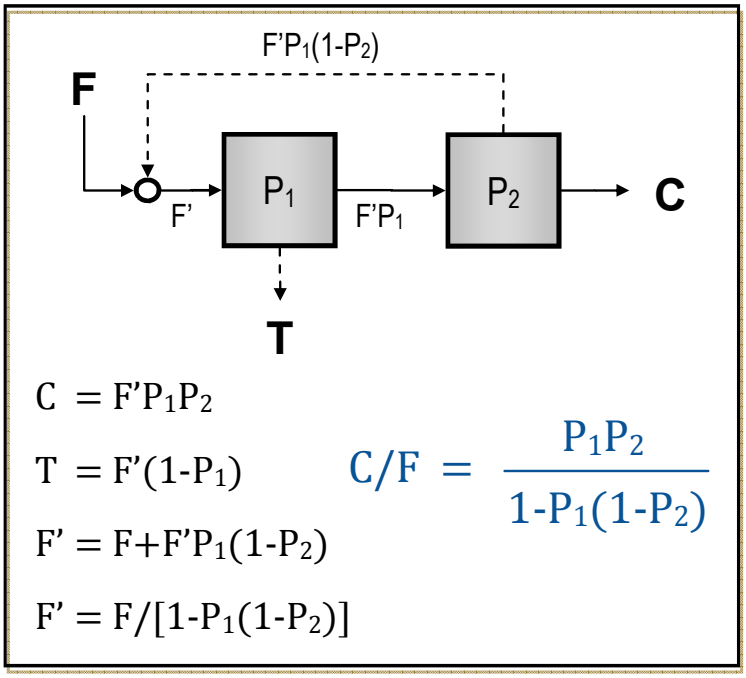

Figure 6.1: Example of circuit analysis algebra.

expression for the circuit is first determined, and terms referring to units not under scrutiny are lumped into a single constant parameter. Next, the partial derivative of the global recovery function is determined with respect to the recovery of the unit under scrutiny. The magnitude of this partial derivative is plotted for various expected values of the individual recovery functions.

Local minima and maxima in the plots indicate the relative sensitivity of the unit under scrutiny. This process is then repeated by taking the partial derivative with respect to each unit, and the overall magnitude of each partial derivative is compared to determine most influential unit in the circuit.

6.3 Analytical Solution Algorithm

After identifying the utility of the analytical circuit solution in fundamental separation analysis, several authors have described procedures for simplifying cumbersome mathematics associated with circuit reduction (Yingling, 1988; M. C. Williams, Fuerstenau, & Meloy, 1992). Unfortunately, these procedures require understanding of flowgraph reduction and graph theory concepts. Even if those concepts are mastered, the algorithms still require

manual calculation and somewhat obtrusive time requirements. M. C. Williams et al. (1992) claims that an experienced practitioner can use the graph theory approach to solve a five unit problem in ten minutes.

Despite these efforts, analytical circuit solutions remain underutilized. To reach their potential value, the derived analytical expressions must meet two criteria: (1) undoubted accuracy and (2) efficient determination. The first criterion refers only to the equation; simply, does the derived equation match the true analytical solution of the circuit. If the circuit designer has any cause to doubt the validity of the analytical expression, the utility of any subsequent method is negated. When the algebraic or flowgraph reduction techniques are followed steadfastly, this criterion will be met. The second criterion reflects the time and effort required to achieve the solution. For many circuits, this value increases exponentially as additional units and complex recycle patterns are introduced to the circuit. For any manual technique, these two objectives cannot be consistently met simultaneously. If more care is placed in ensuring an accurate solution, the process will be inefficient. Alternatively, if the solution technique is hastened, accuracy cannot be undoubtedly confirmed.

This paradox has been resolved through the development of a computational-efficient software-based analytical solution algorithm. This algorithm has been incorporated into a simple user interface based within the Microsoft Excel platform. The resulting software package, the Circuit Analysis Reduction Tool (CART^{TM}), allows users to construct a separation circuit using standard flowsheet drawing tools including separators, nodes, and streams. Once the flowsheet is complete, the calculations are initiated, and the analytical circuit solution, as well as Meloy's circuit strength parameter and other circuit parameters are produced. A prior paper has introduced this tool and shown its applicability in a heavy mineral sands wet plant (Noble, Luttrell, & Silva, 2012).

Since the original presentation, the algorithm has been updated to accommodate different recovery functions for the different units. Formerly, the algorithm produced an analytical solution which assumed the transfer function to be identical for all units. While this assumption allows the calculation of Meloy's circuit strength parameter, it limits the application of the analytical solution to real circuits, since circuit units rarely have identical recoveries. Additionally, the multi-unit analytical solution provides other uses, via streamlined simulation, simple sensitivity analysis, and operational parameter optimization. An example of the software's output is shown in Figure 6.2. This circuit is identical to the one solved algebraically in Figure 6.1.

The analytical solutions produced by the CART^{TM}software meets the two aforementioned criteria. The accuracy of the solutions has been validated by comparing the resulting

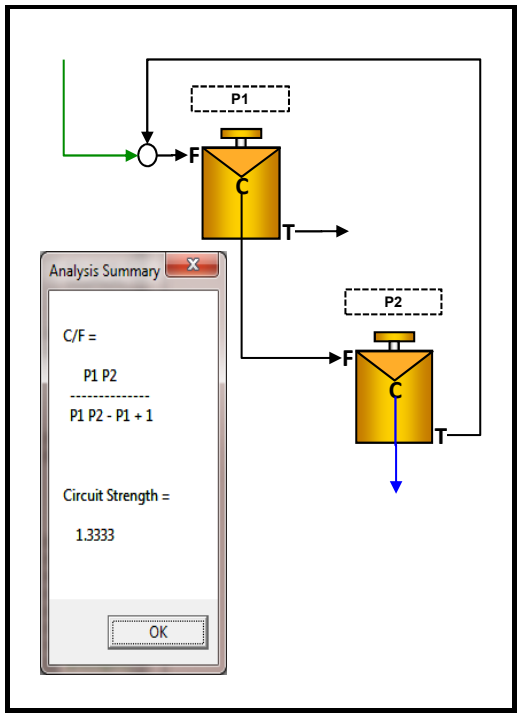

Figure 6.2: Sample output from CART^{TM}software.

solutions to those found from careful manual calculations. Approximately, 25 to 50 simple circuits have been verified in this manner, including circuit sizes ranging from two to seven units. Furthermore, the theory behind the algorithm ensures absolute scalability. The solution algorithm effectively does not distinguish between a small circuit and a large circuit in any respect other than computational time.

With respect to computational efficiency, the algorithm far exceeds manual computation. The actual calculation time for most standard circuits (four to eight units) ranges up to 6 seconds on standard laptop and desktop PC's (Intel Core i7 2.70 GHz processor). If all units are assumed to be identical, the calculation is somewhat faster. As an extreme example, the highly-complex 19 unit circuit presented by McKeon and Luttrell (2012) was solved considering unique unit transition functions. The algorithm produced the solution in 78 seconds.

6.4 Calculation Approaches for Circuit Simulation

Beyond fundamental circuit analysis, analytical solutions provide several supplementary benefits to traditional circuit simulation, especially with regard to the calculation methodology for circuits that contain recirculating loads. In linear circuits (unit performance is independent of unit feed), an analytical solution completely eliminates the need for an iterative or computational solution. The circuit performance may be solved directly by simple algebra. For nonlinear circuits (unit performance is dependent on unit feed), an analytical solution does not completely eliminate the need for iteration, but it does substantially streamline and simplify the simulation procedure.

6.4.1 Iterative Approach

Many traditional circuit simulators employ an iterative technique to accommodate recirculating loads and solve for the final circuit products. In this approach, an initial guess is chosen for the recirculating load, and the recovery calculations are repeated until the values stabilize within some predetermined tolerance or until a specified number of iterations are performed. This approach inherently introduces error unless a large number of iterations are performed. The number of required iterations is arbitrarily defined, since the iterative solution error depends upon the circuit complexity as well as the actual recovery values for individual units.

For nonlinear circuits, two nested iterative loops are required. As in linear circuits, the iteration must stabilize the value of the circulating loads, and the calculation must iteratively solve for each unit's actual recovery value since the recovery is dependent upon the unit feed rate. While the computational power of most PC's is sufficient to handle simple systems, this approach becomes cumbersome for larger problems. Simulations involving double or triple distributed parameters (e.g. flotation plants simulated with size, liberation, and rate-constant classes) can be especially problematic.

6.4.2 Analytical Approach

The CART^{TM}software provides a simplified calculation strategy for circuit simulation. The CART^{TM}algorithm produces an analytical solution to the final circuit concentrate as a function of each unit's individual recovery. For linear circuits, intermediate and circulating streams do not need to be calculated, since the final concentrate value is given analytically. The only information required for simulation is the individual recovery values for each unit. With an analytical solution in hand, these simulations can easily be conducted by hand or with simple spreadsheet software.

Alternatively, non-linear circuits still require an iterative or numeric solution technique. While the analytical solution negates the need for recirculating load calculations, the individual unit recoveries must be determined numerically. One approach to solving these problems is to write a system of equations consisting of the analytical circuit solution and the nonlinear transfer functions for each unit. This system can then be solved by a standard nonlinear numeric technique.

6.5 Optimization Algorithm

In addition to the analytical circuit algorithm, the CART^{TM}software includes an optimization algorithm, based on Meloy's LCA. This optimization algorithm has been developed to specifically address the circuit modification problem. Given an existing circuit, the algorithm determines the best location within the circuit to add another separation unit without altering the structure of the original circuit. The objective function, defining best location, is given by Meloy's circuit strength parameter.

The search algorithm first identifies the feasible and infeasible solution space. Various practical constraints limit the potential solutions and enhance the efficiency of the optimiza-

tion algorithm. Overall, the approach of defining the feasible space is tailored to the circuit modification problem. The additional unit may be fed by any current circuit product or placed between existing units such that the initial downstream unit is fed by the new unit. Otherwise, the products of the new unit may be reintroduced at any point in the circuit. Finally, after the additions, any product stream in the circuit may be recognized as the new circuit concentrate.

The optimization algorithm utilizes a direct search technique which attempts every circuit combination that adheres to the stated constraints and falls within the feasible solution space. The analytical solution is produced and the derivative is calculated for each design alternative. Given the calculation efficiency of the CART^{TM}software, several thousand circuit calculations can be performed within a reasonable time frame. The optimization of adding a fourth unit to an existing three unit circuit performed 350 circuit analysis calculations and took approximately 30 seconds on a standard laptop PC with an Intel Core i7 2.70 GHz processor.

6.6 Application Example

The CART^{TM}software and the optimization algorithm were applied to a hypothetical galena flotation plant, using the FLoatSim circuit simulator to produce quantitative results. The plant has an existing configuration and performance capacity. In this example, the circuit is to be modified by adding an additional unit which will enhance recovery and/or grade without reducing either. Consequently, the addition must fundamentally enhance the separation potential of the circuit rather than just shifting the circuit to a new operating point on the same grade-recovery curve.

The plant consists of two primary circuit legs: a rougher bank and a cleaner bank. High grade concentrate from the first rougher cell is passed directly to the final concentrate, while concentrate from the remaining rougher cells is directed to the cleaning bank. The cleaner cell is supported by a cleaner scavenger. Altogether, the circuit is represented schematically by four binary separators (Figure 6.3a).

Initial simulations show that the circuit produced a lead recovery of 95.7% at a grade of 57.22%. CART^{TM}software indicated that Meloy's circuit strength for this configuration is 1.1901 (Figure 6.3b).

Inefficient trial-and-error simulations were conducted attempting various configurations which added scavenging units to support the rougher section of the plant. None of these sim-

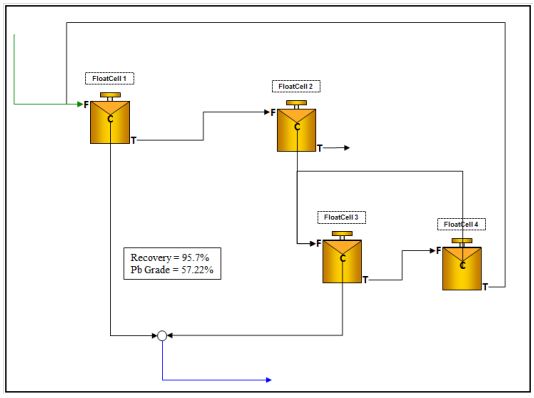

(a) Circuit A - original configuration.

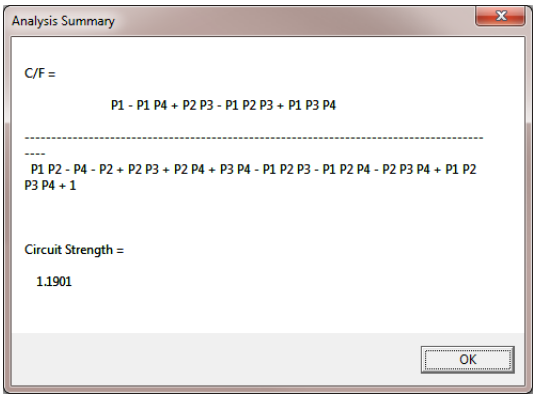

(b) Analysis Summary for Circuit A.

Figure 6.3: Circuit A Analysis

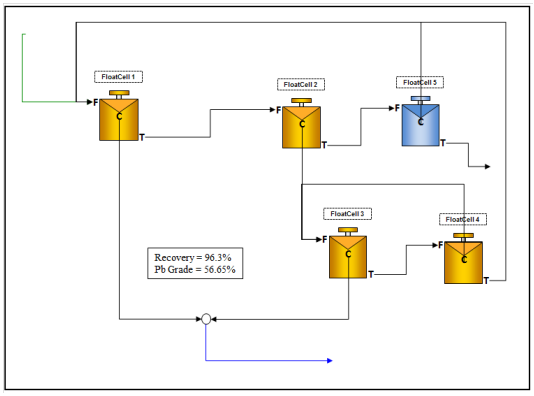

(a) Circuit B - scavenger addition.

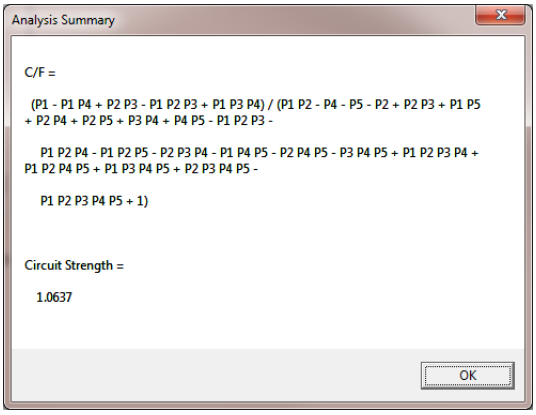

(b) Analysis Summary for Circuit B.

Figure 6.4: Circuit B Analysis

ulations met the modification objectives, and none were able to increase the circuit strength parameter. The best of these results produced a recovery of 96.3% at a grade of 56.65% (Figure 6.4).

After several preliminary simulation attempts, the CART^{TM}optimization algorithm was invoked. The results showed that the circuit strength parameter could be increased to a value of 2.00 by adding a cleaning unit after the initial rougher concentrate (Figure 6.5). The additional cleaning stage naturally produced a higher grade product, but the additional support also permitted the initial rougher cell to run at higher recovery value (via enhanced air flow rate) without compromising the final product. As a result, more total material was recovered in the rougher bank, while the overall circuit showed significantly enhanced lead grade (62.70%) *and* enhanced recovery (96.11%). Table 6.1 summarizes these three

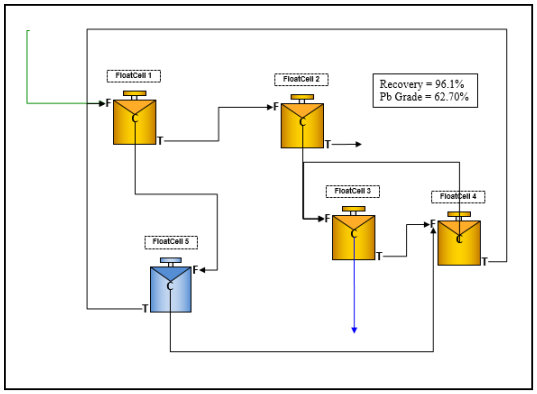

(a) Circuit C - rougher cleaner addition.

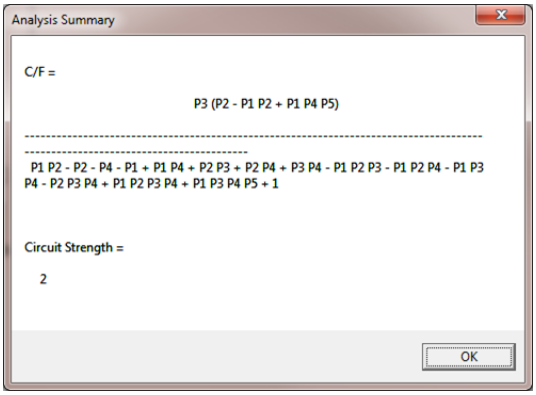

(b) Analysis Summary for Circuit C.

Figure 6.5: Circuit C Analysis

Table 6.1: Summarized Simulation Results

	Circuit A	**Circuit B**	**Circuit C**
Method of Generation	Original Circuit	Trial-and-Error	CART^{TM} Optimization
Recovery (%)	95.7	96.3	96.1
Pb Grade (%)	57.22	56.65	62.70
Circuit Strength	1.1901	1.0637	2.0000

simulations.

This example shows the utility of the CART^{TM}software. Rather than wasting design time in trial-and-error simulation, the designer should first utilize the optimization algorithm as well as circuit strength parameter evaluation to narrow the field of potential alternatives. Simulation efforts can then be focused on the optimization of specific operating parameters and resource volumes without considering the circuit layout.

6.7 Summary and Conclusions

Circuit design is a complex, open-ended engineering design problem. Circuit designers must prescribe the size and type of separation units, the operational parameters of each unit, and how the units will be staged or interconnected in the circuit. Commonly, these questions

are addressed by trial-and-error, either through data-intensive simulation or labor-intensive laboratory experimentation.

This paper has described the Circuit Analysis Reduction Tool (CART^{TM}) and presented its utility as a fundamental tool for separation circuit design. The CART^{TM}uses proprietary algorithms to produce an analytical circuit solutions which subsequently provides several means of analysis and utilization. The derived analytical solution may be used in simple simulations to estimate circuit recoveries and perform simple sensitivity analyses. Additionally, the software automatically calculates Meloy's circuit strength parameter and includes an optimization algorithm which determines the next best place to add a unit to the circuit. The utility of the software has been shown through an application example.

From the information presented in this presented in this paper, four conclusions are derived:

1. The analytical solution produced by the CART^{TM}software meets the two criteria for utility: undoubted accuracy and efficient determination.

2. The analytical solution negates the need for iterative calculation in linear circuits. Appropriate usage can also significantly streamline the simulation of nonlinear circuits.

3. The CART^{TM}software has substantial value in preliminary circuit evaluation. The tool can efficiently guide designers to preferred solutions and substantially reduce the need for trial-and-error.

4. The CART^{TM}software cannot replace model-based simulation. The final solution will require fine parameter tuning and an estimate of expected performance measurements. These tasks are best accomplished through experiments and simulation.

Despite the current power of the CART^{TM}software, additional refinements will enhance the applicability of the analyses to real circuit designs. Most significantly, the objective function to the optimization algorithm must be adapted to reflect more relevant information. Currently, the objective function is Meloy's circuit strength parameter, which only considers the relative efficiency of middling separation. In many separation systems, pure particles represent a significantly higher value per unit weight and a higher portion of the circuit feed (if well liberated). The efficiency of separation units which poorly distinguish these pure particles (i.e. entrainment in flotation, bypass in cyclones) is not reflected in Meloy's circuit strength parameter. Consequently, an optimization routine based on middling separation cannot produce valid results in these systems. Rather, a new objective function must be devised which considers pure particle as well as middling separation.

Acknowledgments

The author would like to thank FLSmidth Minerals for partial financial support for this work. The input and suggestions from the technical staff has been crucial to the progression of this software.

Also, the author would like to recognize Dr. Serhat Keles for his initiative in designing the user interface and providing ideas and suggestions for general software usability.

6.8 Bibliography

Cameron, P., & Morrison, R. (1991). Optimisation in the concentrator - the practical realities. In *Mining industry optimisation conference, sydney, june l991.*

Cisternas, L. A., Mndez, D. A., Glvez, E. D., & Jorquera, R. E. (2006). A milp model for design of flotation circuits with bank/column and regrind/no regrind selection. *International Journal of Mineral Processing*, *79*(4), 253–263.

Do, H. (2010). *Development of a turbulent flotation model from first principles.* Unpublished doctoral dissertation.

Galvez, E. (1998). A shortcut procedure for the design of mineral separation circuits. *Minerals Engineering*, *11*(2), 113–123.

Guria, C., Varma, M., Mehrotra, S. P., & Gupta, S. K. (n.d.). Simultaneous optimization of the performance of flotation circuits and their simplification using the jumping gene adaptations of genetic algorithm-ii: More complex problems. *International Journal of Mineral Processing*, *79*(3), 149–166.

Guria, C., Verma, M., Gupta, S. K., & Mehrotra, S. P. (2005). Simultaneous optimization of the performance of flotation circuits and their simplification using the jumping gene adaptations of genetic algorithm. *International Journal of Mineral Processing*, *77*(3), 165–185.

Hand, P., & Wiseman, D. (2010). Addressing the envelope. *Journal of the South African Institute of Mining & Metallurgy*, *110*(7), 365.

Kelley, K., Noble, A., Luttrell, G., & Yoon, R. (2012). Development of a model-based flotation simulator. In C. Young & G. Luttrell (Eds.), *Separation technologies for minerals, coal, and earth resources* (pp. 699–708). SME.

King, R. (2001). *Modeling and simulation of mineral processing systems.* Elsevier.

Lauder, D., & McKee, D. (1986). The impact of circulating loads on flotation circuit performance. In *l3th congress the council of mining and metallurgical institutions, singapore, 6 volumes* (p. 7).

Loveday, B., & Brouckaert, C. (1995). An analysis of flotation circuit design principles. *The Chemical Engineering Journal and the Biochemical Engineering Journal*, *59*(1), 15–21.

Loveday, B., & Marchant, G. (1972). Simulation of multicomponent flotation plants. *Journal of the South African Institute of Mining and Metallurgy*, *72*, 288–294.

Lucay, F., Mellado, M. E., Cisternas, L. A., & Galvez, E. D. (2012). Sensitivity analysis of separation circuits. *International Journal of Mineral Processing*, *110–111*, 30–45.

Luttrell, G., Forrest, W., & Mankosa, M. (2002). Development of an ideal separation curve for dry beneficiation. In *Sme preprint number 02-178* (p. 8). SME.

Luttrell, G., Kohmuench, J., Stanley, F., & Trump, G. (1998). Improving spiral performance using circuit analysis. *Minerals & Metallurgical Processing*, *15*(4), 16–21.

McKeon, T., & Luttrell, G. (2005). Application of linear circuit analysis in gravity separator circuit design. In *Heavy minerals.*

McKeon, T., & Luttrell, G. (2012). Optimization of multistage circuits for gravity concentration of heavy mineral sands. *Minerals & Metallurgical Processing*, *29*(1), 1-5.

Meloy, T. (1983). Analysis and optimization of mineral processing and coal-cleaning circuits circuit analysis. *International Journal of Mineral Processing*, *10*(1), 61–80.

Mendez, D. A., Galvez, E. D., & Cisternas, L. A. (2009). State of the art in the conceptual design of flotation circuits. *International Journal of Mineral Processing*, *90*(14), 1–15.

Nageswararao, K., Wiseman, D., & Napier-Munn, T. (2004). Two empirical hydrocyclone models revisited. *Minerals Engineering*, *17*(5), 671–687.

Noble, A., Luttrell, G., & Silva, R. (2012). An algorithm for analytical solutions and analysis of mineral processing circuits. In *2012 sme annual meeting and exhibit preprints* (p. 5). SME.

Richardson, R. (2002). Jksimmet: A simulator for analysis, optimisation and design of comminution circuits. *Mineral Processing Plant Design, Practice, and Control Proceedings*, *1*, 442.

Schena, G., Villeneuve, J., & Nol, Y. (1996). A method for a financially efficient design of cell-based flotation circuits. *International Journal of Mineral Processing*, *46*(12), 1–20.

Schena, G., Zanin, M., & Chiarandini, A. (1997). procedures for the automatic design of flotation networks. *International Journal of Mineral Processing*, *52*(23), 137–160.

Sutherland, D. (1981). A study on the optimization of the arrangement of flotation circuits. *International Journal of Mineral Processing*, *7*(4), 319–346.

Williams, M., & Meloy, T. (1991). Feasible designs for separation networks: a selection technique. *International Journal of Mineral Processing*, *32*(34), 161–174.

Williams, M. C., Fuerstenau, D., & Meloy, T. (1992). A graph-theoretic approach to process plant design. *International Journal of Mineral Processing*, *36*(12), 1–8.

Yingling. (1988). *Optimum synthesis of probabilistically-governed separation system with applications to mineral processing circuits*. Unpublished doctoral dissertation, University of Pittsburgh.

Chapter 7

The Partition Moment of Inertia as a Technical-Economic Separation Performance Measure

(ABSTRACT)

The partition curve is widely used in particulate separation to diagnose and compare separation behavior between different operating conditions, feed characteristics, and unit operations. Several traditional surrogate parameters have been defined in the literature and used to consolidate information from the entire curve into a single value. Many of these parameters are based on the curve's slope through the middling transition region, and common formulations include the separation sharpness, Ecart probable, and imperfection. Unfortunately, these surrogate measures fail to fully describe the process economics since the area of interest is isolated to the middling particles. This flaw is further compounded considering the disproportionately high influence pure particles have on final process economics, via increased incremental value and increased feed percentage in well-liberated systems. To account for these common biases, a new performance measure, the partition moment of inertia, is proposed. This paper describes the derivation of the partition moment of inertia and demonstrates the calculation for single-unit partitions as well as simple circuit configurations. Finally, the veracity of the value is demonstrated in a coal separation case study.

7.1 Introduction

7.1.1 Partition Curves

Partition curves are commonly used in the mineral processing discipline to characterize the separation efficiency of binary separators. First introduced by Tromp (1937), the partition curve graphically shows how individual particles are distributed between concentrate and tailings streams in a binary separator. Figure 7.1 shows a generic partition curve, highlighting the difference between an ideal and a real separation. The abscissa of a partition curve is a continuous scale reflecting the magnitude of the separation property of interest (often denoted Z), while the ordinate defines the probability that a particle of a given property will report to the concentrate product (often denoted P). Given the ease of two-dimensional graphical analysis, partition curve curves are common in separations that exploit a single, easily measured physical property.

Partition curves serve as a suitable measure of process performance as long as the separation property corresponds to the process objective. For example, the performance of classification cyclones is often characterized by partition curves showing recovery to underflow as a function of particle size. In this case, the partition curve permits detailed process evaluation since the predominant or sole separation property (particle size in this case) matches the process objective (size classification). Conversely, traditional partition curve analyses are largely absent in more complex processes where the separation property is ill-defined or difficult to measure, such as in froth flotation. Nevertheless, the underlying principles are still present, provided that the separation property corresponds to the process objective (i.e. floatability corresponds to composition).

Several mathematical functions which define the partition curve have been proposed. King (2001) has provided a detailed investigation of 9 different mathematical functions, while Stratford and Napier-Munn (1986) have provided general recommendations for suitable partition function formulations. By mathematically fitting experimental separation data to a known partition function, the parameters of the model may be used for diagnostic or comparative analyses (Armstrong & Whitmore, 1982; Rong & Lyman, 1985; Jowett, 1986; Tamilmani & Kapur, 1986). These comparisons are common when comparing different separation technologies which exploit the same separation property (jigs, vessels, and spirals, for example). One common partition function is given by the Whiten model:

$$P(Z) = (\theta_{High} - \theta_{Low})\frac{1}{1 + e^{\alpha(1-Z)}} + \theta_{Low}. \tag{7.1}$$

where P is the partition probability, θ_{High} and θ_{Low} are the high and low bypass values, α is

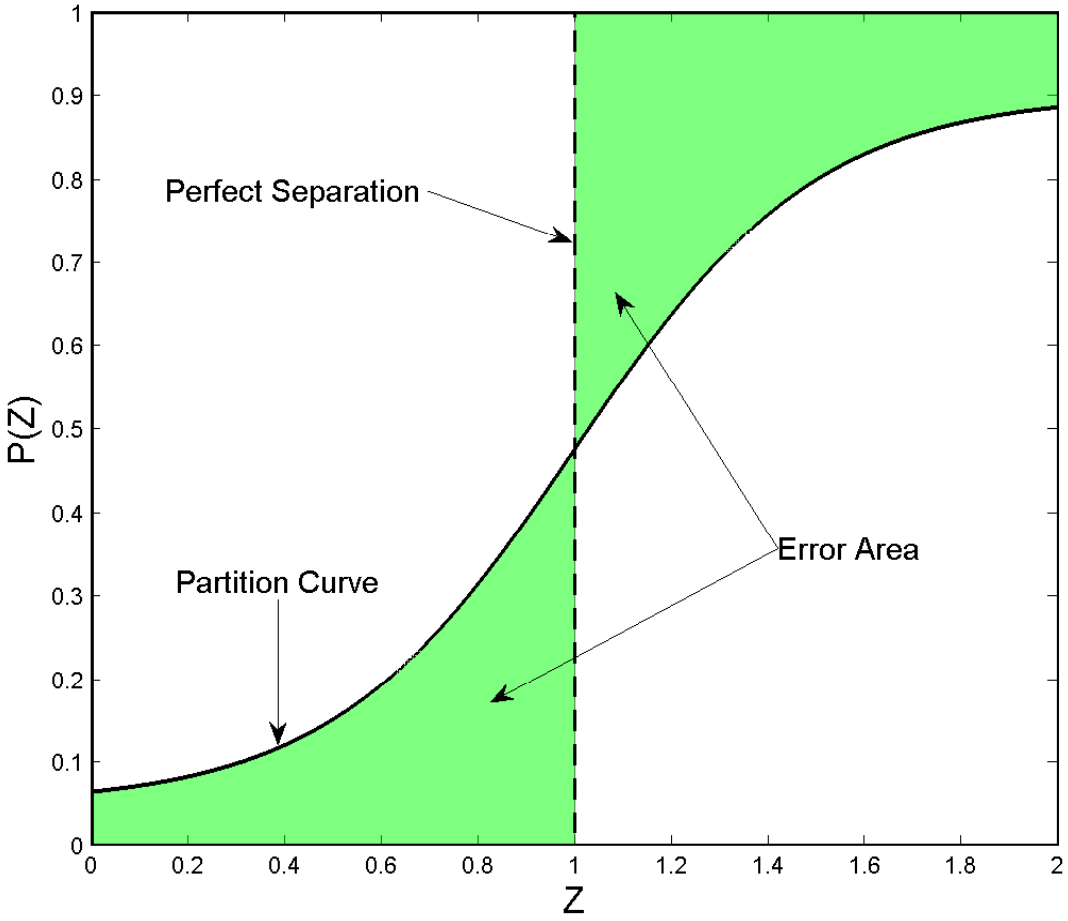

Figure 7.1: Generic partition curve with key components labeled.

a fitting parameter related to the partition slope, and Z is the normalized cut-point.

7.1.2 Traditional Partition Performance Measures

The overall geometric and algebraic characteristics of the partition curve provide information on the type and quantity of misplacement occurring within the particulate separator. For example, the location of the final asymptotes (θ_{High} and θ_{Low}) indicate the separator's susceptibility to bypass of pure particles. If the low property portion of the curve does not close at 0%, some portion of the low quality product will always report to concentrate. The amount of this misplaced portion is quantified by the location of the asymptote. A second geometric feature used to characterize the separation performance is the slope of the partition curve through the transition region. A steeper slope indicates that the separator is increasingly selective, and an infinitively large slope indicates a perfect separation. This value is often cited as the sole indication of performance in a partition separator in diagnostic and comparative studies. Two common formulations of this slope are given by the Ecart probable (E_P) and the imperfection (I) (Leonard, 1991; King, 2001). Many of the mathematical partition functions also include a fitting parameter (often denoted α) which directly corresponds to this slope. The Ecart probable is calculated by:

$$E_p = \frac{|d_{75} - d_{25}|}{2}$$

where d_{75} and d_{25} refer to the x-axis property values which refer to the 75% and 25% partition probabilities. The imperfection provides a way of normalizing the Ecart probable by the 50% partition property value (d_{50}):

$$I = \frac{E_p}{(d_{50} - 1)}.$$

The Ecart probable and the imperfection are commonly used in raw data analysis since the values can be quickly obtained from a simple graphical analysis. A more precise definition of the instantaneous partition slope (or separation sharpness, SS) can be derived by differentiating Equation 7.1 at the cut-point. This reduction yields:

$$SS = \frac{\alpha(\theta_{High} - \theta_{Low})}{4}.$$

Unfortunately, when the partition slope is used as the sole characteristic performance measure, information on the high and low bypass values is lost. A process with a high separation slope could in fact be producing an inadequate product if the bypass is considerably

high. The error area is one measure meant to overcome this limitation, while consolidating information from the entire partition curve. Mathematically, the error area is the difference between the ideal separation and the true separation defined by the partition curve. A graphical example of the error area is presented in Figure 7.1. If the partition function ($P(Z)$) as well as the minimum, maximum, and desired Z values (Z_{Min}, Z_{Max}, and Z_{Desire}) are known, the error area (EA) may be calculated by:

$$EA = \int_A \mathrm{d}A = \int_{Z_{Min}}^{Z_{Desire}} P(Z)\,\mathrm{d}Z + \int_{Z_{Desire}}^{Z_{Max}} (1 - P(Z))\,\mathrm{d}Z. \tag{7.2}$$

While the partition curve analysis is most readily applied to single separation units, its principles are also applicable to full separation circuits. Linear circuit analysis provides one methodology of extending the mathematics from a single unit to a full circuit (Meloy, 1983a). Here, simple algebra is first used to derive an analytical circuit recovery expression as a function of individual unit recoveries. The derivative of this analytical expression is used to determine the slope of the circuit partition curve through the transition zone. Circuit slope values greater than one indicate that the circuit can distinguish middling particles better than a single unit, while values less than one indicate that the circuit reduces middling separation performance. Similarly, the circuit analytical expression can be used to determine how other partition factors (cut-point and bypass) are influenced by the configuration.

In this paper, the separation sharpness, imperfection, and error are are collectively identified as the *traditional* partition performance indicators. These values are commonly used in industrial and academic settings as surrogate measures for real separation performance. They conveniently reduce the full partition data to a single parameter that may be used for comparative or diagnostic studies. Unfortunately, this consolidation results in a loss of information on the real performance of the separation.

7.1.3 Micro-Pricing and Incremental Quality

Smelter and utility contracts often include premium and penalty clauses to incentivize delivery of raw materials that meet a certain quality standard. These price adjustments are applied to a base cost when the delivered quality deviates from a standard quality (i.e., "± \$1.00 per ton for each 100 Btu/lb over/under 13,000 Btu/lb"). The "micro-pricing" principle dictates that individual particles contribute independently to the final recovered revenue (Luttrell, Honaker, & Yoon, 2004; Luttrell & Honaker, 2005; Luttrell, Keles, & Honaker, 2009). Accordingly, the "incremental value" of each particle (or class of particles

with similar composition) is determined by the contract penalty and premium values as applied to that individual particle.

As an example, in a coal-ash system, contract specifications typically apply premiums and penalties for heat content and ash values which deviate from a standard value. By applying these price adjustments, each washability class can be defined by the incremental value the recovered material in that class will contribute to the final revenue. Low ash, high Btu classes will contribute an incremental value substantially above the base price, while pure rock material will contribute a large negative return. Often this principle is extended to show that the ideal cut-point occurs at the washability class that contributes zero incremental value. Furthermore, optimal blending can be achieved when all parallel circuits are operated at the same incremental quality (Salama, 1989; Lyman, 1993; Luttrell, Catarious, Miller, & Stanley, 2000; Luttrell, Barbee, & Stanley, 2003; Luttrell et al., 2009; Mohanta, Chakraborty, & Meikap, 2011).

Unfortunately, the traditional, derivative-based separation indicators fail to reflect the economic incentives of particular separation processes and circuit configurations. Since the partition slope only accounts for middling separation, performance measures derived from this value cannot account for deviant behavior at the end of the curves. According to the micro-pricing principle, particle classes at the ends of the curves have a much stronger influence on process economics than the middling material. Extreme Z values often correspond to classes which invoke high premiums or penalties, provided that the separation property corresponds to the process objective. Additionally, in a well liberated system, these pure particles represent a higher portion of the feed material. When compared to the derivative-based measures, the error area shows marked improvement since it considers misplacement along the entire property axis. However, this value does not inherently give additional weight to the pure particles which have a greater influence on final revenue. Consequently, all of the performance measures fundamentally lack the ability to diagnose separation performance from an economic perspective.

7.1.4 Overview

This paper proposes a new separation performance measure, the partition moment of inertia (MOI). This parameter may be derived from standard partition analysis and is analogous to the mass moment of inertia for rigid-body rotational dynamics. Calculation of the parameter may be conducted for single units or extended to circuit configurations via linear circuit analysis. From the physics perspective, the mass moment of inertia indicates

a body's resistance to rotational motion about a given axis. Mass which is located further away from the rotation axis is more heavily weighted in the calculation. Similarly, the partition moment of inertia evaluates the partition error's ability to "rotate" about a given axis, namely the partition cut-point. In this calculation, misplacement further way from the cut-point (i.e. pure particles) is more heavily weighted than misplacement of middling material. This paper derives this formula using the mass moment of inertia as a blueprint for the methodology. A precise mathematical formulation of the parameter is provided along with sample calculations for single units and simple circuits. Finally, the veracity of the performance indicator is investigated for a coal preparation case study.

7.2 The Moment of Inertia

7.2.1 Mechanical Background

In rotational mechanics, the mass moment of inertia (I) is a parameter which defines a body's resistance to rotation about a given axis. From the perspective of rigid-body kinetics, the moment of inertia is the rotational equivalent of mass. By definition, mass signifies a body's ability to resist linear acceleration; whereas, the moment of inertia signifies the body's ability to resist angular acceleration. Mathematically, a three-dimensional body's moment of inertia is given by:

$$I = \int_V \rho(r) r^2 \, \mathrm{d}V \tag{7.3}$$

where $\mathrm{d}V$ is an incremental volume element, r is the perpendicular radius from the axis of rotation to the volume element, and $\rho(r)$ is the mass density function. For uniform-density bodies, the density function is constant and can be factored out of the integral. These physical dimensions are shown for an arbitrary body in Figure 7.2.

The value of the mass moment of inertia may be increased by increasing the mass of material located away from the axis of rotation. Pragmatically, this increase is most readily achieved by either increasing the radius of the body or by increasing the peripheral density.

7.2.2 Applications to Single Separators

The incremental quality concept asserts that particles with extreme property values have a larger incremental influence on the final recovered revenue. For example, in a simple coal-ash system, pure coal and pure rock particles carry the largest incremental value when

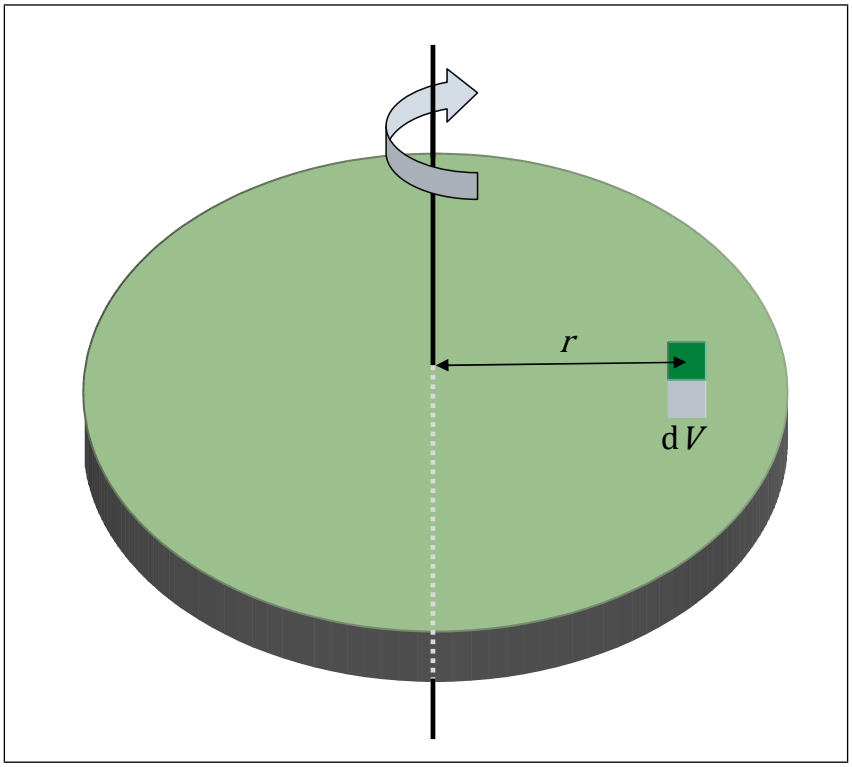

Figure 7.2: The mass moment of inertia for an arbitrary physical body.

compared to intermediate middlings. Furthermore, since most mineral systems are well liberated, the initial mass fraction of pure particles is much greater than the fraction of middlings. Unfortunately, all traditional performance measures fail to explicitly account for this natural economic bias. Conversely, a more descriptive separation performance measure should place a larger emphasis on pure particle misplacement since this material substantially influences the final economic result.

The moment of inertia calculation provides a basis to apply differential weighting based on the property class and its distance from the cut-point. The mechanical analogy is formed by assuming the partition error area to be a thin plate with the thickness going into the paper. The rotational axis is set parallel to the y-axis at the normalized cut-point, and the density of the body is related to the incremental cost function or may be assumed to be uniform if no costing data is available. The rotation of the partition error area plate around the cut-point axis is governed by the moment of inertia. Larger bypass values result in more peripheral mass, leading to a larger moment of inertia. Conversely, a lower partition slope would lead to more overall mass and an increased moment of inertia. However, since this mass is centrally located, it would not be weighted as heavily as the peripheral mass influenced by the unit bypass. A visual representation of this principle is provided in Figure 7.3.

Mathematically, the partition moment of inertia (MOI) may be derived by applying the geometry of Figure 7.3 to the generic mass moment of inertia calculation (Equation 7.3), while assuming that the incremental cost function corresponds to the plate density. The MOI derivation follows a similar pattern as the partition error area calculation (Equation 7.2) since the rotational geometry of interest is identical to the error area. The final value is dependent on the specific partition function ($P(Z)$), the optional cost function ($C(Z)$), as well as the minimum, maximum, and desired normalized property values (Z_{Min}, Z_{Max}, and Z_{Desire}). The generic derivation is given by:

$$MOI = \int_{Z_{Min}}^{Z_{Desire}} C(Z)P(Z)(Z_{Desire} - Z)^2 \,\mathrm{d}Z + \int_{Z_{Desire}}^{Z_{Max}} C(Z)(1 - P(Z))(Z - Z_{Desire})^2 \,\mathrm{d}Z. \tag{7.4}$$

As it is defined, the partition moment of inertia always places a higher weight on pure particles. If incremental costing data is available, these values may be included to account for the "density" difference of the rotated area. If no cost information is available, a "uniform density" may be assumed. In this case, the unweighted MOI value still *indirectly* accounts for the the pure particles (by the square of the moment arm length). In general, the approach supports both methodologies, depending on the availability of data.

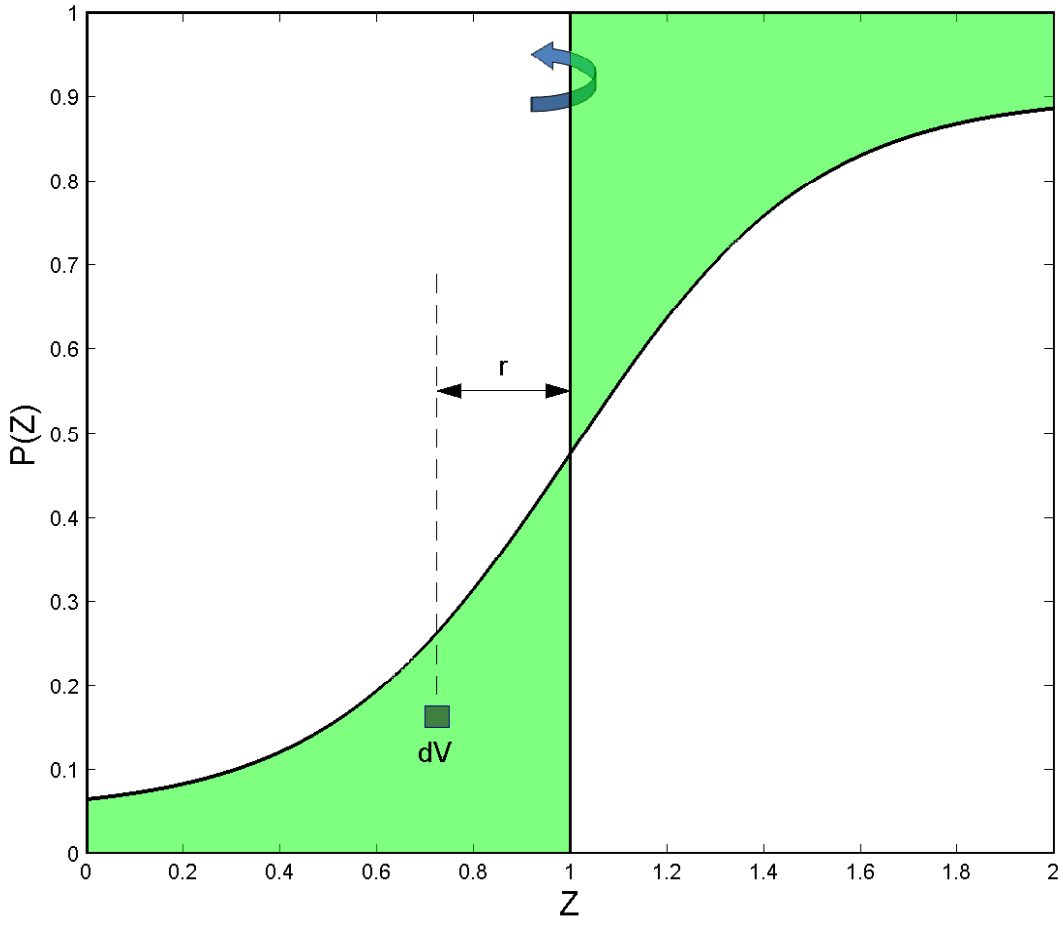

Figure 7.3: The parition moment of inertia for a generic partition curve.

To show how the derived MOI parameter relates to standard partition function parameters (α, high bypass, and low bypass), a simple single unit simulation was conducted. The Whiten partition model (Equation 7.1) was used to produce a partition curve through a factorial sweep of α (1 to 30) and low bypass (0 to 30%) values. Equation 7.4 was used to calculate the partition moment of inertia, assuming a constant cost function ($C(Z)$) and Z values of 0.5, 1.0, and 1.5 for the minimum, desired, and maximum, respectively. Figure 7.4 shows the results with MOI plotted as a function of α and low bypass.

This simulation indicates the theoretical relationship between MOI and α. While the MOI integrals were calculated over a range of 0.5 to 1.0, the relative behavior between the parameters will not change, provided that the cut-point is the average of the two extremes. At low α values, small increases in α correspond to large decreases in MOI. At larger α values (> 15 in this case) incremental changes in the partition slope have very little influence on the partition MOI. Simply, these α values are elevated beyond the point of diminishing returns. While these diminishing returns are intuitively well known, their impact on process economics are ill-defined.

From a technical-economic perspective, the MOI-α-bypass relationship suggests that not all gains in separation sharpness produce proportional increases in economic performance. Despite the perception of diminishing returns, proportional increases in α yield contrasting results. For example, consider two separators operating with 0% bypass and respective α values of 5 and 15. For the first separator (original α of 5), a twofold increase in α produces a 74% reduction in MOI (MOI reduction from 1.19 to 0.31). Alternatively, a two fold increase in the second separator (original α of 10) yields an 87% reduction in MOI (MOI reduction from 0.10 to 0.013).

Alternatively, for a fixed α value, a linear relationship exists between the low bypass and the MOI parameter. As anticipated, absolute reduction in bypass does not show diminishing returns. Each unit of properly placed pure material corresponds directly to an increase in the technical-economic separation performance.

7.2.3 Applications to Separation Circuits

Linear circuit analysis describes how the separation sharpness indicator can be extended from a single unit to a circuit of units by the analytical circuit solution (Meloy, 1983a, 1983b). In an analogous manner, the analytical circuit solution can be used to extend the moment of inertia calculation from a single unit to a full circuit. Many of these steps become increasingly computationally intensive as the circuit complexity increases. Numeric routines

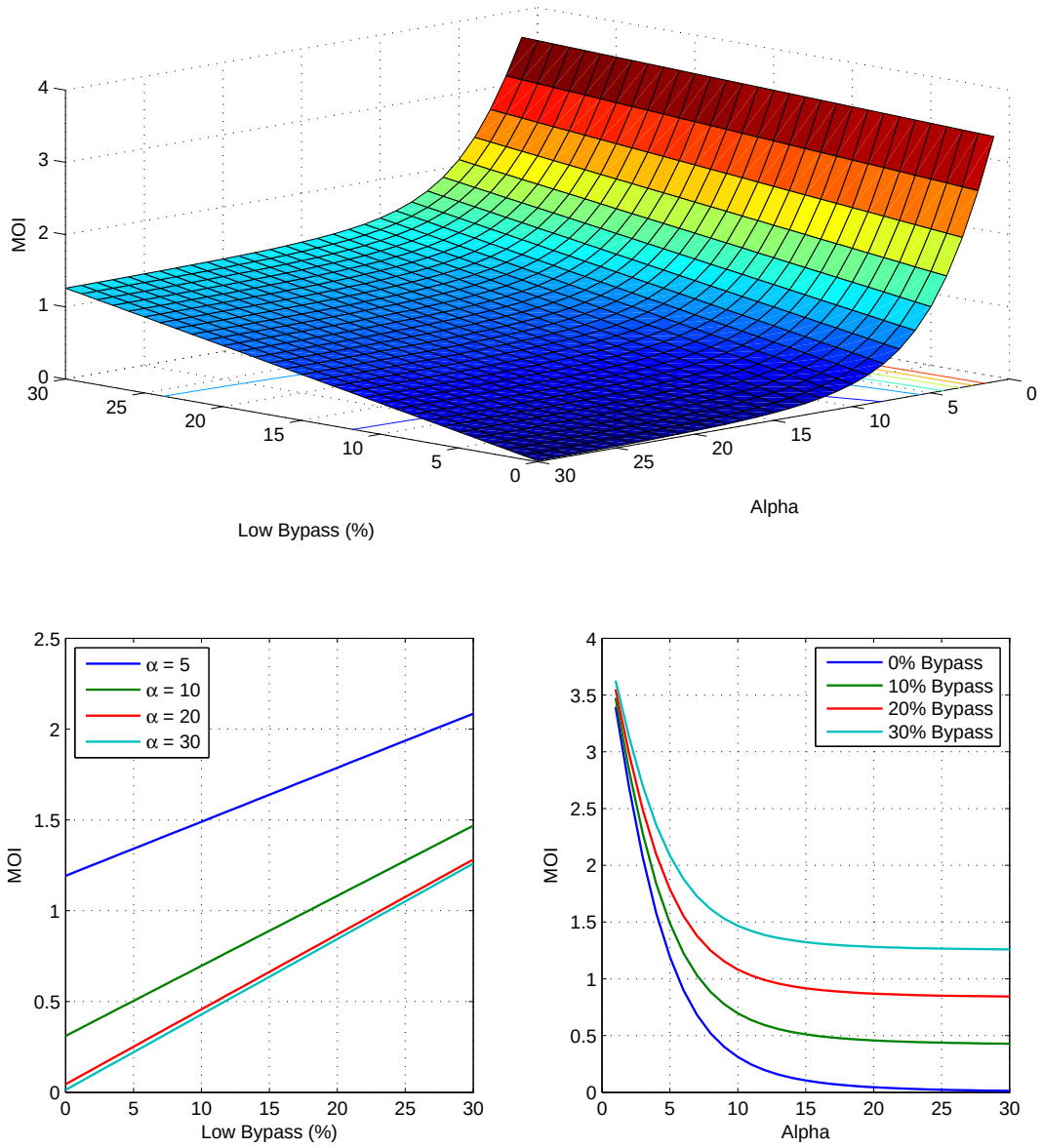

Figure 7.4: Theoretical relationship between MOI, α, and low bypass values.

for the integral calculation are recommended in order to preserve the efficiency and integrity of the performance indicator.

First, algebra or the CART^{TM}algorithm (see Chapter 5) is used to derive an analytical circuit solution in terms of unit P values. Next, all P values are assumed equal to produce a simplified analytical solution. This analytical solution may be plotted against unit P values from 0 to 1 to produce the circuit partition function. The moment of inertia calculation is then applied to this circuit partition function by using Equation 7.4. The circuit recovery expression (C/F) is substituted for $P(Z)$, the x-axis value (P) is substituted for Z, and 0, 0.5, and 1 are assumed as the integration limits. The cost function may be implemented as a function of unit P, or a uniform cost may be assumed if no data is available. The final calculation yields the circuit MOI. Since many of these values are low in absolute magnitude and difficult to compare, the values reported in this paper are always expressed as a percent of the circuit MOI of a single unit (a value of approximately 0.01042). With this convention, circuit MOI values above 100% correspond to configurations worse than a single unit, while values less than 100% indicate improved separation.

To illustrate the calculation methodology, a sample calculation for the circuit MOI of a single unit ($C/F = P$) is shown:

$$\begin{aligned}
MOI &= \int_{Z_{Min}}^{Z_{Desire}} (C/F)(Z_{Desire} - P)^2 \,\mathrm{d}P + \int_{Z_{Desire}}^{Z_{Max}} (1 - (C/F))(P - Z_{Desire})^2 \,\mathrm{d}P \\
&= \int_0^{0.5} (P)(0.5 - P)^2 \,\mathrm{d}P + \int_{0.5}^{1} (1 - P)(P - 0.5)^2 \,\mathrm{d}P \\
&= \int_0^{0.5} [0.25P - P^2 + P^3] \,\mathrm{d}P + \int_{0.5}^{1} [(P^2 - P + 0.25) - (P^3 - P^2 + 0.25P)] \,\mathrm{d}P \\
&= \int_0^{0.5} [0.25P - P^2 + P^3] \,\mathrm{d}P + \int_{0.5}^{1} [0.25 - 1.25P + 2P^2 - P^3] \,\mathrm{d}P \\
&= \left[\frac{0.25}{2}P^2 - \frac{1}{3}P^3 + \frac{1}{4}P^4\right]_0^{0.5} + \left[0.25P - \frac{1.25}{2}P^2 + \frac{2}{3}P^3 - \frac{1}{4}P^4\right]_{0.5}^{1} \\
&= 0.005280 + 0.005208 \\
&= 0.01042
\end{aligned}$$

As more units are included in the circuit configuration, the complexity of the analytical solution increases rapidly, thus reducing the likelihood of a simple integration. As more terms are introduced into the equation, numerical integration becomes a much more useful approach. For example, consider the circuit MOI calculation for a two-unit rougher-cleaner with recycle to the head ($C/F = P^2/(1 - P + P^2)$). A numeric routine is used to solve the

integral after the second step:

$$\begin{aligned} MOI_{Absolute} &= \int_{Z_{Min}}^{Z_{Desire}} (C/F)(Z_{Desire} - P)^2 \, \mathrm{d}P + \int_{Z_{Desire}}^{Z_{Max}} (1 - (C/F))(P - Z_{Desire})^2 \, \mathrm{d}P \\ &= \int_{0}^{0.5} (P^2/(1 - P + P^2))(0.5 - P)^2 \, \mathrm{d}P + \int_{0.5}^{1} (1 - (P^2/(1 - P + P^2)))(P - 0.5)^2 \, \mathrm{d}P \\ &= 0.00743 \\ MOI &= 0.00743/0.01042 = 71.3\% \end{aligned}$$

Consequently, the addition of the cleaner with recycle produces a 71.3% reduction in the MOI from that of a single unit.

To analyze and compare the utility of the circuit MOI parameter, the integral calculation as well as the sharpness indicator (SE) have been evaluated for various two and three-unit circuit configurations. Figure 7.5 shows the configurations that were considered in this demonstration. All circuits were evaluated for both a standard operating condition as well as several "bypass" conditions. In these conditions (as shown in C1 of Figure 7.5), a defined portion of the feed *bypasses* the separation unit and reports directly to the unit concentrate. This model corresponds to real processes which undergo a selective and a non-selective recovery mechanism, such as flotation entrainment or screen blinding.

Figure 7.6 shows the circuit partition curves for the six simple configurations included in this analysis. These plots depict the circuit recovery (C/F) as a function of individual unit recovery, assuming each unit has the same P value. These partition functions indicate whether a circuit is predominantly cleaning (circuit recovery is generally lower than unit recovery) or scavenging (circuit recovery is generally higher than unit recovery). For extremely complex circuits, the predominant function can be difficult to identify by merely studying the configuration. However, when the circuit partition function is plotted with a normalizing line ((0,0) to (1,1)), zones of enriched or reduced recovery are easily denoted.

Table 7.1 summarizes the analytical solution, circuit SE, and circuit MOI values for each of the six circuits under the standard, no bypass conditions. Table 7.2 extends these results for 10%, 20%, and 30% bypass levels.

The aggregate circuit analysis data for the six circuits is summarized in Figure 7.7. In this plot, circuit MOI is plotted against circuit SE for each unique circuit configuration and unit bypass level. The circuit configurations are grouped explicitly by the series color and marker style, while the unit bypass values are denoted only for the C6 data series. Nevertheless, the unit bypass values for the other data series may be interpreted implicitly by applying the same positional pattern. For each data series, the rightmost point (the

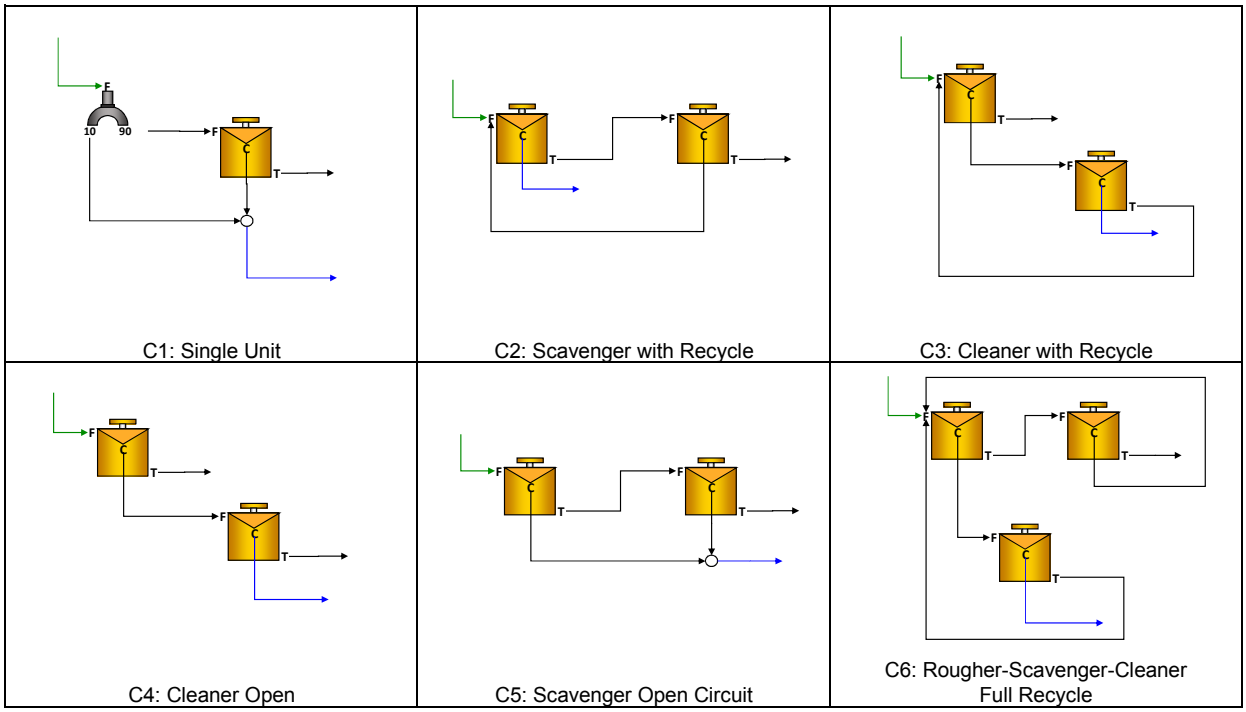

Figure 7.5: Basic circuit configurations used in circuit MOI calculation comparison. Note that from a circuit analysis perspective, each unit cell in the multi-unit circuits (C2 - C6) actually corresponds to a feed splitter followed by a unit cell as depicted in C1. Splitters were omitted from the latter drawings to conserve space.

Table 7.1: Circuit Analysis Comparison for Basic Circuits.

Circuit ID	**Circuit Description**	**Analytical Solution**	**Circuit** SE	**Circuit** MOI
C1	Single Unit	P	1.00	100.0
C2	R-S (r)	$P/(P^2 - P + 1)$	1.33	71.3
C3	R-C (r)	$P^2/(1 - P + P^2)$	1.33	71.3
C4	R-C (o)	P^2	1.00	100.0
C5	R-S (o)	$2P - P^2$	1.00	100.0
C6	R-S-C (r)	$P^2/(2P^2 - 2P + 1)$	2.00	31.8

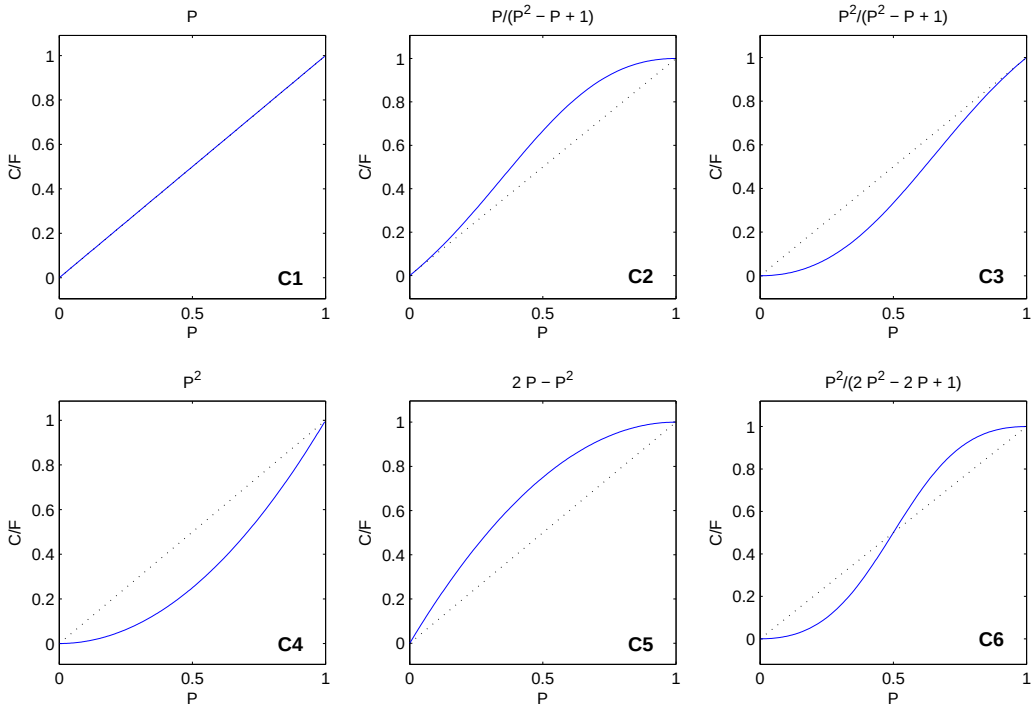

Figure 7.6: Circuit partition curves for six basic circuit configurations.

Table 7.2: Moment of Inertia and Separation Sharpness Values for Basic Circuits at Various Bypass levels

Circuit ID	**Separation Sharpness** *% Bypass* 0%	10%	20%	30%	**Moment of Inertia** *% Bypass* 0%	10%	20%	30%
C1	1.00	0.90	0.80	0.70	100.00	130.00	160.00	190.00
C2	1.33	1.11	0.89	0.68	71.31	113.42	159.79	208.31
C3	1.33	1.27	1.16	1.03	71.31	78.77	95.16	120.81
C4	1.00	0.99	0.96	0.91	100.00	103.00	112.00	127.00
C5	1.00	0.81	0.64	0.49	100.00	157.00	208.00	253.00
C6	2.00	1.75	1.42	1.07	31.78	47.52	77.91	124.68

highest SE value or the lowest MOI value corresponds to the 0% bypass condition. Each successive data point (moving left and up) corresponds to increasing increments of unit bypass.

The aggregated circuit $MOI - SE$ trend mirrors the behavior exemplified in the single-unit partition function analysis (Figure 7.4). At elevated SE values, incremental SE gains yield diminished reductions in MOI, when compared to similar gains at reduced SE values. Furthermore, this general trend does not produce a one-to-one comparison for all data points, implying that the MOI performance measure will not always produce the same rankings as the SE parameter. For example, consider the comparison between the C6, 20% bypass point and the C3, 0% bypass point. The SE ranking shows preference to the C6 configuration (SE value of 1.42 compared to 1.33 for C3), while the MOI ranking shows preference to the C3 configuration (MOI of 71.31 for C3 compared to 77.91 for C6). This result is anticipated since the MOI parameter places a larger penalty on bypassed pure particles.

To further illustrate the discrepancies between the two circuit analysis measures, Figure 7.7 includes quadrant designations centered around the single unit circuit (1,100). These four quadrants indicate differences in comparative behavior. Quadrants I and III indicate divergent conclusions, while Quadrants II and IV show similar conclusions; although, the magnitude of the improvement may not correlate with the magnitude of the value. For example, in Quadrant I, SE shows separation improvement while MOI shows separation deterioration compared to a single unit. Alternatively, in Quadrant IV, both parameters show circuit improvement. In principle, these quadrant axes may be centered around any point on the plot to illustrate differences in comparisons at that point.

7.3 Application Example: Coal Separation Economics

7.3.1 Methodology

To analyze the veracity of the partition moment of inertia and other separation performance indicators, a hypothetical coal cleaning case is presented. The last section, comparing circuit MOI and circuit SE, indicated that the two parameters occasionally produce divergent results in ranking circuit configurations. Furthermore, the two performance measures show a nonlinear relationship, which indicates that both performance measures cannot directly correlate to economic performance simultaneously. These seeming contradictions indicate that one performance measure likely provides a better indication of technical-economic

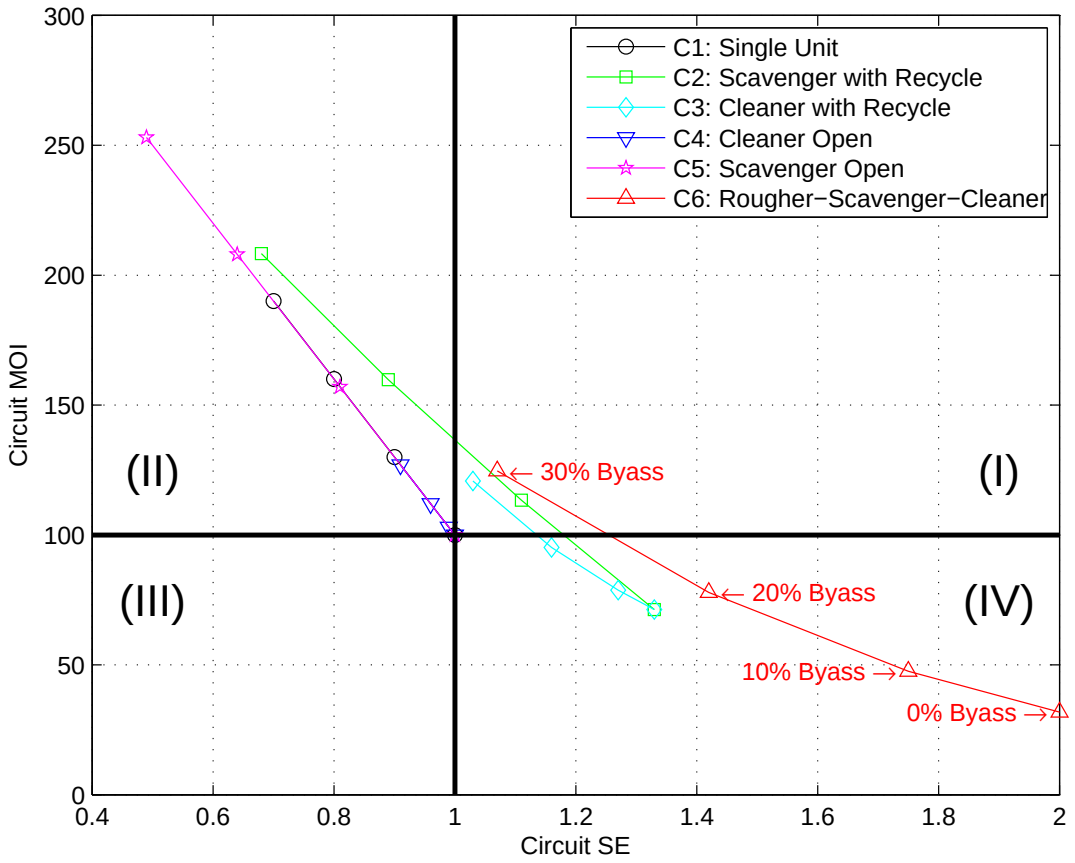

Figure 7.7: Circuit MOI plotted against Circuit SE for six basic circuit configurations. Individual data points refer to different levels of unit bypass. Bypass levels include 0% (rightmost point in each data series), 10%, 20%, and 30% (leftmost point in each data series). Quadrants indicate different predictive behavior: (I) SE indicates improvement from single unit, MOI indicates degradation from single unit; (II) both indicate degradation; (III) MOI indicates improvement, SE indicates degradation; (IV) both indicate improvement.

performance.

This coal economics case study uses washability and sales contract data to calculate the real recovered revenue from a hypothetical density-based separator. The separator is modeled under a number of different operating conditions, using a generic partition function (Equation 7.1) to define the separation. From the calculated partition data, various traditional technical separation performance indicators (separation sharpness, error area, and imperfection) are calculated along with the partition moment of inertia. All of these surrogate measures are then compared to the economic results (recovered revenue and misplaced revenue) to determine which performance indicator produces results which most closely correspond to the economic output.

The coal contract data used in this example is shown in Table 7.3. While these values do not necessarily represent any real contract, they do generally correspond to typical values found in steam coal contracts in the year 2013. These values, including the Btu premium/penalty, ash premium/penalty, and sales penalty are used to calculate the incremental revenue by density class. In this example, impurity clauses, sulfur penalties, and moisture requirements are ignored for the sake of simplicity. Sulfur standards will slightly increase the incremental value if the cleaning unit selectively rejects sulfur, but the general conclusions will remain. Since size and differential moisture reduction are not considered in this example, the addition of a moisture clause in this contract will affect the incremental value consistently for all density fractions. Nevertheless, all cleaned products are assumed to have 8.00% moisture which influences the heat content of the final product.

Despite the assumed simplifications, the contract does include premium and penalty clauses for ash and heat content as well as a sales cost penalty. The washability data (Table 7.4) was used along with the contract to create a cost function formulated solely as a function of particle density. This washability data represents a fairly well liberated, easy to clean coal, with 63.2% of the mass in the two extreme density classes. A plot of 1/SG versus ash (Figure 7.8) shows a near linear relationship between the two washability parameters, supporting the validity of the washability analysis.

Table 7.5 extends the washability data to demonstrate the incremental cost calculation. The base price is constant for all density classes, regardless of the quality. The ash penalty is applied per density class using the individual ash assay for the class as the basis for penalty. The Btu penalty/premium is determined by first calculating the heat content incrementally for each density class. This value is defined as the dry ash free heat (daf, 15,000 Btu/lb in this case) less the portion of in-class ash and moisture. As mentioned above, 8% moisture is assumed for all classes. With the heat content calculated for each class, the Btu adjustment

Table 7.3: Coal Sales Contract Data for Economic Simulation

Cost	**Contract Item**
$50.00	Base Price
12,500	Btu Standard
$0.50	Premium/penalty per 100 Btu
12.00 %	Ash Standard
$1.00	Premium/penalty per 1% ash
8.00%	Standard Moisture
15,000	Btu/lb daf
$2.25	Sales Cost Base Penalty
10%	Sales Cost Revenue Multiplier
100	Feed Rate (tph)

Table 7.4: Coal Washability Data for Economic Simulation

Sink SG	**Float SG**	**Weight %**	**Ash %**
1.20	1.35	45.54	3.54
1.35	1.40	17.64	12.34
1.40	1.45	8.49	19.07
1.45	1.50	5.04	23.16
1.50	1.55	2.20	29.69
1.55	1.60	0.52	33.99
1.60	1.65	0.48	38.73
1.65	1.70	0.25	44.25
1.70	1.75	0.31	47.26
1.75	1.80	0.40	52.98
1.80	1.90	0.63	56.52
1.90	2.00	0.84	59.89
2.00	2.50	17.66	82.08
TOTAL		100.00	23.41

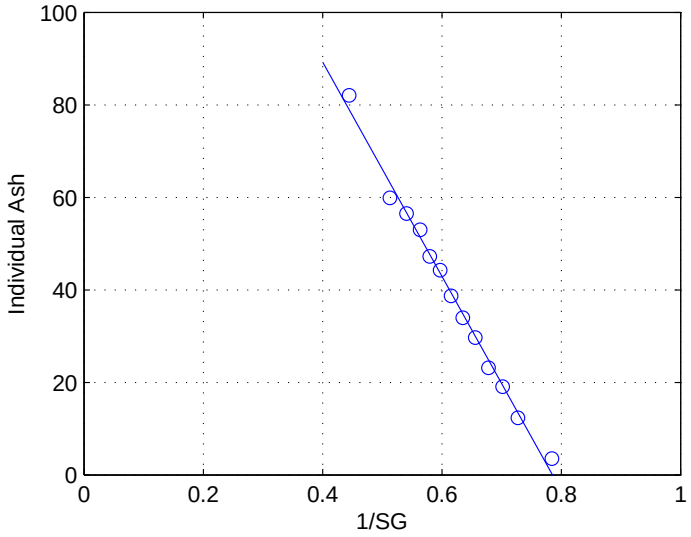

Figure 7.8: Individual ash versus 1/specific gravity from coal washability data.

is applied. The remaining positive revenue in each class (if any is remaining after the heat and ash adjustments) is subjected to a 10% sales cost. A constant $2.25 sales cost is applied to all classes, regardless of net revenue status. The final summation of the base cost and all adjustment yields the net value as a function of SG.

Using the contract and washability data, a cut SG of 1.60 was selected. This value corresponds to the ash class which produces nearly zero incremental revenue. Cut-points greater than this value recover particles which result in a net penalty, while cut-points lower than this value reject particles which result in a net premium. The micro-pricing principle dictates that the optimal revenue is produced from this SG cut-point.

With the cut-point set, a two-dimensional parameter sweep simulation was conducted using a factorial combination of α and low bypass values in the partition function. The low bypass was simulated from 0 to 30% in increments of 1%, while α was simulated from 10 to 30 in increments of 0.5. In total, this matrix produced 1271 independent simulations. For each simulation, the partition function was used to determine the recovery by density class. The contract and washability data was then used to determine the product quality and incremental contract value of each density class. The recovery and incremental value were multiplied and summed to produce the final recovered product value.

In addition to the economic indicators, several performance measures were calculated for each simulation run. The traditional performance indicators included the separation sharpness, the imperfection, and the error area. The moment of inertia was calculated using

Table 7.5: Incremental Value Calculation for Economic Simulation

Washability			**Incremental Value**					
Mean SG	**Weight (%)**	**Ash (%)**	**Clean Btu**	**Base Price**	**Btu Adj**	**Ash Adj**	**Sales Adj**	**Net Value**
1.28	45.54	3.54	13,269	$50.00	$3.85	$8.46	($8.26)	$54.05
1.38	17.64	12.34	11,949	$50.00	($2.76)	($0.34)	($6.72)	$40.19
1.43	8.49	19.07	10,940	$50.00	($7.80)	($7.07)	($5.54)	$29.59
1.48	5.04	23.16	10,326	$50.00	($10.87)	($11.16)	($4.82)	$23.15
1.53	2.20	29.69	9,347	$50.00	($15.77)	($17.69)	($3.68)	$12.86
1.58	0.52	33.99	8,702	$50.00	($18.99)	($21.99)	($2.93)	$6.09
1.63	0.48	38.73	7,991	$50.00	($22.55)	($26.73)	($2.10)	($1.37)
1.68	0.25	44.25	7,163	$50.00	($26.69)	($32.25)	($1.13)	($10.07)
1.73	0.31	47.26	6,711	$50.00	($28.95)	($35.26)	($0.60)	($14.81)
1.78	0.40	52.98	5,853	$50.00	($33.24)	($40.98)	$0.40	($23.82)
1.85	0.63	56.52	5,322	$50.00	($35.89)	($44.52)	$1.02	($29.39)
1.95	0.84	59.89	4,817	$50.00	($38.42)	($47.89)	$1.61	($34.70)
2.25	17.66	82.08	1,488	$50.00	($55.06)	($70.08)	$5.49	($69.65)

both the unweighted (no costing data) and weighted methods. In the weighted case, the absolute value of the incremental cost by density class was used as the density function.

7.3.2 Results and Analysis

In total, 1,271 parameter sweep simulations were conducted to compare recovered revenue against several technical and technical-economic performance measures. The graphical results of these simulations are shown in Figures 7.9 and 7.10. In these plots, the raw economic performance is plotted as a function of the α value and the low bypass used in the simulation. These plots are shown as smooth surfaces with a corresponding color contour on the x-y plane. The misplaced revenue plot (Figure 7.10) was formulated by subtracting the maximum revenue ($3,570) from the recovered revenue. While these parameters are simple inverses of each other, the availability of both curves will allow convenient comparison to inverse performance measures. For example, increased separation sharpness yields increased revenue. Consequently, the separation sharpness parameter can be easily compared to the recovered revenue curve since one should drive the other. Alternatively, increases in the moment of inertia, error area, and imperfection correspond to reductions in separation efficiency. Consequently, these parameters will be compared to the misplaced revenue in order to form a one-to-one correspondence.

Figure 7.11 shows the recovered revenue as a function of the five separation performance indicators as individual plots. The data included on each individual plot corresponds to the 1,271 parameter sweep simulations. Data lines indicate simulations conducted at constant bypass but varying α values. In each case, the lower lines indicate the higher bypass values. A legend is omitted from this plot since too many data series are included, and since the intent is not to compare how bypass and α influence the various parameters. Instead, the intent is to analyze the spread of real performance values (in this case, the recovered revenue) that are represented by a single surrogate performance indicator value. From a metrics standpoint, a more useful surrogate performance measure would represent a small range of real performance values by a single value, with the ideal surrogate measure forming a one-to-one relationship between the derived and real measures. Simply, the different drivers of performance (α and low bypass, in this case) need to be buried into the surrogate performance measure.

Figure 7.11 indicates that both moment of inertia values (and especially the cost-weighted moment of inertia) are much better surrogate measures than the traditional performance indicators, based on the spread of revenue values that a single surrogate value can produce. For example, depending on the specific mix of α and low bypass values, a sepa-

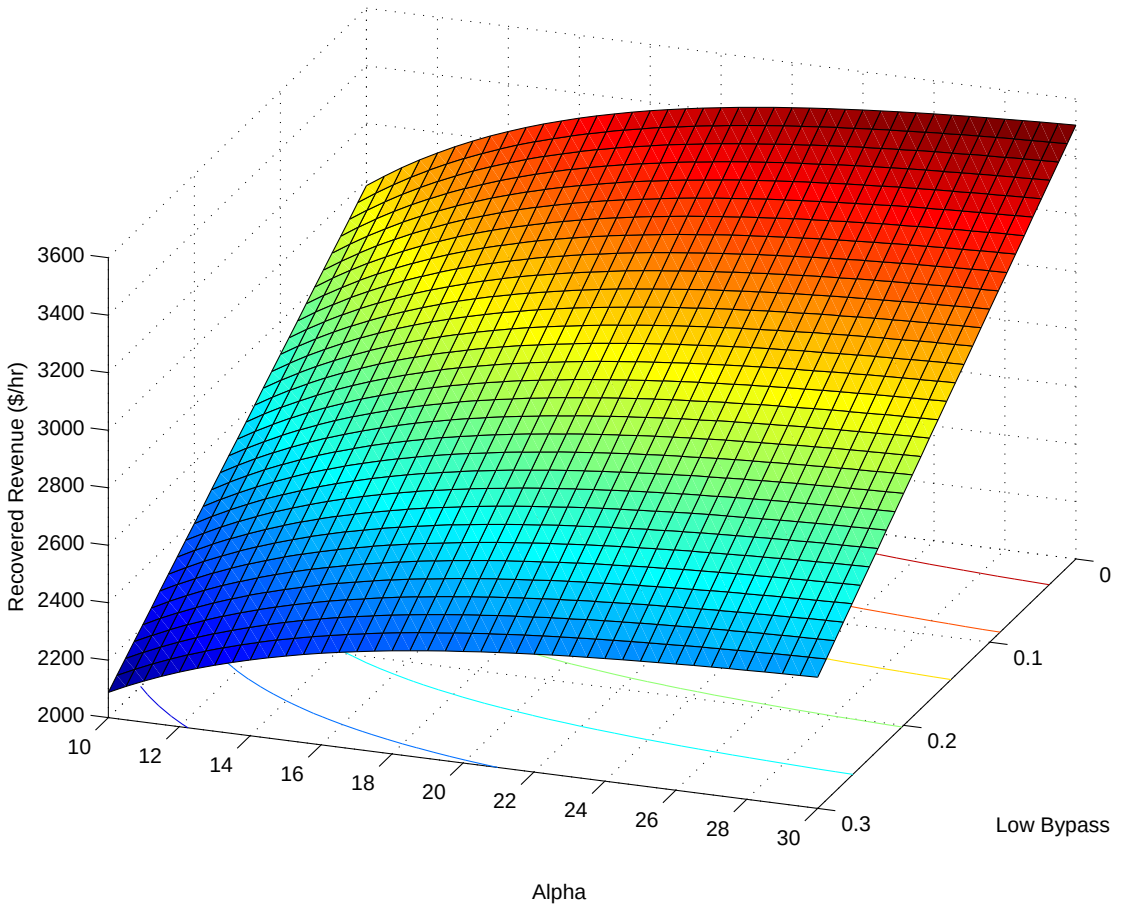

Figure 7.9: Recovered hourly revenue as a function of partition α and low bypass for coal economic simulation.

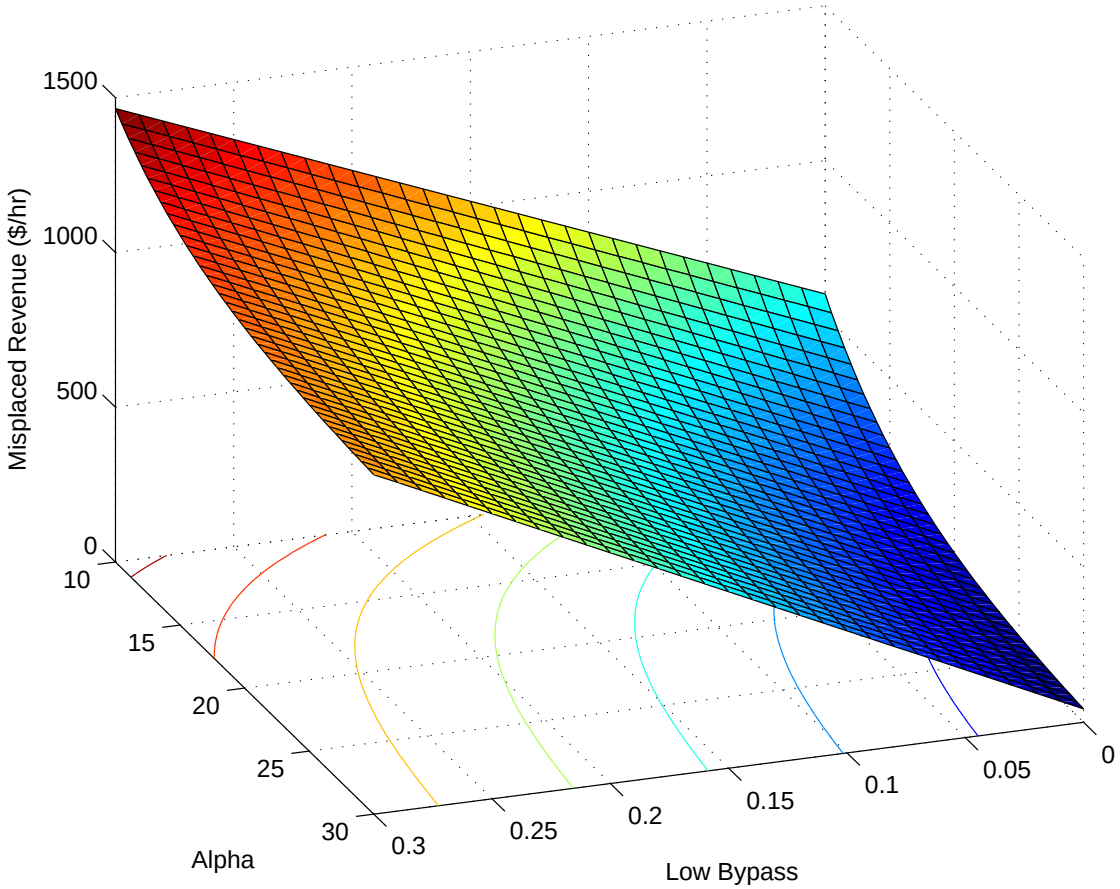

Figure 7.10: Misplaced hourly revenue as a function of partition α and low bypass for coal economic simulation.

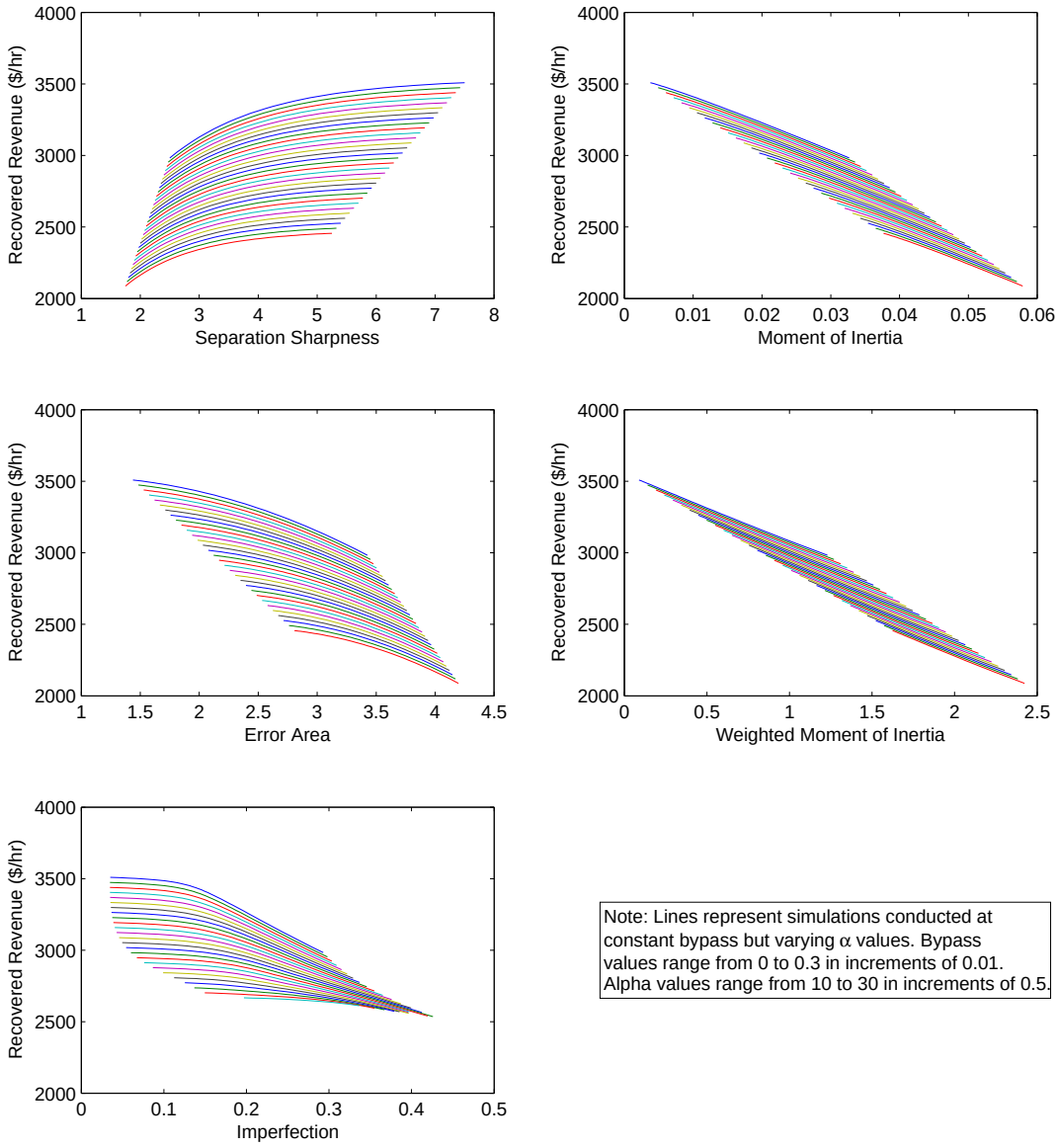

Figure 7.11: Recovered revenue as a function of five performance indicators: separation sharpness, error area, imperfection, moment of inertia, and weighted moment of inertia. Data shown for partition simulations conducted over a factorial sweep of α (10 to 30 in increments of 0.5) and low theta (0 to 0.3 in increments of 0.01).

ration sharpness of 4 can correspond to a recovered revenue of \$2,400 to \$3,300, a range of \$900. Over the full span of the data, this range does not decrease substantially. On the other hand, the widest range of the weighted MOI occurs at a value of approximately 1.5. Here, the recovered revenue only spans a range of \$300 (\$2,500 to \$2,800). Furthermore, as the values extend to the periphery, the range of recovered revenue values reduces substantially. Graphically, these range comparisons show that the moment of inertia parameters produce more aggregate linear behavior, which implies that the "hidden" drivers of recovered revenue are also proportionally driving the moment of inertia.

A second way of making the same comparison is by looking at side-by-side surface contours of the real and the surrogate measurements as a function of α and low bypass. These plots will depict the specific regions where the economic performance behaves similarly to the derived measure. A more ideal surrogate measure would produce similar, though proportionally adjusted, behavior across the entire region. Figures 7.12 and 7.13 show this data for the traditional and moment of inertia performance indicators, respectively. The left column of plots show the derived performance measures, while the right column of plots shows the corresponding real economic measure. In this case, all parameters (with the exception of separation sharpness) were compared side-to-side with misplaced revenue, since higher values in these measurements correspond to decreased performance. Alternatively, separation sharpness was compared directly with recovered revenue to match the appropriate comparison. The missing regions of the imperfection contour indicate that the value is non-defined for those parameter values. This result was often due to the partition curve never crossing 25% which is required for the imperfection calculation.

Visual comparisons between the surface contours indicate that the moment of inertia parameters show close agreement with the financial indicators across the full range of parameter values. Figure 7.12 shows that the separation sharpness and error area values are too heavily influence by the α value when compared to their corresponding economic indicators. The slope of the contour lines in the separation sharpness plot does not change as a function of bypass value. On the other hand, the slope of the moment of inertia parameters does reflect the changes in low bypass value. This visualization can be quantified by counting the number of contour lines that a particular indicator crosses at a fixed y-axis (α) value. At $\alpha = 20$, separation sharpness crosses 1 contour line, error area crosses 2, imperfection crosses 4, unweighted MOI crosses 5, and the weighted MOI crosses 5. For the comparisons, the recovered revenue crosses 6, and the misplaced revenue crosses 5. While the graphical rendering can be manipulated to force these results, the failure of traditional performance measures to account for unit bypass is evident in the geometry of the contours.

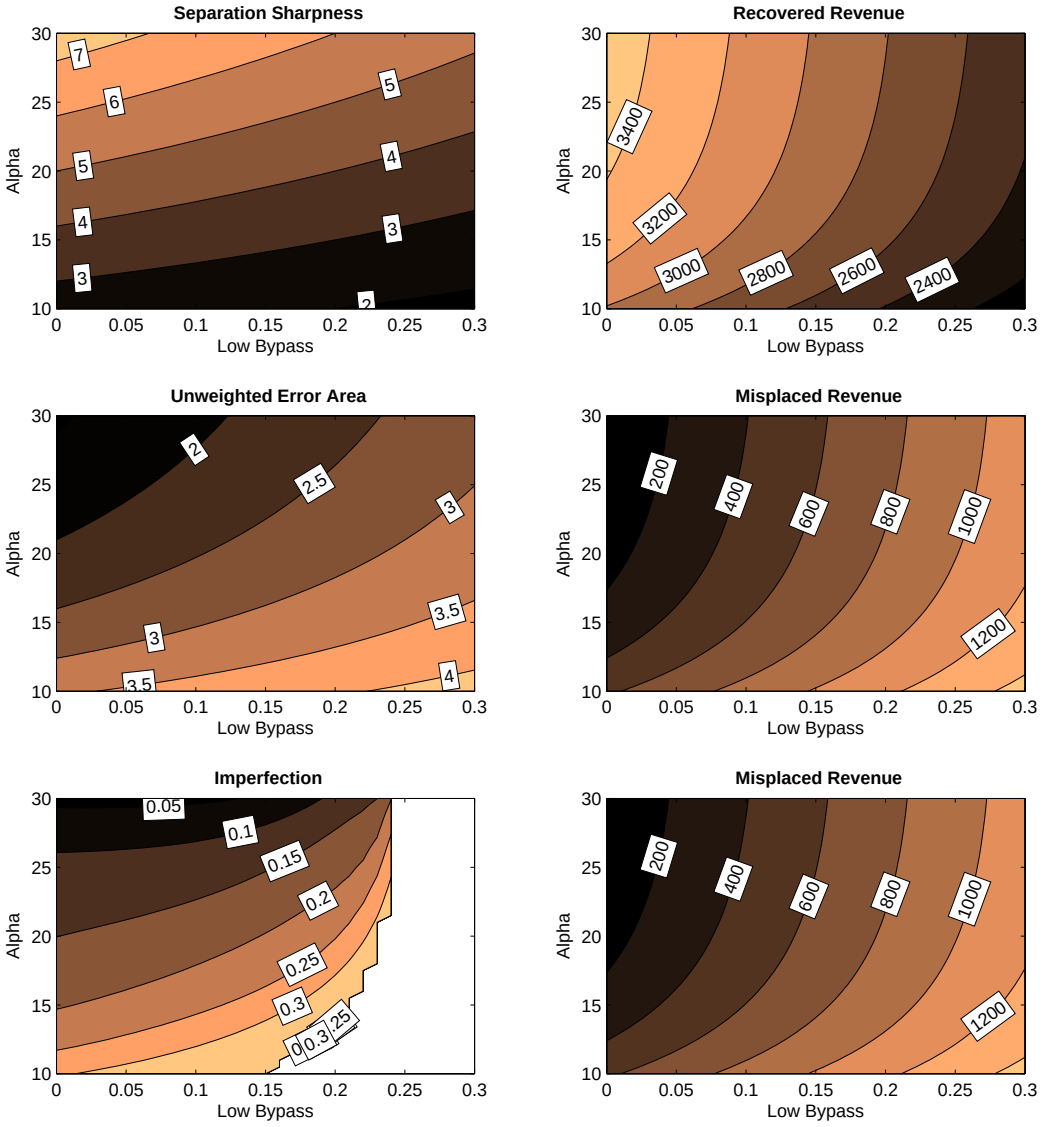

Figure 7.12: Surface contours showing traditional surrogate performance measures (left column) and actual economic measures (right column). Side-by-side plots indicate values presumed to have a direct correspondence (e.g. error area should directly correspond to misplaced revenue). Data shown for partition simulations conducted over a factorial sweep of α (10 to 30 in increments of 0.5) and low theta (0 to 0.3 in increments of 0.01).

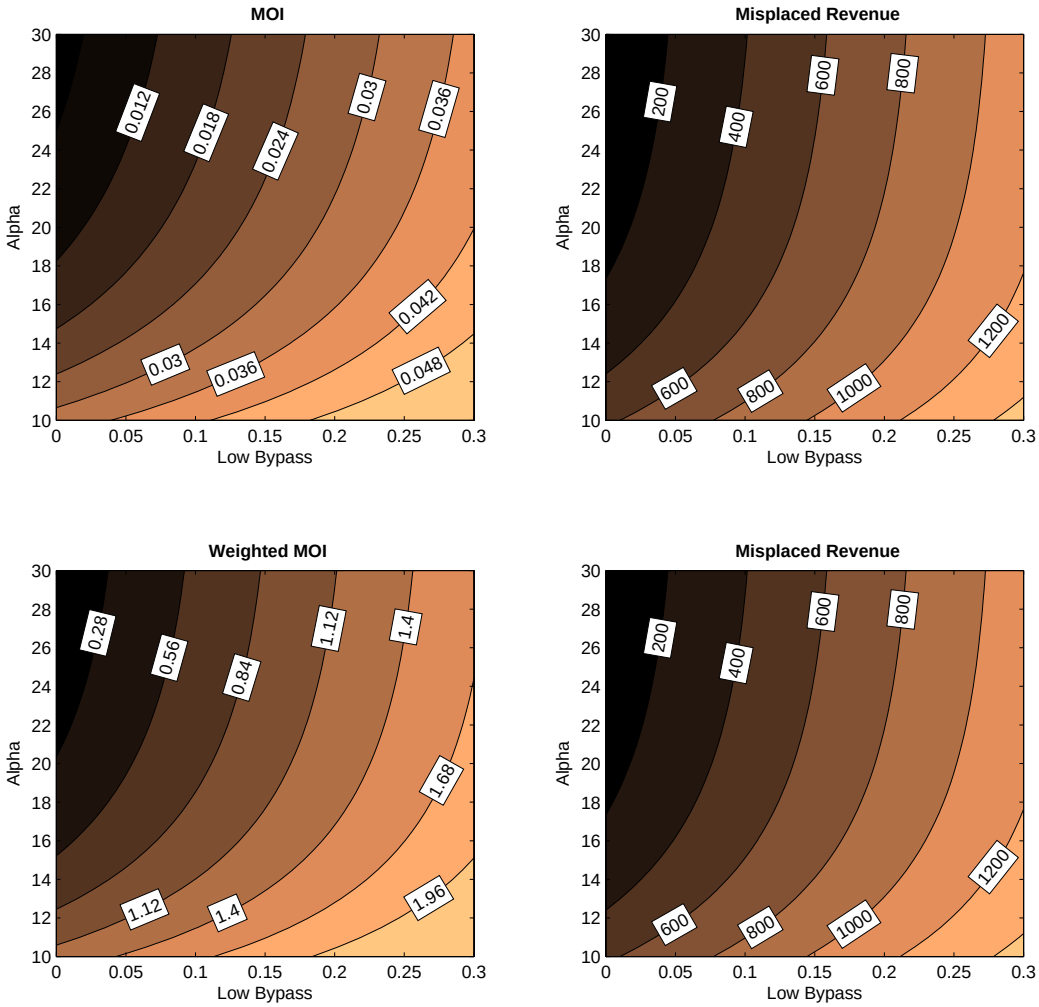

Figure 7.13: Surface contours showing moment of inertia surrogate performance measures (left column) and actual economic measures (right column). Side-by-side plots indicate values presumed to have a direct correspondence (e.g. MOI should directly correspond to misplaced revenue). Data shown for partition simulations conducted over a factorial sweep of α (10 to 30 in increments of 0.5) and low theta (0 to 0.3 in increments of 0.01)

7.4 Summary & Conclusions

This paper has introduced the partition moment of inertia (MOI) as a technical-economic separation performance indicator. This value is derived from the mechanical definition of the mass moment of inertia and used to account for the disproportionately high influence pure particles have on the final process economics. In most systems, these pure particles represent a higher portion of the initial feed weight (via liberation) as well a higher unit economic value (via incremental costing). A robust technical-economic performance indicator must account for this consistent bias.

From a mechanical perspective, the mass moment of inertia penalizes mass in proportion to its distance from the rotational axis. Mass farther away from the axis of rotation contributes more heavily to the final moment of inertia value. In an analogous fashion, a traditional partition curve places the valuable pure particles at the periphery of the x-axis, most distant from the central cut-point. If the error area of the partition curve is modeled as a thin plate rotating about the cut-point, the mass moment of inertia of that plate would disproportionately penalize error area at the periphery. Furthermore, an incremental costing function may be applied to represent the "density" of the thin plate. Thus the final model produces a derived performance indicator, the partition moment of inertia (MOI), which successfully accounts for the value of misplaced pure particles.

Formally, the partition moment of inertia is defined by:

$$MOI = \int_{Z_{Min}}^{Z_{Desire}} C(Z)P(Z)(Z_{Desire} - Z)^2 \,\mathrm{d}Z + \int_{Z_{Desire}}^{Z_{Max}} C(Z)(1 - P(Z))(Z - Z_{Desire})^2 \,\mathrm{d}Z$$

where $C(Z)$ is the cost or density function, $P(Z)$ is the partition function, and Z_{Min}, Z_{Max}, and Z_{Desire} are the the minimum, maximum, and desired normalized property values, respectively. This calculation can be extended to circuit configurations by substituting the analytical circuit solution as ($P(Z)$) and the unit transfer function as Z. The integration limits in the circuit case are defined as 0, 0.5, and 1.

Sample calculations for six basic circuit configurations show that at fixed unit bypass levels, the circuit separation sharpness (SE) produces similar rankings as the partition moment of inertia (MOI). However, as bypass is factored into the system, the two factors often produce conflicting circuit rankings. To defend the partition moment of inertia as the superior measure, a parameter sweep simulation was conducted using coal separation and economic data. The results compared the real economic performance of the separator, in terms of recovered revenue, to several derived performance indicators (separation sharpness, error area, imperfection, unweighted MOI, and cost-weighted MOI). Contour plots and

holistic comparisons show that the MOI behavior correlates very well to the pure economic measures across a full range of separation operating points.

From this work, three final conclusions are formed:

1. Traditional performance indicators do not deliberately or inherently account for the disproportionate value of pure particles. Most are based solely or largely on the separation of middling material which, while difficult to separate, do not account for large incremental values or a large portion of the feed material.

2. In comparing circuit configurations, the circuit MOI and circuit SE produce similar but occasionally slightly divergent trends. With the addition of a costing function this discrepancy is further intensified.

3. The aggregated, near-linear trend between the moment of inertia and the pure economic indicators (Figure 7.11) indicate that the MOI parameter robustly accounts for the various driving parameters of the economic gain. The lack of any aggregate trend among the traditional performance indicators shows their inability to account for synergistic gains and losses by multiple driving parameters. As a result, the traditional performance indicators should be restricted to comparisons along a single dimension (such as only changes in α at a constant bypass value).

7.5 Bibliography

Armstrong, M., & Whitmore, R. (1982). *The mathematical modeling of coal washability, 1st australia coal preparation conf.*

Jowett, A. (1986). An appraisal of partition curves for coal-cleaning processes. *International Journal of Mineral Processing*, *16*(1), 75–95.

King, R. (2001). *Modeling and simulation of mineral processing systems*. Elsevier.

Leonard, J. (1991). *Coal preparation, 5th ed.* SME.

Luttrell, G., Barbee, C., & Stanley, F. (2003). Optimum cutpoints for heavy medium separations. *Advances in Gravity Concentration*, 81.

Luttrell, G., Catarious, D., Miller, J., & Stanley, F. (2000). An evaluation of plantwide control strategies for coal preparation plants. *Control 2000: Mineral and Metallurgical Processing*, 175.

Luttrell, G., & Honaker, R. (2005). Practical optimization of coal preparation plants. *Innovations in Natural Resource Processing*, 367–382.

Luttrell, G., Honaker, R., & Yoon, R. (2004). Optimization of the coal fuel supply chain: A coal preparation perspective. In *Proceedings, 29th international technical conference on coal utilization and fuel systems* (p. 9).

Luttrell, G., Keles, S., & Honaker, R. (2009). Implications of constant incremental quality on fine coal dewatering circuitry. In *2009 sme annual meeting and exhibit preprints* (p. 5). SME.

Lyman, G. (1993). Computational procedures in optimization of beneficiation circuits based on incremental grade or ash content. *Transactions*, *102*, C159–C159.

Meloy, T. (1983a). Analysis and optimization of mineral processing and coal-cleaning circuits circuit analysis. *International Journal of Mineral Processing*, *10*(1), 61–80.

Meloy, T. (1983b). Optimizing for grade or profit in mineral processing circuits circuit analysis. *International Journal of Mineral Processing*, *11*(2), 89–99.

Mohanta, S., Chakraborty, S., & Meikap, B. (2011). Prediction of economic operating conditions for indian coal preparation plants. *Fuel Processing Technology*, *92*(9), 1696–1700.

Rong, R., & Lyman, G. (1985). Computational techniques for coal washery optimization-parallel gravity and flotation separation. *Coal Preparation*, *2*(1), 51–67.

Salama, A. (1989). Theoretical aspects of parallel coal processing circuits optimization and m-curve. *International Journal of Mineral Processing*, *27*(3), 171–187.

Stratford, K., & Napier-Munn, T. (1986). Functions for the mathematical representation of the partition curve for dense medium cyclones. In *Submitted to apcom symposium.*

Tamilmani, M., & Kapur, P. (1986). A heuristic model of the tromp (distribution) curve. *International Journal of Mineral Processing*, *18*(1), 47–56.

Tromp, K. (1937). New methods of computing the washability of coals. *Colliery Guardian*, *154*, 955–959.

Chapter 8

Experimental Validation of Analytical Circuit Design Methodologies

(ABSTRACT)

A virtual experimental study was conducted using the Working Model 2D program to compare various circuit configurations. This dynamic discrete element modeling program provides an environment to construct physical systems and observe how these systems will react to various input conditions. The electrostatic physics model was used to construct a particulate electrostatic separator within the virtual environment. This separator was then arranged into 17 circuit configurations and tested under 3 levels of forced unit bypass. A feed charge consisting of 55 particles of varying electrostatic charges was implemented into the separation circuits and monitored to determine the selectivity of the various configurations. This experimental data was compared to the circuit analysis separation sharpness (SE), moment of inertia (MOI), and yield score (YS) parameters. The results indicate that the circuit analysis methodology provides exceptional capacity to rank circuits on the basis of mass yield and selectivity. Isolated comparisons and holistic results are presented.

8.1 Introduction

8.1.1 Background

Over the past 30 years, numerous scientific and industrial studies have proposed various mineral processing circuit design methodologies which attempt to optimize the allocation of

separation resources within the processing plant. Over this time period, the methodologies have undergone various transitions, including the increased inclusion of process models and computer algorithms as well as the general shift from a purely technical solution (e.g., Lauder & McKee, 1986) to partially economic solutions (Abu-Ali & Sabour, 2003). This author has extensively reviewed the circuit design literature elsewhere (see Chapter 2), but some noteworthy concepts in the development of the discipline include Sutherland's (1981) use of process models to distribute residence time in a flotation circuit, Williams' and Meloy's decade-long development of "circuit analysis" as a means of generically evaluating separation circuits (for example, Meloy, 1983a; Williams, Fuerstenau, & Meloy, 1992), and Yingling's (1990) use of a superstructure and optimization algorithm.

Despite these scientific developments, very few studies include a comprehensive *empirical* validation of separation circuit design methodologies in a controlled experiment. For example, Sutherland (1981) compares 26 flotation circuit configuration designs, with each design distributing the total plant residence time differently between the rougher, cleaner, and scavenger banks. While this work did lead to several generally-accepted principles (such as the benefits of a balanced configuration), the author only considered two different stream configurations: the rougher-cleaner-recleaner and the rougher-scavenger-cleaner. Furthermore, the data was generated from purely mathematical (and purposefully simple) flotation models, rather than real separation devices.

Other circuit design methodologies, such as linear circuit analysis, were originally presented as purely analytical thought exercises with no external validation (Meloy, 1983a, 1983b; Meloy, Clark, & Glista, 1986). The lack of original experimentation likely led to the exclusion of this principle in real industrial circuit design problems for nearly 20 years. Nevertheless, other authors noted the legitimacy of Meloy's mathematical approach (Yingling, 1990; Luttrell, Kohmuench, Stanley, & Trump, 1998), and the the holistic methodology was eventually used to redesign a heavy mineral sands plant, leading to drastic performance improvements (McKeon & Luttrell, 2005, 2012). While this result loosely verifies the principle's applicability, the study only included a binary comparison of two circuit configurations, and the final circuit analysis was not extended to completion, given the overbearing complexity of the circuits. As a result, the outcomes of the design methodology were not quantified, leaving the potential for alternate solutions. Other studies, such as the column flotation circuit comparison presented by Tao, Luttrell, and Yoon (2000) extend the methodology to more circuit designs (six in this case) but still fail to quantify the outcomes in a controlled setting.

8.1.2 Review of Analytical Methods

Traditionally, the circuit analysis methodology encompasses two primary stages. First, the analytical circuit solution is produced via algebraic manipulation. A generic transfer function (P_i) is defined for each binary separation unit, resulting in simple mathematical functions for the concentrate ($C = PF$) and the tailings ($T = (1 - P)F$). These principles are extended to account for multi-unit separations, including open circuits and recirculating loads. An extensive review of this technique is provided in Chapter 5. Second, the analytical circuit solution is used to define a separation sharpness indicator (SE). This value is mathematically defined as the derivative of the analytical circuit solution at $P = 0.5$. For the sake of simplicity in calculating the derivative, all P values are assumed to be equal ($P_i = P$). The resulting SE value defines the relative sharpness of the circuit's partition curve to the sharpness of a single unit. Pragmatically, this value reveals the circuit's capacity to distinguish middling or otherwise indiscriminate particles.

A new software package, the Circuit Analysis Reduction Tool (CART), has streamlined both of these circuit analysis steps. This program provides a graphical interface for user-defined flowsheet input and uses proprietary algorithms to solve the analytical circuit solution and the SE parameter. The utilization and application of this software is presented in Chapter 6.

Various real separation processes include some type of non-selective recovery mechanisms, generally labeled unit bypass. Some examples include entrainment in flotation and hydrocyclones, blinding or plugging in industrial screens, and entrapment in spiral separators). The circuit analysis algebra provides a basis to include these phenomenon via non-selective splitting. In the circuit analysis model, a defined portion of the feed (equal to the bypass) is redirected around the separation, automatically reporting to the appropriate product. Unfortunately, while the algebra provides the potential for inclusion, the SE performance measure cannot entirely account for the performance losses. Typically, the addition of unit bypass does prompt a reduction in the SE parameter; however, since the value only inherently considers middling separation, the influence of unit bypass tends to be understated. This limitation is magnified considering the high incremental value of non-middling particles and the typically high percentage of these particles in well liberated feeds.

To overcome these limitations, this author has proposed a secondary performance measure which is derived from the analytical circuit solution. The partition moment of inertia (MOI) represents the physical resistance of the partition area against rotation about the

cut-point. This derived parameter is analogous to a mechanical moment of inertia which represents a rigid body's resistance to rotation about an axis. In the mechanical moment of inertia, mass further away from the rotational axis contributes exponentially more to the MOI value since that mass is more difficult to rotate. Similarly, partition error further away from the cut-point contributes exponentially more to the partition MOI since these non-middling particles contribute substantially more to lost revenue. An extensive mathematical treatment of the partition MOI as well as its calculation in single units and circuits is given in Chapter 7.

Along with these measures of circuit *selectivity*, the analytical solution may also be used as an indicator of the circuit mass *yield*. When considering two partition separators, the area between the partition curves designates the incremental difference in circuit yield. The same principle applies to circuit partition curves. By integrating the difference between two circuit analytical functions, the differential yield between the two circuits is obtained. Mathematically, this integral is given by:

$$Y_i = \int_0^1 W(Z)\left[(C/F)_2 - (C/F)_1\right] \mathrm{d}P$$

where Y_i is the incremental yield, $W(Z)$ is the mass distribution function, and $(C/F)_i$ are the circuit analytical functions. As it is formulated, a positive Y_i value indicates that circuit 2 produces a greater yield, while a negative value indicates that circuit 1 produces a greater yield. The mass distribution function is included to account for non-uniform feed distributions. If this function is not known, a constant value (i.e. 1) may be substituted and factored out of the integral.

A generic formulation of this incremental yield calculation is given by the *yield score* (YS). This value is defined as the yield differential between a given circuit and the single-unit circuit ($C/F = P$). The yield score indicates the yield gain or loss compared to a single unit and may be used as a holistic ranking parameter used in circuit analysis. Since circuit analysis generally relies on limited data, the weighting function is commonly disregarded in calculating the yield score. Formally, the yield score is given by:

$$YS = \int_0^1 \left[(C/F) - P\right] \mathrm{d}P. \tag{8.1}$$

The yield score inherently carries no information on circuit selectivity. However, the yield score does indicate a circuit's ability to recover pure mass of feed material. While yield is never a sole process objective, the yield score is still useful in intermediate or incremental optimization which targets circuit production since recovered tonnage often strongly influences the circuit's revenue.

8.1.3 Working Model Program

This study evaluates various circuit designs using a virtual experimental analysis conducted with the Working Model 2D software package (Copyright ©2005-2013 Design Simulation Technologies, Inc.). This commercial computer aided engineering program provides an environment for dynamic discrete element modeling, based on various Newtonian physics principles. The Working Model 2D development environment provides an interface to construct simple geometries (circles, arcs, polygons), which model real physical entities in a virtual two-dimensional environment. The intensive physical properties of the user-defined geometries (including friction coefficients, the elastic coefficient, and the particle charge) may be adjusted independently or selected from a default menu which includes common materials (plastic, rubber, steel, rock, etc.) Various physical motion constraints, including locking joints and pin joints, may be applied to the geometries in order to construct simple machines. Finally, the user may apply several constant or potential force sources (point loads, torques, springs, rotational motors, gravity fields) to the original geometries. The Working Model program then uses dynamic Newtonian physics models to predict how the geometries will react to the environmental conditions as a function of time. Physical outputs of the system, body particle position, velocity, and acceleration may be logged during the simulation.

The physical models in the Working Model 2D program include functions for simple collision models as well as various force fields, including gravity, wind, magnetics, and electrostatics. The application of these models has been incorporated in various other scientific studies covering a wide range of disciplines, including prosthetics (Dechev, Cleghorn, & Naumann, 2001), biomechanics (Linnell, Wu, Baudin, & Gervais, 2007; Delattre & Moretto, 2008), energy harvesting (Wang, Chen, & Sung, 2010), and robot design (Thueer & Siegwart, 2010). A cursory review of the literature in the mineral processing field yielded no published studies which have used Working Model. Nevertheless, Working Model was used in this study to analyze a virtual electrostatic separation device arranged in various circuit configurations. The multi-body, dynamic environment provided the means to create discrete particles as well as the actual separator. The simulation then uses the physical models to depict how particles are separated as they flow through the system.

8.1.4 Overview

This study empirically evaluates the circuit analysis design methodologies via controlled and comprehensive experimentation. The Working Model 2D program is used to generate 17 circuit configurations which are tested under various levels of force bypass. This approach

models the behavior of real physical systems while providing the context for unlimited circuit variations and cost-effective, yet rigorous, data analysis. In addition to the experimental separation data, the CART^{TM}program is used to define the SE value and the MOI value for each of the 17 circuit configurations at varying degrees of anticipated bypass.

The remainder of this paper describes the experimental details and the specific bulk experimental results. The virtual experimental setup which utilizes the Working Model 2D program is first presented. The specific geometries of the virtual separator as well as the feed characteristics and data post-processing algorithms are described. Next, comparative results show the correspondence between the analytical circuit evaluations (SE and MOI) and the real separation performance measured in the virtual experiments. Finally, opportunities for further study are described in the conclusions.

8.2 Experimental

8.2.1 Experimental Setup

The Working Model 2D program was used to create a hypothetical electrostatic separator. This device uses a strong positively charged electrostatic plate which causes falling material to either be pulled or thrown depending upon the given charge of the individual particle. Two product bins are arranged to collect the processed material, given the trajectory after being influenced by the electrostatic plate. A range of particle charges was included in the feed to model both "liberated" and middling constituents.

The specific geometry of the standard single-unit separator (Figure 8.1) includes a hopper with a feed distributer, an electrostatic plate, a separation divider, and two product bins. For all simulations, the electrostatic plate was set to a constant charge value, 6.0×10^{-5} Coulombs. This value was selected from initial shakedown testing to produce a moderately inefficient separator. Higher charge values produce better separation; however, high single-unit separation efficiency tends to mask the gains produced by the circuit configuration. In the simulated environment, this electrostatic plate measures 1.1 by 0.3 meters.

The location of the separation divider and the shape of the feed hopper define the cut-point for the separator. These geometries were set so that the standard single unit cut-point would be at the zero-charge particle. The separation divider has a height of 1.8 meters, and the center point is 2.2 meters from the left edge of the bottom plate. The bottom plate has a total length of 4.76 meters. The entire device, including the hopper, is 8.5 meters tall, and

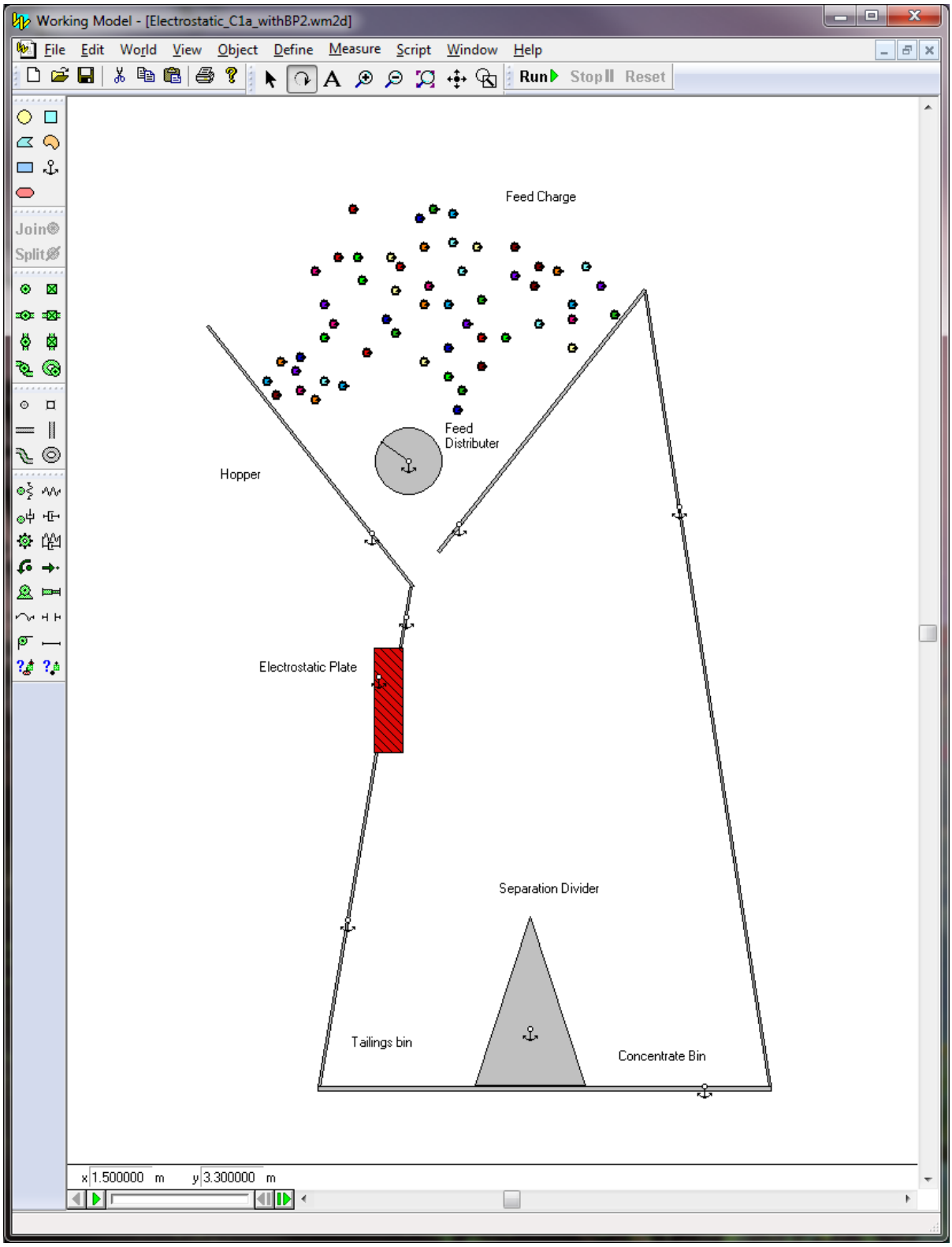

Figure 8.1: Standard single-unit electrostatic separator in Working Model 2D development environment.

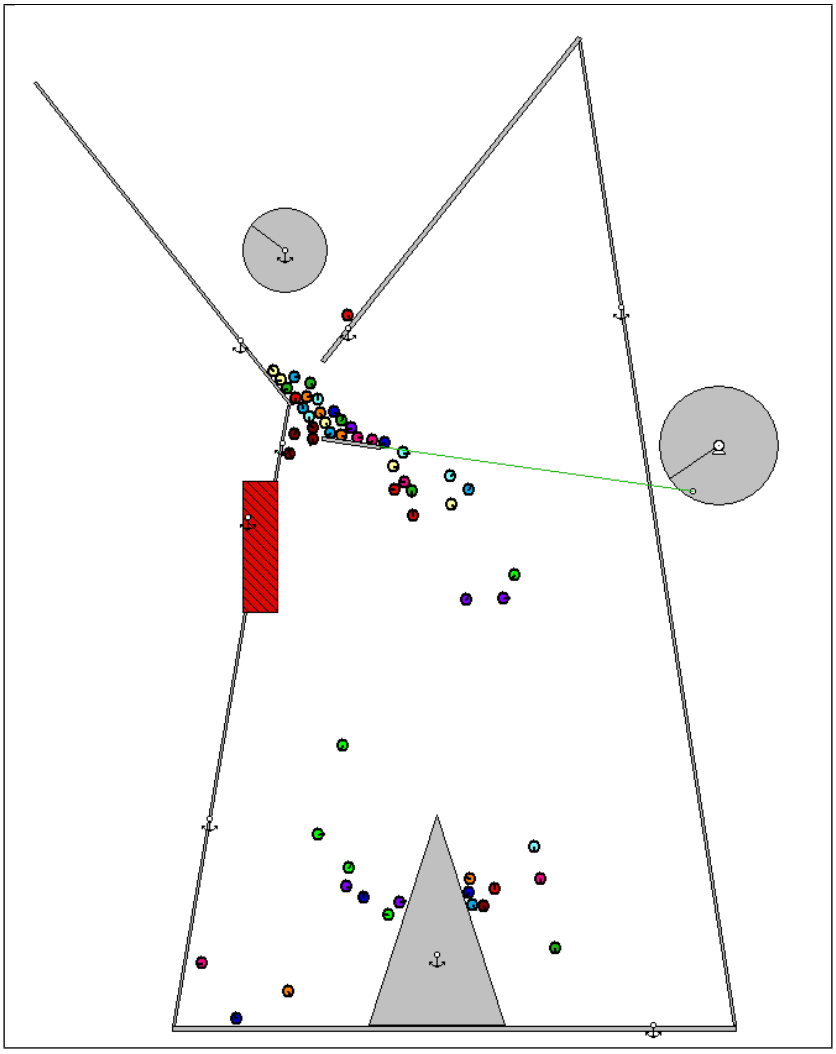

Figure 8.2: Working Model electrostatic simulation with unit bypass.

all structures are approximately 0.05 meters thick.

To study the influence of non-selective bypass on circuit design, an addition was made to the standard electrostatic model. A motor driven platform was placed immediately below the feed hopper (Figure 8.2). This platform incrementally blocks material from entering the separation zone, while indiscriminately forcing material into the concentrate bin. The degree of the bypass was controlled by increasing or reducing the size of the platform, keeping the motor at a constant speed. The platform lengths used in the simulations include 0.3 meters and 0.5 meters. The motor speed was held at a constant 5 radians per second throughout all tests.

The basic geometry of the electrostatic separator does not represent or correspond to any "real" process. Conversely, the Working Model device was designed solely to produce a naturally inefficient separation within a virtual environment. The single-unit separator was then duplicated and reconfigured to produce numerous simple circuit configurations so that the final results of this virtual experiment diagnose efficiency gains and losses due to circuit configuration. An example of a rougher-scavenger-cleaner circuit in the working model environment is shown in Figure 8.3. The intent of this study is not to investigate the realism of the modeled separation process; rather, the intent is to quantitatively study the influence of circuit design on separation performance in an inherently stochastic process. Other merits and criticism of this approach are thoroughly discussed in Section 8.4.1.

The feed charge includes 11 different particle types with charges varying from -1.0×10^{-7} to 1.0×10^{-7} Coulombs in increments of 2.0×10^{-8} Coulombs. Each distinct particle charge corresponds to a specific color, and each measures 10 cm in diameter. Five particles of each charge are included, resulting in a total feed of 55 particles. Table 8.1 summarizes the standard feed charge for the electrostatic separator.

8.2.2 Circuits

During the experiments, 17 unique circuit configurations were tested at three levels of forced bypass. Figure 8.4 shows a simplified circuit analysis schematic for each circuit configuration. Various code letters ranging from C1 to C31 are used to designate the circuits. C1 is the standard single-unit cell, and the remaining configurations fall into one of three generic design approaches:

1. *C2 - C5*: Two unit open and recycle circuits. Configurations include rougher-cleaner and rougher-scavenger arrangements.

2. *C12 - C17*: Various rougher-cleaner-recleaner circuits. Configurations include all potentially beneficial recycle patterns.

3. *C26 - C31* Various balanced rougher-scavenger-cleaner circuits. Configurations include all potentially beneficial recycle patterns.

Deleterious configurations were purposely omitted from the analysis. For example, rougher-cleaner-recleaner circuits which re-direct tailings streams forward in the circuit were

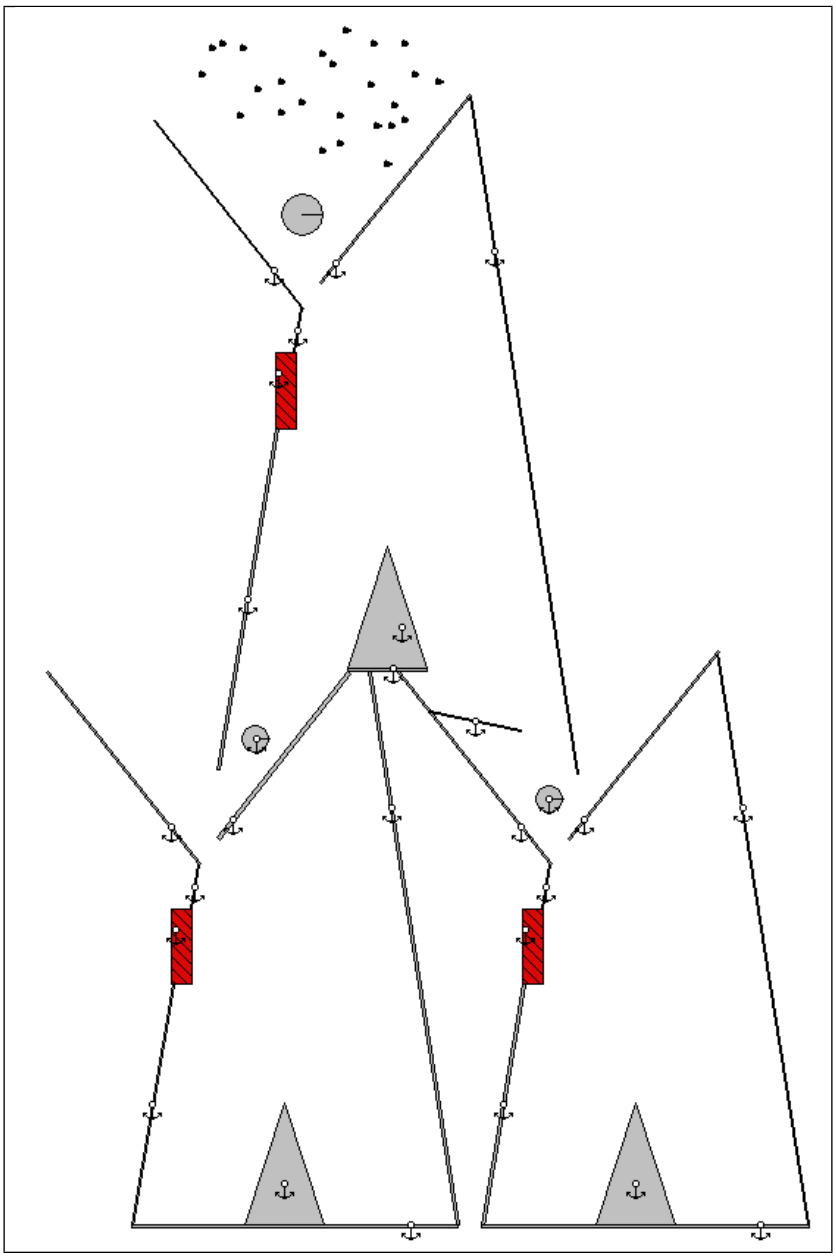

Figure 8.3: Example of a rougher-scavenger-cleaner circuit in the Working Model development environment.

Table 8.1: Working Model Electrostatic Simulation Feed Charge

Ball Color	**Charge ($\times 10^{-7}$ C)**	**Feed Number**
Pink	-1.0	5
Blue	-0.8	5
Purple	-0.6	5
Maroon	-0.4	5
Green	-0.2	5
Yellow	0	5
Red	0.2	5
Orange	0.4	5
Dark Green	0.6	5
Light Blue	0.8	5
Cyan	1	5

not included. Nevertheless, the remaining configurations are only considered *potentially beneficial* as circuit analysis and the expermental results may show that some configurations waste resources and inhibit separation performance.

These particular circuits were selected in order to model common decisions posed to circuit designers. For example, the choice of a recleaner cell or a scavenger cell in the three unit case is common for many flotation circuits. The direction of the force bypass in these experiments disqualified the consideration of rougher-scavenger-scavenger circuits. Since material is short circuited to the concentrate rather than the tailings in these experiments, the additional recleaning circuits were prioritized. Had the bypass forced material to the tailings, the decision would be reversed.

8.2.3 Procedures

The virtual electrostatic separation experiments were conducted within the Working Model 2D program. Upon launching the program, the appropriate single-unit geometry was constructed. This cell was then copied to create the desired circuit superstructure. The 55 particle feed charge was placed in the first hopper using a semi-randomized initial configuration. With all of the geometries, physical properties, and initial conditions of the experiment set, the Working Model virtual test was initiated. While the program was running, the particles were observed as they passed throughout the entire circuit. Once all of the particles came to rest in a final product bin, the total recoveries were tallied by counting the particle colors in each bin.

Recycle streams were implemented manually. For these circuit configurations, specific product bins were modeled to represent recycle streams. After the initial test run was completed, particles which were recovered in these bins were manually moved to the appropriate circuit point and a supplemental run was conducted. During these supplemental runs, all of the original feed charge was maintained in the test; however, the *appearance* of the original feed was turned off, focusing the visual attention on the recirculating particles. As a result, the original feed particles still influenced the separation behavior; however, the supplemental test runs only showed the recirculated particles of interest. Additional supplemental runs were completed until the entire recirculated load eventually came to rest in a final product bin rather than a recirculation bin. For some circuit configurations as many as 10 supplemental runs were required to finalize the circuit.

Each circuit configuration was tested for five independent experimental runs in order to appraise the reproducibility of the results. The additional test runs were reconfigured

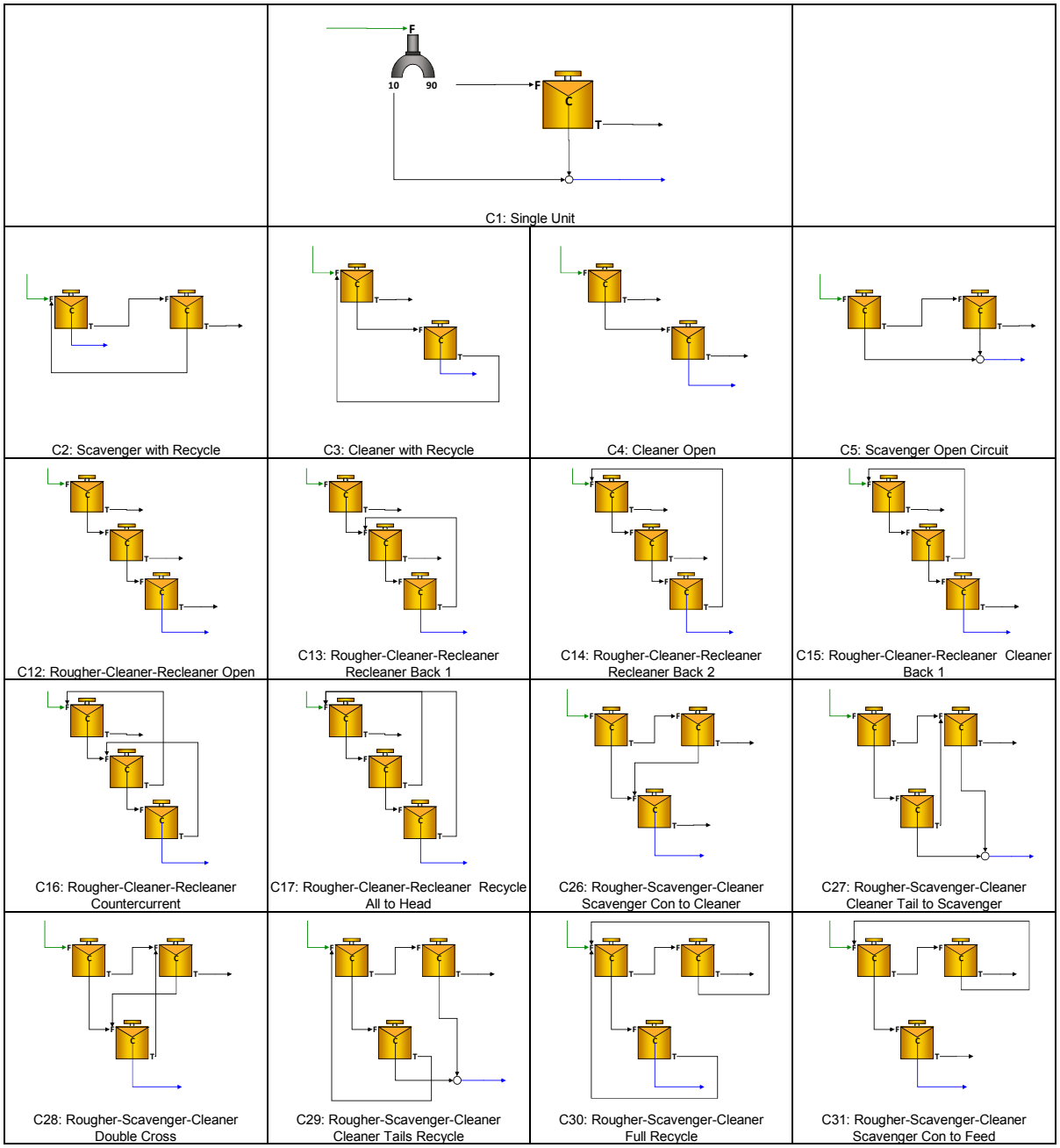

Figure 8.4: Circuit Configurations used in Working Model Simulations. Note that from a circuit analysis perspective, each unit cell in the circuits (C2 - C31) actually corresponds to a feed splitter followed by a unit cell as depicted in C1. Splitters were omitted from the latter drawings to conserve space.

by randomizing the initial feed condition. Various particles were randomly selected and moved to other positions in the feed hopper, and the size and location of the feed distributer were adjusted. This randomization produced slightly varying results, as the specific particle-particle interactions changed with the altered feed conditions. The recovery results presented in this study predominantly reflect the simple average of the five test runs, while the error bars correspond to one standard deviation of the five test population.

In total, 17 circuit configurations were tested at three levels of forced bypass. Each condition was repeated five times, leading to 255 independent virtual experiments.

8.2.4 Experimental Post-Processing

The results of each experimental run were enumerated using a custom MATLAB image analysis script (Copyright ©1994-2013 The MathWorks, Inc.). A screenshot from one of the product bins is input into the routine along with the number of pixels in a single ball. This value is dependent upon the screen resolution and the zoom level in the Working Model program; however, a quick analysis of a single ball easily yields this calibration. The script file then decodes the image using the CIE L*a*b* color space, counting the total number of image pixels with a designated color. Different colors in the L*a*b* color space are designated by two-dimensional coordinates in a 200 x 200 matrix. The Euclidean distance between two points in this plane corresponds directly to color distinction. The actual value in a specific matrix element represents the number of pixels with that color coordinate. The colors selected for the electrostatic particles were sufficiently distanced in the color plane to allow definitive distinction. Figure 8.5 shows a sample 2D histogram depicting the initial ball charge. The white intensity of a given point indicates the number of counted pixels at that point.

With the 2D pixel histogram constructed, the total pixels of each particle color were summed. These totals were divided by the pixels per ball calibration, and the final results were automatically exported into Excel. Figure 8.6 shows the screen output from the MATLAB script for a sample product. This process was repeated for each product bin in a given simulation.

Numerous mathematical and analytical methods were used to consolidate the results. In lieu of artificial pricing or contract data, the true separation capacity of the circuit was determined by the total recovered charge parameter. This value was determined by summing the total charge present in the final concentrate product bin. The number of particles of a given color was multiplied by the charge of that color, and this product was summed for all

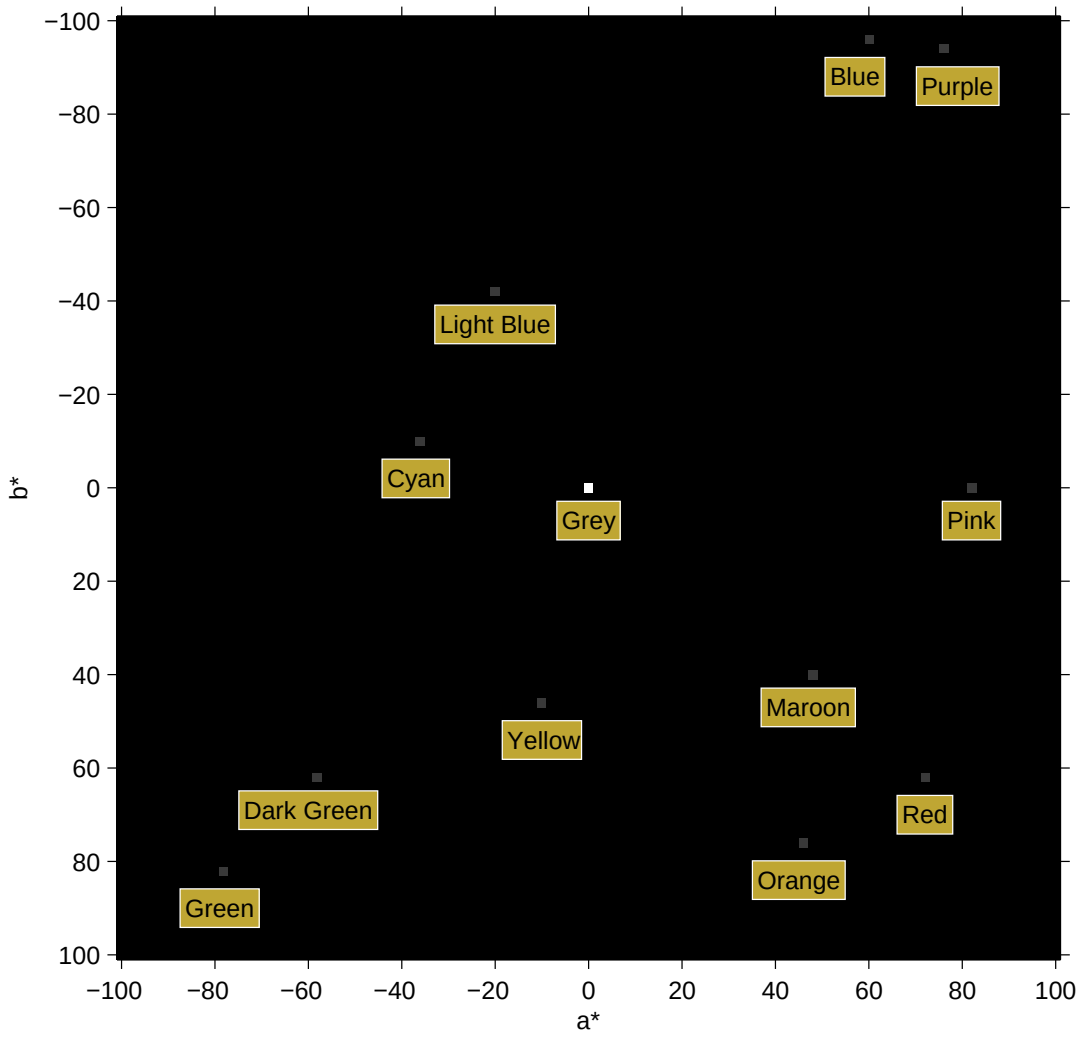

Figure 8.5: Two dimensional L*a*b* histogram. Unique a*b* coordinate pairs corresponds to distinct color value. White intensity of a point on the histogram is directly related to the number of pixels having the designated color. The electrostatic particle colors are denoted on the plot.

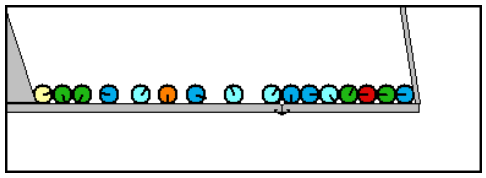

	Particle Count
Pink	0
Blue	0
Purlple	0
Maroon	0
Green	0
Yellow	1
Red	1
Orange	1
Dark Green	4
Light Blue	5
Cyan	4

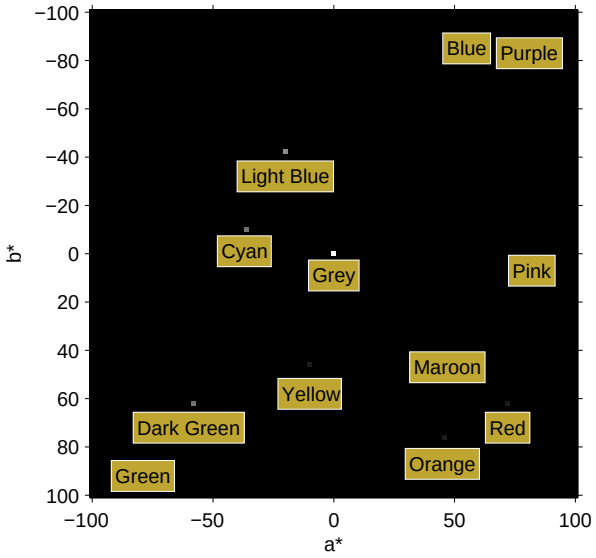

Figure 8.6: Sample image analysis collage used in data post-processing. Collage includes original image, L*a*b* two-dimensional histogram, and final ball count.

particle colors. Mathematically, this values is given by:

$$TC = \sum_{i=1}^{N} N_i C_i$$

where TC is the total recovered charge, N is the number of recovered particles in color class i, and C is the charge of particles in color class i. The TC value applies a natural premium/penalty mechanism since valuable particles contribute an increasingly positive value, while invaluable particles contribute an increasingly negative value. The net sum is subject to both increases and decreases from individual particle classes.

Along with the mass yield and total recovered charge statistics, partition curve fitting was also used to consolidate the data. For this analysis, the parameters of the Whiten partition function, including separation sharpness (α), normalized cut-point (Z), high bypass (θ_H), and low bypass (θ_L), were determined for each averaged experimental run by minimizing the sum-of-the-squared error between the predicted and experimental data points. The Whiten partition function defines the particle recovery (P) by:

$$P = (\theta_H - \theta_L)\left[1 - \frac{1}{1 + e^{\alpha(Z-1)}}\right] + \theta_L. \tag{8.2}$$

For most analyses, the raw experimental data is preferred over the smoothed partition fit; however, these parameters are still useful in identifying how the circuit configuration influences key parameters, including cut-point and bypass.

Several analytical circuit measures were determined for the various experimental circuit configurations. The CART^{TM}program was first used to determine the simplified circuit analytical function, which was then utilized in downstream analysis. The circuit SE and circuit MOI were used as indicators of circuit selectivity, while the yield score was used as the indicator of mass yield. These values were determined for each circuit configuration at various unit bypass levels. These analytically-derived values were then compared to the experimental values to evaluate the correlations.

8.3 Results

8.3.1 Working Model Simulations

The Working Model 2D program was used to simulate 255 circuit runs. This section presents the consolidated data for these experiments as well as detailed data for specific experimental points. The bulk experimental data, including recovery values for each test run is included in the Appendix to this dissertation.

First, the experimental data was used to create partition curves showing recovery to concentrate (right bin) as a function of individual particle charge. Figure 8.7 shows partition curves for the single-unit circuit (C1) at the three levels of forced bypass. The data point represents the average recovery for the five experimental runs, while the error bar represents the standard deviation of the experimental values. The line was found by fitting the Whiten partition model (Equation 8.2) to the data by minimization of the weighted sum-of-the-squared error.

This analysis is extended for the other 16 multi-unit circuit configurations. Figures 8.8, 8.9, and 8.10 show the experimental partition curves for the no, medium, and high bypass conditions, respectively. Collectively, these plots illustrate the circuit's ability to influence the partition cut-point, separation sharpness, unit bypass. Additionally, Table 8.2, shows the fitting parameters used to determine the Whiten partition model for each data set.

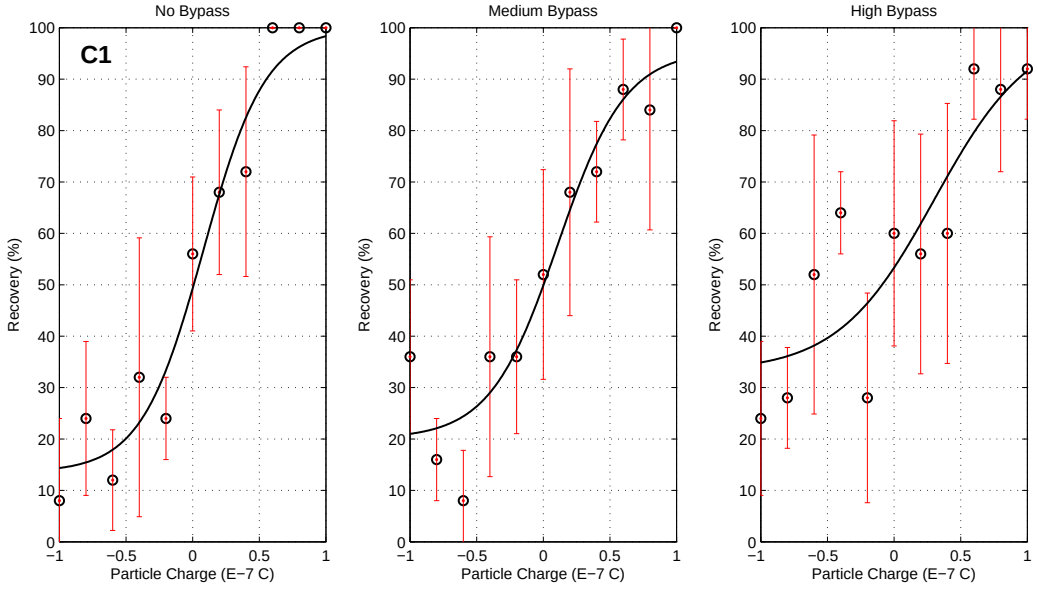

Figure 8.7: Experimental data and fitted partition curves for C1 (single unit). Data points represent the average of 5 experimental runs, while the error bars indicate one standard deviation of the measurements.

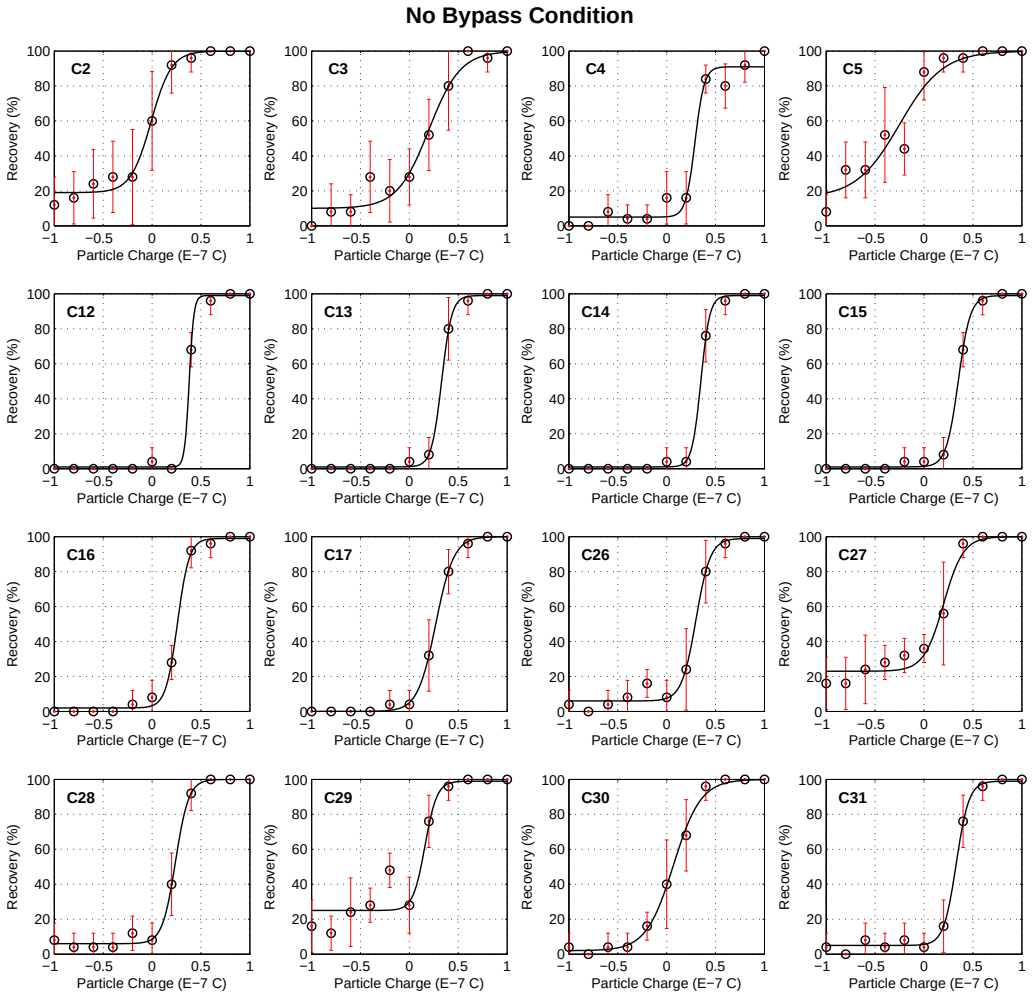

Figure 8.8: Experimental data and fitted partition curves for all circuits, no bypass condition. Data points represent the average of 5 experimental runs, while the error bars indicate one standard deviation of the measurements.

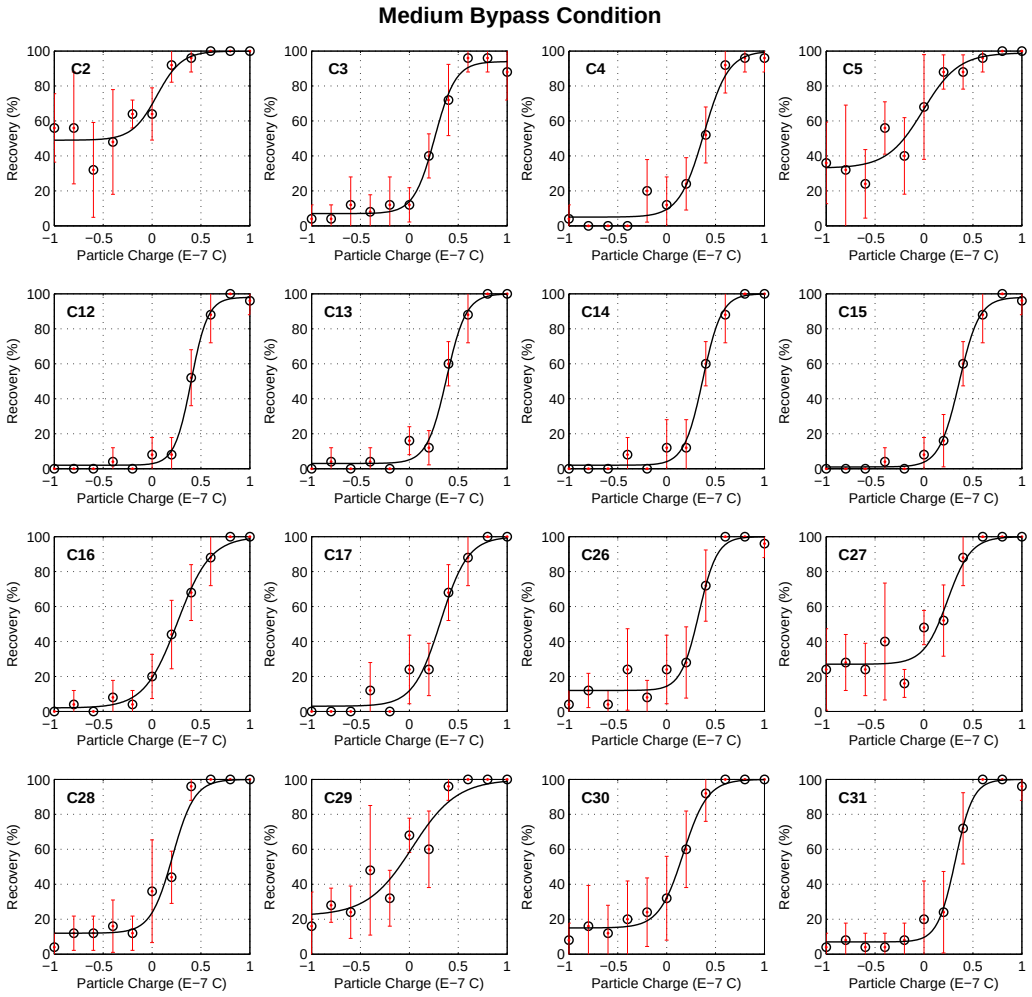

Figure 8.9: Experimental data and fitted partition curves for all circuits, medium bypass condition. Data points represent the average of 5 experimental runs, while the error bars indicate one standard deviation of the measurements.

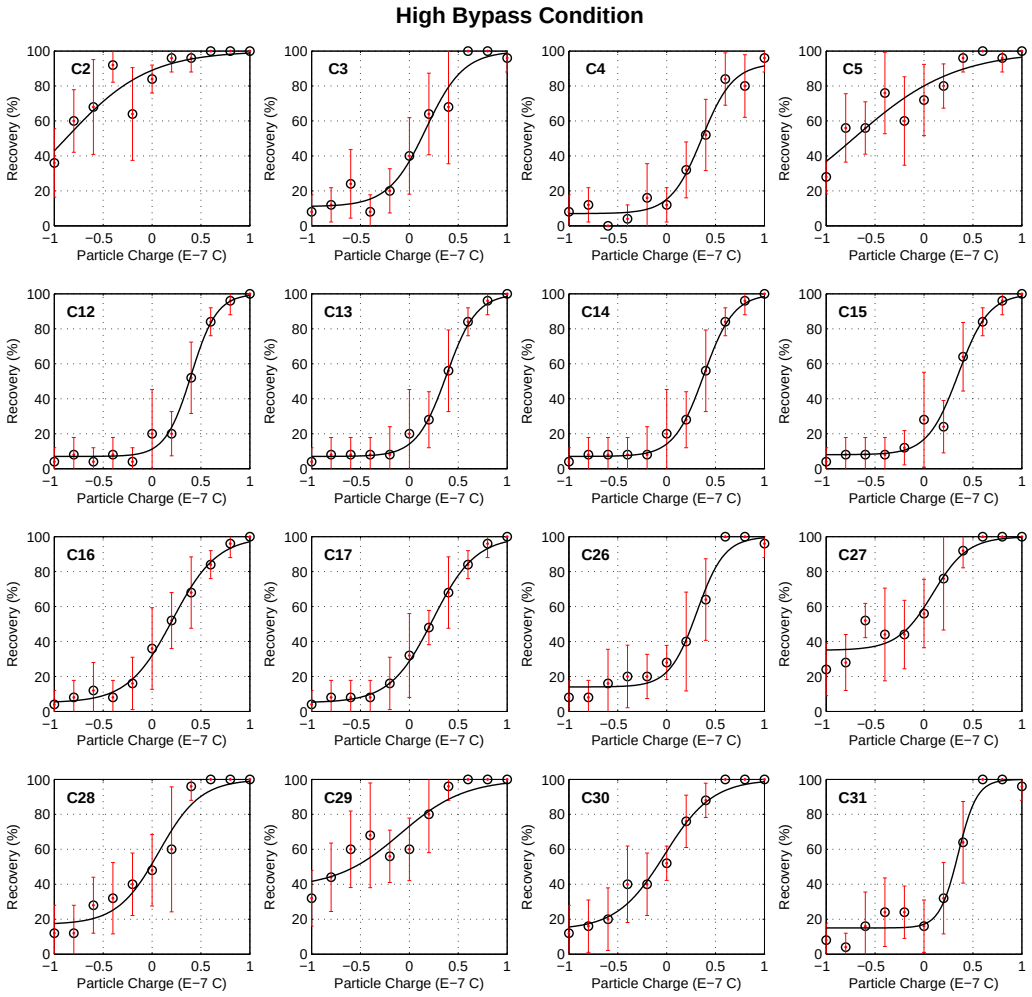

Figure 8.10: Experimental data and fitted partition curves for all circuits, high bypass condition. Data points represent the average of 5 experimental runs, while the error bars indicate one standard deviation of the measurements.

Table 8.2: Working Model Electrostatic Simulation Partition Curve Fitting Parameters

Circuit	**Cut-Point**			**Alpha**			**High Bypass**			**Low Bypass**		
ID	None	Med	High	None	Med	High	None	Med	High	None	Med	High
C1	0.08	0.11	0.30	8.96	8.31	6.39	1.00	0.96	1.00	0.14	0.20	0.33
C2	-0.01	0.05	-0.88	19.04	16.14	2.66	1.00	1.00	1.00	0.19	0.49	0.00
C3	0.20	0.26	0.17	13.65	21.18	11.30	1.00	0.94	1.00	0.10	0.07	0.11
C4	0.29	0.38	0.36	48.25	18.88	14.76	0.91	1.00	0.93	0.05	0.05	0.07
C5	-0.25	-0.01	-0.72	7.89	10.94	2.47	1.00	0.99	1.00	0.16	0.33	0.00
C12	0.38	0.40	0.40	100.54	28.18	18.26	0.99	0.98	1.00	0.01	0.02	0.07
C13	0.33	0.38	0.38	45.21	23.85	15.60	0.99	1.00	1.00	0.01	0.03	0.07
C14	0.35	0.37	0.38	51.90	24.70	15.61	0.99	1.00	1.00	0.01	0.02	0.07
C15	0.35	0.36	0.35	38.20	23.11	15.07	0.99	0.98	1.00	0.01	0.01	0.08
C16	0.26	0.26	0.21	37.76	13.38	9.68	0.99	1.00	1.00	0.02	0.02	0.05
C17	0.27	0.32	0.24	24.58	16.64	10.25	1.00	1.00	1.00	0.00	0.03	0.05
C26	0.30	0.33	0.31	31.45	25.12	16.40	0.99	1.00	1.00	0.06	0.12	0.14
C27	0.20	0.24	0.09	21.74	18.59	11.68	1.00	1.00	1.00	0.23	0.27	0.35
C28	0.24	0.21	0.07	33.26	19.67	9.72	1.00	1.00	1.00	0.06	0.12	0.17
C29	0.16	0.03	-0.09	35.36	8.88	5.81	0.99	1.00	1.00	0.25	0.22	0.38
C30	0.07	0.17	-0.02	14.81	17.47	8.09	1.00	1.00	1.00	0.02	0.15	0.14
C31	0.33	0.32	0.35	35.86	25.61	24.53	0.99	1.00	1.00	0.05	0.07	0.15

Finally, two bulk measures of circuit performance were calculated directly for each circuit configuration: the mass yield and recovered charge. These values were calculated directly from the experimental data and are completely independent from the partition analysis. These values correlate to traditional particulate processing performance indicators and collectively describe the separator's efficiency and selectivity. Tabular data for the yield and recovered charge are presented for each experimental run in Table 8.3.

8.3.2 Circuit Analysis

In addition to the Working Model Simulations, the CART^{TM}(see Chapter 6) program was used to conduct circuit analyses on each of the 17 circuit configurations at various levels of bypass ranging from 0 to 35%. Figure 8.11 shows the circuit partition functions for each of the multi-unit circuits. These graphs present the simplified analytical circuit solution, assuming the recovery in each unit cell is equal and no unit bypass is present. The addition of individual unit bypass changes the circuit analytical function, typically increasing the complexity. The graphs show the final circuit recovery as a function of the individual unit cell recoveries. These partition functions are used to determine the circuit SE and circuit MOI values. Once again, these graphs are only valid in the 0% bypass case.

Tabular data for the circuit analysis parameters are shown in Tables 8.4 and 8.5 for the circuit SE and circuit MOI parameters, respectively. This data is presented as a function of unit bypass, which is identical for all units throughout the circuit. These data indicate that as unit bypass increases, the quality of the separation deteriorates; however, the specific circuit configuration defines the degree of deterioration. Simply, the performance of some circuits is less susceptible to large bypass in individual units. Graphical presentations of this data for the 16 multi-unit circuits is presented in Figures 8.12 and 8.13.

8.4 Discussion

8.4.1 Justification for Experimental Methodology

In this work, the Working Model 2D software package was used to create a virtual separation device based on dynamic discreet element physics-based modeling. While the model does not correspond to or represent any "real" physical process, the virtual device still performs a "real" particulate separation, which is inherently inefficient and probabilistic.

Table 8.3: Bulk Results for Electrostatic Virtual Experiments

	Recovered Charge ($\times 10^{-7}$C)			**Mass Yield (%)**		
Circuit ID	**No Bypass**	**Medium Bypass**	**High Bypass**	**No Bypass**	**Medium Bypass**	**High Bypass**
C1	11.52	9.36	7.20	54.18	54.18	58.55
C2	12.04	7.24	6.16	59.64	73.45	81.45
C3	12.64	11.96	11.84	47.27	40.36	49.09
C4	12.56	12.28	10.76	36.73	36.00	36.00
C5	10.76	9.20	7.12	68.00	66.18	74.55
C12	13.24	12.48	11.76	33.45	32.36	36.36
C13	13.56	12.72	11.76	35.27	34.91	38.18
C14	13.44	12.80	11.76	34.55	34.55	38.18
C15	13.28	12.72	11.84	34.55	33.82	39.64
C16	13.96	13.08	12.04	38.91	39.64	44.00
C17	13.76	13.00	12.12	37.82	37.82	42.91
C26	13.08	12.16	11.68	40.00	42.91	45.45
C27	11.44	10.28	9.40	54.91	56.36	65.09
C28	13.36	12.88	11.56	42.91	48.36	57.09
C29	11.64	10.60	7.64	57.09	61.09	72.36
C30	14.04	12.40	11.48	48.36	51.27	58.55
C31	12.96	12.68	11.64	37.82	40.00	44.00

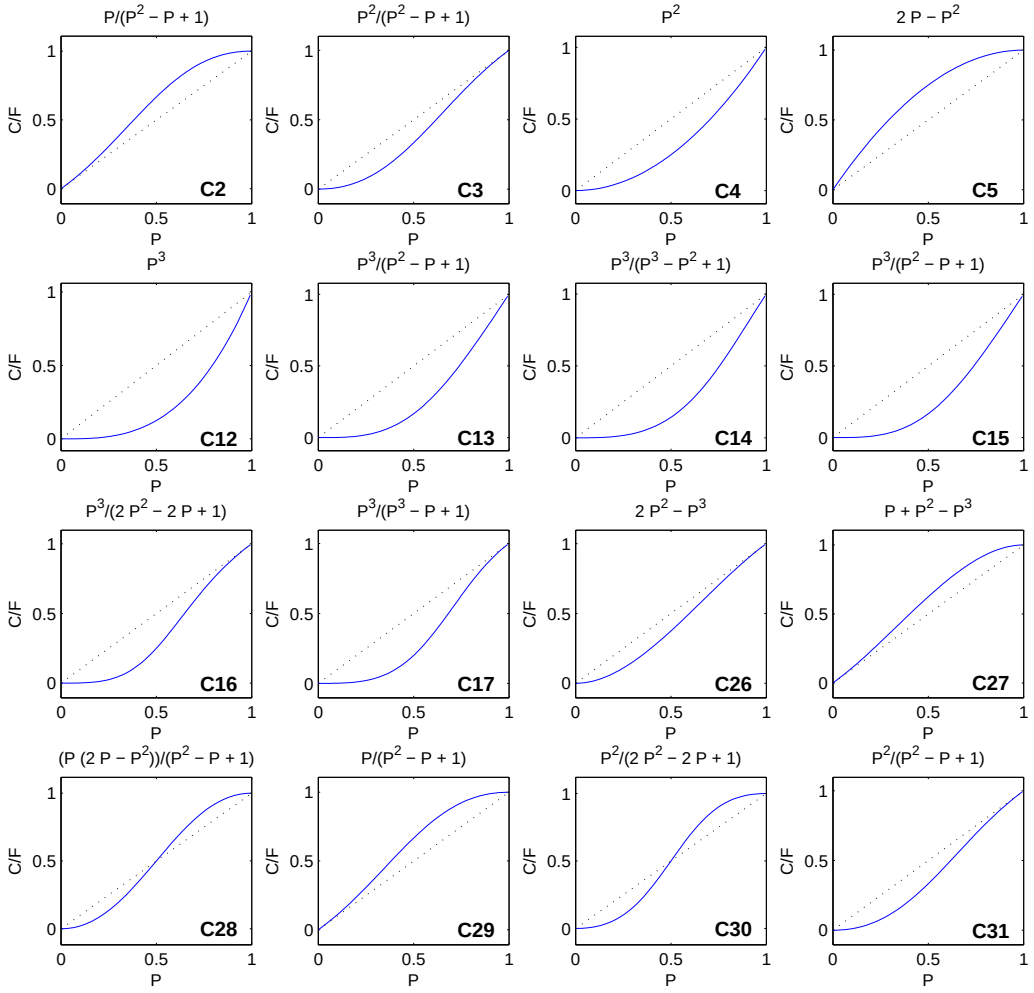

Figure 8.11: Circuit partition curves for circuits included in Working Model experiments.

Table 8.4: Separation Sharpness Values for Simulated Circuit Configurations

Circuit ID	**Relative Separation Sharpness (SE)**							
	% Bypass							
	0%	5%	10%	15%	20%	25%	30%	35%
C1	1.000	0.950	0.900	0.850	0.800	0.750	0.700	0.650
C2	1.333	1.221	1.109	0.997	0.886	0.780	0.677	0.581
C3	1.333	1.306	1.268	1.220	1.163	1.100	1.029	0.954
C4	1.000	0.998	0.990	0.978	0.960	0.938	0.910	0.878
C5	1.000	0.903	0.810	0.723	0.640	0.563	0.490	0.423
C12	0.750	0.786	0.817	0.843	0.864	0.879	0.887	0.889
C13	1.000	1.034	1.059	1.073	1.077	1.070	1.052	1.023
C14	0.898	0.945	0.984	1.016	1.038	1.049	1.050	1.038
C15	1.000	1.034	1.059	1.073	1.077	1.070	1.052	1.023
C16	1.500	1.512	1.500	1.464	1.406	1.330	1.240	1.139
C17	1.280	1.330	1.362	1.374	1.366	1.338	1.289	1.221
C26	1.250	1.210	1.163	1.112	1.056	0.996	0.933	0.867
C27	1.250	1.162	1.073	0.984	0.896	0.809	0.723	0.639
C28	1.667	1.577	1.476	1.366	1.250	1.129	1.007	0.885
C29	1.333	1.221	1.109	0.997	0.886	0.780	0.677	0.581
C30	2.000	1.886	1.747	1.589	1.420	1.246	1.072	0.905
C31	1.333	1.306	1.268	1.220	1.163	1.100	1.029	0.954

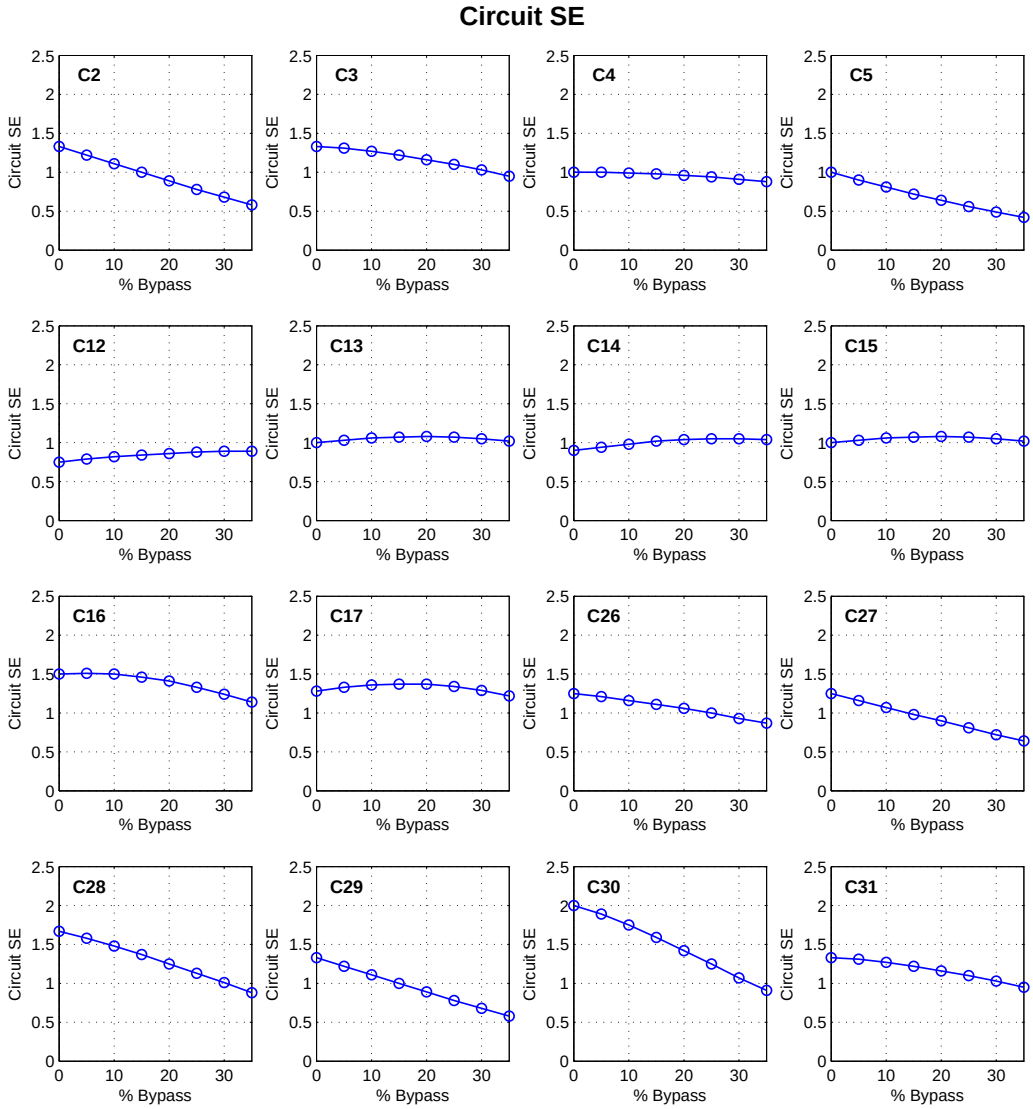

Figure 8.12: Circuit SE as a function of unit bypass for 16 multi-unit circuit configurations included in Working Model experiments.

Table 8.5: Moment of Inertia Values for Simulated Circuit Configurations

Circuit ID	**Partition Moment of Inertia (MOI)**							
	% Bypass							
	0%	5%	10%	15%	20%	25%	30%	35%
C1	100.0	115.0	130.0	145.0	160.0	175.0	190.0	205.0
C2	71.3	91.7	113.4	136.2	159.8	183.9	208.3	232.5
C3	71.3	74.0	78.8	85.8	95.2	106.8	120.8	136.9
C4	100.0	100.8	103.0	106.8	112.0	118.8	127.0	136.8
C5	100.0	129.3	157.0	183.3	208.0	231.3	253.0	273.3
C12	125.0	121.5	118.5	116.4	115.2	115.2	116.7	119.7
C13	100.0	97.2	95.4	94.6	95.4	97.9	102.5	109.4
C14	104.2	101.0	98.4	96.8	96.4	97.5	100.5	105.5
C15	100.0	97.2	95.4	94.6	95.4	97.9	102.5	109.4
C16	65.9	64.7	64.9	66.9	71.4	78.7	89.5	104.1
C17	72.3	70.2	69.1	69.5	71.7	76.3	83.7	94.3
C26	75.0	80.0	87.5	97.1	108.8	122.3	137.3	153.8
C27	75.0	94.3	114.5	135.4	156.8	178.5	200.3	222.0
C28	42.6	50.7	62.2	77.0	95.0	115.8	139.1	164.4
C29	71.3	91.7	113.4	136.2	159.8	183.9	208.3	232.5
C30	31.8	38.0	47.5	60.7	77.9	99.3	124.7	153.6
C31	71.3	74.0	78.8	85.8	95.2	106.8	120.8	136.9

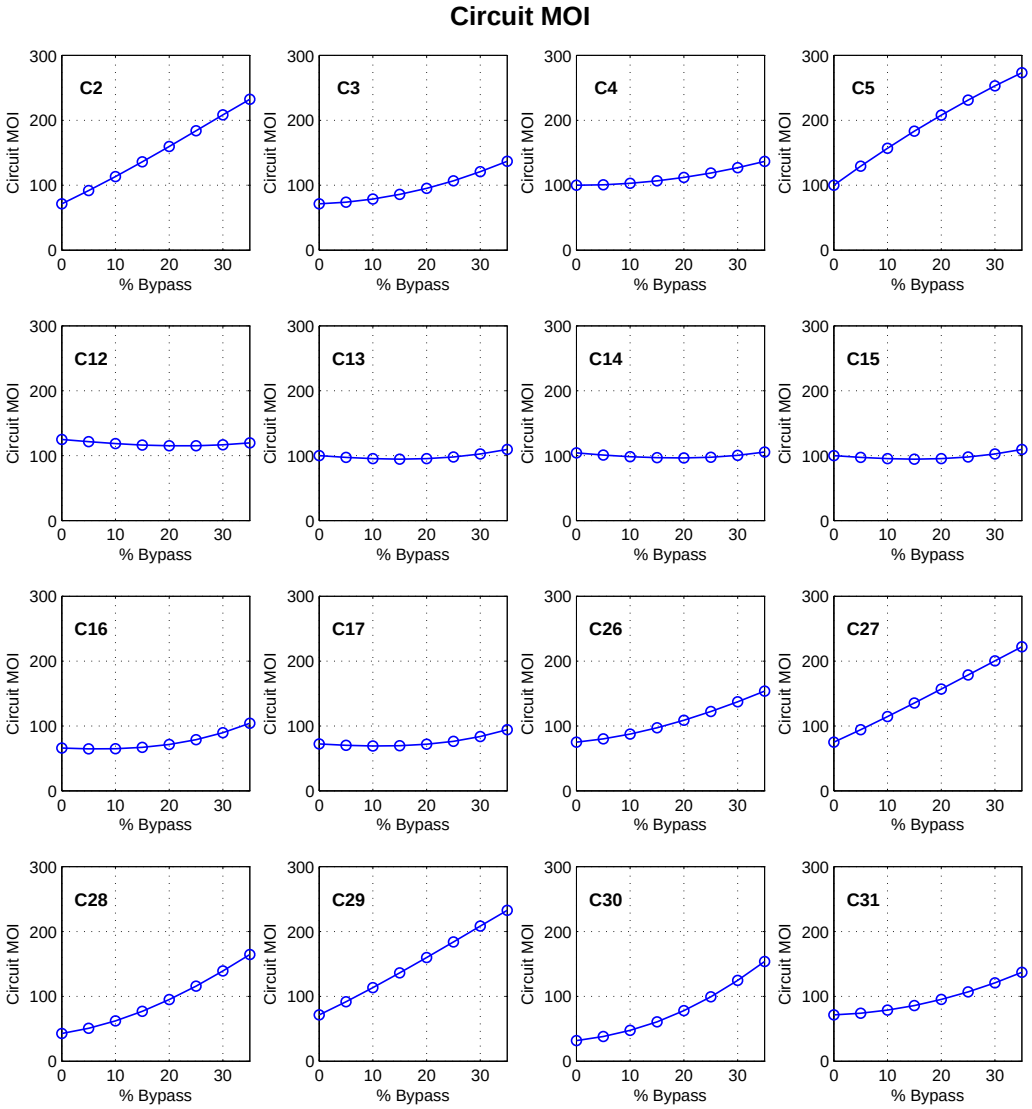

Figure 8.13: Circuit MOI as a function of unit bypass for 16 multi-unit circuit configurations included in Working Model experiments.

Unlike a pure numeric model, the Working Model experiment provides a distribution of results. The separation is predominantly influenced by the intensive physical properties of the feed material; however, the specific loading of the particles into the separator creates natural particle-particle interactions which also ultimately influence the separation performance. Changes in the specific particle arrangement generate slightly different results; however, the bulk distributions show that the device produces a meaningful separation.

In principle, circuit analysis only describes the role of unit interconnection in manipulating separation behavior; the actual separation process is irrelevant. Since the circuit analysis principles are fundamentally derived for generic binary separations, the results are universally applicable to any inefficient particulate separation device, regardless of the process model or operation. From the mineral processing perspective, the principles and implications of circuit analysis are applicable to any unit operation which generates a naturally inefficient binary separation, including dense-media vessels, hydrocyclones, magnetic separators, screens, flotation cells, etc. As a result, the circuit analysis methodology can be validated by considering any separation device, even a virtual device, provided that the separation is probabilistic and that the unit can be arranged in a circuit.

The inclusion of the forced bypass element provides an additional non-selective recovery mechanism creating systemic bias. Many real separation devices undergo similar inefficiencies, often denoted entrainment or entrapment. While these non-selective recovery mechanisms are ever-present in real separation devices, the magnitude of the bypass is often proportional to some other operational parameter. For example, entrainment is a non-selective recovery mechanism inherent to flotation and hydrocyclones, whereby fine particles are carried into products by hydraulic flow rather than by the separation mechanism. In these cases, the amount of entrained material is often proportional to the amount of recovered water. The virtual separator mimics this phenomenon through the forced bypass element. The proportion of the bypass is independently controlled by the geometry of the device.

From a pragmatic perspective, practitioners understand that bypass inefficiencies can be mitigated by the circuit design. Circuit analysis provides a mechanism to incorporate non-selective recovery, provided that the magnitude of bypass is known *a priori*. Given the design of the virtual separator, the bypass parameter may be adjusted independently without influencing other process variables. This factor is hard to predict and control in real processes since the factors controlling bypass often influence other selective recovery mechanisms as well. For example, water recovery in flotation may be increase or decreased by adjusting froth level, air flow rates, or frother dosages; however, all three of these parameters are also

known to influence true flotation rates as well.

Finally, the Working Model platform enabled the efficient analysis of numerous experimental runs, including repeat trials to gauge experimental consistency. In this study, 255 independent trials were conducted. The resource required to pursue this degree of experimental work exorbitant in the laboratory scale and absolutely prohibitive in the industrial scale, especially when one considers the analytical costs, including sample preparation and assays. Furthermore, the lack of feed consistency in any real experiment would likely invalidate the work since this variability could likely exceed the measured performance difference between some circuits.

8.4.2 Circuit Yield Rankings

The ultimate goal of circuit analysis is to provide holistic, semi-quantitative rankings of circuit configurations in order to distinguish more efficient from less efficient designs. While direct correlation is beneficial, a direct mathematical relationship between the circuit analysis parameters and the true separation performance is not necessary to form general rankings. Ultimately, these rankings may be used to select a limited number of top circuit candidates which may then be subject to downstream experimental analysis, modeling, and circuit simulation.

Applying this principle, the results from the Working model experimental study must be interpreted holistically. Rather than forming a direct correlation between the various parameters and scrutinizing every point, a better aggregate analytical method looks at all the rankings simultaneously. While ignoring the respective values, this type of analysis questions whether circuit analysis produces the same conclusions as the experimental data in terms of identifying good, moderate, and bad configurations.

In this section, polar plots are used side-by-side to compare the experimental results and the circuit analysis parameters. A generic, instructional polar plot is shown in Figure 8.14 which explains how to interpret the remaining polar plots in this section. By analogy, the polar plot is a bar graph that has been rolled around a single point. Angular positions on the polar graph indicate different circuit configurations, while the radial distance from the central point indicates the magnitude of the given value. The three circular segments of the graph distinguish the three general types of circuits considered in this study. Finally a concentric red circuit indicates the average parameter value for all 17 configurations. Figure 8.14 includes angular labels which identifying circuit position. All other polar plots follow this same angular convention.

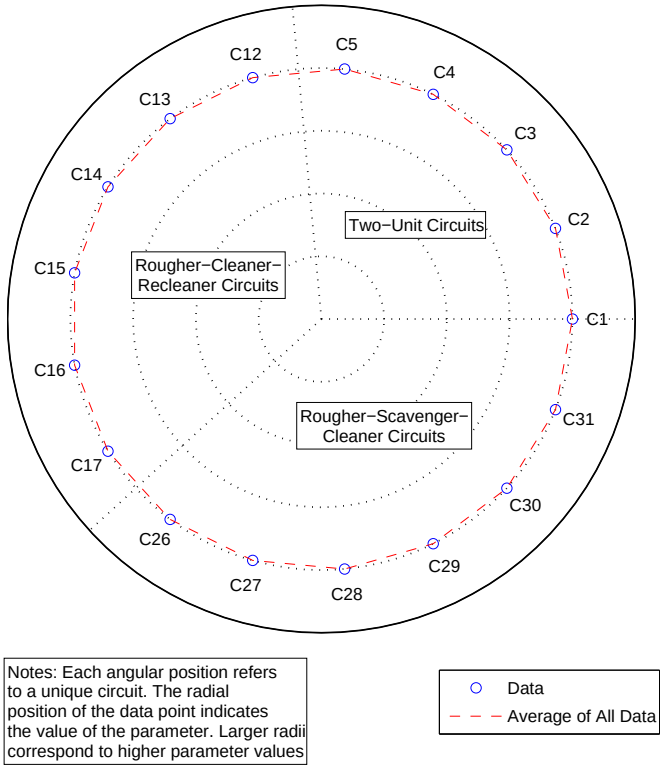

Figure 8.14: Generic polar plot.

The polar plot is used to provide quick side-by-side comparisons between the experimental parameter and the corresponding circuit analysis parameter(s). Since qualitative conclusions are desired, the magnitude difference between the individual polar plots is irrelevant. Instead, a "good" comparison produces a similar shape with similar circuit configurations exceeding the average. This condition indicates that the circuit analysis parameter produces results which agree with the experimental data. Given the number of circuit configurations in this study, the polar plot holds a visual advantage over side-by-side or overlapping bar graphs. The angular positions and relative magnitude are easily identified and compared by examining the shape of the polar plot. Alternatively, the bar graph begins to loose convenience beyond the comparison of six to ten elements.

The circuit mass yield is analyzed first. Figures 8.15, 8.16, and 8.17 show the comparative polar plots for the no, medium, and high forced bypass conditions, respectively. In each of these plots, the experimental yield is shown in the left plot, while the circuit analysis yield score is shown in the right plot. The circuit analysis bypass values selected for the comparison were based off of the partition curve for the single unit circuit (C1). For the single unit, the natural unforced bypass was determined to be approximately 10%. As a result, this experimental data was compared to the circuit analysis parameters calculated with a unit bypass of 10%. Following the same logic, 25% and 35% were selected as the unit bypass levels for the medium and high bypass conditions, respectively.

In all three bypass cases, the experimental yield shows good correlation to the circuit analysis yield score. C2, C5, C27, and C29 consistently show the highest yield values, as well as elevated yield scores. All of these circuits represent a net scavenging condition which logically leads to increased yield values. All of the rougher-cleaner-recleaner circuits show reduced yield values which also correspond to expectation, since additional cleaning stages increase product quality at the expense of reduced yield. As anticipated, C12 (the rougher-cleaner-recleaner open circuit) shows the lowest yield value, which is additionally corroborated by the lowest yield score in all three bypass conditions.

Figure 8.18 summarizes the yield-yield score comparison for all the available data. Each data point indicates a unique circuit conditions with the bypass level noted in the legend. This plot shows exceptional agreement between the yield and the yield score. The Pearson's correlation between the two data sets is 0.936, statistically confirming the strong positive correlation. While the trend is not purely linear, the relationship indicates that the yield score is a good indicator of circuit yield for the purpose of comparison.

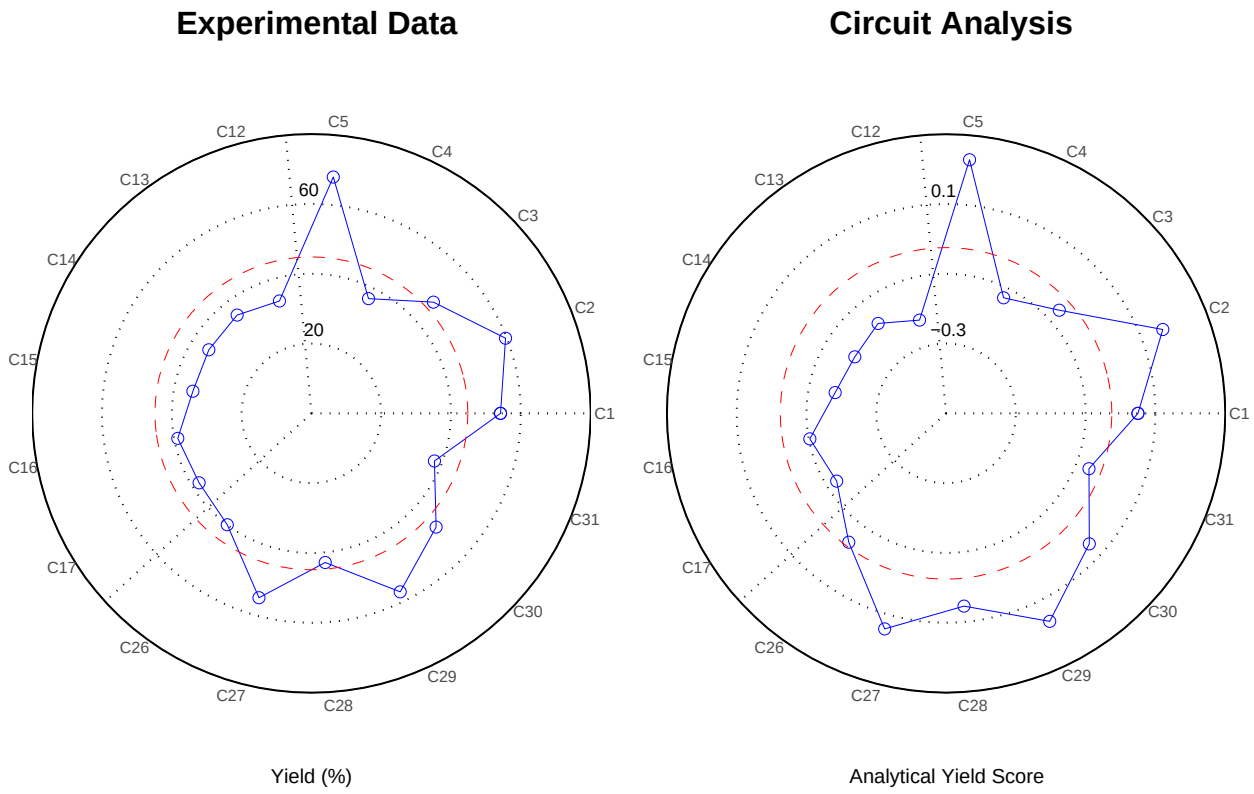

Figure 8.15: Polar yield plot for no forced bypass condition. Actual bypass value used for the circuit analysis calculation is 10%.

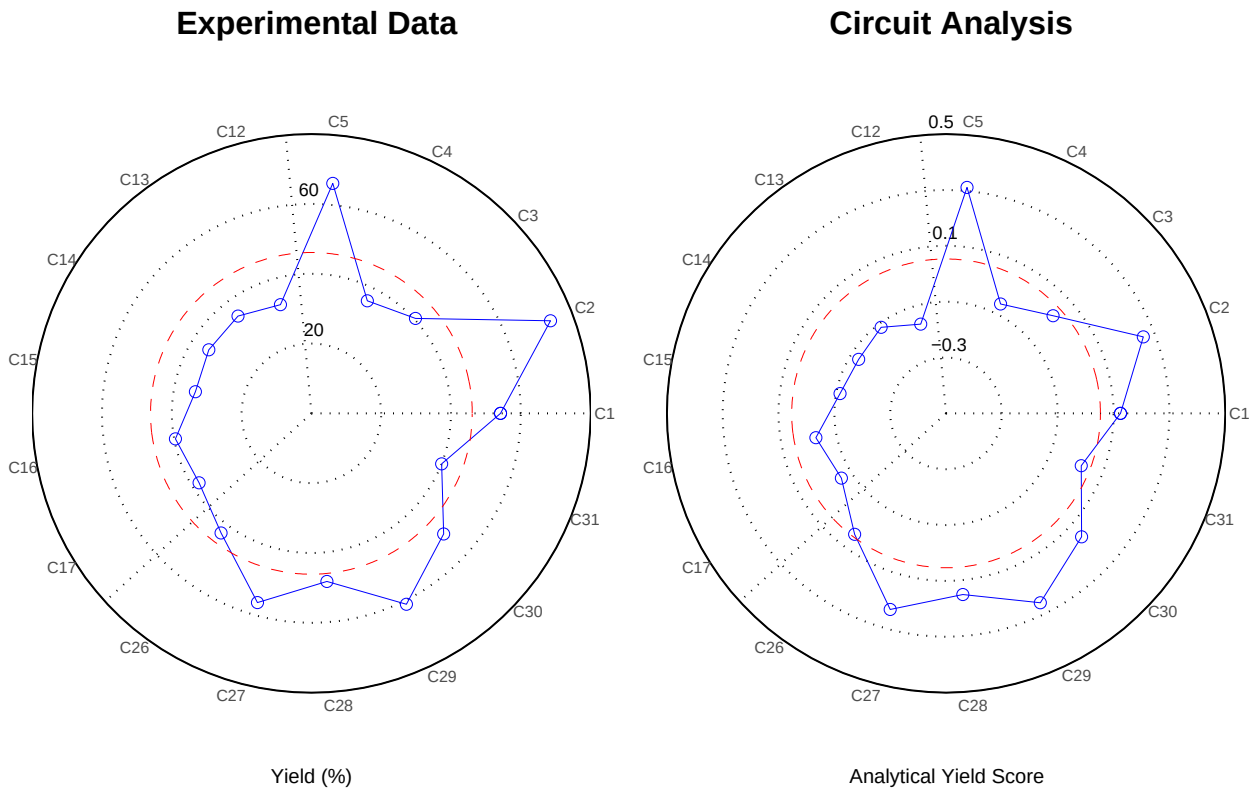

Figure 8.16: Polar yield plot for medium forced bypass condition. Actual bypass value used for the circuit analysis calculation is 25%.

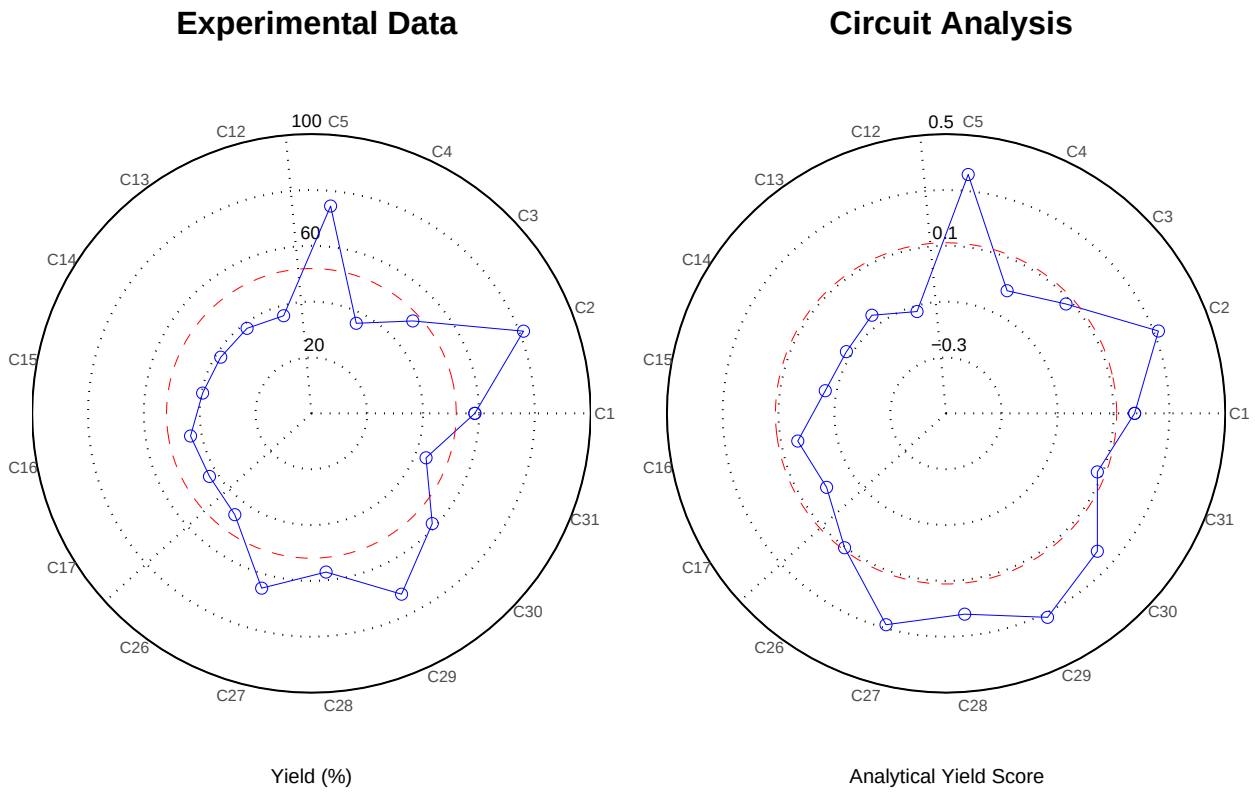

Figure 8.17: Polar yield plot for high bypass condition. Actual bypass value used for the circuit analysis calculation is 35%.

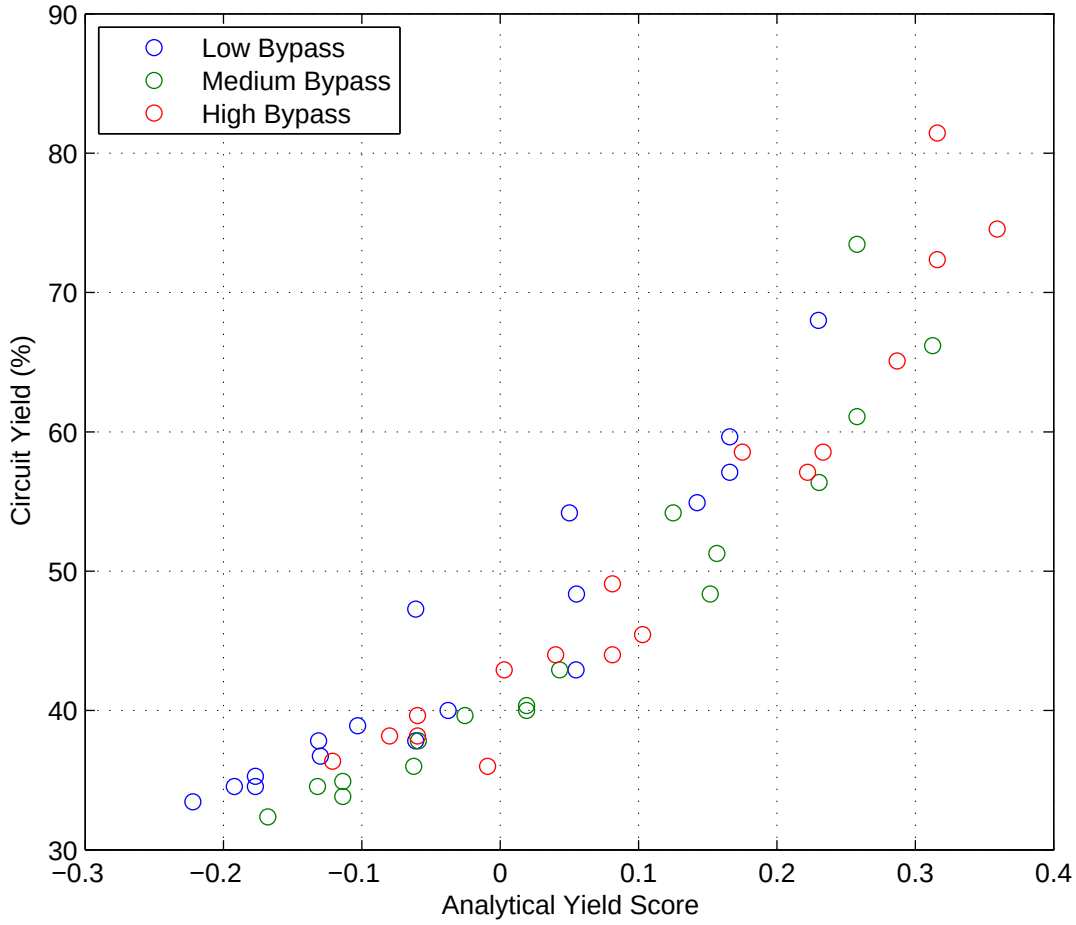

Figure 8.18: Aggregate experimental results: circuit yield plotted against yield score.

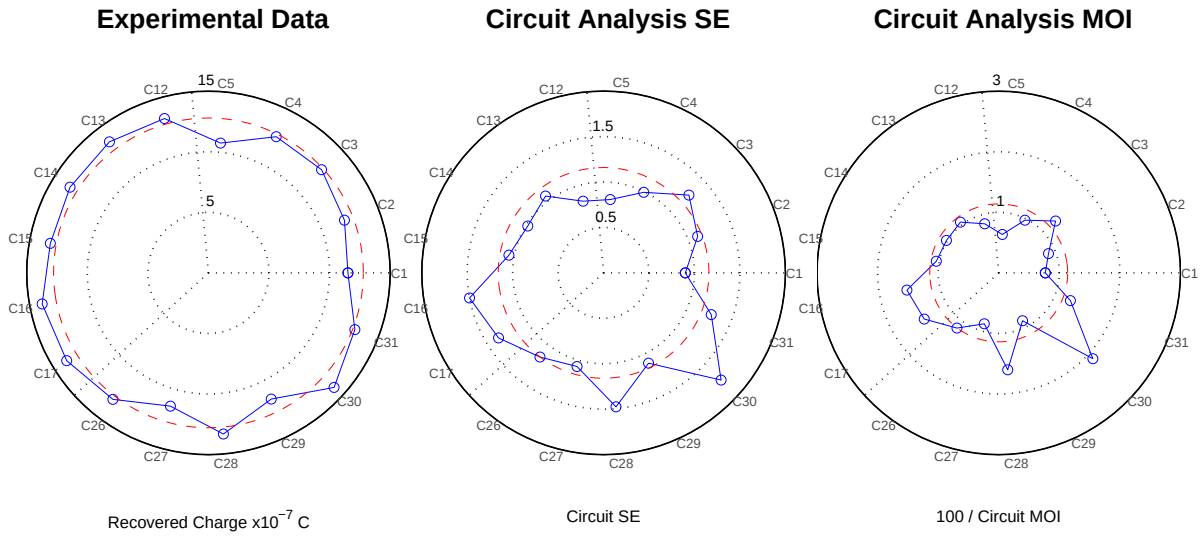

Figure 8.19: Polar selectivity plot for no forced bypass condition. Actual bypass value used for the circuit analysis calculation is 10%.

8.4.3 Circuit Selectivity Rankings

In addition to circuit mass yield, the circuit selectivity can be analyzed via circuit analysis and the experimental data. In this case, two circuit analysis parameters were used as indicators of circuit selectivity: the separation sharpness (SE) and the circuit moment of inertia (MOI). Once again, the side-by-side polar plots are used to compare the data sets. Figures 8.19, 8.20, and 8.21 show the comparisons for the no, medium, and high bypass data. As in the yield score calculation, the circuit MOI and circuit SE values were calculated at unit bypass levels of 10%, 25% and 35% for the no, medium, and high bypass levels, respectively. These values were determined from the partition curve analysis of the single unit circuit (C1).

In the MOI polar plot, the radial axis is plotted as 100/circuit MOI. This manipulation was implemented to ease the visual comparison between the plots. In the calculation of circuit MOI, smaller values correspond to more selective circuits. In this data set, the other two parameters (recovered charge and circuit SE) reflect inverse behavior: larger values correspond to more selective circuits. To ensure consistent comparisons, the inverse of the circuit MOI is used so that larger values correspond to more selective circuits.

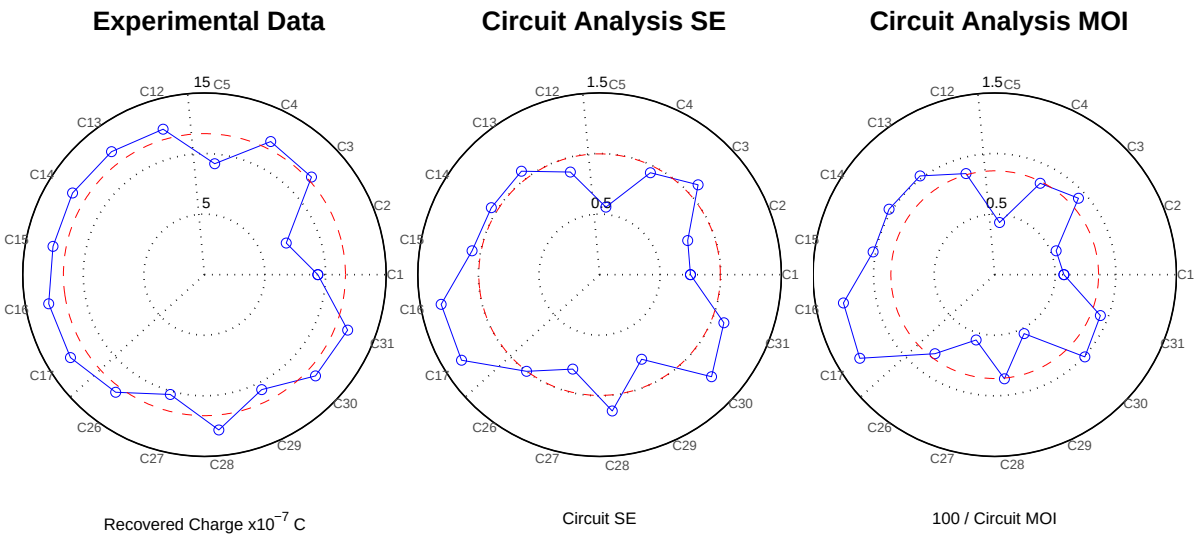

Figure 8.20: Polar selectivity plot for medium bypass condition. Actual bypass value used for the circuit analysis calculation is 25%.

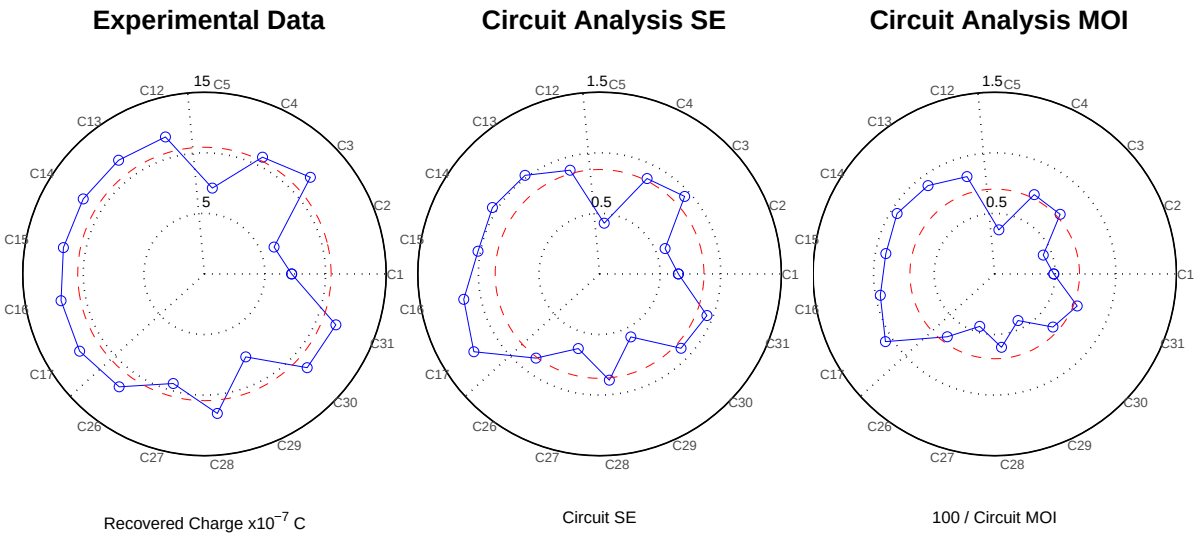

Figure 8.21: Polar selectivity plot for high bypass condition. Actual bypass value used for the circuit analysis calculation is 35%.

In general, the experimental data compares well to both circuit analysis parameters. In the no bypass condition (Figure 8.19), both circuit analysis parameters show high preference to C16, C28, and C30, while largely dismissing C1 and C5. The experimental data agrees on both accounts. Under the no bypass condition, C16 and C30 show the best selectivity in terms of recovered charge, while C1 and C5 are the worst circuits, experimentally.

As the unit bypass was increased, the circuit analysis parameters (especially, the circuit MOI) show stronger preference to the rougher-cleaner-recleaner circuits. This result is confirmed experimentally, as many of these circuits show similar elevated performance at the medium and high bypass conditions (Figures 8.20 and 8.21).

Figure 8.22 summarizes the recovered charge-SE and recovered charge-MOI comparisons for all of the available data. Each data point indicates a unique circuit configuration at different bypass levels. In both cases, the overall trends strongly correlate, implying that both factors are applicable for circuit ranking. Quantitatively, the Pearson's correlation between the recovered charge and SE is 0.805, while the correlation between the recovered charge and MOI is -0.916.

Further analysis of Figure 8.22 shows regions where the circuit analysis parameters are better predictors of actual performance. In both case, intermediate selectivity values (recovered charge between 8 and 13 $\times 10^{-7} C$) are predicted well by both parameters, as indicated by the consistent linearity in this region. Alternatively, neither parameter predicts performance of poor circuits well, as the points strongly deviate from the otherwise overwhelming trend. Finally, highly selective circuits are better predicted by the MOI parameters. This graph retains linearity through this region, while the SE parameter shows substantial deviation. This result indicates that the MOI parameter values are scalable and comparable along most levels of meaningful selectivity. Since few instances will require selection between two poor circuits, the deviation in this region is unsubstantial.

8.4.4 Three-Unit Utilization

One criticism of traditional circuit analysis is evident in a common three-unit utilization problem. Without consideration of unit bypass, the circuit analysis SE parameter dictates that the rougher-scavenger-cleaner, closed circuit is the best utilization of three units. This configuration (C30) produces an SE value of 2.0, with the next best option being the rougher-scavenger-cleaner double cross (C28, $SE = 1.667$). However, many industrial flotation applications often utilize rougher-cleaner-recleaner circuits to pursue various process objectives and meet quality specifications. Thus a discrepancy is produced between

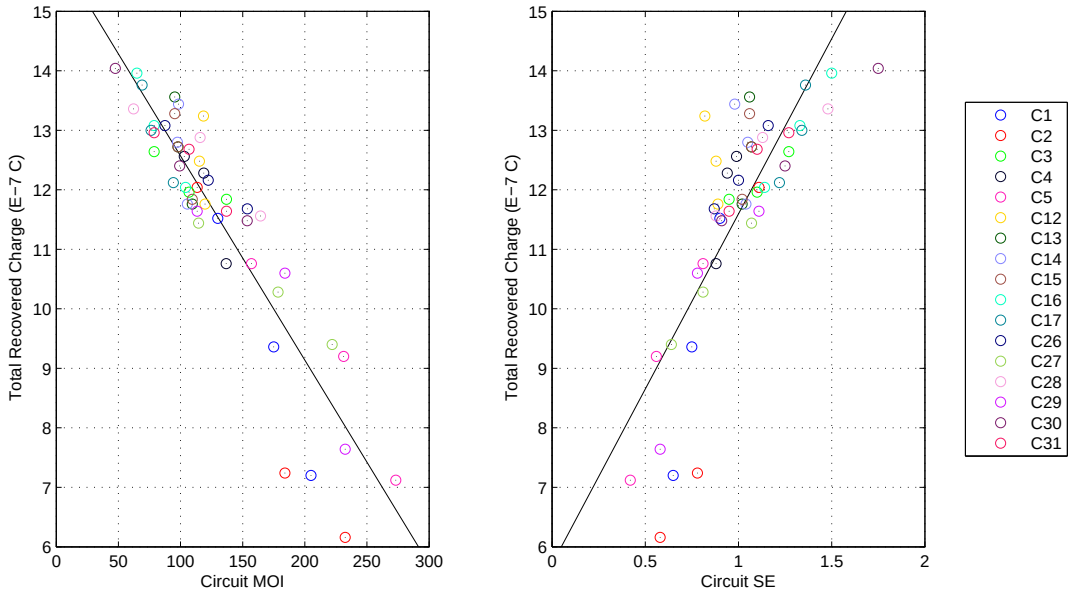

Figure 8.22: Aggregate experimental results: total recovered charge plotted against MOI and SE.

the suggestion of circuit analysis and the industrial trend.

One method that overcomes this disagreement is the inclusion of unit bypass in the circuit analysis SE calculation. As unit bypass is increased, the selection of a recleaning unit over a scavenging unit becomes intuitively more favorable, and this intuition is matched by the circuit analysis projection. While the SE parameter is slightly influenced by unit bypass, the overall parameter only inherently reflects the separation of middling particles. As a result, the SE parameter will tend to undervalue the bypass misplacement, thus retaining a scavenging unit at elevated bypass values that are not justified economically.

To overcome this limitation of the SE parameter, the circuit MOI value was derived (see Chapter 7). This parameter placed additional weight on pure material that has bypassed the separation stage. Consequently, the MOI parameter should be a better indicator of real separation performance as unit bypass becomes more significant.

The experimental Working Model data verifies this hypothesis. As an isolated comparison, the performance of C1 (single unit), C17 (rougher-cleaner-recleaner), and C30 (rougher-scavenger-cleaner) is compared. Figure 8.23 shows the partition curves for these three circuits at the three levels of forced bypass. In all three instances, C17 shows the most substantial bypass reduction, while C30 shows the greatest separation sharpness increase. Finally, C17

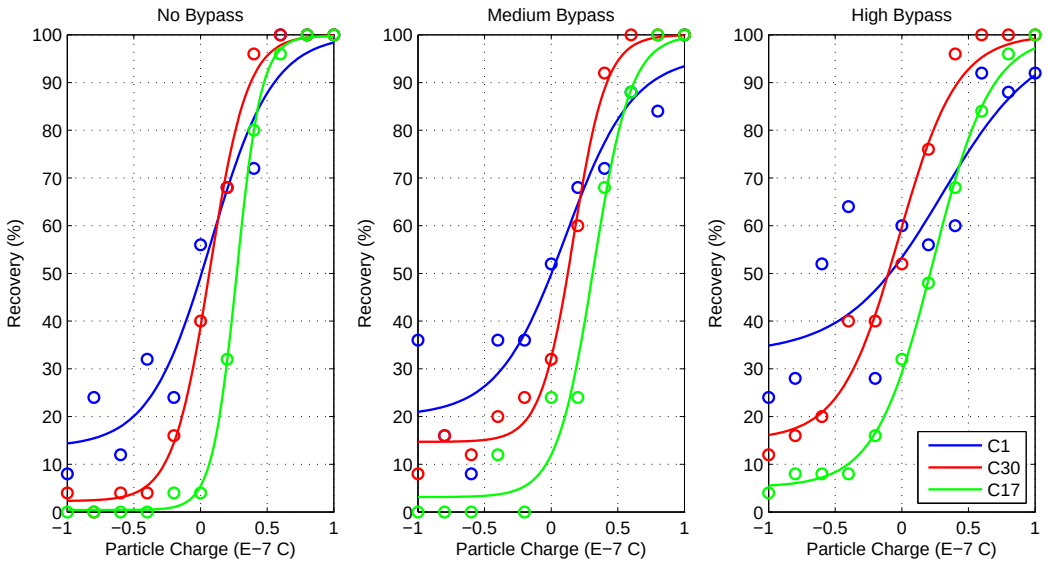

Figure 8.23: Experimental data and fitted partition curves for C1, C17, and C30. C1 = single unit; C17 = rougher-cleaner-recleaner, all recycles to feed; C30 = rougher-scavenger-cleaner, all recycles to feed;.

shows the greatest cut-point shift, while C30 tends to retain the cut-point of a single unit.

The overall performance of these three circuits is compared as a function of unit bypass (Figure 8.24). The top plot shows the experimental selectivity expressed as total recovered charge. Obviously, as the bypass increases, the total recovered charge diminishes due to additional recovery of negatively charged material. The lower two plots show the circuit SE parameter and the circuit MOI parameter calculated as a function of unit bypass. In all three cases, the single unit circuit is not a valid alternative for selection, but is shown as a baseline for other two data sets. The experimental data indicates that the rougher-scavenger-cleaner circuit is preferred for unit bypass values less than 15%. At higher bypass values, the scavenger should be alternatively utilized as a recleaner. The SE parameter predicts this crossover occurring at 22%, while the MOI predicts it at 18%. While neither parameter strictly corresponds to the experimental data, this example does confirm the circuit SE's tendency to undervalue unit bypass. Instead, the moment of inertia parameter is better formulated to account for this phenomenon.

As an additional note, C17 and C30 were experimentally and analytically selected as the best circuits (out of the original 17) over the given bypass range. The only distinction between the three data sets is the point of the crossover.

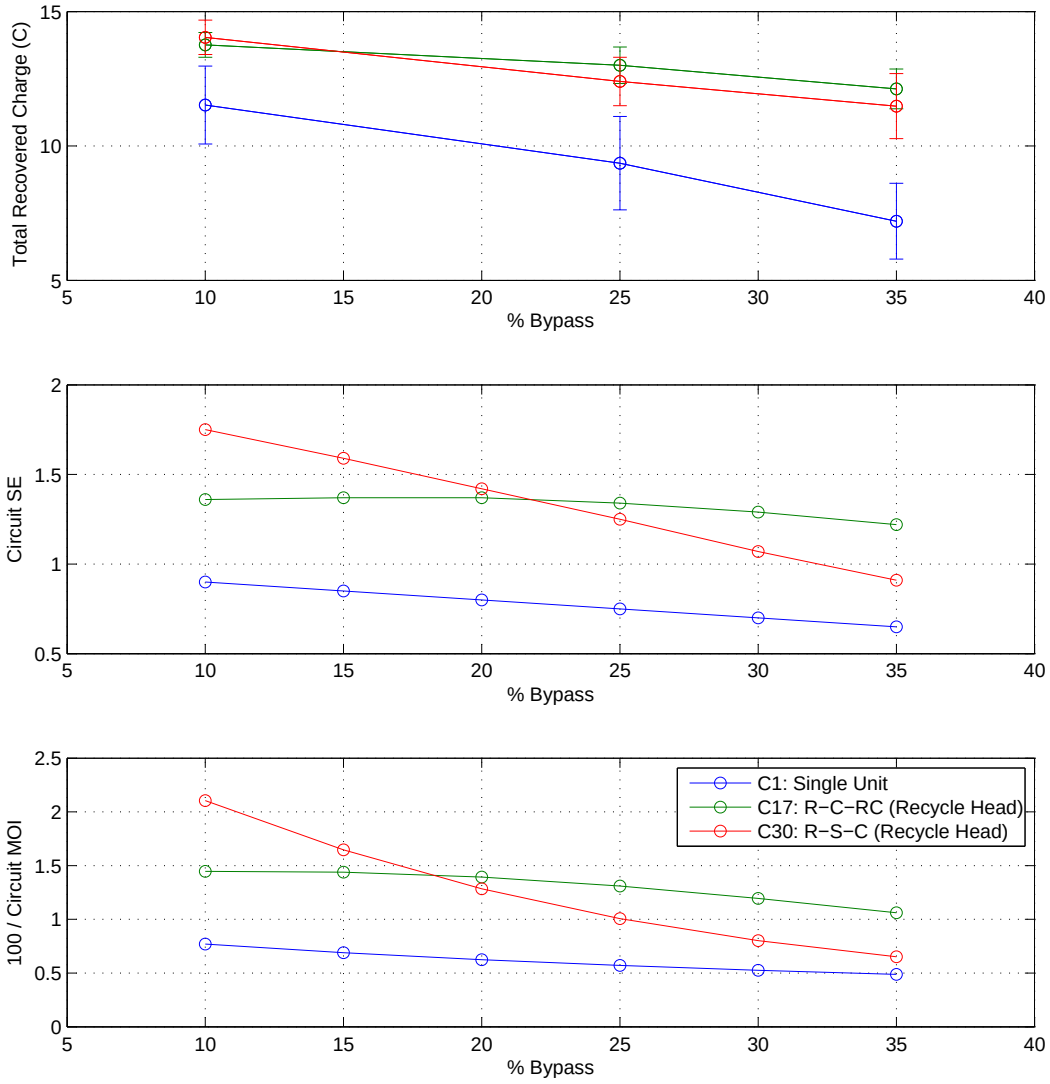

Figure 8.24: Experimental and analytical comparison for C1, C17, and C30. Plot shows three performance measures (experimentally recovered charge, Circuit SE, and 100/Circuit MOI as a function of unit bypass).

8.4.5 Comparison of Performance Measures

The aggregated circuit analysis data for all 17 circuit configurations is summarized in Figure 8.25. In this plot, circuit MOI is plotted against circuit SE for each unique circuit configuration and unit bypass level. The circuit configurations are grouped explicitly by the series color and marker style, while the unit bypass levels are implied by the point position. For each data series, the general rightmost point (the highest SE value or the lowest MOI value) corresponds to the 0% bypass condition. Each successive data point (moving left and up) corresponds to increasing increments of unit bypass.

The aggregated circuit $MOI - SE$ trend mirrors the theoretical behavior exemplified in the single-unit partition function analysis (see Chapter 7). At elevated SE values, incremental SE gains yield diminished reductions in MOI when compared to similar gains at reduced SE values. Furthermore, this general trend does not produce a one-to-one comparison for all data points, implying that the MOI performance measure will not always produce the same rankings as the SE parameter.

To further illustrate the discrepancies between the two circuit analysis measures, Figure 8.25 also includes quadrant designations centered around the single unit circuit (1,100). These four quadrants indicate differences in comparative behavior. Quadrants I and III indicate divergent conclusions, while Quadrants II and IV show similar conclusions; although, the magnitude of the improvement may not correlate with the magnitude of the value. For example, in Quadrant I, SE shows separation improvement while MOI shows separation deterioration. Alternatively, in Quadrant IV, both parameters show circuit improvement. In principle, these quadrant axes may be centered around any point on the plot to illustrate the differences in comparisons to that point.

Given these apparent discrepancies, both performance measures cannot simultaneous predict real circuit performance to the same precision. However, the working model experimental data has repeatedly shown superior correlation to the MOI parameter, especially when unit bypass is substantial. Both the consistent linear trend, even for highly selective circuits (Figure 8.22), and the improved ability to select the appropriate three-unit utilization (Figure 8.24) support utilization of the circuit MOI in addition to, or in favor of, the circuit SE.

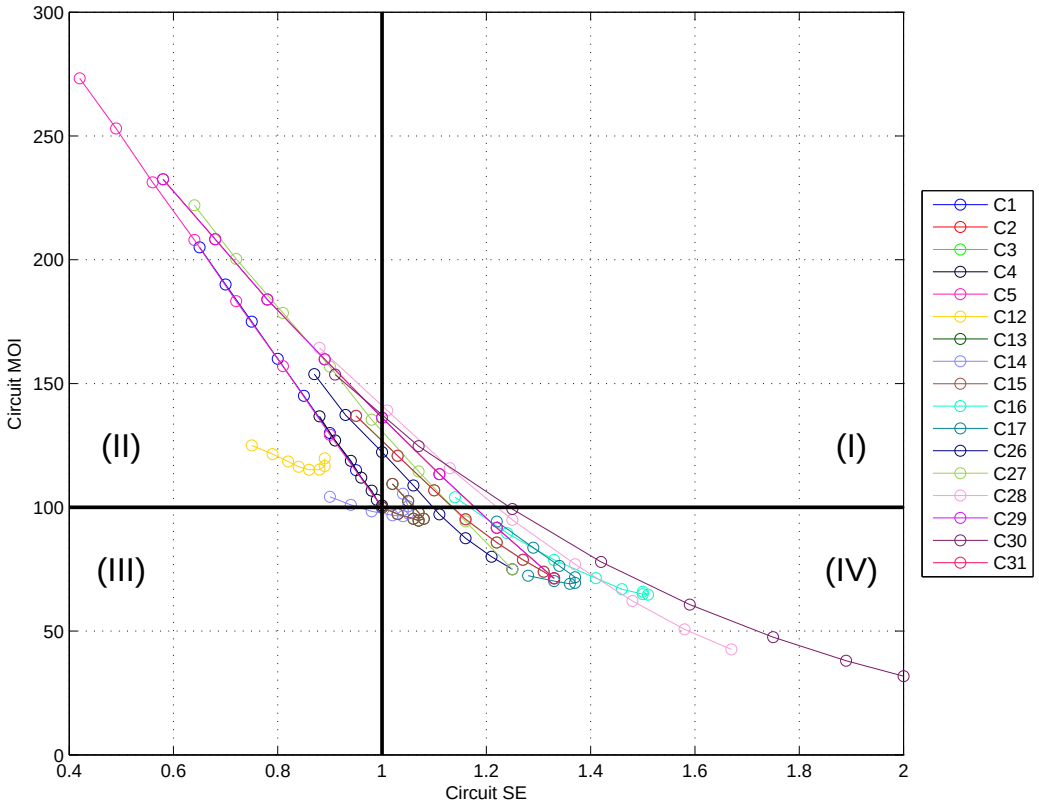

Figure 8.25: Circuit MOI plotted against circuit SE for all 17 circuits included in Working Model Simulations. Individual data points refer to different levels of unit bypass. Quadrants indicate different predictive behavior: (I) SE indicates improvement compared to single unit, MOI indicates degradation compared to single unit; (II) both indicate degradation; (III) MOI indicates improvement, SE indicates degradation; (IV) both indicate improvement.

8.5 Summary and Conclusions

This paper has described a virtual experimental analysis that was used to evaluate the separation efficiency of various circuit designs. The Working Model 2D dynamic discreet element modeling environment was used to construct and analyze a virtual electrostatic separation device. This device was incorporated into 17 distinct circuit configurations and tested at three levels of forced unit bypass. The results of the experimental analysis were compared to the circuit analysis projections, using the yield score (YS), relative separation sharpness (SE), and partition moment of inertia (MOI) as analytical performance indices.

The results of this study yield four conclusions:

1. The Working Model 2D program is suitable for circuit comparisons. Though the specific geometry of the device used in this study did not mimic any real separation process, the virtual separator showed generally stochastic behavior and mimicked real separation phenomenon. Particle interaction and feed loading influence the final separation performance; however, the general behavior fits standard partition curves very well.

2. The selection of an optimal separation circuit is often dependent upon the degree of unit bypass. For the two unit case, the circuit analysis and the experimental data show that C3 (rougher-cleaner with recycle) and C4 (rougher-cleaner open circuit) are the best configurations in this study. Had the direction of the forced bypass been reversed to the tailings streams, the rougher-scavenger circuits would likely have been selected instead.

3. For the three unit-case, the selection between C30 (rougher-scavenger-cleaner, all recycled to feed) and C17 (rougher-cleaner-recleaner, all recycle to the feed) is strongly governed by the unit bypass. The experimental data shows that for bypass levels lower than 14-16% the rougher-scavenger cleaner is the better option, while the decision is reversed for greater bypass values. The circuit SE shows this crossover occurring at 22%, while the circuit MOI shows the crossover at 18%.

4. The bulk results indicate that both circuit analysis methods correspond very well with real circuit performance. While the comparisons are not always direct correlations,the overall results show that the circuit analysis methodology is suitable for making gross comparisons which are needed in the preliminary circuit design stages. The yield score shows excellent capacity to predict and compare circuit yield, while the MOI value

provides greater implied realism and proves to be a better selectivity indicator than SE when substantial bypass is present.

Finally, an unanticipated result of this study shows that the circuit configuration design not only provides the capacity for better *separation*, but the circuit configuration also provides the capacity to reduce *uncertainty*. A simple comparison of size of the error bars in Figures 8.8, 8.9, and 8.10 shows that the two circuits reduce uncertainty when compared to the single unit. Furthermore, this single-point comparison shows that different circuits reduce the uncertainty to varying degrees. Further analysis on the current data set may reveal trends and heuristics which analytically define the uncertainty reduction potential of a given circuit design.

8.6 Bibliography

Abu-Ali, M., & Sabour, S. A. (2003). Optimizing the design of flotation circuits: an economic approach. *Minerals Engineering*, *16*(1), 55–58.

Dechev, N., Cleghorn, W., & Naumann, S. (2001). Multiple finger, passive adaptive grasp prosthetic hand. *Mechanism and machine theory*, *36*(10), 1157–1173.

Delattre, N., & Moretto, P. (2008). A new dimensionless number highlighted from mechanical energy exchange during running. *Journal of Biomechanics*, *41*(13), 2895–2898.

Lauder, D., & McKee, D. (1986). The impact of circulating loads on flotation circuit performance. In *l3th congress the council of mining and metallurgical institutions, singapore, 6 volumes* (p. 7).

Linnell, W., Wu, T., Baudin, P., & Gervais, P. (2007). Analysis of the volleyball spike using working model 2d. *Journal of Biomechanics*, *40*(2), S760.

Luttrell, G., Kohmuench, J., Stanley, F., & Trump, G. (1998). Improving spiral performance using circuit analysis. *Minerals & Metallurgical Processing*, *15*(4), 16–21.

McKeon, T., & Luttrell, G. (2005). Application of linear circuit analysis in gravity separator circuit design. In *Heavy minerals.*

McKeon, T., & Luttrell, G. (2012). Optimization of multistage circuits for gravity concentration of heavy mineral sands. *Minerals & Metallurgical Processing*, *29*(1), 1-5.

Meloy, T. (1983a). Analysis and optimization of mineral processing and coal-cleaning circuits circuit analysis. *International Journal of Mineral Processing*, *10*(1), 61–80.

Meloy, T. (1983b). Optimizing for grade or profit in mineral processing circuits circuit analysis. *International Journal of Mineral Processing*, *11*(2), 89–99.

Meloy, T., Clark, N., & Glista, J. J. (1986). Effect of density variations in heavy-media rougher-cleaner-scavenger cells circuit analysis. *International Journal of Mineral Processing*, *16*(34), 169–178.

Sutherland, D. (1981). A study on the optimization of the arrangement of flotation circuits. *International Journal of Mineral Processing*, *7*(4), 319–346.

Tao, D., Luttrell, G., & Yoon, R.-H. (2000). An experimental investigation on column flotation circuit configuration. *International Journal of Mineral Processing*, *60*(1), 37–56.

Thueer, T., & Siegwart, R. (2010). Mobility evaluation of wheeled all-terrain robots. *Robotics and Autonomous Systems*, *58*(5), 508–519.

Wang, Y.-J., Chen, C.-D., & Sung, C.-K. (2010). Design of a frequency-adjusting device for harvesting energy from a rotating wheel. *Sensors and Actuators A: Physical*, *159*(2), 196–203.

Williams, M. C., Fuerstenau, D., & Meloy, T. (1992). A graph-theoretic approach to process plant design. *International Journal of Mineral Processing*, *36*(12), 1–8.

Yingling. (1990). Circuit analysis: optimizing mineral processing flowsheet layouts and steady state control specifications. *International Journal of Mineral Processing*, *29*(34), 149–174.

Yingling. (1993). Parameter and configuration optimization of flotation circuits, part i. a review of prior work. *International Journal of Mineral Processing*, *38*(12), 21–40.

Chapter 9

Conclusions and Recommendations

Most generally, mineral processing is the art and science of particulate separation as applied to mining products. Run-of-mine material is typically not of sufficient quality to justify shipment to downstream users, including smelters, utilities, and other end-users. Mineral processing separation systems seek to upgrade this material such that the value of the final product justifies the cost of beneficiation. Often single unit operations are not capable of producing products which meet these specifications, both in terms of product quality and product loss. Consequently, operators utilize staged units in various circuit configurations to produce synergistic improvements which eventually produce a sufficient product.

This work has provided a treatise on circuit design. Despite the development of sophisticated process models, astute analytical methods, and robust numeric optimization strategies, the industrial design of process circuits is still largely based on empirical knowledge as well as trial-and-error approaches. As a result, many greenfield designs and circuit modifications pursue "better" designs often at the expense of man hours and design resources. In many cases, the optimal circuit design remains elusive. Given the plurality of modern engineering design tools, the circuit design process should be streamlined while producing optimal results.

Many circuit design tools have been refined, reanalyzed, and developed as a part of this work. First, a robust, graphically-based flotation modeling and simulation software package was developed as a means to quantitatively define circuit performance. This program provides the framework to use laboratory, pilot-plant, or full-scale data sets to predict performance in a user-defined circuit configuration.

Second, rate-compositing equations were derived to assist in flotation data inquiry and error analysis. Most contemporary flotation models are based on a distributed rate model. Traditional methods do not provide a means to composite multiple rate constants in order to form an average; however, these new compositing equations describe the mathematical approach necessary to determine weighted averages for rate values. These equations are useful in rate fitting and error prediction applications.

Third, a unique algorithm was developed to derive analytical circuit solutions when given the circuit configuration. The analytical solution may then be used for non-iterative circuit simulation as well as circuit analysis, via the separation sharpness parameter. This value can be used to rank various circuit configurations based on the circuits' inherent ability to distinguish middlings. The evaluation of this parameter only requires the circuit configuration; extensive feed and performance data is not necessary.

Fourth, an optimization algorithm was developed to define the ideal circuit location of an additional unit when given an existing configuration. This optimization is based on the aforementioned analytical circuit solution algorithm and the separation sharpness parameter.

Fifth, a new technical-economic separation performance measure, the partition moment of inertia, was developed to incorporate micro-pricing and incremental value concepts into traditional partition analysis. The resultant parameter inherently reflects the technical-economic capacity of the separation and is defined for both individual units as well as circuit analysis applications. This parameter becomes increasingly useful as unit bypass becomes more pronounced.

Both circuit analysis indicators were evaluated and compared in an extensive experimental investigation. A virtual electrostatic separator was generated in the Working Model 2D program and tested in 17 circuit configurations. The virtual experiments were used to determine the real separation capacity of the various circuits, and these results were compared to the general rankings derived from circuit analysis. In general, the moment of inertia parameter provided slightly better predictions; however, both methodologies showed excellent agreement with the experimental results.

Collectively, these tools may be utilized interdependently to streamline the circuit design process while pursuing optimal circuit designs for physical separation systems. During the preliminary greenfield design stages, when extensive data sets are costly and largely non-existent, the circuit analysis and incremental optimization tools may be used to define a small number of potential alternatives. Further experimental and simulation work may then be used to evaluate this constrained solution space, thus eliminating trial-and-error

while ensuring only near-optimal solutions are considered. Since circuit analysis can only be used for relative comparisons, the final simulation is necessary to quantitatively define the anticipated circuit performance. Finally, error analysis and rate-constant compositing may be used to determine the inherent degree of uncertainty in the simulation.

For circuit redesign and modification problems, the incremental optimization tool as well as the analytical circuit solution may be used to evaluate circuit sensitivity and define the units in the circuit that provide the best opportunity for growth at the lowest cost. Further experimental work can then be focused in these areas, and eventually incorporated into detailed circuit simulations. Once again, the final simulation is necessarily to provide quantitative justification for the circuit modification.

To the author's knowledge, seven original contributions have been presented in this work:

1. A four-reactor flotation model and resulting simulation package. This model uniquely considers process kinetics as well as carrying capacity, thus placing a large significance on the machine parameters and characteristics.

2. Generic rate compositing equations. While distributed rate models are common for flotation modeling, no simple formula has previously been presented which predicts apparent rate values from a truncated distribution. Such formulas have been derived analytically for the plug-flow and perfectly-mixed reactor models. A numeric methodology has been proposed for the axially-dispersed reactor model.

3. The matrix reduction algorithm to determine analytical circuit solutions. Though many researchers utilize analytical solutions in their theory and analysis, no streamlined methodology exists which simultaneously provides undoubted accuracy and time efficiency. The author's algorithm meets both specifications, while incorporating a graphical interface for convenient circuit input.

4. The optimization algorithm for circuit modification based on the separation sharpness parameter. Several circuit superstructure optimization algorithms have been reported; however, this is the only one which uses the analytical solution and the separation sharpness parameter as the objective function. Furthermore, the search algorithm easily accommodates other performance measures derived from the analytical solution (i.e. MOI, YS).

5. The partition moment of inertia as a technical-economic separation performance indicator. No other derived partition curve parameter inherently accounts for process

economics and the biased influence pure particles have on final revenue. The moment of inertia value provides mechanisms for this type of analysis with or without detailed contract data.

6. The yield score as a derived circuit analysis indicator. While circuit analysis has been used in the past to asses circuit selectivity, no current methodology accurately accounts for yield variations between circuit configurations. The yield score has been proven as an exceptional indicator and ranking parameter by both fundamental derivation and empirical evidence.

7. The large-scale empirical evaluation of separation circuits using virtual experiments. Most literature studies of circuit performance are restricted to small sample sizes (usually two or three configurations) or purely mathematical treatment. Both of these types of investigations fail to account for the natural and probabilistic inefficiency of real separators as well as the multitude of available configurations. This research has included a virtual experiments which analyzed a significant breadth of configuration types, while validating much of the proposed methodology.

Finally, the author of this dissertation recommends the following items for continued study:

1. Refined data fitting and analysis modules for flotation model building. The current data fitting approach limits the data set to three floatability classes. While this routine performs adequately in most situations, not all flotation systems are optimally defined by three rigid floatability classes. Furthermore, the current fitting routine is not capable of analyzing data which has experienced a chemical or physical change during the experiment. Advanced fitting routines may also use an assumed or known floatability distribution to derive multiple rates from single-residence time data sets (i.e. pilot-plant data).

2. Evaluation of simulation confidence. All current commercial simulation packages as well as the simulation package described in this dissertation produce deterministic solutions, with no means to incorporate the uncertainty inherent to the experimental data. As a result, users cannot reasonably estimate the confidence and precision associated with a particular deterministic solution. The circuit analytical solution, Monte Carlo simulation, and sensitivity analysis may be used to provide better indications of simulation confidence.

3. Quantification of uncertainty reduction as a function of circuit configuration. As empirically observed in Chapter 8, changes in the circuit configuration produce changes in the experimental uncertainty related to individual class recovery. Intuitively, this circuit is a function of the circuit configuration, dictating that some circuits possess a natural ability to reduce uncertainty, just as some circuits have a natural ability to distinguish middlings or increase yield. Mathematical manipulation of the analytical solution will likely produce a function capable of predicting this reduction.

4. Further validation of the circuit analysis methodology in real mineral processing systems. While the virtual experiments provide numerous qualitative and quantitative benefits, the ultimate measure of the methodology must be proven in real systems. Such experiments require due consideration in order to isolate the circuit configuration as the single cause of performance changes. In the virtual experiment, extraneous influences are mitigated since the feed condition was fixed. However, in physical experiments, feed degradation, environmental factors, as well as unknown factors are all difficult to control but contribute to the final outcome.

5. Quantified correlation of circuit analysis parameters to real separation performance measures. Currently, the circuit analysis parameters are ill-defined in terms of real performance gain and only applicable for comparative analysis. However, further empirical testing, especially in real separation systems, may produce general rules relating the incremental circuit analysis parameter change to real changes in measured performance.

Appendix A

Appendix: Working Model Data

The following 17 pages include the raw data sheets compiled from the Working Model 2D virtual experiments.

Working Model Electrostatic Simulation

Simulation Information	
Date:	3.13.2013
Time:	7:00 PM
File Name1	Electrostatic_C1a_noBP.wm2d
File Name2	Electrostatic_C1a_withBP1.wm2d
File Name 3	Electrostatic_C1a_withBP2.wm2d
Circuit Name:	Single Unit
Circuit No:	1
By:	Noble

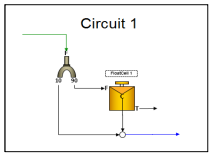

Summary					
Color --	Charge (*10^-7 C)	Feed Number	No BP Recovery	Med BP Recovery	High BP Recovery
Pink	-1	5	8	36	24
Blue	-0.8	5	24	16	28
Purple	-0.6	5	12	8	52
Maroon	-0.4	5	32	36	64
Green	-0.2	5	24	36	28
Yellow	0	5	56	52	60
Red	0.2	5	68	68	56
Orange	0.4	5	72	72	60
Dark Green	0.6	5	100	88	92
Light Blue	0.8	5	100	84	88
Cyan	1	5	100	100	92
Recovered Charge:		0	11.52	9.36	7.2

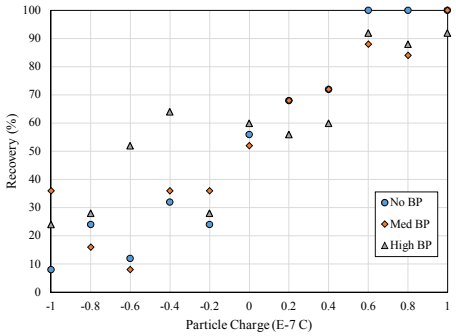

Condition 1

Separation Plate	0.00006	C
BP board	NA	m
Bypass Motor	NA	rad/sec

Total Recovered Charge: **11.52**

	Charge (*10^-7 C)	Number Recovered to Right Side, Test Run 1	2	3	4	5	Average	Sum
Pink	-1	0	2	0	0	0	0.4	25
Blue	-0.8	1	2	1	0	2	1.2	25
Purple	-0.6	1	1	0	0	1	0.6	25
Maroon	-0.4	4	1	1	0	2	1.6	25
Green	-0.2	1	1	1	1	2	1.2	25
Yellow	0	2	3	3	2	4	2.8	25
Red	0.2	3	4	4	2	4	3.4	25
Orange	0.4	3	4	5	2	4	3.6	25
Dark Green	0.6	5	5	5	5	5	5	25
Light Blue	0.8	5	5	5	5	5	5	25
Cyan	1	5	5	5	5	5	5	25

	Number Recovered to Left Side, Test Run 1	2	3	4	5	Average
Pink	5	3	5	5	5	4.6
Blue	4	3	4	5	3	3.8
Purple	4	4	5	5	4	4.4
Maroon	1	4	4	5	3	3.4
Green	4	4	4	4	3	3.8
Yellow	3	2	2	3	1	2.2
Red	2	1	1	3	1	1.6
Orange	2	1	0	3	1	1.4
Dark Green	0	0	0	0	0	0
Light Blue	0	0	0	0	0	0
Cyan	0	0	0	0	0	0

Condition 2

Separation Plate	0.00006	C
BP board	0.3	m
Bypass Motor	5	rad/sec

Total Recovered Charge: **9.36**

	Charge (*10^-7 C)	Number Recovered to Right Side, Test Run 1	2	3	4	5	Average	Sum
Pink	-1	2	2	1	1	3	1.8	25
Blue	-0.8	1	1	1	1	0	0.8	25
Purple	-0.6	0	1	0	0	1	0.4	25
Maroon	-0.4	3	0	1	2	3	1.8	25
Green	-0.2	1	1	2	3	2	1.8	25
Yellow	0	1	4	3	2	3	2.6	25
Red	0.2	5	2	4	2	4	3.4	25
Orange	0.4	4	3	4	4	3	3.6	25
Dark Green	0.6	4	4	5	5	4	4.4	25
Light Blue	0.8	4	2	5	5	5	4.2	25
Cyan	1	5	5	5	5	5	5	25

	Number Recovered to Left Side, Test Run 1	2	3	4	5	Average
Pink	3	3	4	4	2	3.2
Blue	4	4	4	4	5	4.2
Purple	5	4	5	5	4	4.6
Maroon	2	5	4	3	2	3.2
Green	4	4	3	2	3	3.2
Yellow	4	1	2	3	2	2.4
Red	0	3	1	3	1	1.6
Orange	1	2	1	1	2	1.4
Dark Green	1	1	0	0	1	0.6
Light Blue	1	3	0	0	0	0.8
Cyan	0	0	0	0	0	0

Condition 3

Separation Block	0.00006	C
BP board	0.5	m
Bypass Motor	5	rad/sec

Total Recovered Charge: **7.2**

	Charge (*10^-7 C)	Number Recovered to Right Side, Test Run 1	2	3	4	5	Average	Sum
Pink	-1	2	1	2	1	0	1.2	25
Blue	-0.8	1	1	2	1	2	1.4	25
Purple	-0.6	2	2	3	1	5	2.6	25
Maroon	-0.4	3	3	3	3	4	3.2	25
Green	-0.2	2	0	1	1	3	1.4	25
Yellow	0	2	5	2	3	3	3	25
Red	0.2	2	5	2	2	3	2.8	25
Orange	0.4	4	1	4	2	4	3	25
Dark Green	0.6	5	4	5	4	5	4.6	25
Light Blue	0.8	5	4	5	5	3	4.4	25
Cyan	1	5	4	5	5	4	4.6	25

	Number Recovered to Left Side, Test Run 1	2	3	4	5	Average
Pink	3	4	3	4	5	3.8
Blue	4	4	3	4	3	3.6
Purple	3	3	2	4	0	2.4
Maroon	2	2	2	2	1	1.8
Green	3	5	4	4	2	3.6
Yellow	3	0	3	2	2	2
Red	3	0	3	3	2	2.2
Orange	1	4	1	3	1	2
Dark Green	0	1	0	1	0	0.4
Light Blue	0	1	0	0	2	0.6
Cyan	0	1	0	0	1	0.4

Working Model Electrostatic Simulation

Simulation Information	
Date:	3.20.2013
Time:	10:00 AM
File Name1	Electrostatic_C2a_noBP.wm2d
File Name2	Electrostatic_C2a_withBP1.wm2d
File Name 3	Electrostatic_C2a_withBP2.wm2d
Circuit Name:	Scavenger with Recycle
Circuit No:	2
By:	Noble

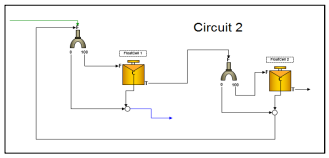

Summary					
Color --	Charge (*10^-7 C)	Feed Number	No BP Recovery	Med BP Recovery	High BP Recovery
Pink	-1	5	12	56	36
Blue	-0.8	5	16	56	60
Purple	-0.6	5	24	32	68
Maroon	-0.4	5	28	48	92
Green	-0.2	5	28	64	64
Yellow	0	5	60	64	84
Red	0.2	5	92	92	96
Orange	0.4	5	96	96	96
Dark Green	0.6	5	100	100	100
Light Blue	0.8	5	100	100	100
Cyan	1	5	100	100	100
Total Charge:		0	12.04	7.24	6.16

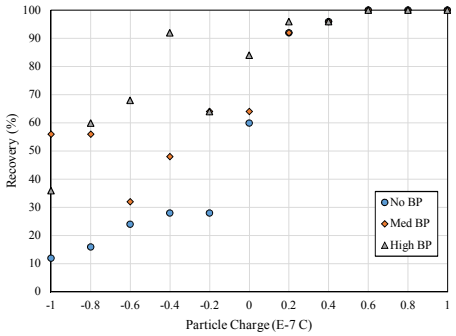

Condition 1

Separation Plate	0.00006	C
BP board	NA	m
Bypass Motor	NA	rad/sec

Total Recovered Charge: **12.04**

	Charge (*10^-7 C)	Number Recovered to Right Side, Test Run 1	2	3	4	5	Average	Sum
Pink	-1	1	0	0	0	2	0.6	25
Blue	-0.8	1	2	1	0	0	0.8	25
Purple	-0.6	1	1	3	0	1	1.2	25
Maroon	-0.4	1	2	1	3	0	1.4	25
Green	-0.2	0	3	3	1	0	1.4	25
Yellow	0	5	4	3	2	1	3	25
Red	0.2	5	5	5	5	3	4.6	25
Orange	0.4	4	5	5	5	5	4.8	25
Dark Green	0.6	5	5	5	5	5	5	25
Light Blue	0.8	5	5	5	5	5	5	25
Cyan	1	5	5	5	5	5	5	25

	Number Recovered to Left Side, Test Run 1	2	3	4	5	Average
Pink	4	5	5	5	3	4.4
Blue	4	3	4	5	5	4.2
Purple	4	4	2	5	4	3.8
Maroon	4	3	4	2	5	3.6
Green	5	2	2	4	5	3.6
Yellow	0	1	2	3	4	2
Red	0	0	0	0	2	0.4
Orange	1	0	0	0	0	0.2
Dark Green	0	0	0	0	0	0
Light Blue	0	0	0	0	0	0
Cyan	0	0	0	0	0	0

Condition 2

Separation Plate	0.00006	C
BP board	0.3	m
Bypass Motor	5	rad/sec

Total Recovered Charge: **7.24**

	Charge (*10^-7 C)	Number Recovered to Right Side, Test Run 1	2	3	4	5	Average	Sum
Pink	-1	4	2	4	2	2	2.8	25
Blue	-0.8	4	2	4	4	0	2.8	25
Purple	-0.6	1	2	1	4	0	1.6	25
Maroon	-0.4	3	2	1	5	1	2.4	25
Green	-0.2	3	3	3	4	3	3.2	25
Yellow	0	3	4	3	4	2	3.2	25
Red	0.2	5	4	5	5	4	4.6	25
Orange	0.4	5	4	5	5	5	4.8	25
Dark Green	0.6	5	5	5	5	5	5	25
Light Blue	0.8	5	5	5	5	5	5	25
Cyan	1	5	5	5	5	5	5	25

	Number Recovered to Left Side, Test Run 1	2	3	4	5	Average
Pink	1	3	1	3	3	2.2
Blue	1	3	1	1	5	2.2
Purple	4	3	4	1	5	3.4
Maroon	2	3	4	0	4	2.6
Green	2	2	2	1	2	1.8
Yellow	2	1	2	1	3	1.8
Red	0	1	0	0	1	0.4
Orange	0	1	0	0	0	0.2
Dark Green	0	0	0	0	0	0
Light Blue	0	0	0	0	0	0
Cyan	0	0	0	0	0	0

Condition 3

Separation Block	0.00006	C
BP board	0.5	m
Bypass Motor	5	rad/sec

Total Recovered Charge: **6.16**

	Charge (*10^-7 C)	Number Recovered to Right Side, Test Run 1	2	3	4	5	Average	Sum
Pink	-1	1	1	1	3	3	1.8	25
Blue	-0.8	2	4	2	4	3	3	25
Purple	-0.6	3	1	5	4	4	3.4	25
Maroon	-0.4	5	4	5	4	5	4.6	25
Green	-0.2	1	3	3	5	4	3.2	25
Yellow	0	4	4	5	4	4	4.2	25
Red	0.2	5	5	4	5	5	4.8	25
Orange	0.4	5	5	5	4	5	4.8	25
Dark Green	0.6	5	5	5	5	5	5	25
Light Blue	0.8	5	5	5	5	5	5	25
Cyan	1	5	5	5	5	5	5	25

	Number Recovered to Left Side, Test Run 1	2	3	4	5	Average
Pink	4	4	4	2	2	3.2
Blue	3	1	3	1	2	2
Purple	2	4	0	1	1	1.6
Maroon	0	1	0	1	0	0.4
Green	4	2	2	0	1	1.8
Yellow	1	1	0	1	1	0.8
Red	0	0	1	0	0	0.2
Orange	0	0	0	1	0	0.2
Dark Green	0	0	0	0	0	0
Light Blue	0	0	0	0	0	0
Cyan	0	0	0	0	0	0

Working Model Electrostatic Simulation

Simulation Information	
Date:	3.19.2013
Time:	7:30 PM
File Name1	Electrostatic_C3a_noBP.wm2d
File Name2	Electrostatic_C3a_withBP1.wm2d
File Name 3	Electrostatic_C3a_withBP2.wm2d
Circuit Name:	Cleaner with Recycle
Circuit No:	3
By:	Noble

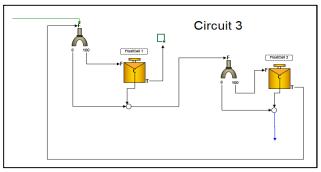

Summary					
Color --	Charge (*10^-7 C)	Feed Number	No BP Recovery	Med BP Recovery	High BP Recovery
Pink	-1	5	0	4	8
Blue	-0.8	5	8	4	12
Purple	-0.6	5	8	12	24
Maroon	-0.4	5	28	8	8
Green	-0.2	5	20	12	20
Yellow	0	5	28	12	40
Red	0.2	5	52	40	64
Orange	0.4	5	80	72	68
Dark Green	0.6	5	100	96	100
Light Blue	0.8	5	96	96	100
Cyan	1	5	100	88	96
Total Charge:		0	12.64	11.96	11.84

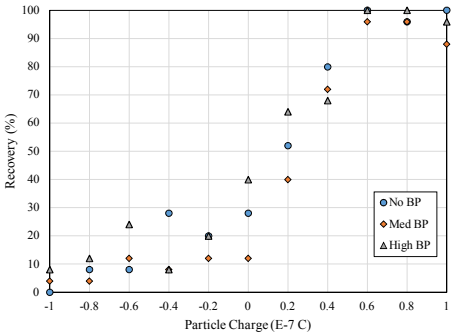

Condition 1

Separation Plate	0.00006	C
BP board	NA	m
Bypass Motor	NA	rad/sec

Total Recovered Charge: **12.64**

	Charge (*10^-7 C)	Number Recovered to Right Side, Test Run 1	2	3	4	5	Average	Sum
Pink	-1	0	0	0	0	0	0	25
Blue	-0.8	0	0	0	2	0	0.4	25
Purple	-0.6	1	0	0	1	0	0.4	25
Maroon	-0.4	1	0	3	1	2	1.4	25
Green	-0.2	0	2	2	1	0	1	25
Yellow	0	3	1	1	1	1	1.4	25
Red	0.2	4	3	1	3	2	2.6	25
Orange	0.4	5	2	3	5	5	4	25
Dark Green	0.6	5	5	5	5	5	5	25
Light Blue	0.8	4	5	5	5	5	4.8	25
Cyan	1	5	5	5	5	5	5	25

	Number Recovered to Left Side, Test Run 1	2	3	4	5	Average
Pink	5	5	5	5	5	5
Blue	5	5	5	3	5	4.6
Purple	4	5	5	4	5	4.6
Maroon	4	5	2	4	3	3.6
Green	5	3	3	4	5	4
Yellow	2	4	4	4	4	3.6
Red	1	2	4	2	3	2.4
Orange	0	3	2	0	0	1
Dark Green	0	0	0	0	0	0
Light Blue	1	0	0	0	0	0.2
Cyan	0	0	0	0	0	0

Condition 2

Separation Plate	0.00006	C
BP board	0.3	m
Bypass Motor	5	rad/sec

Total Recovered Charge: **11.96**

	Charge (*10^-7 C)	Number Recovered to Right Side, Test Run 1	2	3	4	5	Average	Sum
Pink	-1	0	1	0	0	0	0.2	25
Blue	-0.8	0	1	0	0	0	0.2	25
Purple	-0.6	0	0	0	1	2	0.6	25
Maroon	-0.4	0	0	0	1	1	0.4	25
Green	-0.2	1	0	0	2	0	0.6	25
Yellow	0	1	0	1	0	1	0.6	25
Red	0.2	1	2	2	3	2	2	25
Orange	0.4	4	3	2	5	4	3.6	25
Dark Green	0.6	5	5	5	4	5	4.8	25
Light Blue	0.8	4	5	5	5	5	4.8	25
Cyan	1	5	4	5	5	3	4.4	25

	Number Recovered to Left Side, Test Run 1	2	3	4	5	Average
Pink	5	4	5	5	5	4.8
Blue	5	4	5	5	5	4.8
Purple	5	5	5	4	3	4.4
Maroon	5	5	5	4	4	4.6
Green	4	5	5	3	5	4.4
Yellow	4	5	4	5	4	4.4
Red	4	3	3	2	3	3
Orange	1	2	3	0	1	1.4
Dark Green	0	0	0	1	0	0.2
Light Blue	1	0	0	0	0	0.2
Cyan	0	1	0	0	2	0.6

Condition 3

Separation Block	0.00006	C
BP board	0.5	m
Bypass Motor	5	rad/sec

Total Recovered Charge: **11.84**

	Charge (*10^-7 C)	Number Recovered to Right Side, Test Run 1	2	3	4	5	Average	Sum
Pink	-1	1	1	0	0	0	0.4	25
Blue	-0.8	0	1	1	0	1	0.6	25
Purple	-0.6	0	3	1	1	1	1.2	25
Maroon	-0.4	1	0	0	0	1	0.4	25
Green	-0.2	2	1	1	1	0	1	25
Yellow	0	4	1	2	2	1	2	25
Red	0.2	4	2	3	5	2	3.2	25
Orange	0.4	5	5	4	2	1	3.4	25
Dark Green	0.6	5	5	5	5	5	5	25
Light Blue	0.8	5	5	5	5	5	5	25
Cyan	1	5	5	4	5	5	4.8	25

	Number Recovered to Left Side, Test Run 1	2	3	4	5	Average
Pink	4	4	5	5	5	4.6
Blue	5	4	4	5	4	4.4
Purple	5	2	4	4	4	3.8
Maroon	4	5	5	5	4	4.6
Green	3	4	4	4	5	4
Yellow	1	4	3	3	4	3
Red	1	3	2	0	3	1.8
Orange	0	0	1	3	4	1.6
Dark Green	0	0	0	0	0	0
Light Blue	0	0	0	0	0	0
Cyan	0	0	1	0	0	0.2

Working Model Electrostatic Simulation

Simulation Information	
Date:	3.19.2013
Time:	5:20 PM
File Name1	Electrostatic_C4a_noBP.wm2d
File Name2	Electrostatic_C4a_withBP1.wm2d
File Name 3	Electrostatic_C4a_withBP2.wm2d
Circuit Name:	Cleaner no Recycle
Circuit No:	4
By:	Noble

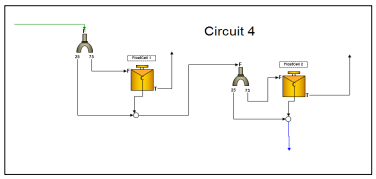

Summary					
Color --	Charge (*10^-7 C)	Feed Number	No BP Recovery	Med BP Recovery	High BP Recovery
Pink	-1	5	0	4	8
Blue	-0.8	5	0	0	12
Purple	-0.6	5	8	0	0
Maroon	-0.4	5	4	0	4
Green	-0.2	5	4	20	16
Yellow	0	5	16	12	12
Red	0.2	5	16	24	32
Orange	0.4	5	84	52	52
Dark Green	0.6	5	80	92	84
Light Blue	0.8	5	92	96	80
Cyan	1	5	100	96	96
Total Charge:		0	12.56	12.28	10.76

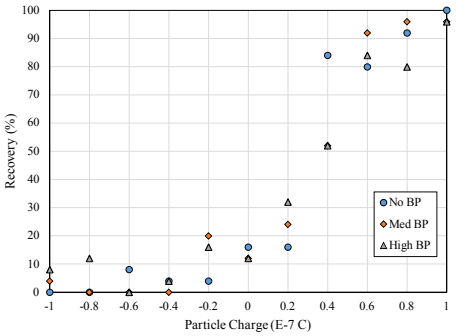

Condition 1

Separation Plate	0.00006	C
BP board	NA	m
Bypass Motor	NA	rad/sec

Total Recovered Charge: **12.56**

	Charge (*10^-7 C)	Number Recovered to Right Side, Test Run 1	2	3	4	5	Average	Sum
Pink	-1	0	0	0	0	0	0	25
Blue	-0.8	0	0	0	0	0	0	25
Purple	-0.6	0	0	1	0	1	0.4	25
Maroon	-0.4	0	0	1	0	0	0.2	25
Green	-0.2	1	0	0	0	0	0.2	25
Yellow	0	0	1	2	0	1	0.8	25
Red	0.2	1	0	0	2	1	0.8	25
Orange	0.4	4	4	4	5	4	4.2	25
Dark Green	0.6	4	4	4	3	5	4	25
Light Blue	0.8	5	4	5	5	4	4.6	25
Cyan	1	5	5	5	5	5	5	25

	Number Recovered to Left Side, Test Run 1	2	3	4	5	Average
Pink	5	5	5	5	5	5
Blue	5	5	5	5	5	5
Purple	5	5	4	5	4	4.6
Maroon	5	5	4	5	5	4.8
Green	4	5	5	5	5	4.8
Yellow	5	4	3	5	4	4.2
Red	4	5	5	3	4	4.2
Orange	1	1	1	0	1	0.8
Dark Green	1	1	1	2	0	1
Light Blue	0	1	0	0	1	0.4
Cyan	0	0	0	0	0	0

Condition 2

Separation Plate	0.00006	C
BP board	0.3	m
Bypass Motor	5	rad/sec

Total Recovered Charge: **12.28**

	Charge (*10^-7 C)	Number Recovered to Right Side, Test Run 1	2	3	4	5	Average	Sum
Pink	-1	0	0	1	0	0	0.2	25
Blue	-0.8	0	0	0	0	0	0	25
Purple	-0.6	0	0	0	0	0	0	25
Maroon	-0.4	0	0	0	0	0	0	25
Green	-0.2	2	0	2	1	0	1	25
Yellow	0	2	0	0	0	1	0.6	25
Red	0.2	2	2	1	0	1	1.2	25
Orange	0.4	3	1	3	3	3	2.6	25
Dark Green	0.6	5	3	5	5	5	4.6	25
Light Blue	0.8	5	5	5	5	4	4.8	25
Cyan	1	5	5	4	5	5	4.8	25

	Number Recovered to Left Side, Test Run 1	2	3	4	5	Average
Pink	5	5	4	5	5	4.8
Blue	5	5	5	5	5	5
Purple	5	5	5	5	5	5
Maroon	5	5	5	5	5	5
Green	3	5	3	4	5	4
Yellow	3	5	5	5	4	4.4
Red	3	3	4	5	4	3.8
Orange	2	4	2	2	2	2.4
Dark Green	0	2	0	0	0	0.4
Light Blue	0	0	0	0	1	0.2
Cyan	0	0	1	0	0	0.2

Condition 3

Separation Block	0.00006	C
BP board	0.5	m
Bypass Motor	5	rad/sec

Total Recovered Charge: **10.76**

	Charge (*10^-7 C)	Number Recovered to Right Side, Test Run 1	2	3	4	5	Average	Sum
Pink	-1	0	0	1	0	1	0.4	25
Blue	-0.8	0	0	1	1	1	0.6	25
Purple	-0.6	0	0	0	0	0	0	25
Maroon	-0.4	0	1	0	0	0	0.2	25
Green	-0.2	0	2	2	0	0	0.8	25
Yellow	0	1	1	1	0	0	0.6	25
Red	0.2	2	2	2	0	2	1.6	25
Orange	0.4	3	1	4	2	3	2.6	25
Dark Green	0.6	5	4	3	5	4	4.2	25
Light Blue	0.8	4	3	3	5	5	4	25
Cyan	1	5	5	5	5	4	4.8	25

	Number Recovered to Left Side, Test Run 1	2	3	4	5	Average
Pink	5	5	4	5	4	4.6
Blue	5	5	4	4	4	4.4
Purple	5	5	5	5	5	5
Maroon	5	4	5	5	5	4.8
Green	5	3	3	5	5	4.2
Yellow	4	4	4	5	5	4.4
Red	3	3	3	5	3	3.4
Orange	2	4	1	3	2	2.4
Dark Green	0	1	2	0	1	0.8
Light Blue	1	2	2	0	0	1
Cyan	0	0	0	0	1	0.2

Working Model Electrostatic Simulation

Simulation Information	
Date:	3.19.2013
Time:	11:20 AM
File Name1	Electrostatic_C5a_noBP.wm2d
File Name2	Electrostatic_C5a_withBP1.wm2d
File Name 3	Electrostatic_C5a_withBP2.wm2d
Circuit Name:	Scavenger no Recycle
Circuit No:	5
By:	Noble

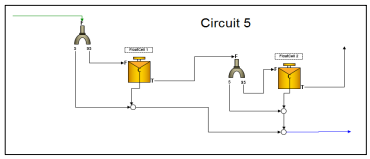

Summary					
Color --	Charge (*10^-7 C)	Feed Number	No BP Recovery	Med BP Recovery	High BP Recovery
Pink	-1	5	8	36	28
Blue	-0.8	5	32	32	56
Purple	-0.6	5	32	24	56
Maroon	-0.4	5	52	56	76
Green	-0.2	5	44	40	60
Yellow	0	5	88	68	72
Red	0.2	5	96	88	80
Orange	0.4	5	96	88	96
Dark Green	0.6	5	100	96	100
Light Blue	0.8	5	100	100	96
Cyan	1	5	100	100	100
Total Charge:		15	10.76	9.2	7.12

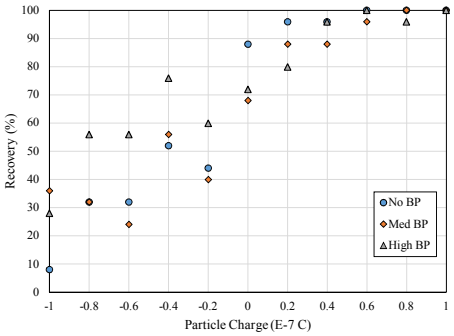

Condition 1

Separation Plate	0.00006	C
BP board	NA	m
Bypass Motor	NA	rad/sec

Total Recovered Charge: **10.76**

	Charge (*10^-7 C)	Number Recovered to Right Side, Test Run 1	2	3	4	5	Average	Sum
Pink	-1	0	1	0	0	1	0.4	25
Blue	-0.8	1	1	2	3	1	1.6	25
Purple	-0.6	1	3	1	2	1	1.6	25
Maroon	-0.4	4	3	0	3	3	2.6	25
Green	-0.2	3	2	3	2	1	2.2	25
Yellow	0	5	3	4	5	5	4.4	25
Red	0.2	5	4	5	5	5	4.8	25
Orange	0.4	5	5	5	5	4	4.8	25
Dark Green	0.6	5	5	5	5	5	5	25
Light Blue	0.8	5	5	5	5	5	5	25
Cyan	1	5	5	5	5	5	5	25

	Number Recovered to Left Side, Test Run 1	2	3	4	5	Average
Pink	5	4	5	5	4	4.6
Blue	4	4	3	2	4	3.4
Purple	4	2	4	3	4	3.4
Maroon	1	2	5	2	2	2.4
Green	2	3	2	3	4	2.8
Yellow	0	2	1	0	0	0.6
Red	0	1	0	0	0	0.2
Orange	0	0	0	0	1	0.2
Dark Green	0	0	0	0	0	0
Light Blue	0	0	0	0	0	0
Cyan	0	0	0	0	0	0

Condition 2

Separation Plate	0.00006	C
BP board	0.3	m
Bypass Motor	5	rad/sec

Total Recovered Charge: **9.2**

	Charge (*10^-7 C)	Number Recovered to Right Side, Test Run 1	2	3	4	5	Average	Sum
Pink	-1	1	3	0	2	3	1.8	25
Blue	-0.8	0	2	1	0	5	1.6	25
Purple	-0.6	2	2	0	2	0	1.2	25
Maroon	-0.4	4	3	3	2	2	2.8	25
Green	-0.2	2	3	0	3	2	2	25
Yellow	0	3	5	3	1	5	3.4	25
Red	0.2	5	5	4	4	4	4.4	25
Orange	0.4	5	4	5	4	4	4.4	25
Dark Green	0.6	4	5	5	5	5	4.8	25
Light Blue	0.8	5	5	5	5	5	5	25
Cyan	1	5	5	5	5	5	5	25

	Number Recovered to Left Side, Test Run 1	2	3	4	5	Average
Pink	4	2	5	3	2	3.2
Blue	5	3	4	5	0	3.4
Purple	3	3	5	3	5	3.8
Maroon	1	2	2	3	3	2.2
Green	3	2	5	2	3	3
Yellow	2	0	2	4	0	1.6
Red	0	0	1	1	1	0.6
Orange	0	1	0	1	1	0.6
Dark Green	1	0	0	0	0	0.2
Light Blue	0	0	0	0	0	0
Cyan	0	0	0	0	0	0

Condition 3

Separation Block	0.00006	C
BP board	0.5	m
Bypass Motor	5	rad/sec

Total Recovered Charge: **7.12**

	Charge (*10^-7 C)	Number Recovered to Right Side, Test Run 1	2	3	4	5	Average	Sum
Pink	-1	1	1	1	2	2	1.4	25
Blue	-0.8	4	2	2	2	4	2.8	25
Purple	-0.6	2	2	3	4	3	2.8	25
Maroon	-0.4	3	5	4	5	2	3.8	25
Green	-0.2	2	2	2	4	5	3	25
Yellow	0	4	2	5	3	4	3.6	25
Red	0.2	3	4	4	4	5	4	25
Orange	0.4	5	5	5	5	4	4.8	25
Dark Green	0.6	5	5	5	5	5	5	25
Light Blue	0.8	5	4	5	5	5	4.8	25
Cyan	1	5	5	5	5	5	5	25

	Number Recovered to Left Side, Test Run 1	2	3	4	5	Average
Pink	4	4	4	3	3	3.6
Blue	1	3	3	3	1	2.2
Purple	3	3	2	1	2	2.2
Maroon	2	0	1	0	3	1.2
Green	3	3	3	1	0	2
Yellow	1	3	0	2	1	1.4
Red	2	1	1	1	0	1
Orange	0	0	0	0	1	0.2
Dark Green	0	0	0	0	0	0
Light Blue	0	1	0	0	0	0.2
Cyan	0	0	0	0	0	0

Working Model Electrostatic Simulation

Simulation Information	
Date:	4.5.2013
Time:	4:11 PM
File Name1	Electrostatic_C12a_noBP.wm2d
File Name2	Electrostatic_C12a_withBP1.wm2d
File Name 3	Electrostatic_C12a_withBP2.wm2d
Circuit Name:	Cleaner-Recleaner Open
Circuit No:	12
By:	Noble

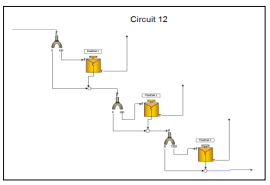

Summary					
Color --	Charge (*10^-7 C)	Feed Number	No BP Recovery	Med BP Recovery	High BP Recovery
Pink	-1	5	0	0	4
Blue	-0.8	5	0	0	8
Purple	-0.6	5	0	0	4
Maroon	-0.4	5	0	4	8
Green	-0.2	5	0	0	4
Yellow	0	5	4	8	20
Red	0.2	5	0	8	20
Orange	0.4	5	68	52	52
Dark Green	0.6	5	96	88	84
Light Blue	0.8	5	100	100	96
Cyan	1	5	100	96	100
Total Charge:		15	13.24	12.48	11.76

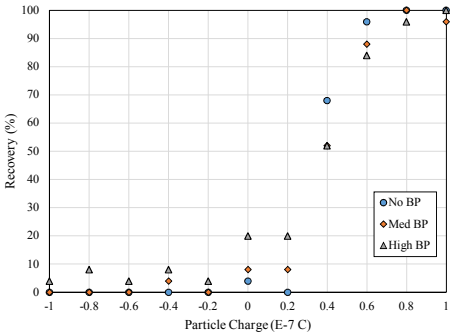

Condition 1

Separation Plate	0.00006	C
BP board	NA	m
Bypass Motor	NA	rad/sec

Total Recovered Charge: **13.24**

	Charge (*10^-7 C)	Number Recovered to Right Side, Test Run 1	2	3	4	5	Average	Sum
Pink	-1	0	0	0	0	0	0	25
Blue	-0.8	0	0	0	0	0	0	25
Purple	-0.6	0	0	0	0	0	0	25
Maroon	-0.4	0	0	0	0	0	0	25
Green	-0.2	0	0	0	0	0	0	25
Yellow	0	0	1	0	0	0	0.2	25
Red	0.2	0	0	0	0	0	0	25
Orange	0.4	3	3	4	3	4	3.4	25
Dark Green	0.6	5	5	4	5	5	4.8	25
Light Blue	0.8	5	5	5	5	5	5	25
Cyan	1	5	5	5	5	5	5	25

	Number Recovered to Left Side, Test Run 1	2	3	4	5	Average
Pink	5	5	5	5	5	5
Blue	5	5	5	5	5	5
Purple	5	5	5	5	5	5
Maroon	5	5	5	5	5	5
Green	5	5	5	5	5	5
Yellow	5	4	5	5	5	4.8
Red	5	5	5	5	5	5
Orange	2	2	1	2	1	1.6
Dark Green	0	0	1	0	0	0.2
Light Blue	0	0	0	0	0	0
Cyan	0	0	0	0	0	0

Condition 2

Separation Plate	0.00006	C
BP board	0.3	m
Bypass Motor	5	rad/sec

Total Recovered Charge: **12.48**

	Charge (*10^-7 C)	Number Recovered to Right Side, Test Run 1	2	3	4	5	Average	Sum
Pink	-1	0	0	0	0	0	0	25
Blue	-0.8	0	0	0	0	0	0	25
Purple	-0.6	0	0	0	0	0	0	25
Maroon	-0.4	0	1	0	0	0	0.2	25
Green	-0.2	0	0	0	0	0	0	25
Yellow	0	0	0	1	0	1	0.4	25
Red	0.2	0	0	1	0	1	0.4	25
Orange	0.4	2	2	4	3	2	2.6	25
Dark Green	0.6	5	5	3	4	5	4.4	25
Light Blue	0.8	5	5	5	5	5	5	25
Cyan	1	5	5	5	5	4	4.8	25

	Number Recovered to Left Side, Test Run 1	2	3	4	5	Average
Pink	5	5	5	5	5	5
Blue	5	5	5	5	5	5
Purple	5	5	5	5	5	5
Maroon	5	4	5	5	5	4.8
Green	5	5	5	5	5	5
Yellow	5	5	4	5	4	4.6
Red	5	5	4	5	4	4.6
Orange	3	3	1	2	3	2.4
Dark Green	0	0	2	1	0	0.6
Light Blue	0	0	0	0	0	0
Cyan	0	0	0	0	1	0.2

Condition 3

Separation Block	0.00006	C
BP board	0.5	m
Bypass Motor	5	rad/sec

Total Recovered Charge: **11.76**

	Charge (*10^-7 C)	Number Recovered to Right Side, Test Run 1	2	3	4	5	Average	Sum
Pink	-1	0	0	0	0	1	0.2	21
Blue	-0.8	1	0	0	1	0	0.4	25
Purple	-0.6	0	0	0	1	0	0.2	25
Maroon	-0.4	0	0	0	1	1	0.4	25
Green	-0.2	0	0	1	0	0	0.2	25
Yellow	0	0	0	0	3	2	1	25
Red	0.2	0	1	1	2	1	1	25
Orange	0.4	3	2	4	3	1	2.6	25
Dark Green	0.6	5	4	4	4	4	4.2	25
Light Blue	0.8	5	5	4	5	5	4.8	25
Cyan	1	5	5	5	5	5	5	25

	Number Recovered to Left Side, Test Run 1	2	3	4	5	Average
Pink	1	5	5	5	4	4
Blue	4	5	5	4	5	4.6
Purple	5	5	5	4	5	4.8
Maroon	5	5	5	4	4	4.6
Green	5	5	4	5	5	4.8
Yellow	5	5	5	2	3	4
Red	5	4	4	3	4	4
Orange	2	3	1	2	4	2.4
Dark Green	0	1	1	1	1	0.8
Light Blue	0	0	1	0	0	0.2
Cyan	0	0	0	0	0	0

Working Model Electrostatic Simulation

Simulation Information	
Date:	4.5.2013
Time:	4:11 PM
File Name1	Electrostatic_C12a_noBP.wm2d
File Name2	Electrostatic_C12a_withBP1.wm2d
File Name 3	Electrostatic_C12a_withBP2.wm2d
Circuit Name:	Cleaner-Recleaner/Recleaner Back 1
Circuit No:	13
By:	Noble

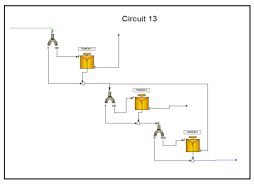

Summary					
Color --	Charge (*10^-7 C)	Feed Number	No BP Recovery	Med BP Recovery	High BP Recovery
Pink	-1	5	0	0	4
Blue	-0.8	5	0	4	8
Purple	-0.6	5	0	0	8
Maroon	-0.4	5	0	4	8
Green	-0.2	5	0	0	8
Yellow	0	5	4	16	20
Red	0.2	5	8	12	28
Orange	0.4	5	80	60	56
Dark Green	0.6	5	96	88	84
Light Blue	0.8	5	100	100	96
Cyan	1	5	100	100	100
Total Charge:		15	13.56	12.72	11.76

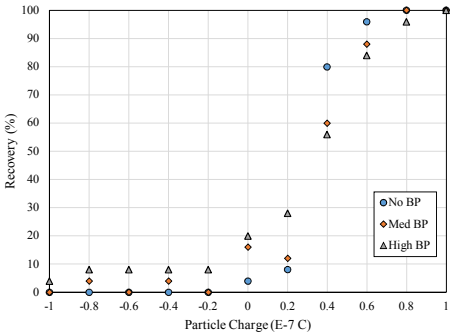

Condition 1

Separation Plate	0.00006	C
BP board	NA	m
Bypass Motor	NA	rad/sec

Total Recovered Charge: **13.56**

	Charge (*10^-7 C)	Number Recovered to Right Side, Test Run 1	2	3	4	5	Average	Sum
Pink	-1	0	0	0	0	0	0	25
Blue	-0.8	0	0	0	0	0	0	25
Purple	-0.6	0	0	0	0	0	0	25
Maroon	-0.4	0	0	0	0	0	0	25
Green	-0.2	0	0	0	0	0	0	25
Yellow	0	0	1	0	0	0	0.2	25
Red	0.2	0	1	0	1	0	0.4	24
Orange	0.4	5	3	4	3	5	4	26
Dark Green	0.6	5	5	4	5	5	4.8	25
Light Blue	0.8	5	5	5	5	5	5	25
Cyan	1	5	5	5	5	5	5	25

	Number Recovered to Left Side, Test Run 1	2	3	4	5	Average
Pink	5	5	5	5	5	5
Blue	5	5	5	5	5	5
Purple	5	5	5	5	5	5
Maroon	5	5	5	5	5	5
Green	5	5	5	5	5	5
Yellow	5	4	5	5	5	4.8
Red	5	4	5	4	4	4.4
Orange	0	2	1	2	1	1.2
Dark Green	0	0	1	0	0	0.2
Light Blue	0	0	0	0	0	0
Cyan	0	0	0	0	0	0

Condition 2

Separation Plate	0.00006	C
BP board	0.3	m
Bypass Motor	5	rad/sec

Total Recovered Charge: **12.72**

	Charge (*10^-7 C)	Number Recovered to Right Side, Test Run 1	2	3	4	5	Average	Sum
Pink	-1	0	0	0	0	0	0	25
Blue	-0.8	0	0	0	1	0	0.2	25
Purple	-0.6	0	0	0	0	0	0	25
Maroon	-0.4	0	1	0	0	0	0.2	25
Green	-0.2	0	0	0	0	0	0	25
Yellow	0	1	1	1	0	1	0.8	25
Red	0.2	1	0	1	0	1	0.6	25
Orange	0.4	3	3	4	3	2	3	25
Dark Green	0.6	5	5	3	4	5	4.4	25
Light Blue	0.8	5	5	5	5	5	5	25
Cyan	1	5	5	5	5	5	5	25

	Number Recovered to Left Side, Test Run 1	2	3	4	5	Average
Pink	5	5	5	5	5	5
Blue	5	5	5	4	5	4.8
Purple	5	5	5	5	5	5
Maroon	5	4	5	5	5	4.8
Green	5	5	5	5	5	5
Yellow	4	4	4	5	4	4.2
Red	4	5	4	5	4	4.4
Orange	2	2	1	2	3	2
Dark Green	0	0	2	1	0	0.6
Light Blue	0	0	0	0	0	0
Cyan	0	0	0	0	0	0

Condition 3

Separation Block	0.00006	C
BP board	0.5	m
Bypass Motor	5	rad/sec

Total Recovered Charge: **11.76**

	Charge (*10^-7 C)	Number Recovered to Right Side, Test Run 1	2	3	4	5	Average	Sum
Pink	-1	0	0	0	0	1	0.2	21
Blue	-0.8	1	0	0	1	0	0.4	25
Purple	-0.6	0	0	1	1	0	0.4	25
Maroon	-0.4	0	0	0	1	1	0.4	25
Green	-0.2	0	0	2	0	0	0.4	25
Yellow	0	0	0	0	3	2	1	25
Red	0.2	0	2	2	2	1	1.4	25
Orange	0.4	4	2	4	3	1	2.8	25
Dark Green	0.6	5	4	4	4	4	4.2	25
Light Blue	0.8	5	5	4	5	5	4.8	25
Cyan	1	5	5	5	5	5	5	25

	Number Recovered to Left Side, Test Run 1	2	3	4	5	Average
Pink	1	5	5	5	4	4
Blue	4	5	5	4	5	4.6
Purple	5	5	4	4	5	4.6
Maroon	5	5	5	4	4	4.6
Green	5	5	3	5	5	4.6
Yellow	5	5	5	2	3	4
Red	5	3	3	3	4	3.6
Orange	1	3	1	2	4	2.2
Dark Green	0	1	1	1	1	0.8
Light Blue	0	0	1	0	0	0.2
Cyan	0	0	0	0	0	0

Working Model Electrostatic Simulation

Simulation Information	
Date:	4.5.2013
Time:	4:11 PM
File Name1	Electrostatic_C12a_noBP.wm2d
File Name2	Electrostatic_C12a_withBP1.wm2d
File Name 3	Electrostatic_C12a_withBP2.wm2d
Circuit Name:	Cleaner-Recleaner/Recleaner Back 2
Circuit No:	14
By:	Noble

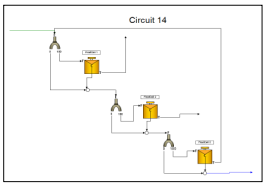

Summary					
Color --	Charge (*10^-7 C)	Feed Number	No BP Recovery	Med BP Recovery	High BP Recovery
Pink	-1	5	0	0	4
Blue	-0.8	5	0	0	8
Purple	-0.6	5	0	0	8
Maroon	-0.4	5	0	8	8
Green	-0.2	5	0	0	8
Yellow	0	5	4	12	20
Red	0.2	5	4	12	28
Orange	0.4	5	76	60	56
Dark Green	0.6	5	96	88	84
Light Blue	0.8	5	100	100	96
Cyan	1	5	100	100	100
Total Charge:		15	13.44	12.8	11.76

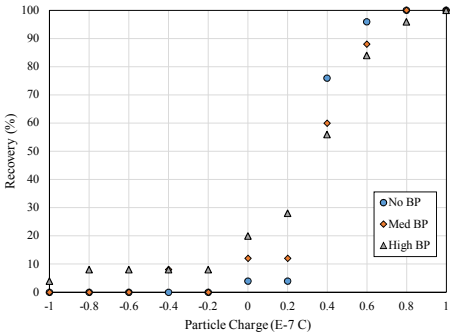

Condition 1

Separation Plate	0.00006	C
BP board	NA	m
Bypass Motor	NA	rad/sec

Total Recovered Charge: **13.44**

	Charge (*10^-7 C)	Number Recovered to Right Side, Test Run 1	2	3	4	5	Average	Sum
Pink	-1	0	0	0	0	0	0	25
Blue	-0.8	0	0	0	0	0	0	25
Purple	-0.6	0	0	0	0	0	0	25
Maroon	-0.4	0	0	0	0	0	0	25
Green	-0.2	0	0	0	0	0	0	25
Yellow	0	0	1	0	0	0	0.2	25
Red	0.2	0	1	0	0	0	0.2	25
Orange	0.4	4	3	4	3	5	3.8	25
Dark Green	0.6	5	5	4	5	5	4.8	25
Light Blue	0.8	5	5	5	5	5	5	25
Cyan	1	5	5	5	5	5	5	25

	Number Recovered to Left Side, Test Run 1	2	3	4	5	Average
Pink	5	5	5	5	5	5
Blue	5	5	5	5	5	5
Purple	5	5	5	5	5	5
Maroon	5	5	5	5	5	5
Green	5	5	5	5	5	5
Yellow	5	4	5	5	5	4.8
Red	5	4	5	5	5	4.8
Orange	1	2	1	2	0	1.2
Dark Green	0	0	1	0	0	0.2
Light Blue	0	0	0	0	0	0
Cyan	0	0	0	0	0	0

Condition 2

Separation Plate	0.00006	C
BP board	0.3	m
Bypass Motor	5	rad/sec

Total Recovered Charge: **12.8**

	Charge (*10^-7 C)	Number Recovered to Right Side, Test Run 1	2	3	4	5	Average	Sum
Pink	-1	0	0	0	0	0	0	25
Blue	-0.8	0	0	0	0	0	0	25
Purple	-0.6	0	0	0	0	0	0	25
Maroon	-0.4	0	1	0	1	0	0.4	25
Green	-0.2	0	0	0	0	0	0	25
Yellow	0	0	0	1	0	2	0.6	25
Red	0.2	0	0	2	0	1	0.6	25
Orange	0.4	3	3	4	3	2	3	25
Dark Green	0.6	5	5	3	4	5	4.4	25
Light Blue	0.8	5	5	5	5	5	5	25
Cyan	1	5	5	5	5	5	5	25

	Number Recovered to Left Side, Test Run 1	2	3	4	5	Average
Pink	5	5	5	5	5	5
Blue	5	5	5	5	5	5
Purple	5	5	5	5	5	5
Maroon	5	4	5	4	5	4.6
Green	5	5	5	5	5	5
Yellow	5	5	4	5	3	4.4
Red	5	5	3	5	4	4.4
Orange	2	2	1	2	3	2
Dark Green	0	0	2	1	0	0.6
Light Blue	0	0	0	0	0	0
Cyan	0	0	0	0	0	0

Condition 3

Separation Block	0.00006	C
BP board	0.5	m
Bypass Motor	5	rad/sec

Total Recovered Charge: **11.76**

	Charge (*10^-7 C)	Number Recovered to Right Side, Test Run 1	2	3	4	5	Average	Sum
Pink	-1	0	0	0	0	1	0.2	21
Blue	-0.8	1	0	0	1	0	0.4	25
Purple	-0.6	0	0	1	1	0	0.4	25
Maroon	-0.4	0	0	0	1	1	0.4	25
Green	-0.2	0	0	2	0	0	0.4	25
Yellow	0	0	0	0	3	2	1	25
Red	0.2	0	2	2	2	1	1.4	25
Orange	0.4	4	2	4	3	1	2.8	25
Dark Green	0.6	5	4	4	4	4	4.2	25
Light Blue	0.8	5	5	4	5	5	4.8	25
Cyan	1	5	5	5	5	5	5	25

	Number Recovered to Left Side, Test Run 1	2	3	4	5	Average
Pink	1	5	5	5	4	4
Blue	4	5	5	4	5	4.6
Purple	5	5	4	4	5	4.6
Maroon	5	5	5	4	4	4.6
Green	5	5	3	5	5	4.6
Yellow	5	5	5	2	3	4
Red	5	3	3	3	4	3.6
Orange	1	3	1	2	4	2.2
Dark Green	0	1	1	1	1	0.8
Light Blue	0	0	1	0	0	0.2
Cyan	0	0	0	0	0	0

Working Model Electrostatic Simulation

Simulation Information	
Date:	4.5.2013
Time:	4:11 PM
File Name1	Electrostatic_C12a_noBP.wm2d
File Name2	Electrostatic_C12a_withBP1.wm2d
File Name 3	Electrostatic_C12a_withBP2.wm2d
Circuit Name:	Cleaner-Recleaner/Cleaner Back
Circuit No:	15
By:	Noble

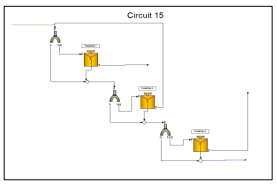

Summary					
Color --	Charge (*10^-7 C)	Feed Number	No BP Recovery	Med BP Recovery	High BP Recovery
Pink	-1	5	0	0	4
Blue	-0.8	5	0	0	8
Purple	-0.6	5	0	0	8
Maroon	-0.4	5	0	4	8
Green	-0.2	5	4	0	12
Yellow	0	5	4	8	28
Red	0.2	5	8	16	24
Orange	0.4	5	68	60	64
Dark Green	0.6	5	96	88	84
Light Blue	0.8	5	100	100	96
Cyan	1	5	100	96	100
Total Charge:		15	13.28	12.72	11.84

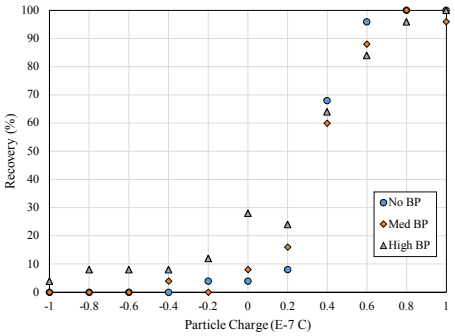

Condition 1

Separation Plate	0.00006	C
BP board	NA	m
Bypass Motor	NA	rad/sec

Total Recovered Charge: **13.28**

	Charge (*10^-7 C)	Number Recovered to Right Side, Test Run 1	2	3	4	5	Average	Sum
Pink	-1	0	0	0	0	0	0	25
Blue	-0.8	0	0	0	0	0	0	25
Purple	-0.6	0	0	0	0	0	0	25
Maroon	-0.4	0	0	0	0	0	0	25
Green	-0.2	0	1	0	0	0	0.2	25
Yellow	0	0	1	0	0	0	0.2	25
Red	0.2	1	1	0	0	0	0.4	25
Orange	0.4	3	3	4	3	4	3.4	25
Dark Green	0.6	5	5	4	5	5	4.8	25
Light Blue	0.8	5	5	5	5	5	5	25
Cyan	1	5	5	5	5	5	5	25

	Number Recovered to Left Side, Test Run 1	2	3	4	5	Average
Pink	5	5	5	5	5	5
Blue	5	5	5	5	5	5
Purple	5	5	5	5	5	5
Maroon	5	5	5	5	5	5
Green	5	4	5	5	5	4.8
Yellow	5	4	5	5	5	4.8
Red	4	4	5	5	5	4.6
Orange	2	2	1	2	1	1.6
Dark Green	0	0	1	0	0	0.2
Light Blue	0	0	0	0	0	0
Cyan	0	0	0	0	0	0

Condition 2

Separation Plate	0.00006	C
BP board	0.3	m
Bypass Motor	5	rad/sec

Total Recovered Charge: **12.72**

	Charge (*10^-7 C)	Number Recovered to Right Side, Test Run 1	2	3	4	5	Average	Sum
Pink	-1	0	0	0	0	0	0	25
Blue	-0.8	0	0	0	0	0	0	25
Purple	-0.6	0	0	0	0	0	0	25
Maroon	-0.4	0	1	0	0	0	0.2	25
Green	-0.2	0	0	0	0	0	0	25
Yellow	0	0	0	1	0	1	0.4	25
Red	0.2	1	0	1	0	2	0.8	25
Orange	0.4	3	3	4	3	2	3	25
Dark Green	0.6	5	5	3	4	5	4.4	25
Light Blue	0.8	5	5	5	5	5	5	25
Cyan	1	5	5	5	5	4	4.8	25

	Number Recovered to Left Side, Test Run 1	2	3	4	5	Average
Pink	5	5	5	5	5	5
Blue	5	5	5	5	5	5
Purple	5	5	5	5	5	5
Maroon	5	4	5	5	5	4.8
Green	5	5	5	5	5	5
Yellow	5	5	4	5	4	4.6
Red	4	5	4	5	3	4.2
Orange	2	2	1	2	3	2
Dark Green	0	0	2	1	0	0.6
Light Blue	0	0	0	0	0	0
Cyan	0	0	0	0	1	0.2

Condition 3

Separation Block	0.00006	C
BP board	0.5	m
Bypass Motor	5	rad/sec

Total Recovered Charge: **11.84**

	Charge (*10^-7 C)	Number Recovered to Right Side, Test Run 1	2	3	4	5	Average	Sum
Pink	-1	0	0	0	0	1	0.2	21
Blue	-0.8	1	0	0	1	0	0.4	25
Purple	-0.6	0	0	1	1	0	0.4	25
Maroon	-0.4	0	0	0	1	1	0.4	25
Green	-0.2	1	0	1	1	0	0.6	25
Yellow	0	0	0	1	3	3	1.4	25
Red	0.2	0	2	1	2	1	1.2	25
Orange	0.4	3	2	5	3	3	3.2	25
Dark Green	0.6	5	4	4	4	4	4.2	25
Light Blue	0.8	5	5	4	5	5	4.8	25
Cyan	1	5	5	5	5	5	5	25

	Number Recovered to Left Side, Test Run 1	2	3	4	5	Average
Pink	1	5	5	5	4	4
Blue	4	5	5	4	5	4.6
Purple	5	5	4	4	5	4.6
Maroon	5	5	5	4	4	4.6
Green	4	5	4	4	5	4.4
Yellow	5	5	4	2	2	3.6
Red	5	3	4	3	4	3.8
Orange	2	3	0	2	2	1.8
Dark Green	0	1	1	1	1	0.8
Light Blue	0	0	1	0	0	0.2
Cyan	0	0	0	0	0	0

Working Model Electrostatic Simulation

Simulation Information	
Date:	4.5.2013
Time:	4:11 PM
File Name1	Electrostatic_C12a_noBP.wm2d
File Name2	Electrostatic_C12a_withBP1.wm2d
File Name 3	Electrostatic_C12a_withBP2.wm2d
Circuit Name:	Cleaner-Recleaner/Countercurrent
Circuit No:	16
By:	Noble

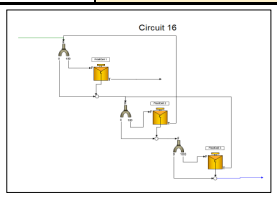

Summary					
Color --	Charge (*10^-7 C)	Feed Number	No BP Recovery	Med BP Recovery	High BP Recovery
Pink	-1	5	0	0	4
Blue	-0.8	5	0	4	8
Purple	-0.6	5	0	0	12
Maroon	-0.4	5	0	8	8
Green	-0.2	5	4	4	16
Yellow	0	5	8	20	36
Red	0.2	5	28	44	52
Orange	0.4	5	92	68	68
Dark Green	0.6	5	96	88	84
Light Blue	0.8	5	100	100	96
Cyan	1	5	100	100	100
Total Charge:		15	13.96	13.08	12.04

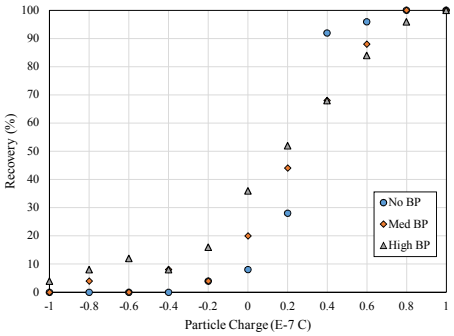

Condition 1

Separation Plate	0.00006	C
BP board	NA	m
Bypass Motor	NA	rad/sec

Total Recovered Charge: **13.96**

	Charge (*10^-7 C)	Number Recovered to Right Side, Test Run 1	2	3	4	5	Average	Sum
Pink	-1	0	0	0	0	0	0	25
Blue	-0.8	0	0	0	0	0	0	25
Purple	-0.6	0	0	0	0	0	0	25
Maroon	-0.4	0	0	0	0	0	0	25
Green	-0.2	0	1	0	0	0	0.2	25
Yellow	0	0	1	0	0	1	0.4	25
Red	0.2	1	2	1	2	1	1.4	25
Orange	0.4	5	5	4	4	5	4.6	25
Dark Green	0.6	5	5	4	5	5	4.8	25
Light Blue	0.8	5	5	5	5	5	5	25
Cyan	1	5	5	5	5	5	5	25

	Number Recovered to Left Side, Test Run 1	2	3	4	5	Average
Pink	5	5	5	5	5	5
Blue	5	5	5	5	5	5
Purple	5	5	5	5	5	5
Maroon	5	5	5	5	5	5
Green	5	4	5	5	5	4.8
Yellow	5	4	5	5	4	4.6
Red	4	3	4	3	4	3.6
Orange	0	0	1	1	0	0.4
Dark Green	0	0	1	0	0	0.2
Light Blue	0	0	0	0	0	0
Cyan	0	0	0	0	0	0

Condition 2

Separation Plate	0.00006	C
BP board	0.3	m
Bypass Motor	5	rad/sec

Total Recovered Charge: **13.08**

	Charge (*10^-7 C)	Number Recovered to Right Side, Test Run 1	2	3	4	5	Average	Sum
Pink	-1	0	0	0	0	0	0	25
Blue	-0.8	0	0	0	1	0	0.2	25
Purple	-0.6	0	0	0	0	0	0	25
Maroon	-0.4	0	1	0	0	1	0.4	25
Green	-0.2	0	0	1	0	0	0.2	25
Yellow	0	2	1	1	0	1	1	25
Red	0.2	4	2	2	1	2	2.2	25
Orange	0.4	4	4	4	3	2	3.4	25
Dark Green	0.6	5	5	3	4	5	4.4	25
Light Blue	0.8	5	5	5	5	5	5	25
Cyan	1	5	5	5	5	5	5	25

	Number Recovered to Left Side, Test Run 1	2	3	4	5	Average
Pink	5	5	5	5	5	5
Blue	5	5	5	4	5	4.8
Purple	5	5	5	5	5	5
Maroon	5	4	5	5	4	4.6
Green	5	5	4	5	5	4.8
Yellow	3	4	4	5	4	4
Red	1	3	3	4	3	2.8
Orange	1	1	1	2	3	1.6
Dark Green	0	0	2	1	0	0.6
Light Blue	0	0	0	0	0	0
Cyan	0	0	0	0	0	0

Condition 3

Separation Block	0.00006	C
BP board	0.5	m
Bypass Motor	5	rad/sec

Total Recovered Charge: **12.04**

	Charge (*10^-7 C)	Number Recovered to Right Side, Test Run 1	2	3	4	5	Average	Sum
Pink	-1	0	0	0	0	1	0.2	21
Blue	-0.8	1	0	0	1	0	0.4	25
Purple	-0.6	0	0	2	1	0	0.6	25
Maroon	-0.4	0	0	0	1	1	0.4	24
Green	-0.2	1	0	2	1	0	0.8	26
Yellow	0	0	1	2	3	3	1.8	25
Red	0.2	2	4	3	2	2	2.6	25
Orange	0.4	4	2	5	3	3	3.4	25
Dark Green	0.6	5	4	4	4	4	4.2	25
Light Blue	0.8	5	5	4	5	5	4.8	25
Cyan	1	5	5	5	5	5	5	25

	Number Recovered to Left Side, Test Run 1	2	3	4	5	Average
Pink	1	5	5	5	4	4
Blue	4	5	5	4	5	4.6
Purple	5	5	3	4	5	4.4
Maroon	4	5	5	4	4	4.4
Green	5	5	3	4	5	4.4
Yellow	5	4	3	2	2	3.2
Red	3	1	2	3	3	2.4
Orange	1	3	0	2	2	1.6
Dark Green	0	1	1	1	1	0.8
Light Blue	0	0	1	0	0	0.2
Cyan	0	0	0	0	0	0

Working Model Electrostatic Simulation

Simulation Information	
Date:	4.5.2013
Time:	4:11 PM
File Name1	Electrostatic_C12a_noBP.wm2d
File Name2	Electrostatic_C12a_withBP1.wm2d
File Name 3	Electrostatic_C12a_withBP2.wm2d
Circuit Name:	Cleaner-Recleaner/All to Head
Circuit No:	17
By:	Noble

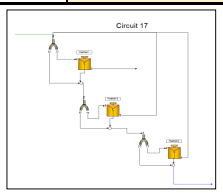

Summary					
Color --	Charge (*10^-7 C)	Feed Number	No BP Recovery	Med BP Recovery	High BP Recovery
Pink	-1	5	0	0	4
Blue	-0.8	5	0	0	8
Purple	-0.6	5	0	0	8
Maroon	-0.4	5	0	12	8
Green	-0.2	5	4	0	16
Yellow	0	5	4	24	32
Red	0.2	5	32	24	48
Orange	0.4	5	80	68	68
Dark Green	0.6	5	96	88	84
Light Blue	0.8	5	100	100	96
Cyan	1	5	100	100	100
Total Charge:		15	13.76	13	12.12

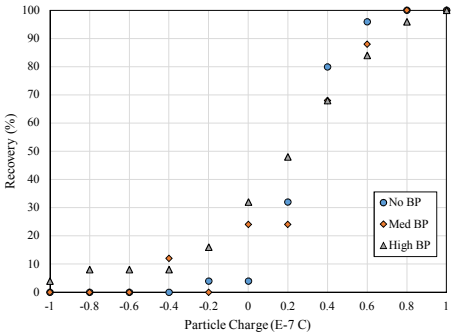

Condition 1

Separation Plate	0.00006	C
BP board	NA	m
Bypass Motor	NA	rad/sec

Total Recovered Charge: **13.76**

	Charge (*10^-7 C)	Number Recovered to Right Side, Test Run 1	2	3	4	5	Average	Sum
Pink	-1	0	0	0	0	0	0	25
Blue	-0.8	0	0	0	0	0	0	25
Purple	-0.6	0	0	0	0	0	0	25
Maroon	-0.4	0	0	0	0	0	0	25
Green	-0.2	0	1	0	0	0	0.2	25
Yellow	0	0	1	0	0	0	0.2	25
Red	0.2	1	3	0	2	2	1.6	25
Orange	0.4	4	3	4	4	5	4	25
Dark Green	0.6	5	5	4	5	5	4.8	25
Light Blue	0.8	5	5	5	5	5	5	25
Cyan	1	5	5	5	5	5	5	25

	Number Recovered to Left Side, Test Run 1	2	3	4	5	Average
Pink	5	5	5	5	5	5
Blue	5	5	5	5	5	5
Purple	5	5	5	5	5	5
Maroon	5	5	5	5	5	5
Green	5	4	5	5	5	4.8
Yellow	5	4	5	5	5	4.8
Red	4	2	5	3	3	3.4
Orange	1	2	1	1	0	1
Dark Green	0	0	1	0	0	0.2
Light Blue	0	0	0	0	0	0
Cyan	0	0	0	0	0	0

Condition 2

Separation Plate	0.00006	C
BP board	0.3	m
Bypass Motor	5	rad/sec

Total Recovered Charge: **13**

	Charge (*10^-7 C)	Number Recovered to Right Side, Test Run 1	2	3	4	5	Average	Sum
Pink	-1	0	0	0	0	0	0	25
Blue	-0.8	0	0	0	0	0	0	25
Purple	-0.6	0	0	0	0	0	0	25
Maroon	-0.4	0	1	0	2	0	0.6	25
Green	-0.2	0	0	0	0	0	0	25
Yellow	0	1	1	1	0	3	1.2	25
Red	0.2	1	1	2	0	2	1.2	25
Orange	0.4	4	4	4	3	2	3.4	25
Dark Green	0.6	5	5	3	4	5	4.4	25
Light Blue	0.8	5	5	5	5	5	5	25
Cyan	1	5	5	5	5	5	5	25

	Number Recovered to Left Side, Test Run 1	2	3	4	5	Average
Pink	5	5	5	5	5	5
Blue	5	5	5	5	5	5
Purple	5	5	5	5	5	5
Maroon	5	4	5	3	5	4.4
Green	5	5	5	5	5	5
Yellow	4	4	4	5	2	3.8
Red	4	4	3	5	3	3.8
Orange	1	1	1	2	3	1.6
Dark Green	0	0	2	1	0	0.6
Light Blue	0	0	0	0	0	0
Cyan	0	0	0	0	0	0

Condition 3

Separation Block	0.00006	C
BP board	0.5	m
Bypass Motor	5	rad/sec

Total Recovered Charge: **12.12**

	Charge (*10^-7 C)	Number Recovered to Right Side, Test Run 1	2	3	4	5	Average	Sum
Pink	-1	0	0	0	0	1	0.2	25
Blue	-0.8	1	0	0	1	0	0.4	25
Purple	-0.6	0	0	1	1	0	0.4	25
Maroon	-0.4	0	0	0	1	1	0.4	25
Green	-0.2	1	0	2	1	0	0.8	25
Yellow	0	1	0	1	3	3	1.6	25
Red	0.2	2	3	3	2	2	2.4	25
Orange	0.4	4	2	5	3	3	3.4	25
Dark Green	0.6	5	4	4	4	4	4.2	25
Light Blue	0.8	5	5	4	5	5	4.8	25
Cyan	1	5	5	5	5	5	5	25

	Number Recovered to Left Side, Test Run 1	2	3	4	5	Average
Pink	5	5	5	5	4	4.8
Blue	4	5	5	4	5	4.6
Purple	5	5	4	4	5	4.6
Maroon	5	5	5	4	4	4.6
Green	4	5	3	4	5	4.2
Yellow	4	5	4	2	2	3.4
Red	3	2	2	3	3	2.6
Orange	1	3	0	2	2	1.6
Dark Green	0	1	1	1	1	0.8
Light Blue	0	0	1	0	0	0.2
Cyan	0	0	0	0	0	0

Working Model Electrostatic Simulation

Simulation Information	
Date:	3.21.2013
Time:	10:30 AM
File Name1	Electrostatic_C26a_noBP.wm2d
File Name2	Electrostatic_C26a_withBP1.wm2d
File Name 3	Electrostatic_C26a_withBP2.wm2d
Circuit Name:	RSC - Scav. Con to cleaner
Circuit No:	26
By:	Noble

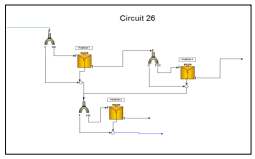

Summary					
Color --	Charge (*10^-7 C)	Feed Number	No BP Recovery	Med BP Recovery	High BP Recovery
Pink	-1	5	4	4	8
Blue	-0.8	5	0	12	8
Purple	-0.6	5	4	4	16
Maroon	-0.4	5	8	24	20
Green	-0.2	5	16	8	20
Yellow	0	5	8	24	28
Red	0.2	5	24	28	40
Orange	0.4	5	80	72	64
Dark Green	0.6	5	96	100	100
Light Blue	0.8	5	100	100	100
Cyan	1	5	100	96	96
Total Charge:		15	13.08	12.16	11.68

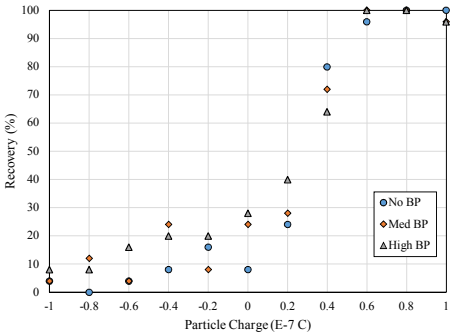

Condition 1

Separation Plate	0.00006	C
BP board	NA	m
Bypass Motor	NA	rad/sec

Total Recovered Charge: **13.08**

	Charge (*10^-7 C)	Number Recovered to Right Side, Test Run 1	2	3	4	5	Average	Sum
Pink	-1	0	0	0	1	0	0.2	25
Blue	-0.8	0	0	0	0	0	0	25
Purple	-0.6	1	0	0	0	0	0.2	25
Maroon	-0.4	1	1	0	0	0	0.4	25
Green	-0.2	1	1	1	1	0	0.8	25
Yellow	0	1	1	0	0	0	0.4	25
Red	0.2	1	0	3	2	0	1.2	25
Orange	0.4	3	3	4	5	5	4	25
Dark Green	0.6	5	5	4	5	5	4.8	25
Light Blue	0.8	5	5	5	5	5	5	25
Cyan	1	5	5	5	5	5	5	25

	Number Recovered to Left Side, Test Run 1	2	3	4	5	Average
Pink	5	5	5	4	5	4.8
Blue	5	5	5	5	5	5
Purple	4	5	5	5	5	4.8
Maroon	4	4	5	5	5	4.6
Green	4	4	4	4	5	4.2
Yellow	4	4	5	5	5	4.6
Red	4	5	2	3	5	3.8
Orange	2	2	1	0	0	1
Dark Green	0	0	1	0	0	0.2
Light Blue	0	0	0	0	0	0
Cyan	0	0	0	0	0	0

Condition 2

Separation Plate	0.00006	C
BP board	0.3	m
Bypass Motor	5	rad/sec

Total Recovered Charge: **12.16**

	Charge (*10^-7 C)	Number Recovered to Right Side, Test Run 1	2	3	4	5	Average	Sum
Pink	-1	0	0	1	0	0	0.2	25
Blue	-0.8	1	1	0	1	0	0.6	25
Purple	-0.6	0	0	1	0	0	0.2	25
Maroon	-0.4	3	1	0	2	0	1.2	25
Green	-0.2	0	0	0	1	1	0.4	25
Yellow	0	1	1	1	0	3	1.2	25
Red	0.2	0	2	1	3	1	1.4	25
Orange	0.4	2	3	4	5	4	3.6	25
Dark Green	0.6	5	5	5	5	5	5	25
Light Blue	0.8	5	5	5	5	5	5	25
Cyan	1	5	5	5	5	4	4.8	25

	Number Recovered to Left Side, Test Run 1	2	3	4	5	Average
Pink	5	5	4	5	5	4.8
Blue	4	4	5	4	5	4.4
Purple	5	5	4	5	5	4.8
Maroon	2	4	5	3	5	3.8
Green	5	5	5	4	4	4.6
Yellow	4	4	4	5	2	3.8
Red	5	3	4	2	4	3.6
Orange	3	2	1	0	1	1.4
Dark Green	0	0	0	0	0	0
Light Blue	0	0	0	0	0	0
Cyan	0	0	0	0	1	0.2

Condition 3

Separation Block	0.00006	C
BP board	0.5	m
Bypass Motor	5	rad/sec

Total Recovered Charge: **11.68**

	Charge (*10^-7 C)	Number Recovered to Right Side, Test Run 1	2	3	4	5	Average	Sum
Pink	-1	0	0	1	1	0	0.4	25
Blue	-0.8	0	0	1	1	0	0.4	25
Purple	-0.6	0	0	2	0	2	0.8	25
Maroon	-0.4	1	2	0	2	0	1	25
Green	-0.2	1	1	0	2	1	1	25
Yellow	0	1	2	1	1	2	1.4	25
Red	0.2	0	1	4	2	3	2	25
Orange	0.4	3	4	4	4	1	3.2	25
Dark Green	0.6	5	5	5	5	5	5	25
Light Blue	0.8	5	5	5	5	5	5	25
Cyan	1	5	4	5	5	5	4.8	25

	Number Recovered to Left Side, Test Run 1	2	3	4	5	Average
Pink	5	5	4	4	5	4.6
Blue	5	5	4	4	5	4.6
Purple	5	5	3	5	3	4.2
Maroon	4	3	5	3	5	4
Green	4	4	5	3	4	4
Yellow	4	3	4	4	3	3.6
Red	5	4	1	3	2	3
Orange	2	1	1	1	4	1.8
Dark Green	0	0	0	0	0	0
Light Blue	0	0	0	0	0	0
Cyan	0	1	0	0	0	0.2

Working Model Electrostatic Simulation

Simulation Information	
Date:	3.21.2013
Time:	11:00 AM
File Name1	Electrostatic_C27a_noBP.wm2d
File Name2	Electrostatic_C27a_withBP1.wm2d
File Name 3	Electrostatic_C27a_withBP2.wm2d
Circuit Name:	RSC - Cleaner tail to Scavenger
Circuit No:	27
By:	Noble

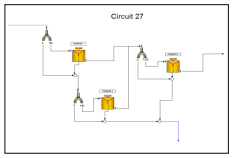

Summary					
Color --	Charge (*10^-7 C)	Feed Number	No BP Recovery	Med BP Recovery	High BP Recovery
Pink	-1	5	16	24	24
Blue	-0.8	5	16	28	28
Purple	-0.6	5	24	24	52
Maroon	-0.4	5	28	40	44
Green	-0.2	5	32	16	44
Yellow	0	5	36	48	56
Red	0.2	5	56	52	76
Orange	0.4	5	96	88	92
Dark Green	0.6	5	100	100	100
Light Blue	0.8	5	100	100	100
Cyan	1	5	100	100	100
Total Charge:		15	11.44	10.28	9.4

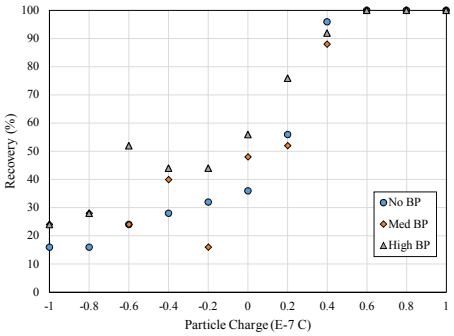

Condition 1

Separation Plate	0.00006	C
BP board	NA	m
Bypass Motor	NA	rad/sec

Total Recovered Charge: **11.44**

	Charge (*10^-7 C)	Number Recovered to Right Side, Test Run 1	2	3	4	5	Average	Sum
Pink	-1	0	0	1	1	2	0.8	25
Blue	-0.8	1	2	1	0	0	0.8	25
Purple	-0.6	3	1	1	0	1	1.2	25
Maroon	-0.4	1	1	2	1	2	1.4	25
Green	-0.2	2	1	2	2	1	1.6	25
Yellow	0	1	2	2	2	2	1.8	25
Red	0.2	3	3	4	4	0	2.8	25
Orange	0.4	5	5	4	5	5	4.8	25
Dark Green	0.6	5	5	5	5	5	5	25
Light Blue	0.8	5	5	5	5	5	5	25
Cyan	1	5	5	5	5	5	5	25

	Number Recovered to Left Side, Test Run 1	2	3	4	5	Average
Pink	5	5	4	4	3	4.2
Blue	4	3	4	5	5	4.2
Purple	2	4	4	5	4	3.8
Maroon	4	4	3	4	3	3.6
Green	3	4	3	3	4	3.4
Yellow	4	3	3	3	3	3.2
Red	2	2	1	1	5	2.2
Orange	0	0	1	0	0	0.2
Dark Green	0	0	0	0	0	0
Light Blue	0	0	0	0	0	0
Cyan	0	0	0	0	0	0

Condition 2

Separation Plate	0.00006	C
BP board	0.3	m
Bypass Motor	5	rad/sec

Total Recovered Charge: **10.28**

	Charge (*10^-7 C)	Number Recovered to Right Side, Test Run 1	2	3	4	5	Average	Sum
Pink	-1	0	2	1	0	3	1.2	25
Blue	-0.8	2	2	0	2	1	1.4	25
Purple	-0.6	1	0	2	1	2	1.2	25
Maroon	-0.4	5	2	0	2	1	2	25
Green	-0.2	1	1	0	1	1	0.8	25
Yellow	0	2	2	3	2	3	2.4	25
Red	0.2	3	3	2	4	1	2.6	25
Orange	0.4	4	3	5	5	5	4.4	25
Dark Green	0.6	5	5	5	5	5	5	25
Light Blue	0.8	5	5	5	5	5	5	25
Cyan	1	5	5	5	5	5	5	25

	Number Recovered to Left Side, Test Run 1	2	3	4	5	Average
Pink	5	3	4	5	2	3.8
Blue	3	3	5	3	4	3.6
Purple	4	5	3	4	3	3.8
Maroon	0	3	5	3	4	3
Green	4	4	5	4	4	4.2
Yellow	3	3	2	3	2	2.6
Red	2	2	3	1	4	2.4
Orange	1	2	0	0	0	0.6
Dark Green	0	0	0	0	0	0
Light Blue	0	0	0	0	0	0
Cyan	0	0	0	0	0	0

Condition 3

Separation Block	0.00006	C
BP board	0.5	m
Bypass Motor	5	rad/sec

Total Recovered Charge: **9.4**

	Charge (*10^-7 C)	Number Recovered to Right Side, Test Run 1	2	3	4	5	Average	Sum
Pink	-1	1	1	2	2	0	1.2	25
Blue	-0.8	1	1	3	1	1	1.4	25
Purple	-0.6	3	2	3	2	3	2.6	25
Maroon	-0.4	4	2	0	2	3	2.2	25
Green	-0.2	4	2	1	2	2	2.2	25
Yellow	0	3	4	1	3	3	2.8	25
Red	0.2	1	5	4	4	5	3.8	25
Orange	0.4	5	5	4	5	4	4.6	25
Dark Green	0.6	5	5	5	5	5	5	25
Light Blue	0.8	5	5	5	5	5	5	25
Cyan	1	5	5	5	5	5	5	25

	Number Recovered to Left Side, Test Run 1	2	3	4	5	Average
Pink	4	4	3	3	5	3.8
Blue	4	4	2	4	4	3.6
Purple	2	3	2	3	2	2.4
Maroon	1	3	5	3	2	2.8
Green	1	3	4	3	3	2.8
Yellow	2	1	4	2	2	2.2
Red	4	0	1	1	0	1.2
Orange	0	0	1	0	1	0.4
Dark Green	0	0	0	0	0	0
Light Blue	0	0	0	0	0	0
Cyan	0	0	0	0	0	0

Working Model Electrostatic Simulation

Simulation Information	
Date:	3.21.2013
Time:	11:00 AM
File Name1	Electrostatic_C28a_noBP.wm2d
File Name2	Electrostatic_C28a_withBP1.wm2d
File Name 3	Electrostatic_C28a_withBP2.wm2d
Circuit Name:	RSC - Double Cross
Circuit No:	28
By:	Noble

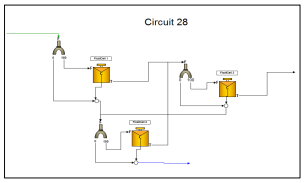

Summary					
Color --	Charge (*10^-7 C)	Feed Number	No BP Recovery	Med BP Recovery	High BP Recovery
Pink	-1	5	8	4	12
Blue	-0.8	5	4	12	12
Purple	-0.6	5	4	12	28
Maroon	-0.4	5	4	16	32
Green	-0.2	5	12	12	40
Yellow	0	5	8	36	48
Red	0.2	5	40	44	60
Orange	0.4	5	92	96	96
Dark Green	0.6	5	100	100	100
Light Blue	0.8	5	100	100	100
Cyan	1	5	100	100	100
Total Charge:		15	13.36	12.88	11.56

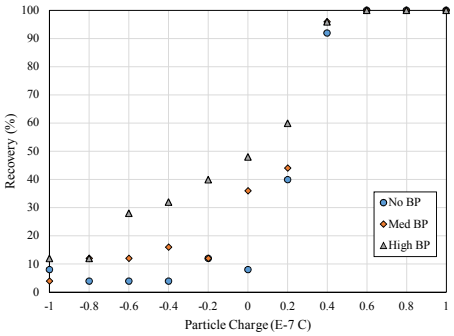

Condition 1

Separation Plate	0.00006	C
BP board	NA	m
Bypass Motor	NA	rad/sec

Total Recovered Charge: **13.36**

	Charge (*10^-7 C)	Number Recovered to Right Side, Test Run 1	2	3	4	5	Average	Sum
Pink	-1	0	0	0	1	1	0.4	25
Blue	-0.8	0	1	0	0	0	0.2	25
Purple	-0.6	1	0	0	0	0	0.2	25
Maroon	-0.4	0	1	0	0	0	0.2	25
Green	-0.2	1	0	0	1	1	0.6	25
Yellow	0	1	1	0	0	0	0.4	25
Red	0.2	3	1	2	3	1	2	25
Orange	0.4	5	4	5	4	5	4.6	25
Dark Green	0.6	5	5	5	5	5	5	25
Light Blue	0.8	5	5	5	5	5	5	25
Cyan	1	5	5	5	5	5	5	25

	Number Recovered to Left Side, Test Run 1	2	3	4	5	Average
Pink	5	5	5	4	4	4.6
Blue	5	4	5	5	5	4.8
Purple	4	5	5	5	5	4.8
Maroon	5	4	5	5	5	4.8
Green	4	5	5	4	4	4.4
Yellow	4	4	5	5	5	4.6
Red	2	4	3	2	4	3
Orange	0	1	0	1	0	0.4
Dark Green	0	0	0	0	0	0
Light Blue	0	0	0	0	0	0
Cyan	0	0	0	0	0	0

Condition 2

Separation Plate	0.00006	C
BP board	0.3	m
Bypass Motor	5	rad/sec

Total Recovered Charge: **12.88**

	Charge (*10^-7 C)	Number Recovered to Right Side, Test Run 1	2	3	4	5	Average	Sum
Pink	-1	0	0	1	0	0	0.2	25
Blue	-0.8	1	1	0	1	0	0.6	25
Purple	-0.6	0	0	1	1	1	0.6	25
Maroon	-0.4	1	0	0	2	1	0.8	25
Green	-0.2	0	0	1	1	1	0.6	25
Yellow	0	1	1	3	0	4	1.8	25
Red	0.2	1	2	2	3	3	2.2	25
Orange	0.4	4	5	5	5	5	4.8	25
Dark Green	0.6	5	5	5	5	5	5	25
Light Blue	0.8	5	5	5	5	5	5	25
Cyan	1	5	5	5	5	5	5	25

	Number Recovered to Left Side, Test Run 1	2	3	4	5	Average
Pink	5	5	4	5	5	4.8
Blue	4	4	5	4	5	4.4
Purple	5	5	4	4	4	4.4
Maroon	4	5	5	3	4	4.2
Green	5	5	4	4	4	4.4
Yellow	4	4	2	5	1	3.2
Red	4	3	3	2	2	2.8
Orange	1	0	0	0	0	0.2
Dark Green	0	0	0	0	0	0
Light Blue	0	0	0	0	0	0
Cyan	0	0	0	0	0	0

Condition 3

Separation Block	0.00006	C
BP board	0.5	m
Bypass Motor	5	rad/sec

Total Recovered Charge: **11.56**

	Charge (*10^-7 C)	Number Recovered to Right Side, Test Run 1	2	3	4	5	Average	Sum
Pink	-1	0	0	1	2	0	0.6	25
Blue	-0.8	0	0	2	0	1	0.6	25
Purple	-0.6	1	0	2	2	2	1.4	25
Maroon	-0.4	2	2	0	3	1	1.6	25
Green	-0.2	3	2	1	3	1	2	25
Yellow	0	2	3	1	4	2	2.4	25
Red	0.2	0	5	4	2	4	3	25
Orange	0.4	5	5	5	5	4	4.8	25
Dark Green	0.6	5	5	5	5	5	5	25
Light Blue	0.8	5	5	5	5	5	5	25
Cyan	1	5	5	5	5	5	5	25

	Number Recovered to Left Side, Test Run 1	2	3	4	5	Average
Pink	5	5	4	3	5	4.4
Blue	5	5	3	5	4	4.4
Purple	4	5	3	3	3	3.6
Maroon	3	3	5	2	4	3.4
Green	2	3	4	2	4	3
Yellow	3	2	4	1	3	2.6
Red	5	0	1	3	1	2
Orange	0	0	0	0	1	0.2
Dark Green	0	0	0	0	0	0
Light Blue	0	0	0	0	0	0
Cyan	0	0	0	0	0	0

Working Model Electrostatic Simulation

Simulation Information	
Date:	3.21.2013
Time:	4:00 PM
File Name1	Electrostatic_C29a_noBP.wm2d
File Name2	Electrostatic_C29a_withBP1.wm2d
File Name 3	Electrostatic_C29a_withBP2.wm2d
Circuit Name:	RSC - Cleaner tails to Feed
Circuit No:	29
By:	Noble

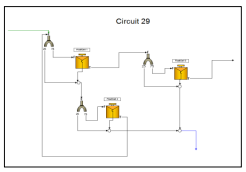

Summary					
Color --	Charge (*10^-7 C)	Feed Number	No BP Recovery	Med BP Recovery	High BP Recovery
Pink	-1	5	16	16	32
Blue	-0.8	5	12	28	44
Purple	-0.6	5	24	24	60
Maroon	-0.4	5	28	48	68
Green	-0.2	5	48	32	56
Yellow	0	5	28	68	60
Red	0.2	5	76	60	80
Orange	0.4	5	96	96	96
Dark Green	0.6	5	100	100	100
Light Blue	0.8	5	100	100	100
Cyan	1	5	100	100	100
Total Charge:		15	11.64	10.6	7.64

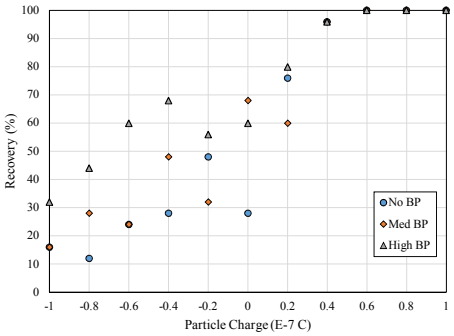

Condition 1

Separation Plate	0.00006	C
BP board	NA	m
Bypass Motor	NA	rad/sec

Total Recovered Charge: **11.64**

	Charge (*10^-7 C)	Number Recovered to Right Side, Test Run 1	2	3	4	5	Average	Sum
Pink	-1	0	0	1	1	2	0.8	25
Blue	-0.8	1	1	1	0	0	0.6	25
Purple	-0.6	3	1	1	0	1	1.2	25
Maroon	-0.4	2	1	1	1	2	1.4	25
Green	-0.2	3	2	2	3	2	2.4	25
Yellow	0	1	2	0	2	2	1.4	25
Red	0.2	4	3	4	5	3	3.8	25
Orange	0.4	4	5	5	5	5	4.8	25
Dark Green	0.6	5	5	5	5	5	5	25
Light Blue	0.8	5	5	5	5	5	5	25
Cyan	1	5	5	5	5	5	5	25

	Number Recovered to Left Side, Test Run 1	2	3	4	5	Average
Pink	5	5	4	4	3	4.2
Blue	4	4	4	5	5	4.4
Purple	2	4	4	5	4	3.8
Maroon	3	4	4	4	3	3.6
Green	2	3	3	2	3	2.6
Yellow	4	3	5	3	3	3.6
Red	1	2	1	0	2	1.2
Orange	1	0	0	0	0	0.2
Dark Green	0	0	0	0	0	0
Light Blue	0	0	0	0	0	0
Cyan	0	0	0	0	0	0

Condition 2

Separation Plate	0.00006	C
BP board	0.3	m
Bypass Motor	5	rad/sec

Total Recovered Charge: **10.6**

	Charge (*10^-7 C)	Number Recovered to Right Side, Test Run 1	2	3	4	5	Average	Sum
Pink	-1	0	0	2	0	2	0.8	25
Blue	-0.8	2	1	1	2	1	1.4	25
Purple	-0.6	1	0	2	1	2	1.2	25
Maroon	-0.4	5	2	0	4	1	2.4	25
Green	-0.2	2	3	1	1	1	1.6	25
Yellow	0	4	3	3	3	4	3.4	25
Red	0.2	3	3	2	5	2	3	25
Orange	0.4	4	5	5	5	5	4.8	25
Dark Green	0.6	5	5	5	5	5	5	25
Light Blue	0.8	5	5	5	5	5	5	25
Cyan	1	5	5	5	5	5	5	25

	Number Recovered to Left Side, Test Run 1	2	3	4	5	Average
Pink	5	5	3	5	3	4.2
Blue	3	4	4	3	4	3.6
Purple	4	5	3	4	3	3.8
Maroon	0	3	5	1	4	2.6
Green	3	2	4	4	4	3.4
Yellow	1	2	2	2	1	1.6
Red	2	2	3	0	3	2
Orange	1	0	0	0	0	0.2
Dark Green	0	0	0	0	0	0
Light Blue	0	0	0	0	0	0
Cyan	0	0	0	0	0	0

Condition 3

Separation Block	0.00006	C
BP board	0.5	m
Bypass Motor	5	rad/sec

Total Recovered Charge: **7.64**

	Charge (*10^-7 C)	Number Recovered to Right Side, Test Run 1	2	3	4	5	Average	Sum
Pink	-1	1	1	3	2	1	1.6	25
Blue	-0.8	2	2	4	2	1	2.2	25
Purple	-0.6	4	1	4	3	3	3	25
Maroon	-0.4	5	3	1	5	3	3.4	25
Green	-0.2	4	3	2	3	2	2.8	25
Yellow	0	2	2	4	3	4	3	25
Red	0.2	2	4	5	5	4	4	25
Orange	0.4	5	5	5	5	4	4.8	25
Dark Green	0.6	5	5	5	5	5	5	25
Light Blue	0.8	5	5	5	5	5	5	25
Cyan	1	5	5	5	5	5	5	25

	Number Recovered to Left Side, Test Run 1	2	3	4	5	Average
Pink	4	4	2	3	4	3.4
Blue	3	3	1	3	4	2.8
Purple	1	4	1	2	2	2
Maroon	0	2	4	0	2	1.6
Green	1	2	3	2	3	2.2
Yellow	3	3	1	2	1	2
Red	3	1	0	0	1	1
Orange	0	0	0	0	1	0.2
Dark Green	0	0	0	0	0	0
Light Blue	0	0	0	0	0	0
Cyan	0	0	0	0	0	0

Working Model Electrostatic Simulation

Simulation Information	
Date:	3.21.2013
Time:	10:15 PM
File Name1	Electrostatic_C30a_noBP.wm2d
File Name2	Electrostatic_C30a_withBP1.wm2d
File Name 3	Electrostatic_C30a_withBP2.wm2d
Circuit Name:	RSC - Full Recylce
Circuit No:	30
By:	Noble

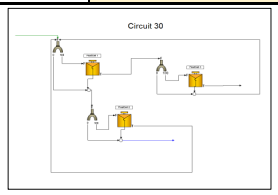

Summary					
Color --	Charge (*10^-7 C)	Feed Number	No BP Recovery	Med BP Recovery	High BP Recovery
Pink	-1	5	4	8	12
Blue	-0.8	5	0	16	16
Purple	-0.6	5	4	12	20
Maroon	-0.4	5	4	20	40
Green	-0.2	5	16	24	40
Yellow	0	5	40	32	52
Red	0.2	5	68	60	76
Orange	0.4	5	96	92	88
Dark Green	0.6	5	100	100	100
Light Blue	0.8	5	100	100	100
Cyan	1	5	100	100	100
Total Charge:		15	14.04	12.4	11.48

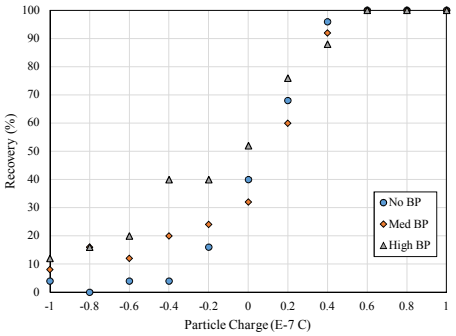

Condition 1

Separation Plate	0.00006	C
BP board	NA	m
Bypass Motor	NA	rad/sec

Total Recovered Charge: **14.04**

	Charge (*10^-7 C)	Number Recovered to Right Side, Test Run 1	2	3	4	5	Average	Sum
Pink	-1	0	0	0	1	0	0.2	25
Blue	-0.8	0	0	0	0	0	0	25
Purple	-0.6	1	0	0	0	0	0.2	25
Maroon	-0.4	0	1	0	0	0	0.2	25
Green	-0.2	1	0	1	1	1	0.8	25
Yellow	0	3	1	0	3	3	2	25
Red	0.2	5	3	3	2	4	3.4	25
Orange	0.4	5	5	5	4	5	4.8	25
Dark Green	0.6	5	5	5	5	5	5	25
Light Blue	0.8	5	5	5	5	5	5	25
Cyan	1	5	5	5	5	5	5	25

	Number Recovered to Left Side, Test Run 1	2	3	4	5	Average
Pink	5	5	5	4	5	4.8
Blue	5	5	5	5	5	5
Purple	4	5	5	5	5	4.8
Maroon	5	4	5	5	5	4.8
Green	4	5	4	4	4	4.2
Yellow	2	4	5	2	2	3
Red	0	2	2	3	1	1.6
Orange	0	0	0	1	0	0.2
Dark Green	0	0	0	0	0	0
Light Blue	0	0	0	0	0	0
Cyan	0	0	0	0	0	0

Condition 2

Separation Plate	0.00006	C
BP board	0.3	m
Bypass Motor	5	rad/sec

Total Recovered Charge: **12.4**

	Charge (*10^-7 C)	Number Recovered to Right Side, Test Run 1	2	3	4	5	Average	Sum
Pink	-1	0	0	1	0	1	0.4	25
Blue	-0.8	0	1	0	3	0	0.8	25
Purple	-0.6	0	0	2	0	1	0.6	25
Maroon	-0.4	1	1	0	3	0	1	25
Green	-0.2	3	0	1	1	1	1.2	25
Yellow	0	3	0	1	1	3	1.6	25
Red	0.2	3	4	1	4	3	3	25
Orange	0.4	3	5	5	5	5	4.6	25
Dark Green	0.6	5	5	5	5	5	5	25
Light Blue	0.8	5	5	5	5	5	5	25
Cyan	1	5	5	5	5	5	5	25

	Number Recovered to Left Side, Test Run 1	2	3	4	5	Average
Pink	5	5	4	5	4	4.6
Blue	5	4	5	2	5	4.2
Purple	5	5	3	5	4	4.4
Maroon	4	4	5	2	5	4
Green	2	5	4	4	4	3.8
Yellow	2	5	4	4	2	3.4
Red	2	1	4	1	2	2
Orange	2	0	0	0	0	0.4
Dark Green	0	0	0	0	0	0
Light Blue	0	0	0	0	0	0
Cyan	0	0	0	0	0	0

Condition 3

Separation Block	0.00006	C
BP board	0.5	m
Bypass Motor	5	rad/sec

Total Recovered Charge: **11.48**

	Charge (*10^-7 C)	Number Recovered to Right Side, Test Run 1	2	3	4	5	Average	Sum
Pink	-1	0	0	2	1	0	0.6	25
Blue	-0.8	0	0	1	1	2	0.8	25
Purple	-0.6	1	0	2	0	2	1	25
Maroon	-0.4	3	2	0	3	2	2	25
Green	-0.2	2	1	1	3	3	2	25
Yellow	0	3	3	2	2	3	2.6	25
Red	0.2	3	3	5	4	4	3.8	25
Orange	0.4	4	5	5	4	4	4.4	25
Dark Green	0.6	5	5	5	5	5	5	25
Light Blue	0.8	5	5	5	5	5	5	25
Cyan	1	5	5	5	5	5	5	25

	Number Recovered to Left Side, Test Run 1	2	3	4	5	Average
Pink	5	5	3	4	5	4.4
Blue	5	5	4	4	3	4.2
Purple	4	5	3	5	3	4
Maroon	2	3	5	2	3	3
Green	3	4	4	2	2	3
Yellow	2	2	3	3	2	2.4
Red	2	2	0	1	1	1.2
Orange	1	0	0	1	1	0.6
Dark Green	0	0	0	0	0	0
Light Blue	0	0	0	0	0	0
Cyan	0	0	0	0	0	0

Working Model Electrostatic Simulation

Simulation Information	
Date:	3.21.2013
Time:	9:00 PM
File Name1	Electrostatic_C31a_noBP.wm2d
File Name2	Electrostatic_C31a_withBP1.wm2d
File Name 3	Electrostatic_C31a_withBP2.wm2d
Circuit Name:	RSC - Scavenger con to feed
Circuit No:	31
By:	Noble

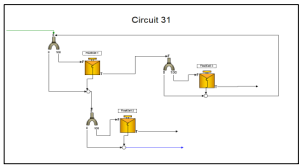

Summary					
Color --	Charge (*10^-7 C)	Feed Number	No BP Recovery	Med BP Recovery	High BP Recovery
Pink	-1	5	4	4	8
Blue	-0.8	5	0	8	4
Purple	-0.6	5	8	4	16
Maroon	-0.4	5	4	4	24
Green	-0.2	5	8	8	24
Yellow	0	5	4	20	16
Red	0.2	5	16	24	32
Orange	0.4	5	76	72	64
Dark Green	0.6	5	96	100	100
Light Blue	0.8	5	100	100	100
Cyan	1	5	100	96	96
Total Charge:		15	12.96	12.68	11.64

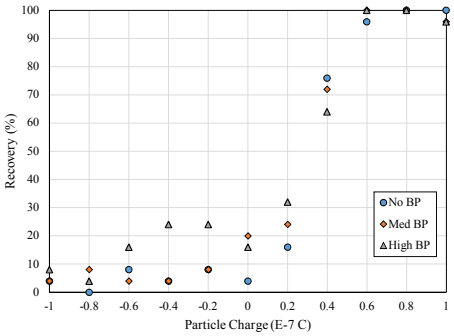

Condition 1

Separation Plate	0.00006	C
BP board	NA	m
Bypass Motor	NA	rad/sec

Total Recovered Charge: **12.96**

	Charge (*10^-7 C)	Number Recovered to Right Side, Test Run 1	2	3	4	5	Average	Sum
Pink	-1	0	0	0	1	0	0.2	25
Blue	-0.8	0	0	0	0	0	0	25
Purple	-0.6	1	0	1	0	0	0.4	25
Maroon	-0.4	0	1	0	0	0	0.2	25
Green	-0.2	1	0	0	1	0	0.4	25
Yellow	0	1	0	0	0	0	0.2	25
Red	0.2	1	0	2	1	0	0.8	25
Orange	0.4	3	3	4	4	5	3.8	25
Dark Green	0.6	5	5	4	5	5	4.8	25
Light Blue	0.8	5	5	5	5	5	5	25
Cyan	1	5	5	5	5	5	5	25

	Number Recovered to Left Side, Test Run 1	2	3	4	5	Average
Pink	5	5	5	4	5	4.8
Blue	5	5	5	5	5	5
Purple	4	5	4	5	5	4.6
Maroon	5	4	5	5	5	4.8
Green	4	5	5	4	5	4.6
Yellow	4	5	5	5	5	4.8
Red	4	5	3	4	5	4.2
Orange	2	2	1	1	0	1.2
Dark Green	0	0	1	0	0	0.2
Light Blue	0	0	0	0	0	0
Cyan	0	0	0	0	0	0

Condition 2

Separation Plate	0.00006	C
BP board	0.3	m
Bypass Motor	5	rad/sec

Total Recovered Charge: **12.68**

	Charge (*10^-7 C)	Number Recovered to Right Side, Test Run 1	2	3	4	5	Average	Sum
Pink	-1	0	0	1	0	0	0.2	25
Blue	-0.8	0	1	0	1	0	0.4	25
Purple	-0.6	0	0	1	0	0	0.2	25
Maroon	-0.4	0	0	0	1	0	0.2	25
Green	-0.2	0	0	0	1	1	0.4	25
Yellow	0	1	1	0	0	3	1	25
Red	0.2	0	2	0	3	1	1.2	25
Orange	0.4	2	3	4	5	4	3.6	25
Dark Green	0.6	5	5	5	5	5	5	25
Light Blue	0.8	5	5	5	5	5	5	25
Cyan	1	5	5	5	5	4	4.8	25

	Number Recovered to Left Side, Test Run 1	2	3	4	5	Average
Pink	5	5	4	5	5	4.8
Blue	5	4	5	4	5	4.6
Purple	5	5	4	5	5	4.8
Maroon	5	5	5	4	5	4.8
Green	5	5	5	4	4	4.6
Yellow	4	4	5	5	2	4
Red	5	3	5	2	4	3.8
Orange	3	2	1	0	1	1.4
Dark Green	0	0	0	0	0	0
Light Blue	0	0	0	0	0	0
Cyan	0	0	0	0	1	0.2

Condition 3

Separation Block	0.00006	C
BP board	0.5	m
Bypass Motor	5	rad/sec

Total Recovered Charge: **11.64**

	Charge (*10^-7 C)	Number Recovered to Right Side, Test Run 1	2	3	4	5	Average	Sum
Pink	-1	0	0	1	1	0	0.4	25
Blue	-0.8	0	0	1	0	0	0.2	26
Purple	-0.6	0	0	2	0	2	0.8	24
Maroon	-0.4	2	2	0	2	0	1.2	25
Green	-0.2	1	2	0	2	1	1.2	25
Yellow	0	0	1	1	0	2	0.8	25
Red	0.2	0	2	3	1	2	1.6	25
Orange	0.4	3	4	4	4	1	3.2	25
Dark Green	0.6	5	5	5	5	5	5	25
Light Blue	0.8	5	5	5	5	5	5	25
Cyan	1	5	4	5	5	5	4.8	25

	Number Recovered to Left Side, Test Run 1	2	3	4	5	Average
Pink	5	5	4	4	5	4.6
Blue	5	5	5	5	5	5
Purple	5	5	2	5	3	4
Maroon	3	3	5	3	5	3.8
Green	4	3	5	3	4	3.8
Yellow	5	4	4	5	3	4.2
Red	5	3	2	4	3	3.4
Orange	2	1	1	1	4	1.8
Dark Green	0	0	0	0	0	0
Light Blue	0	0	0	0	0	0
Cyan	0	1	0	0	0	0.2